The performance of phaselocked loops for frequency control in single sideband land mobile radio receivers.

Sladen, J. P. H.

Award date:
1983

Awarding institution:
University of Bath

THE PERFORMANCE OF PHASELOCKED LOOPS FOR FREQUENCY CONTROL IN SINGLE SIDEBAND LAND MOBILE RADIO RECEIVERS

submitted by J.P.H. Sladen

for the degree of Ph.D.

of the University of Bath

1983

COPYRIGHT

J. P. H. Sladen

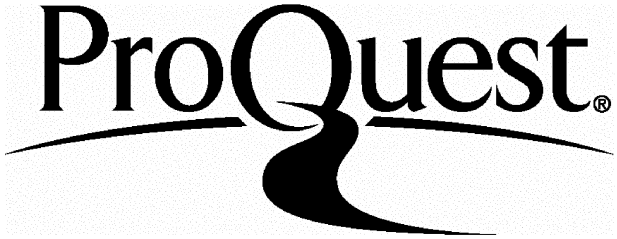

TO

MARIANNE

AND MY PARENTS

ACKNOWLEDGEMENTS

I am most grateful to my supervisor, Dr. J.P. McGeehan, for his advice and guidance throughout this work. I also wish to express my thanks for the help I have received from my colleagues and friends in the Wolfson Laboratory. Finally, I am most grateful to the UK Science and Engineering Research Council for the award of a research studentship and to Professor T.E. Rozzi, head of the Electronics Group, for the provision of laboratory facilities.

SYNOPSIS

All of the single sideband systems currently being considered for the land mobile radio service transmit a pilot tone in addition to the wanted information. The pilot is required in the receiver for automatic gain control and automatic frequency control. In particular, a phase-locked loop is often employed to perform receiver frequency control. This thesis begins by presenting background information on phaselocked receiver design and the problem caused by excess time delay introduced into the loop of a conventional phaselocked receiver. A novel phase-locked loop configuration is introduced and shown to overcome the effects of the excess time delay. The same technique is shown to greatly improve the adjacent channel selectivity performance of a phaselocked receiver.

Random phase and amplitude variations are impressed upon a signal transmitted through the land mobile multipath environment. After discussing several models of the propagation medium, some of the limitations it imposes on phaselocked SSB receiver performance are introduced.

CONTENTS

		Page
	SYNOPSIS	iv
	ABBREVIATIONS	ix
	SYMBOLS	x
	PUBLICATIONS	xvi
1	INTRODUCTION	1.1
	1.1 Land mobile radio	1.1
	1.2 Pilot tone SSB	1.1
	1.3 Pilot tone SSB receiver frequency stability and AFC	1.3
	1.4 Structure of thesis	1.5
2	THE PHASELOCKED LOOP AND ITS APPLICATION TO RECEIVER DESIGN	2.1
	2.1 The basic PLL	2.1
	2.2 PLL linearisation	2.4
	2.3 Steady state tracking performance of an input frequency offset	2.7
	2.4 Acquisition	2.9
	2.5 Aided frequency acquisition	2.11

2.6 Higher order loops 2.12

2.7 Heterodyne phaselocked receivers 2.12

2.8 False locking 2.18

2.9 Development of phaselocked SSB mobile radio receivers 2.19

3 THE SPLIT LOOP TECHNIQUE AND FALSE LOCK ELIMINATION 3.1

3.1 Introduction 3.1

3.2 The split loop receiver 3.2

3.3 Experimental study of the acquisition time of PLLs incorporating pure time delay 3.6

3.4 Experimental study of the acquisition time of a phaselocked SSB receiver 3.13

3.5 The implementation of the split loop technique incorporating acquisition aids 3.18

3.6 The effect of time delay on loop noise bandwidth 3.19

4 THE ADJACENT CHANNEL PERFORMANCE OF A PHASELOCKED SSB RECEIVER 4.1

4.1 Adjacent channel selectivity definitions 4.3

4.2 Receiver characterisation 4.5

4.3 Adjacent channel induced instability 4.7

4.4 Reciprocal mixing 4.23

4.5 Overall adjacent channel selectivity performance of the Wolfson receiver 4.32

5 LAND MOBILE RADIO PROPAGATION 5.1

5.1 The land mobile radio communications medium 5.1

5.2 Short term fading - multiple path case 5.2

5.3 Short term fading - twin path case 5.9

5.4 Multipath distortion correction techniques 5.13

5.5 Implications of fading for phaselocked AFC design 5.16

6 FEEDFORWARD AGC PERFORMANCE IN A PHASELOCKED RECEIVER 6.1

6.1 AGC in land mobile SSB receivers 6.2

6.2 The behaviour of a coupled PLL/FFAGC system in fading 6.5

6.3 Computer simulation of a coupled PLL/FFAGC system 6.8

6.4 Experimental verification 6.15

6.5 Field trials of the coupled PLL/FFAGC system 6.19

7 THE TRACKING PERFORMANCE OF NARROWBAND PHASELOCKED LOOPS IN A LAND MOBILE RECEIVER 7.1

7.1 Field trial recording procedure 7.2

7.2 Experimental configuration for tracking study 7.2

7.3 PLL tracking performance 7.3

8 CONCLUSIONS AND SUGGESTIONS FOR FUTURE WORK 8.1

APPENDIX 1 VHF RECEIVER A1.1

APPENDIX 2 TWO TONE ADJACENT CHANNEL INDUCED INSTABILITY SOLUTIONS A2.1

ABBREVIATIONS

AFC	automatic frequency control
AGC	automatic gain control
AM	amplitude modulation
CCD	charge coupled device
ECL	emitter coupled logic
FFAGC	feedforward automatic gain control
FFT	fast Fourier transform
FM	frequency modulation
IF	intermediate frequency
PD	potential difference
PLL	phaselocked loop
PMR	private mobile radio
PSD	phase sensitive detector
RF	radio frequency
RMS	root mean square
SINAD	signal plus noise plus distortion to noise plus distortion ratio
SSB	single sideband
UHF	ultra high frequency
VCO	voltage controlled oscillator
VHF	very high frequency

SYMBOLS

A	IF gain
B	bandwidth of baseband noise
B_n	PLL noise bandwidth
C	signal amplitude
E	signal amplitude
$F(s)$	loop filter transfer function
$F_1(s)$, $F_2(s)$	split loop filter transfer functions
$G(\omega)$	IF filter response
$H(s)$	closed loop transfer function
J_k	kth order Bessel function of the first kind
K	complete elliptical integral of the first kind
K_d	PSD gain
K_v	DC loop gain
K_1, K_2	VCO gains
N_r	level crossing rate
P_S	signal power
R	signal or voltage ratio
RC	resistor capacitor product
S	reference tone signal to noise ratio
$S_e(\omega)$	power spectrum of electric field

$S_r(\omega)$	power spectrum of envelope modulation
$S_{\dot{\theta}}(\omega)$	power spectrum of frequency modulation
SS1, SS2	scattering sources
T	duration of fade
T_p	pull-in time
U	speed
V_a	peak amplitude of adjacent channel signal
V_b	peak amplitude of demodulated tone
V_g	peak amplitude of demodulated reference
V_i	peak amplitude of input
V_n	RMS noise voltage
V_r	peak amplitude of receiver reference
V_t	peak amplitude of audio signal
V_0	peak amplitude of VCO output
V_1	peak amplitude of first local oscillator output
V_2	peak amplitude of second local oscillator output
W_i	noise power spectral density
X, X_1, X_2	distances on X-Y rectangular co-ordinates
Y, Y_1, Y_2	distances on X-Y rectangular co-ordinates
b	mean received power
dB	decibels
dBm	decibels with respect to 1 mW

e	2.71828...
f	frequency (Hz)
f_r	frequency of receiver reference
f_s	frequency spacing between adjacent channel signal and wanted carrier
f_t, f_t'	frequencies of audio tones
k	an integer
m	modulation index
p	probability density
r, r'	signal envelopes
s	Laplace operator
t	time
v_a	adjacent channel signal
v_b	demodulated tone
v_c	VCO control voltage
v_d	PSD output
v_g, v_g'	demodulated reference signals
v_i	input signal
v_r	receiver reference
v_t	audio signal
v_0	VCO output
v_1	first local oscillator output

v_2	second local oscillator output
x	output signal
α	ratio of modulation tone to reference tone level
$\Delta\omega$	initial frequency offset
$\Delta\omega_p$	pull-in limit
$\Delta\omega_{rms}$	RMS oscillator deviation
δ	phase shift
δ_1, δ_2	angles
$\delta\omega$	beat frequency
ζ	PLL damping factor
θ	phase
θ_a	phase of adjacent channel signal
θ_b	phase of demodulated tone
θ_e	phase error
θ_g	phase of demodulated reference
θ_i	phase of input
θ_r	phase of receiver reference
θ_s	phase of adjacent channel signal relative to $\theta_1 + \theta_2$
θ_t	phase of audio signal
θ_v	static phase error
θ_0	phase of VCO output
θ_1	phase of first local oscillator output

θ_2	phase of second local oscillator output
$\overline{\theta_{no}^2}$	output phase variance
$\dot{\theta}$	frequency modulation
π	3.14159...
τ	time delay
τ_1, τ_2	time constants
ψ	phase shift
ω	frequency (rad)
ω_a	frequency of adjacent channel signal
ω_b	frequency of demodulated tone
ω_c	carrier frequency
ω_d	maximum Doppler frequency
ω_f	fade rate
ω_i, ω_i'	input frequencies
ω_m	modulating frequency
ω_n	PLL natural frequency
ω_r	frequency of receiver reference
ω_s	frequency spacing between adjacent channel signal and wanted carrier
ω_t, ω_t', ω_t''	frequencies of audio tones
ω_0	VCO centre frequency
ω_1	frequency of first local oscillator output

ω_2 frequency of second local oscillator output

Unless otherwise stated, SI units are used throughout the text.

PUBLICATIONS

1 "Elimination of false locking in long loop phase-locked receivers", IEEE Trans., Special issue on phase-locked loops, October 1982, Vol. COM-30, pp. 2391-2397.
Co-author, J.P. McGeehan.

2 "Comparative adjacent-channel selectivity performance of phase-locked pilot-tone SSB mobile radio receivers with particular reference to the long-, short- and split-loop configurations", Proc. IEE, December 1982, Vol. 129F, pp. 439-446.
Co-author, J.P. McGeehan.

3 "The performance of a phaselocked single sideband land mobile receiver in the multipath environment", IEE colloquium on the characterisation and mitigation of multipath interference effects, London, May 1983, pp. 6/1 - 6/3.
Co-author, J.P. McGeehan.

4 "Feedforward automatic gain control performance in a phaselocked single sideband mobile radio receiver", accepted for publication, IEE Proceedings, Part F.
Co-author, J.P. McGeehan.

5 "The tracking performance of a narrowband phaselocked loop in the mobile multipath environment", submitted for publication, IEE Proceedings, Part F.

Co-author, J.P. McGeehan.

The first two of these papers are included at the back of the thesis.

CHAPTER 1

INTRODUCTION

1.1 Land mobile radio

The use of the UK private mobile radio (PMR) service has been growing for many years and this trend seems likely to continue, with an estimated growth rate of 10 % per annum (1). The demand for the service now far exceeds the capacity, particularly in the larger metropolitan areas, and the situation has led to interest in the use of single sideband (SSB) operating in 5 kHz channels as a more spectrally efficient mode of modulation for the service. At present, frequency modulation (FM) and full carrier amplitude modulation (AM), operated in 12.5 kHz channels, are employed at VHF, and FM, operated in 25 kHz channels, is used at UHF. Although the narrow channel spacings required by SSB do not necessarily produce improved spectral usage, results of extensive trials comparing its performance with that of FM and AM systems indicate this to be the case (2).

A similar situation has arisen in the USA, where FM, operated in 25 kHz and 30 kHz channels at both VHF and UHF, is presently employed. The increasing demand for channels has led the Federal Communications Commission to investigate the use of SSB as an alternative mode of modulation for the land mobile service (3).

1.2 Pilot tone SSB

All the SSB systems which have been proposed for PMR use transmit

a pilot tone, some 10 dB to 15 dB below peak envelope power, in addition to the modulation. The tone is required in the receiver for automatic gain control (AGC) and automatic frequency control (AFC). The systems under investigation can be categorized by the position of the pilot relative to the wanted modulation's frequency band and are:

(i) *Pilot carrier SSB.*

(ii) *Tone-in-band SSB.* The pilot is transmitted at some frequency within a notch in the modulation's spectrum.

(iii) *Tone-above-band SSB.* The pilot is transmitted at some frequency above the modulation's spectrum.

It is desirable to be able to choose the frequency spacing between the pilot and nearest modulation component from system considerations. Clearly, the constraint of the standard 300 Hz to 3 kHz audio channel makes this impossible in the pilot carrier case. In both the tone-above-band and pilot carrier systems, the pilot is positioned at the edge of the transmitted spectrum. This makes it vulnerable to adjacent channel interference (4) and also reduces the correlation between modulation and pilot tone fading (5). The tone-in-band system has been criticized because transmission of the pilot within the band necessitates removal of part of the transmitted modulation's baseband spectrum. To overcome this difficulty, the transparent tone-in-band system has been developed (6). Prior to transmission, the audio spectrum is split into two segments, the top portion is shifted up in frequency and the pilot is inserted between the two halves. After demodulation in the receiver, a complementary process removes the pilot and recombines the spectrum.

The system gives a full 300 Hz to 3 kHz 'transparent' spectrum to the user and allows more flexibility in choosing the pilot tone notch width.

1.3 Pilot tone SSB receiver frequency stability and AFC

SSB generation consists of a linear frequency translation of the modulation's baseband spectrum. SSB detection or demodulation is the reverse process and is achieved by one or more mixing processes which translate the sideband back to its original audio spectrum. Any frequency error in the receiver oscillators used for this process will result in frequency errors at the SSB detector output. For instance, if an SSB signal at 450 MHz is demodulated with a carrier 50 Hz offset, the resulting audio spectrum will also be offset by 50 Hz. Voice signals are very sensitive to frequency errors and, in order to avoid loosing the naturalness of speech and introducing noticeable distortion, the errors should be limited to less than 20 Hz (7). This form of distortion is peculiar to SSB systems and gives rise to a much more stringent frequency stability specification than is required for FM and AM systems. A 450 MHz oscillator with a maximum frequency uncertainty of 20 Hz requires a stability of $\pm 4.4 \times 10^{-8}$ to be maintained over its operating temperature range for a period of many months. At present, such performance is far beyond that of an inexpensive temperature compensated crystal oscillator and could only be met by an oven controlled type. The high cost, as well as high power consumption, yield oven controlled oscillators unsuitable for incorporation in mobile receivers, although they can be used to provide a stable reference at base stations.

There is a second, less stringent, constraint on receiver frequency stability and, although applicable to AM and FM systems as well as SSB, it becomes more critical as the channel spacing for mobile radio transmissions is further reduced. Generally, filtering at intermediate frequency (IF) stages determines the selectivity of a receiver. Provided the wanted modulation is passed, narrower filtering gives improved performance due to rejection of adjacent channel transmissions and noise. However, any frequency error of the receiver's local oscillators prior to the main selectivity stage will have to be accomodated by the use of larger IF bandwidths. Clearly, it is important that these oscillators are stable if good selectivity is to be achieved and sideband cutting prevented.

These considerations have led to the incorporation of AFC in the majority of the current SSB mobile radio receivers, and, in particular, the use of a phaselocked loop (PLL) for this purpose. In most cases, the pilot, having been demodulated to some audio frequency, is compared in phase to a precise locally generated reference frequency tone. The resulting error signal, after filtering, is then used to control the first local oscillator of the receiver. In comparison with other AFC schemes, the popularity of the PLL is probably due to its wide use in coherent receiver design, the simplicity of the circuitry, its ability to reject interference from neighbouring modulation components and noise, and to the possibility of achieving zero frequency error when the loop maintains small phase error between the demodulated pilot and the local reference.

1.4 Structure of thesis

The thesis concentrates on three major problems concerning the use of a PLL in a mobile radio receiver:

(i) *Time delay.* It is well known that the inclusion of an IF filter within a PLL can severely degrade the loop's performance due to the introduction of time delay. To some extent, the problem is exacerbated in a SSB receiver by the need for a narrow IF filter.

(ii) *Adjacent channel interference.* Modulation components which enter the PLL modulate the receiver's first local oscillator. As this oscillator is exposed to adjacent channel transmissions, a consequence of the PLL could well be to reduce the receiver's adjacent channel selectivity. (It should be noted that the associated problem of distortion of the demodulated signal caused by the presence of modulation components within the loop, termed 'speech pulling' has been analysed elsewhere (8) and will not be considered in detail here.)

(iii) *Multipath propagation.* Random phase and amplitude variations will be impressed upon the received pilot due to the propagation characteristics of a mobile communications channel. Clearly, the variations will hinder the loop's ability to track the pilot tone.

In chapter 2, background information on the PLL is given, leading to an example of its use in a tone-in-band SSB mobile radio receiver.

Chapter 3 introduces a novel PLL configuration which is shown to minimize the effects of time delay on loop performance and, in chapter 4, the same technique is shown to greatly improve a phaselocked receiver's adjacent channel selectivity performance.

Chapter 5 through 7 deal with multipath propagation and its consequences for PLL design. Chapter 5 discusses land mobile radio propagation and the need to combat the fading encountered in the field by the use of fast acting AGC circuitry. The action of the PLL on the effectiveness of this circuitry is the subject of chapter 6, while the tracking performance of PLLs in the multipath environment is investigated in chapter 7.

In conclusion, chapter 8 summarizes the implications of this study for phaselocked receiver design and suggests further areas of research in the field of mobile radio AFC.

REFERENCES

1) Pannel, W.: "A study of the future frequency spectrum requirements for private mobile radio in the United Kingdom", Pye Telecommunications Ltd., 1976.

2) "Report on comparative tests of modulation methods for private mobile radio", Home Office Directorate of Radio Technology, April 1982.

3) Lusignan, B.B.: "Single-sideband transmission for land mobile radio", IEEE Spectrum, July 1978, pp. 33-37.

4) Gosling, W., McGeehan, J.P., and Holland, P.G.: "Receivers for the Wolfson single-sideband VHF land mobile radio system", Radio and Electronic Engineer, May 1979, Vol. 49, pp. 231-235.

5) McGeehan, J.P., and Burrows, D.F.: "Performance limits of feedforward automatic gain control in mobile radio receivers", Proc. IEE, November 1981, Vol. 128F, pp. 385-392.

6) McGeehan, J.P., Bateman, A.J., and Burrows, D.F.: "The use of 'transparent' tone-in-band (TTIB) and feedforward signal regeneration (FFSR) in single sideband mobile communication systems", conference on communications equipment and systems, IEE, April 1982, pp. 121-124.

7) Pappenfus, E.W., Bruene, W.B., and Schoenike, E.O.: "Single Sideband Principles and Circuits" (McGraw-Hill, 1964), chapter 3.

8) McGeehan, J.P., and Lymer, A.: "The problem of speech pulling and its implication for the design of phase-locked SSB radio systems", Proc. IEE, November 1981, Vol. 128F, pp. 361-369

CHAPTER 2

THE PHASELOCKED LOOP AND ITS APPLICATION TO RECEIVER DESIGN

This chapter provides a general introduction to the PLL. Its use in a superheterodyne receiver is discussed and, in particular, the associated problem of loop time delay. Previous work on phaselocked SSB receivers is then summarised. This leads to the receiver configuration investigated subsequently in this thesis.

2.1 The basic PLL

A block diagram of the basic PLL configuration is given in figure 2.1. It consists of the following three major components:

(i) *Voltage controlled oscillator (VCO)*. The VCO output frequency is determined by the control voltage, $v_c(t)$ and is given by:

$$v_0 = V_0 \cos(\omega_0 t + \theta_0) \qquad (2.1)$$

where ω_0 and V_0 are the VCO's centre frequency and peak amplitude respectively, and:

$$\frac{d\theta_0}{dt} = K_1 v_c \qquad (2.2)$$

where K_1 is the VCO gain constant.

(ii) *Phase sensitive detector (PSD)*. The phases of the input signal, $v_i(t)$, and the VCO output, $v_0(t)$, are compared in the PSD. The input signal is written as:

$$v_i = V_i \sin(\omega_0 t + \theta_i) \qquad (2.3)$$

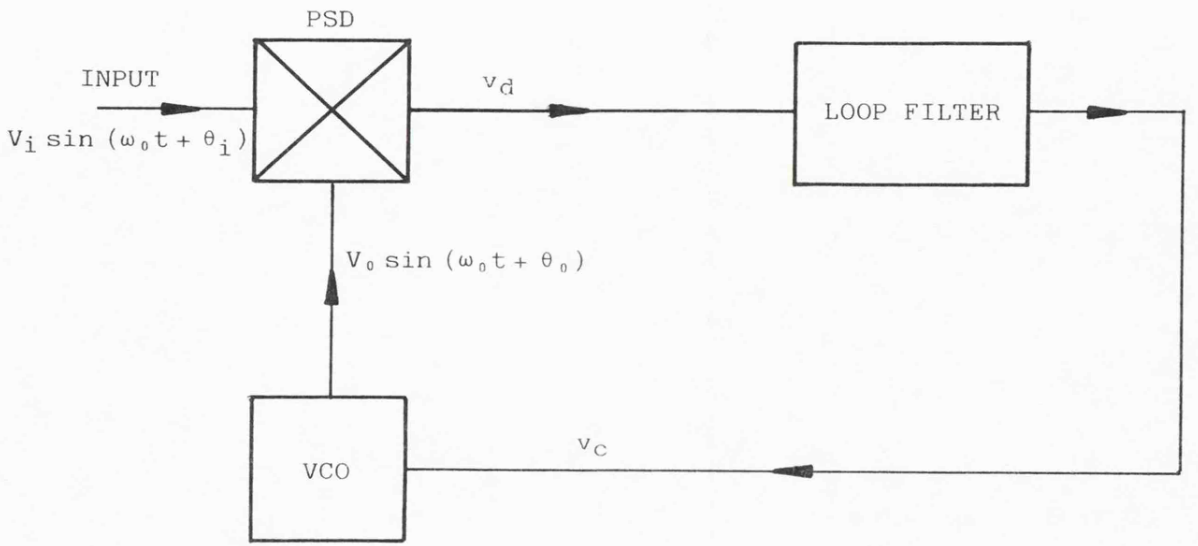

Figure 2.1 Basic PLL block diagram

where V_i is the peak amplitude and θ_i is the input phase relative to $\omega_0 t$. Assuming this is a perfect multiplier and that the high frequency output term is removed by filtering, then:

$$v_d = K_d \sin(\theta_i - \theta_0) \qquad (2.4)$$

where the proportionality constant, K_d, is known as the PSD gain or sensitivity. The multiplier only behaves as a linear phase detector for small values of the sine argument. Other types of PSD are available which extend this linear region, and are useful in certain applications. Examples are the triangular and sawtooth PSDs which have linear regions from $-\pi/2$ to $\pi/2$ and $-\pi$ to π respectively. However, in the following chapters, a sinusoidal PSD will always be assumed because of the following justification:

(a) The bulk of the results applicable to receiver design in the PLL literature are obtained for the sinusoidal PSD case.

(b) It has been established in the literature (1) that the advantage of extended range PSDs is completely lost when subject to noisy fading signals and that the sinusoidal PSD is preferable.

(c) The use of extended range PSDs would not be significant in overcoming any of the problems associated with phaselocked receivers addressed in later chapters.

(iii) *The loop filter.* The transfer function of the loop filter is

denoted by F(s). In mixed notation:

$$v_c = F(s)v_d \tag{2.5}$$

Eliminating $v_c(t)$ and $v_d(t)$ from equations 2.2, 2.4 and 2.5, then:

$$\frac{d\theta_o}{dt} = K_1K_dF(s)\sin(\theta_i - \theta_o) \tag{2.6}$$

If the phase error term is denoted by:

$$\theta_e = \theta_i - \theta_o \tag{2.7}$$

then we obtain:

$$\frac{d\theta_e}{dt} = \frac{d\theta_i}{dt} - K_1K_dF(s)\sin\theta_e \tag{2.8}$$

This is the well known equation of operation of the PLL in the absence of noise (2).

2.2 PLL linearisation

For small phase errors, of magnitude less than, say, 30 degrees, the nonlinearity in equation 2.8 can be removed by the approximation (3):

$$\sin\theta_e = \theta_e \tag{2.9}$$

In this case transfer functions for the loop output phase and phase error can be written:

$$\frac{\theta_o(s)}{\theta_i(s)} = H(s) = \frac{K_1K_dF(s)}{s + K_1K_dF(s)} \tag{2.10}$$

where H(s) is the closed loop transfer function, and:

$$\frac{\theta_e(s)}{\theta_i(s)} = 1 - H(s) = \frac{s}{s + K_1K_dF(s)} \tag{2.11}$$

The order of a PLL is defined as the highest power of s in the denominator of the closed loop transfer function. For example, a first order loop is obtained if F(s) = 1, in which case H(s) becomes:

$$H(s) = \frac{K_1 K_d}{s + K_1 K_d} \tag{2.12}$$

There are two loop filters which are commonly used for a second order PLL. The first, the passive lag-lead filter, has transfer function:

$$F(s) = \frac{s\tau_2 + 1}{s\tau_1 + 1} \tag{2.13}$$

where τ_1 and τ_2 are time constants. This gives a closed loop transfer function:

$$H(s) = \frac{s(2\zeta\omega_n - \omega_n^2/K_1K_d) + \omega_n^2}{s^2 + 2\zeta\omega_n s + \omega_n^2} \tag{2.14}$$

where ω_n is the loop natural frequency and ζ is the damping factor, given by:

$$\omega_n = \left(\frac{K_1 K_d}{\tau_1}\right)^{1/2} \tag{2.15}$$

$$\zeta = \frac{1}{2}\left(\frac{K_1 K_d}{\tau_1}\right)^{1/2}\left(\tau_2 + \frac{1}{K_1 K_d}\right) \tag{2.16}$$

The second loop filter requires an active implementation and has transfer function:

$$F(s) = \frac{s\tau_2 + 1}{s\tau_1} \tag{2.17}$$

The resulting closed loop transfer function is:

$$H(s) = \frac{2\zeta\omega_n s + \omega_n^2}{s^2 + 2\zeta\omega_n s + \omega_n^2} \tag{2.18}$$

where:

$$\omega_n = \left(\frac{K_1 K_d}{\tau_1}\right)^{1/2} \tag{2.19}$$

and:

$$\zeta = \frac{\tau_2 \omega_n}{2} \tag{2.20}$$

The type of the loop is defined as the number of perfect integrators it contains. Because of the VCO, any PLL is at least type 1. Equations 2.12 and 2.14 represent type 1 loops, whereas equation 2.18 is that of a type 2.

The noise bandwidth, B_n, of the PLL is a useful measure when studying its linear performance in noise and is defined as:

$$B_n = \int_0^\infty |H(j2\pi f)|^2 df \text{ Hz} \tag{2.21}$$

For an input tone accompanied by additive white Gaussian noise, the variance of the output phase, $\overline{\theta_{no}^2}$, is given by (4):

$$\overline{\theta_{no}^2} = B_n \frac{W_i}{P_s} \text{ rad}^2 \tag{2.22}$$

where W_i is the noise power spectral density in W/Hz and P_s is the signal power in Watts.

The noise bandwidth of a first order loop is given by:

$$B_n = \frac{K_1 K_d}{4} \tag{2.23}$$

and for a second order type two loop:

$$B_n = \frac{1}{2}\omega_n \left(\zeta + \frac{1}{4\zeta}\right) \tag{2.24}$$

For fixed ω_n, the noise bandwidth of equation 2.24 is minimised by putting ζ equal to ½ (4). However PLLs are usually designed with critical damping, i.e. with ζ equal to $1/\sqrt{2}$. This is optimum for frequency tracking a signal in additive white Gaussian noise and gives rise to little increase in loop noise bandwidth (4).

2.3 Steady state tracking performance of an input frequency offset

It is unlikely that the frequency of the input signal is identical to that of the VCO. Clearly, if this were always the case, any PLL AFC system would be superfluous. It is useful, therefore, to compare the steady state loop phase errors due to an input frequency offset for first and second order loops (5). The results serve to highlight the superiority of the second order type two loop.

2.3.1 Linear tracking

Provided the phase error remains small enough to justify the linear approximation, the loop transfer function can be used to examine the response to a specified input. The steady state phase error can be obtained by applying the final value theorem of Laplace transforms to equation 2.11:

$$\lim_{t\to\infty} \theta_e(t) = \lim_{s\to 0} \frac{s^2\theta_i(s)}{s + K_1K_dF(s)} \qquad (2.25)$$

For a step change in input frequency of magnitude $\Delta\omega$, we have:

$$\theta_i(s) = \Delta\omega/s^2 \qquad (2.26)$$

and

$$\lim_{t\to\infty} \theta_e(t) = \frac{\Delta\omega}{s + K_1 K_d F(s)} = \frac{\Delta\omega}{K_1 K_d F(0)} \qquad (2.27)$$

or

$$\theta_v = \frac{\Delta\omega}{K_v} \qquad (2.28)$$

where θ_v is the static phase error and K_v is the DC loop gain. Comparing the three loop transfer functions mentioned in section 2.2, zero static phase error would only result by the use of the type two loop. Although a filter with infinite DC gain cannot be realized, a very good approximation can be obtained by the incorporation of a modern high gain operational amplifier. Furthermore, for the first order loop, $F(0) = 1$, and the static phase error can only be reduced by increasing $K_1 K_d$. This implies, from equation 2.23, an increase in loop noise bandwidth. In the second order loop, low static phase error can be obtained without sacrificing loop noise performance.

2.3.2 Nonlinear tracking

The nonlinearity of the sinusoidal PSD was neglected in the derivation of equation 2.28. The exact expression should be:

$$\sin \theta_v = \frac{\Delta\omega}{K_v} \qquad (2.29)$$

As $|\sin \theta_v| \leq 1$, there is no solution to this equation if $|\Delta\omega| > K_v$. Instead, the loop falls out of lock, indicating that a PLL is unable to track a signal with an offset frequency of magnitude greater than K_v.

Unlike the first order case, a second order design can possess a large frequency tracking range together with good noise immunity.

2.4 Acquisition

Before phaselock to the input tone is achieved, the PLL is operating in the acquisition mode and the assumption of PSD linearity cannot be made. In a first order loop acquisition occurs without any skipped cycles, that is, without more than one beat period, appearing at the PSD output (6). This is termed lock-up or phase acquisition. A second order loop may undergo a period of cycle skipping called frequency acquisition or pull-in before it too undergoes phase acquisition and achieves lock.

2.4.1 First order loop - phase acquisition

Unlike the case of higher order loops, the acquisition equation of the first order PLL can be solved exactly (6). Cycle skipping does not occur and acquisition is only possible if the signal frequency offset is less than K_1K_d, known as the lock-in limit. A large acquisition range cannot be obtained without a large noise bandwidth. The time required to lock up depends on the initial values of phase and frequency but is in the order of $3/K_1K_d$ seconds.

2.4.2 Second order loop - frequency acquisition

For small frequency offsets, up to the lock-in limit, the second order loop behaves similarly to the first order and will acquire the

input tone without skipping cycles. Gardner (6) argues that the lock-in limit for the second order loop with active or passive lag lead filter is around $2\zeta\omega_n$. For larger offsets, the loop may acquire after skipping cycles, the highest frequency offset for which this can occur being known as the pull-in limit. Usually the frequency acquisition period is slow and, in comparison, the lock-in time can be neglected.

It is at first surprising that a PLL can pull-in at all, as there is no open loop frequency error signal. When an input tone is applied to the closed loop, however, the PSD output beat note has a non-zero mean. This small DC level is integrated in the loop filter and serves to pull the VCO towards lock. The presence of the DC level can be explained as follows. The fundamental frequency of the PSD output is the difference frequency between the input tone and the VCO output. After passing through the loop filter, the beat note frequency modulates the VCO. The frequencies of the input tone and one of the VCO sidebands coincide and yield a DC term at the PSD output. In order to find approximate formulas for the pull-in performance of second order PLL's, several authors (6,7,8) made the assumption that the PSD output beat frequency term passes solely through a constant gain AC loop filter path while the DC term passes only through an integrator term with zero high frequency gain. For example, the loop filter of equation 2.17 can be split up into a constant high frequency gain term, τ_2/τ_1, and a perfect integrator term, $1/\tau_1 s$. Using this approximation, the pull-in time, T_p, defined as the time required for the average frequency error to change from its initial condition, $\Delta\omega$, to the lock-in limit $2\zeta\omega_n$, is given by (6):

$$T_p = \frac{(\Delta\omega)^2}{2\zeta\omega_n^3} \qquad (2.30)$$

The equation is valid for second order loops with either the passive or active lag-lead filter and is an excellent approximation, provided, $\Delta\omega$ is appreciably greater than the lock-in limit and less than the pull-in limit, denoted $\Delta\omega_p$. For the loop with a perfect integrator, $\Delta\omega_p$ is theoretically infinite, restricted only by circuit limiting or DC offsets. For the loop with a passive lag-lead filter, the pull-in limit is given approximately by (6):

$$\Delta\omega_p = K_1 K_d \sqrt{\left(\frac{2\tau_2}{\tau_1}\right)} \qquad (2.31)$$

2.5 Aided frequency acquisition

As shown in equation 2.30, the acquisition time is dependent on the loop's natural frequency and damping factor. As far as possible, these loop parameters should be chosen to optimise tracking, which is the true purpose of the PLL. In doing this, values will often be chosen which are too low to obtain an acceptable acquisition time. As a result, many schemes have been devised to speed up acquisition (6,9). A dual bandwidth loop can be designed, with a large bandwidth for fast acquisition and a small bandwidth for good tracking. A technique which speeds up acquisition and preserves the narrow noise bandwidth of the loop is to sweep the VCO over the expected range of input frequencies until lock is achieved. More complex methods include frequency discriminator aided acquisition and the derived rate rejection technique (10). The latter involves switching circuitry designed to

increase the reduction of loop frequency error for each PSD output beat cycle.

It is important that the acquisition aid does not degrade the loop performance in the tracking mode and as a result will usually be switched out once acquisition is complete. To achieve this, some form of lock detection is required and the usual scheme (6) is shown in figure 2.2. It consists of an auxiliary PSD fed by a quadrature VCO output, and a smoothing filter. The quadrature PSD output is proportional to cos θ_e and in the acquisition mode consists of a beat note with a small DC bias. Once phaselock is achieved, cos $\theta_e \simeq 1$ and a large DC level appears at the quadrature PSD output. When passed through a filter to sufficiently attenuate the beat note, the quadrature PSD output can be used to indicate phaselock.

2.6 Higher order loops

Loops of third or higher order have not found wide application in receiver design. One reason is that they are more difficult to stabilize (2) but, more importantly, they do not usually offer any worthwile performance advantages over a second order PLL. However, third order loops have found applications where it is necessary to track an accelerating input phase with zero steady state phase error (5).

2.7 Heterodyne phaselocked receivers

A block diagram of a simple heterodyne PLL receiver is given in figure 2.3. Such a PLL, containing no IF within it, is termed a short

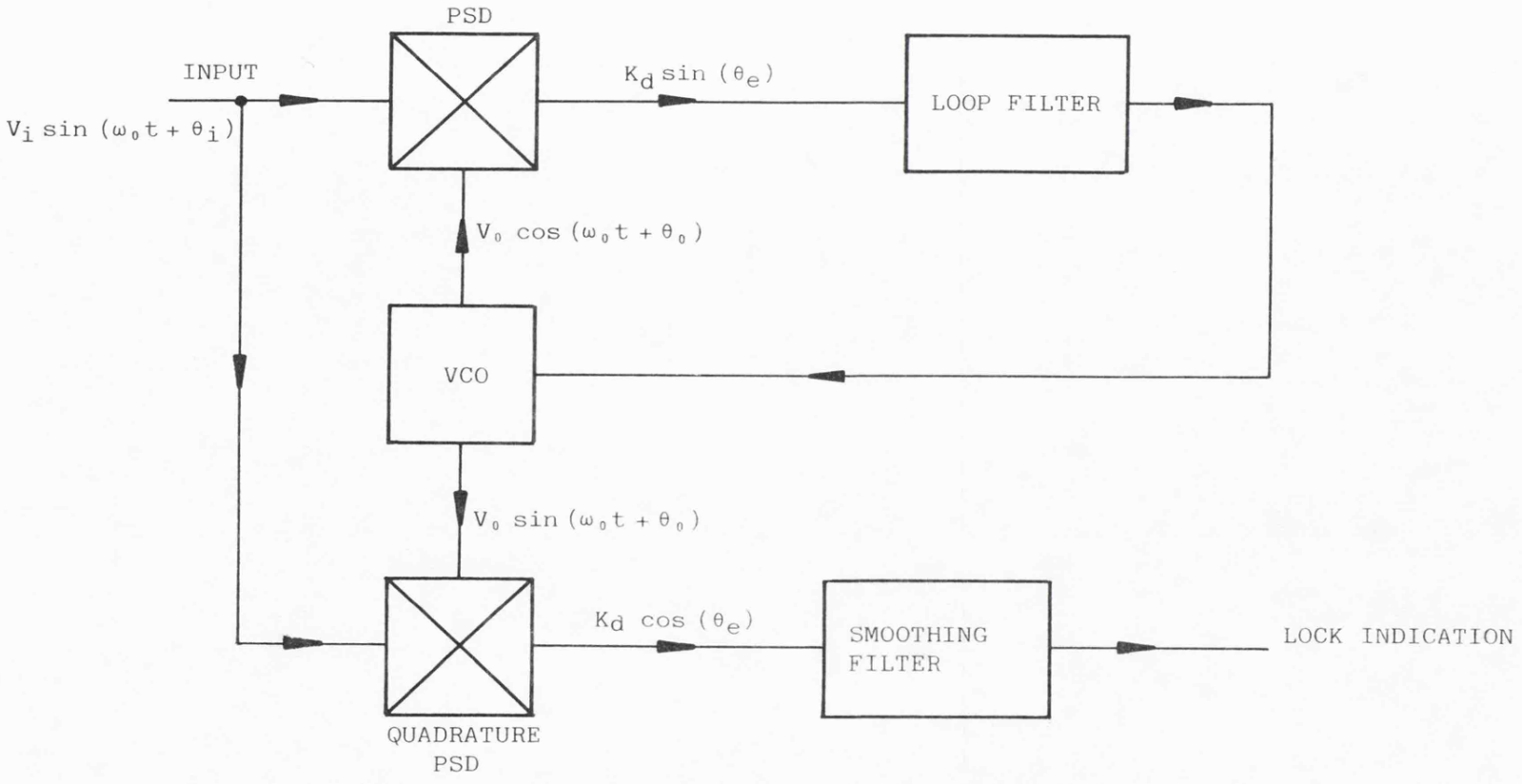

Figure 2.2 PLL with lock indicator

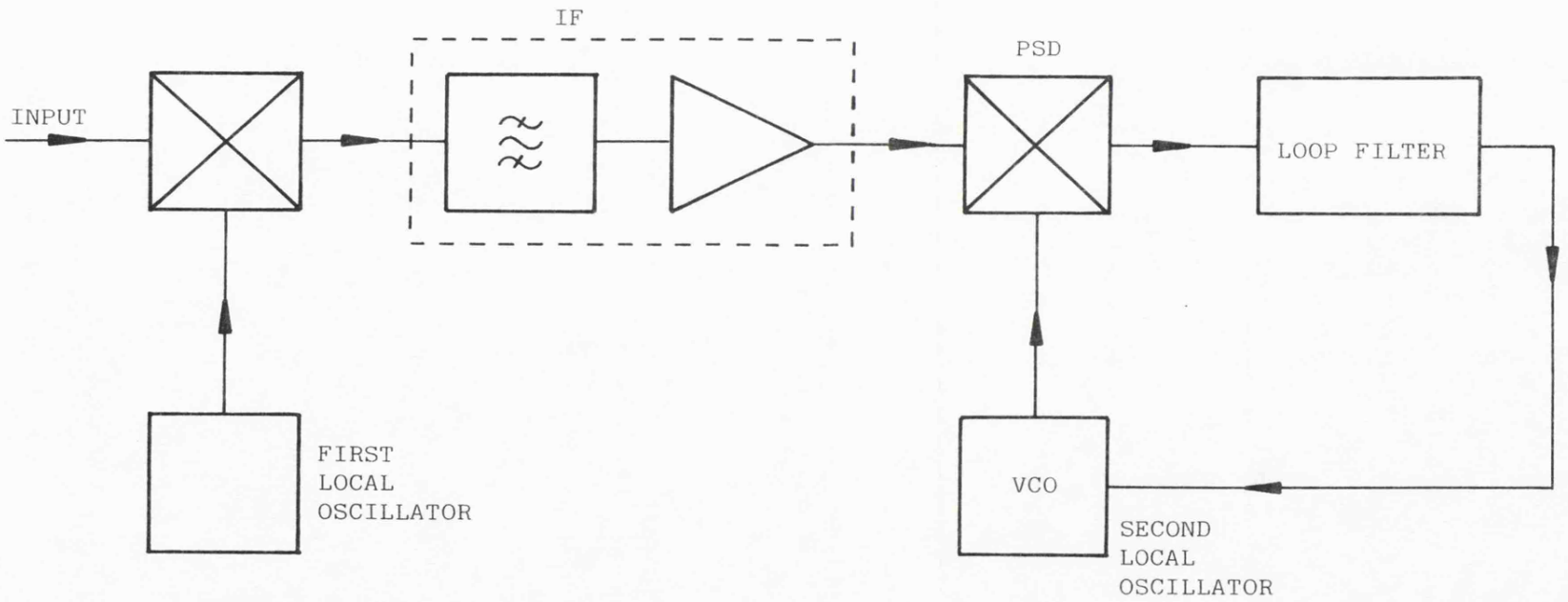

Figure 2.3 Short loop phaselocked receiver

loop. A serious disadvantage of the short loop receiver is that frequency drifts of the input or first local oscillator are not tracked out before the IF filter. There is therefore a requirement to widen the IF filter to accomodate these drifts at the expense of the IF signal to noise ratio. This problem can be overcome by incorporating IF stages within the loop in what is termed a long loop configuration (11). Such a receiver containing one IF stage is shown in figure 2.4 and the equation of the loop will now be derived. The voltage controlled first local oscillator output, $v_1(t)$, is given by:

$$v_1 = V_1 \cos(\omega_1 t + \theta_1) \tag{2.32}$$

with peak output voltage V_1, centre frequency ω_1 and phase θ_1 governed by:

$$\frac{d\theta_1}{dt} = K_1 v_C \tag{2.33}$$

K_1 is the VCO gain constant and $v_C(t)$ is its control voltage. $v_1(t)$ is mixed with the input signal, $v_i(t)$, where:

$$v_i = V_i \sin(\omega_i t + \theta_i) \tag{2.34}$$

$$\omega_i = \omega_1 + \omega_2 \tag{2.35}$$

and θ_i is the input phase relative to $\omega_i t$. The second local oscillator output, $v_2(t)$, which is not voltage controlled, is of the form:

$$v_2 = V_2 \cos(\omega_2 t + \theta_2) \tag{2.36}$$

where ω_2 is its frequency and θ_2 is a constant phase. Ignoring mixer output sum terms and, for the present, the effect of the IF filter characteristic, we can write the PSD output, $v_d(t)$ as:

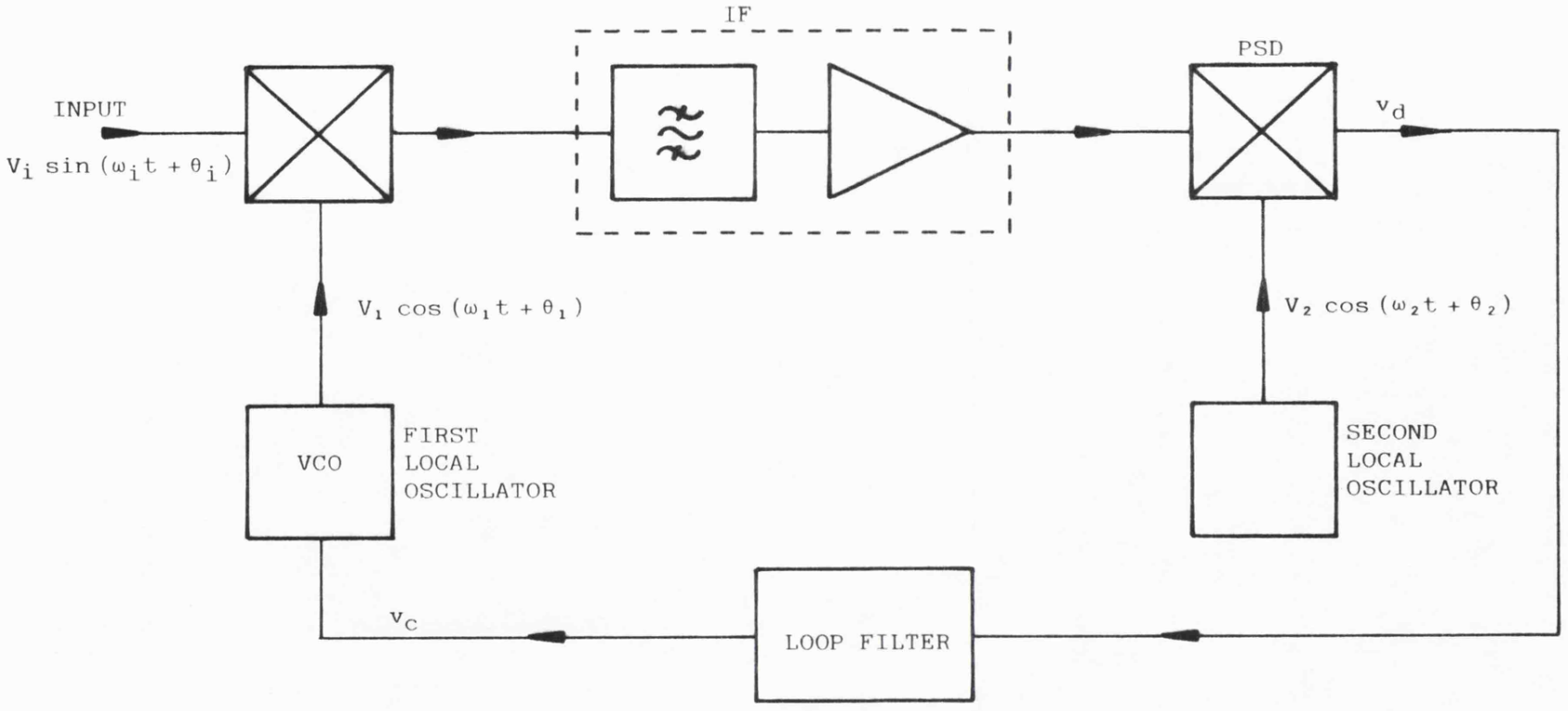

Figure 2.4 Long loop phaselocked receiver

$$v_d = K_d \sin \theta_e \qquad (2.37)$$

where K_d is the PSD gain, and the phase error is given by:

$$\theta_e = \theta_i - \theta_1 - \theta_2 \qquad (2.38)$$

Combining the differential of equation 2.38 with equations 2.5, 2.33 and 2.37, we obtain:

$$\frac{d\theta_e}{dt} = \frac{d\theta_i}{dt} - K_1 K_d F(s) \sin \theta_e \qquad (2.39)$$

This equation is identical to equation 2.8 and illustrates the equivalence of the long and short PLL's. However, in the long loop case, the locked PLL tracks out frequency variations of the input or first local oscillator before the IF stage, thus a narrower filter can be employed. Some allowance may have to be made for drifts in the second local oscillator but, as the oscillator will generally be of much lower frequency, its absolute frequency error will usually be much lower.

Unfortunately, by neglecting the IF filter characteristic, the above derivation is over simplified. Inclusion can have serious consequences for the long loop peformance and the loop cannot, as equation 2.38 implies, be treated as a simple PLL. In particular, the group delay of a narrow IF filter can increase the loop noise bandwidth (12) and introduce instability (11). Furthermore the frequency acquisition performance can be severely degraded and a phenomenon known as false locking (11) can occur, whereby the VCO comes to rest at an incorrect frequency, and phase synchronisation is never achieved. A description of false locking is given in the next section and more

details of an IF filter's effect on the linear performance of the PLL will be left until chapter 3.

2.8 False locking

Several authors (11,13,14,15) have investigated false locking either for an IF filter with arbitrary phase shift versus frequency characteristic or for the case of pure time delay in the loop. The long loop can be analysed as a simple short loop by combining the loop filter response with the equivalent low pass version of the IF filter. It is assumed that the additional filtering does not cause loop instability, so that a stable locked condition exists. For convenience, the IF filter is often treated as a pure time delay element. At the centre of its passband, its phase response will usually be sufficiently linear to make this a good approximation.

The mechanism of false locking is best understood by recalling the explanation of PLL frequency acquisition in section 2.4.2. The PSD beat frequency output is assumed to pass through the loop filter with a frequency-flat gain of τ_2/τ_1 and then modulate the VCO, giving rise to a sideband at the same frequency as the input tone. The PSD output DC component (which drives the VCO towards lock) is the product of this sideband and the input tone, and its polarity depends only on whether the input frequency is above or below that of the VCO. If additional filtering is now introduced into the loop, the phase relationship between the input tone and the VCO sideband of the same frequency will be altered. This, in turn, effects the PSD DC output and, in particular, may reduce it to zero or reverse its polarity, causing the VCO to be

pulled away from lock. Gardner (11) has shown that the DC output becomes proportional to cos ψ where ψ is the additional loop phase shift at the beat frequency. This result is for a type two second order loop and applies when the magnitude of the beat frequency is appreciably higher than the lock-in limit. If the phase shift is produced by a pure time delay, τ, then the DC PSD output becomes proportional to cos $\delta\omega\tau$ where $\delta\omega$ is the beat frequency. For values of $|\delta\omega|\tau$ slightly greater than $\pi/2$, the DC component changes polarity and acts to drive the VCO away from lock towards the first stable false lock positions at a frequency offset of $\pm 3\pi/2\tau$ radians/s. In order for the PLL to achieve phaselock, it is necessary that the magnitude of the initial frequency offset, $\Delta\omega$, is given by:

$$|\Delta\omega| < \frac{\pi}{2\tau} \text{ radians/s} \qquad (2.40)$$

This result, which was reached by Develet (13), indicates that the restriction of loop acquisition range caused by the presence of time delay, is independent of the loop bandwidth. The acquisition range cannot be increased by widening the loop bandwidth and in fact, such a procedure could well lead to loop instability.

2.9 Development of phaselocked SSB mobile radio receivers

The use of a phaselocked loop for frequency control in a SSB radio receiver has been known for many years (16) and it was first applied to a land mobile receiver in 1979 by Gosling *et al.* (17) who described a tone-in-band design. Since then, tone-above-band (18) and pilot carrier (19,20) systems have also incorporated phaselocked AFC.

A block diagram of a tone-in-band or tone-above-band phaselocked receiver is shown in figure 2.5, and the pilot carrier case is illustrated in figure 2.6. In figure 2.5, the demodulated pilot tone is compared in phase to the output of a reference tone generator whereas, in the pilot carrier scheme, the SSB demodulator itself acts as the PSD. However, some pilot carrier designs (20) have found advantage in mixing the carrier down to an audio IF for phase comparison and the resulting receiver more closely resembles figure 2.5. Nevertheless, the loop performance is essentially the same in all cases, as the PSD output, after passing through the loop filter, controls the receiver's first local oscillator in a long loop configuration. The tone-in-band system is advantageous, however, since the pilot is centrally positioned in the IF filter passband. AGC circuitry is, of course, vital and is only omitted from the figures for simplicity. The AGC control voltage is derived from the pilot after the modulation components have been removed by filtering, and is used to control the RF and IF amplifier stages. Some workers have incorporated the tone extraction filter within the PLL. For instance, Ball and Holmes (20) mix down the pilot carrier to an audio IF of 5 kHz and pass it through a narrow bandpass filter before phase comparison to a 5 kHz reference. However, McGeehan and Lymer (21) do not recommend this approach since the additional filtering only aggravates the problem of PLL instability. Frequency acquisition circuitry has also been omitted from the block diagrams for simplicity. Several methods, such as those described in section 2.5, have been used and some are further mentioned in chapter 3. However, acquisition aids are not dealt with in detail in this

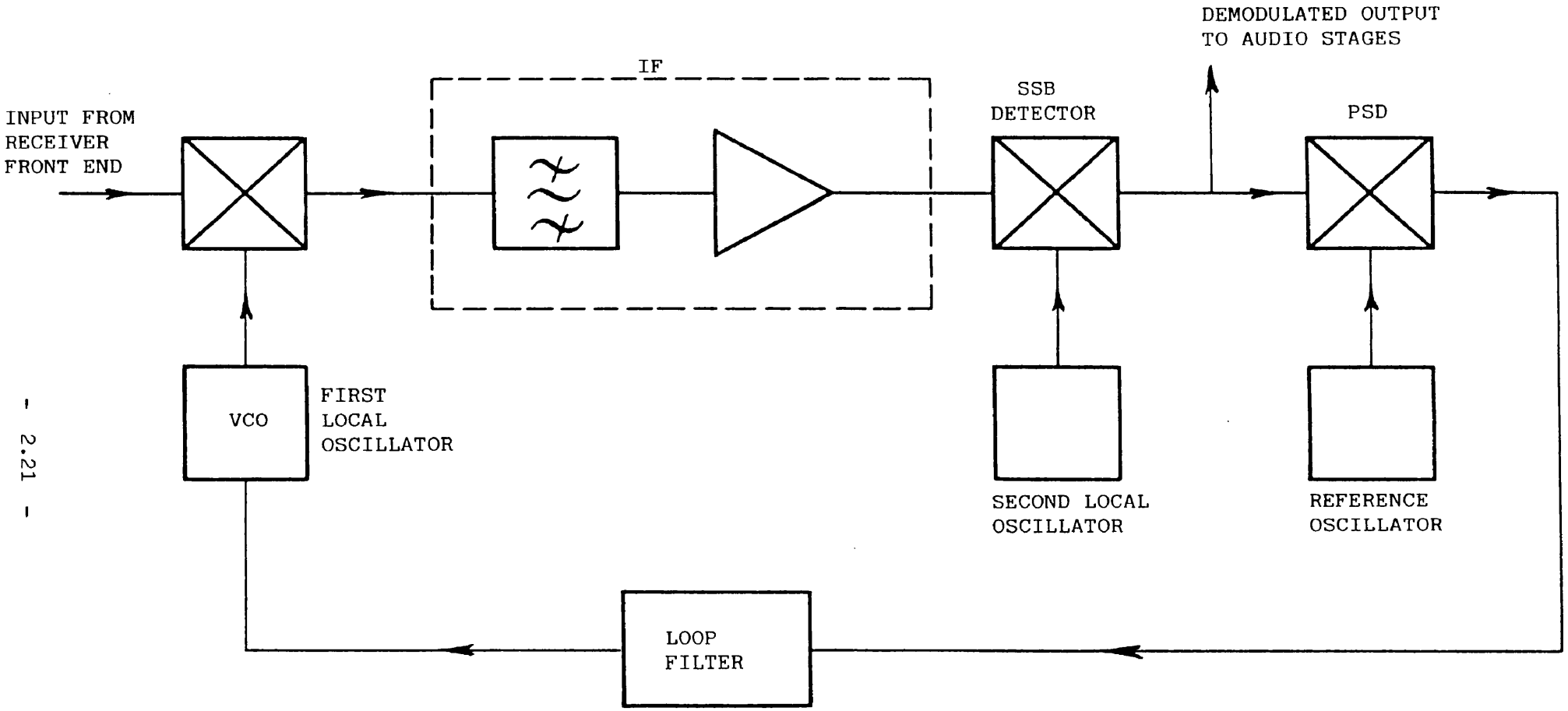

Figure 2.5 Tone-in-band or tone-above-band receiver

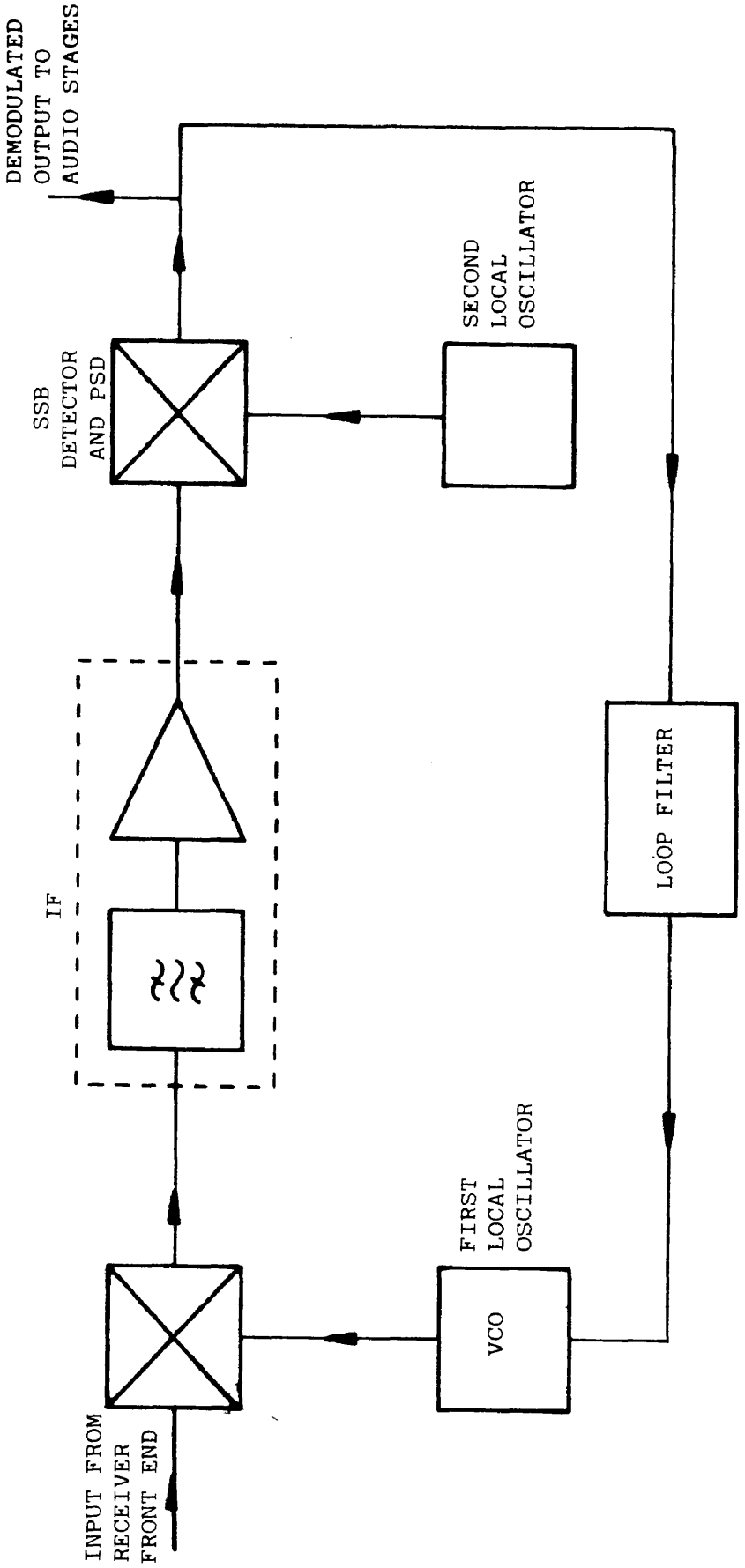

Figure 2.6 Pilot carrier receiver

thesis. Although their use may be necessary, a study of the straightforward PLL peformance was first required before the need for any additional circuitry could be gauged. To conclude this chapter, details of the Wolfson tone-in-band VHF SSB receiver (21,22) are given and, in particular, the design criteria of the second order type two PLL. The study described in the following chapters was initiated by the requirement to understand the performance of such a receiver more fully, with a hope of improving on its effectiveness.

After passing through a conventional front end, the input signal (carrier frequency, 86.2875 MHz) is mixed down with a 75.5875 MHz first local oscillator to a 10.7 MHz IF. The IF stage consists of an upper sideband filter followed by amplification. SSB detection is performed by mixing the IF output with a fixed, 10.7 MHz, second local oscillator. The pilot tone is transmitted at a frequency of 86.289172 MHz and hence demodulates to 1672 Hz. It is then compared with an internally generated 1672 Hz reference frequency oscillator in the PSD, and the resulting error signal is used to control the first local oscillator. The choice of 1672 Hz for the reference frequency was arbitrary, and any frequency in the range around 1.2 kHz to 2.5 kHz is acceptable. The level of the transmitted pilot tone to peak speech power was chosen as -15 dB and was seen as a compromise between risk of cochannel interference and wasting of transmitter power on the one hand, and ease of received pilot detection on the other. Because the demodulated information is not filtered out from the pilot before the PSD, it is not possible to use a limiter to maintain the demodulated pilot level constant at the PSD input. Consequently, it is necessary to rely on

feedback AGC to ensure that the demodulated pilot, and hence K_d, are kept at the correct levels. An important consideration in the choice of PLL bandwidth was the ability of the loop to reject interference caused by the presence of the modulation. Clearly, if modulation components were transmitted sufficiently close to the pilot and were of sufficient magnitude, there is a possibility that the loop will loose lock from the pilot and begin to track the modulation tone. Even if loss of lock does not occur, the modulation component may still give rise to unacceptable distortion at the SSB detector output. This is caused by the modulation component mixing with the receiver reference in the PSD and, after passing through the loop filter, modulating the receiver's first local oscillator. Before combining the pilot tone and modulation in the transmitter, there is, therefore, a requirement to filter out the modulation components close to the pilot frequency. McGeehan and Lymer (21) have extended Blanchard's analysis of the effect of interfering tones on PLL peformance (23) and developed design equations relating this transmitter filter bandwidth to the receiver PLL bandwidth, the transmitted pilot to peak speech power ratio and to the modulation index of the PLL's VCO. In order to ensure that the distortion products remain at least 20 dB below the required modulation at the SSB detector output, the maximum allowable modulation index was set at .2 for the Wolfson system. The PLL bandwidth was chosen as the maximum permissable, consistent with a reasonable level of transmitter filtering. A notch filter with a bandwidth of about 770 Hz was found to be acceptable for removing transmitter modulation components from the vicinity of the pilot and, to ensure distortion below 20 dB, the

receiver's PLL natural frequency was chosen as 10 Hz with damping factor of $1/\sqrt{2}$. For a short period at the start of each transmission, it is necesssary to transmit the pilot tone without any additional modulation. This ensures that the receiver locks onto the reference tone.

REFERENCES

1) Biswas, B.N., Ray, S.K., Bhattacharya, A.K., Sarkar, B.C., and Banerjee, P.: "Phase detector response to noisy and noisy fading signals", IEEE Trans., March 1980, Vol. AES-16, pp. 150-156.

2) Lindsey, W.C.: "Synchronization systems in communication and control" (Prentice Hall, 1972), chapter 3.

3) Gardner, F.M.: "Phaselock techniques" (Wiley, 1979), chapter 2.

4) Blanchard, A.: "Phase-locked loops" (Wiley, 1976), chapter 7.

5) Gardner, F.M.: "Phaselock techniques" (Wiley, 1979), chapter 4.

6) Gardner, F.M.: "Phaselock techniques" (Wiley, 1979), chapter 5.

7) Richman, D.: "Color-carrier reference phase synchronization accuracy in NTSC color television", Proc. IRE, January 1954, Vol. 42, pp. 106-133.

8) Meer, S.A.: "Analysis of phase-locked loop acquisition: a quasi-stationary approach", IEEE Int. Conv. Rec., 1966, Vol. 14, pp. 85-106.

9) Blanchard, A.: "Phase-locked loops" (Wiley, 1976), chapter 11.

10) Hiroshige, K.: "A simple technique for improving the pull-in capability of phase-lock loops", IEEE Trans., March 1965, Vol. SET-11, pp. 40-46.

11) Gardner, F.M.: "Phaselock techniques" (Wiley, 1979), chapter 8.

12) Klapper, J., and Frankle, J.T.: "Phase-locked and frequency feedback systems" (Academic, 1971), chapter 5.

13) Develet, J.A.: "The influence of time delay on second-order phase-lock loop acquisition range", Proc. int. telem. conf., London, September 1963, pp. 432-437.

14) Johnson, W.A.: "A general analysis of the false-lock problem associated with the phase-lock loop", Report TOR-269 (4250-45)-1, Aerospace Corporation, October 1963.

15) Tausworthe, R.C.: "Acquisition and false-lock behavior of phase-locked loops with noisy inputs", JPL SPS 37-46, Jet Propulsion Laboratory, August 1967, Vol. IV, pp. 226-234.

16) Pappenfus, E.W., Bruene, W.B., and Schoenike, E.O.: "Single Sideband Principles and Circuits" (McGraw-Hill, 1964), chapter 17.

17) Gosling, W., McGeehan, J.P., and Holland, P.G.: "Receivers for the Wolfson single-sideband VHF land mobile radio system", Radio and Electronic Engineer, May 1979, Vol. 49, pp. 231-235.

18) Lusignan, B.B.: "AGC, AFC, tone select circuits for narrow-band mobile radio", int. Telecommun. Expo., Dallas, Texas, February 1979.

19) Kadokawa, Y., and Tsukado, F.: "SSB lincompex transmitter and receiver for land mobile communications", 31st IEEE veh. tech. conf., Washington, 1981, pp. 149-154.

20) Ball, J.R., and Holmes, D.W.J.: "An SSB with pilot receiver for mobile radio", Clerk Maxwell commemorative conference on radio receivers and associated systems, IERE, July 1981, pp. 429-435.

21) McGeehan, J.P., and Lymer, A.: "The problem of speech pulling and its implication for the design of phase-locked SSB radio systems", Proc. IEE, November 1981, Vol. 128F, pp. 361-369.

22) McGeehan, J.P., Lightfoot, G., Lymer, A., and Gosling, W.: "Optimisation of the Wolfson SSB radio receiver", Clerk Maxwell commemorative conference on radio receivers and associated systems, IERE, July 1981, pp. 417-428.

23) Blanchard, A.: "Interferences in phase-locked loops", IEEE Trans., September 1974, Vol. AES-10, pp. 686-697.

CHAPTER 3

THE SPLIT LOOP TECHNIQUE AND FALSE LOCK ELIMINATION

This chapter deals with the problem of excess time delay incorporated in the loop of a long loop receiver and, in particular, the phenomenon of false locking. A novel phaselocked receiver configuration is described which eliminates false locking and results in loop characteristics similar to those obtained with zero time delay, while maintaining the advantages of long loop control.

3.1 Introduction

In addition to filtering in the IF stages, there are several other possible causes of excess phase shift within the long loop of a receiver. For instance, it may be necessary to filter the output of the first local oscillator in order to improve its spectral purity. On the other hand, the first local oscillator may be generated from a PLL frequency synthesiser with its own inherent phase shift. Whatever the cause, the result of the excess phase shift is a degradation of the loop's pull-in performance. Acquisition is reported to have been impaired even when a frequency acquisition aid is incorporated (1,2).

A technique for avoiding false locking has been proposed by Biswas et al. (3). Referring to figure 2.4, the technique involves incorporating an electronic phase shifter between the IF output and the PSD. This introduces a phase shift, δ, proportional to the rectified output of the loop filter. If the excess loop phase shift is equal and

opposite to δ, its effect is removed. However, if this is not the case, the loop analysis is greatly complicated by the additional circuitry and no explanation of its behaviour has been given. The technique proposed in the next section is easier to implement and does not complicate the loop analysis.

3.2 The split loop receiver

The proposed method for false locking elimination has been termed the split loop technique since it involves 'splitting' the loop filter in order to feed two voltage controlled local oscillators. A split loop receiver containing one IF is shown in figure 3.1. It can be seen that the PSD output controls both the first and second local oscillators through the filters $F_1(s)$ and $F_2(s)$. The equation of the loop is now derived in a similar manner to that of the long loop in section 2.7.

The voltage controlled first and second local oscillator outputs are given by $v_1(t)$ and $v_2(t)$ respectively where:

$$v_1 = V_1 \cos(\omega_1 t + \theta_1) \qquad (3.1)$$

$$v_2 = V_2 \cos(\omega_2 t + \theta_2) \qquad (3.2)$$

with peak values V_1 and V_2, and centre frequencies ω_1 and ω_2. Their phases are governed by:

$$\frac{d\theta_1}{dt} = K_1 F_1(s) v_d \qquad (3.3)$$

$$\frac{d\theta_2}{dt} = K_2 F_2(s) v_d \qquad (3.4)$$

where K_1 and K_2 are the respective VCO gain constants and $v_d(t)$ is the PSD output voltage. $v_1(t)$ is mixed with the input signal, $v_i(t)$ where:

$$v_i = V_i \sin(\omega_i t + \theta_i) \qquad (3.5)$$

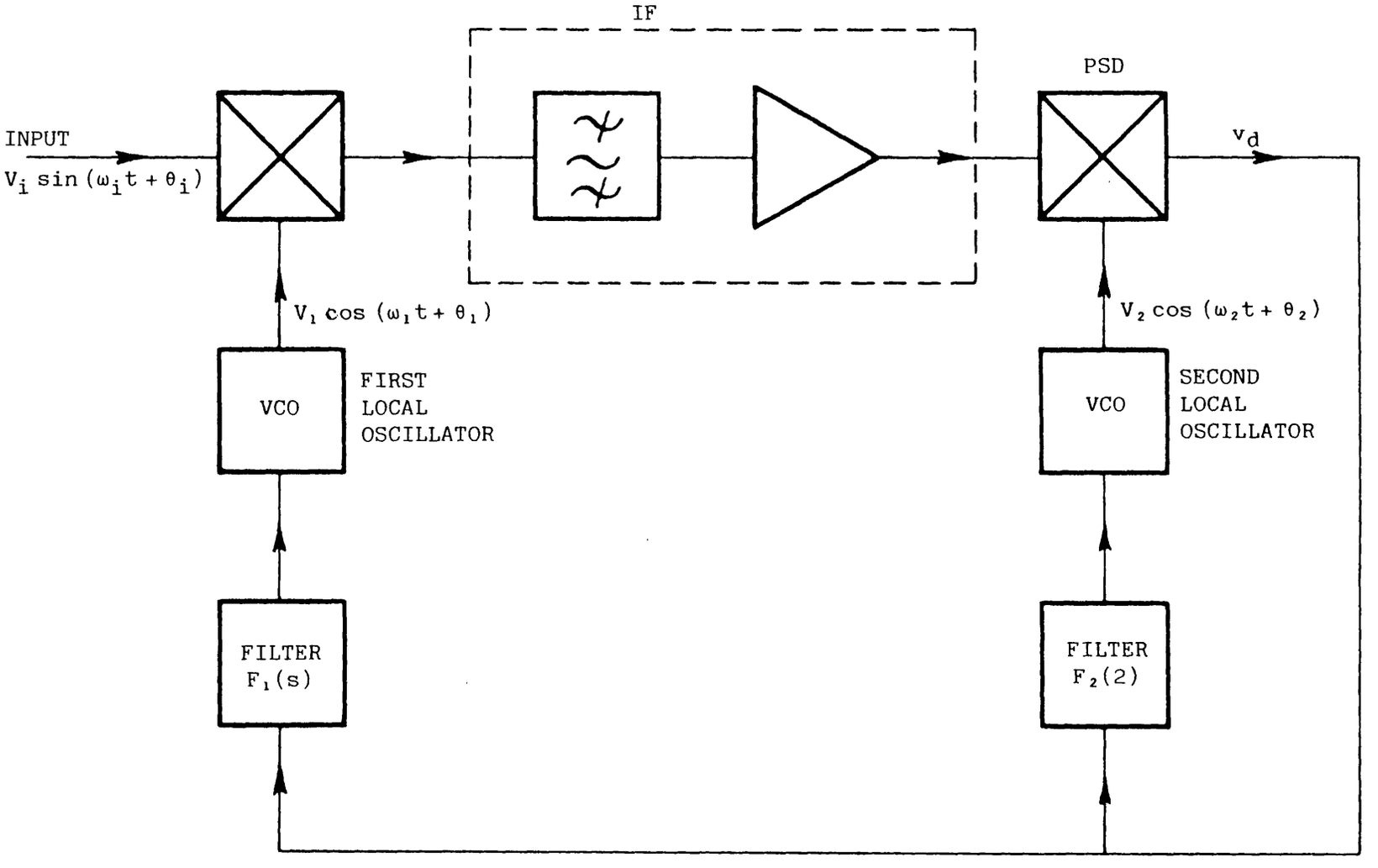

Figure 3.1 Split loop phaselocked receiver

$$\omega i = \omega_1 + \omega_2 \qquad (3.6)$$

and θ_i is the input phase relative to $\omega_i t$. Ignoring mixer output sum terms and, for the present, the effect of the IF filter characteristic, the PSD output can be written as:

$$v_d = K_d \sin \theta_e \qquad (3.7)$$

where K_d is the PSD gain and the phase error, θ_e, is given by:

$$\theta_e = \theta_i - \theta_1 - \theta_2 \qquad (3.8)$$

Combining the differential of equation 3.8 with equations 3.3, 3.4 and 3.7, gives:

$$\frac{d\theta_e}{dt} = \frac{d\theta_i}{dt} - [K_1 F_1(s) + K_2 F_2(s)] K_d \operatorname{Sin} \theta_e \qquad (3.9)$$

Writing F(s) in the form:

$$F(s) = F_1(s) + \frac{K_2}{K_1} F_2(s) \qquad (3.10)$$

then equation 3.9 reduces to that of a simple PLL, with VCO gain K_1 and loop filter transfer function F(s), given by equation 2.8. The split loop is therefore equivalent to a simple PLL except, of course, that the IF filter characteristic is contained within the $F_2(s)$ path.

To proceed further, it is necessary to define $F_1(s)$ and $F_2(s)$ more fully. Meer (4) states that for a loop filter with equal numbers of poles and zeros it is reasonable to consider the filter as composed of a constant gain high frequency term and a low pass term which decays to zero for frequencies outside the loop noise bandwidth. All filters which are Wiener-optimised for tracking or demodulation in the presence of additive white Gaussian noise possess this property. Therefore it is

permissable to rewrite equation 3.10 as:

$$F(s) = \frac{K_2}{K_1} F_2 + F_1(s) \qquad (3.11)$$

where F_2 is independent of the Laplace operator, s, and F_1 (s) is the low pass term with zero high frequency gain. Some loop filters cannot be written in this form. For example, filters with zero high frequency gain are sometimes employed in PLL synthesisers. However, the equation holds for the majority of filters used in coherent receiver design and they are the only ones which need be considered here.

The advantage of employing the split loop technique is apparent when the excess phase shift introduced into the loop by the IF stages is taken into account. As mentioned in section 2.8, the degradation of the loop acquisition performance is due to the excess phase shift of the PSD beat frequency output, and it is justifiable to assume that the beat frequency passes through the high frequency constant gain section of the loop filter. In terms of the split loop receiver, this high frequency path is through F_2 and the second local oscillator. As a result, the PSD beat frequency bypasses the IF stages and the possibility of false locking is eliminated. Despite requiring control of both the receiver's local oscillators, the advantages of the long loop receiver in tracking out large frequency drifts before the IF stage is maintained. For instance, in a second order type two PLL with loop filter defined by equation 2.17, the corresponding split loop filters are given by:

$$F_1(s) = 1/s\tau_1 \qquad (3.12)$$

$$F_2(s) = \frac{K_1 \tau_2}{K_2 \tau_1} \qquad (3.13)$$

The maximum frequency deviation of the second local oscillator is then $\pm K_1 K_d \tau_2/\tau_1$ or simply $\pm 2\zeta\omega_n$. Acquisition and tracking of frequency offsets is accomplished by the integrator in the first local oscillator path.

Results are now presented to confirm the validity of the method in improving long loop performance.

3.3 Experimental study of the acquisition time of PLLs incorporating pure time delay

A comparison was made of the acquisition performance of second order type two split and long PLLs incorporating pure time delay. To avoid the necessity of incorporating an IF stage within the loop, the experiment was performed using the simple PLL as shown in figure 3.2. By inserting the time delay element at either points 1 or 2, it was possible to simulate the performance of either the split or the conventional long loop with time delay in the IF stage.

3.3.1 Experimental configuration

The PLL and variable delay circuit used for the acquisition measurements have been described elsewhere (5) and so only relevant details will be given here. Both the loop's in-phase and quadrature PSDs were implemented with analogue multipliers, type AD534JD, with K_d set at 1 V/rad. The VCO had a centre frequency of 1.67 kHz and a gain of 135 Hz/V. Accurate sine and cosine VCO outputs were synthesised from digital coefficients stored in a programmable read only memory, with the

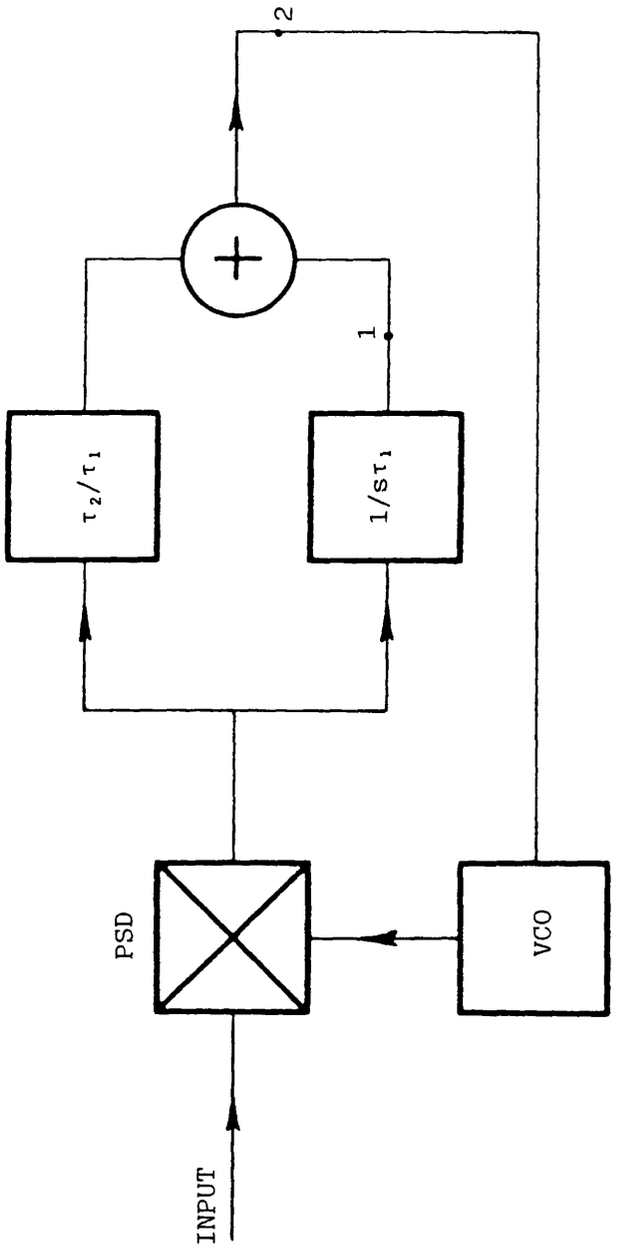

Figure 3.2 Second order, type two PLL

introduction of negligible excess time delay into the loop. Voltage control of the memory address counter clock frequency was achieved with an XR-2209 function generator. The loop filter components were switchable to give loop natural frequencies of 3 Hz, 10 Hz, 30 Hz, 100 Hz, 300 Hz and 1 kHz with a fixed damping factor of $1/\sqrt{2}$. For the acquisition measurements a loop natural frequency of 100 Hz was chosen and the loop filter was modified to allow inclusion of the time delay unit at either of points 1 or 2 in figure 3.2. The notch filters available at the PSD's outputs to remove the sum frequency terms were not used. The DC coupled time delay circuit, based on the SAD512D CCD delay line with crystal controlled clock, provided time delays from .25 ms to 32 ms in .125 ms increments.

A block diagram of the measurement configuration is shown in figure 3.3. For each acquisition measurement, the output of the specially designed signal generator was initially set at the nominal VCO centre frequency, with the loop phaselocked. The generator was then switched to a predetermined offset frequency which triggered the acquisition time counter. The counter was stopped by a high output from the lock detector, which consisted of a RC smoothing filter and a voltage comparator. The acquisition times obtained with this method are a good approximation to the loop's frequency acquisition time since, for frequency offsets well outside the loop bandwidth, errors due to the additional phase acquisition time and the lock detector's RC time constant are negligible. Before each measurement, it was necessary to null the voltage offsets of the PSD output and the loop filter operational amplifiers.

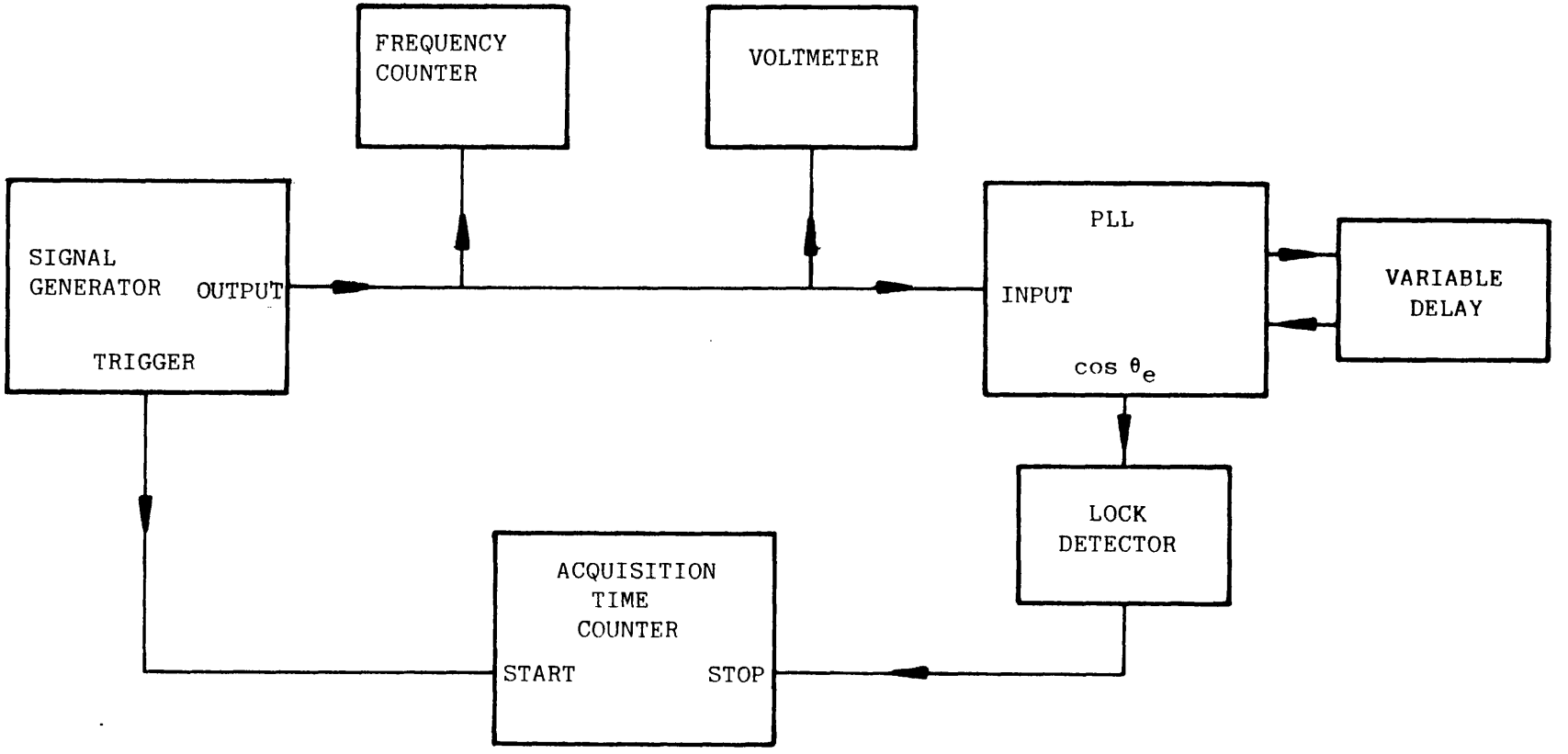

Figure 3.3 PLL acquisition time measurement configuration

3.3.2 Results

The results for the long loop case are shown in figure 3.4. Each point represents the average of ten acquisition time measurements, although little spread was observed between individual readings. Input frequency offset from the VCO centre frequency is plotted against the measured acquisition time, with time delay, τ, as the parameter. Similar results were obtained with negative frequency offsets. In the zero time delay case, acquisition occured without difficulty and the observed results are in close agreement with the theoretical acquisition times given by equation 2.30. However, when time delay was introduced, an increase in acquisition time and a dramatic reduction in pull-in range were observed. Above a critical offset frequency, the loop would not pull-in and false locking occured. The pull-in frequency limits are given in table 3.1. Inspection shows that they compare favourably with the theoretical values predicted by equation 2.40.

DELAY, ms	PULL-IN LIMIT, Hz	
	EXPERIMENTAL	THEORETICAL
.25	950	1000
.50	450	500
.75	310	333

Table 3.1 Long loop pull-in limits

In contrast, the split loop results of figure 3.5 show that the effect of delay is substantially reduced and false locking is eliminated. In fact, for large frequency offsets, increasing the time delay up to

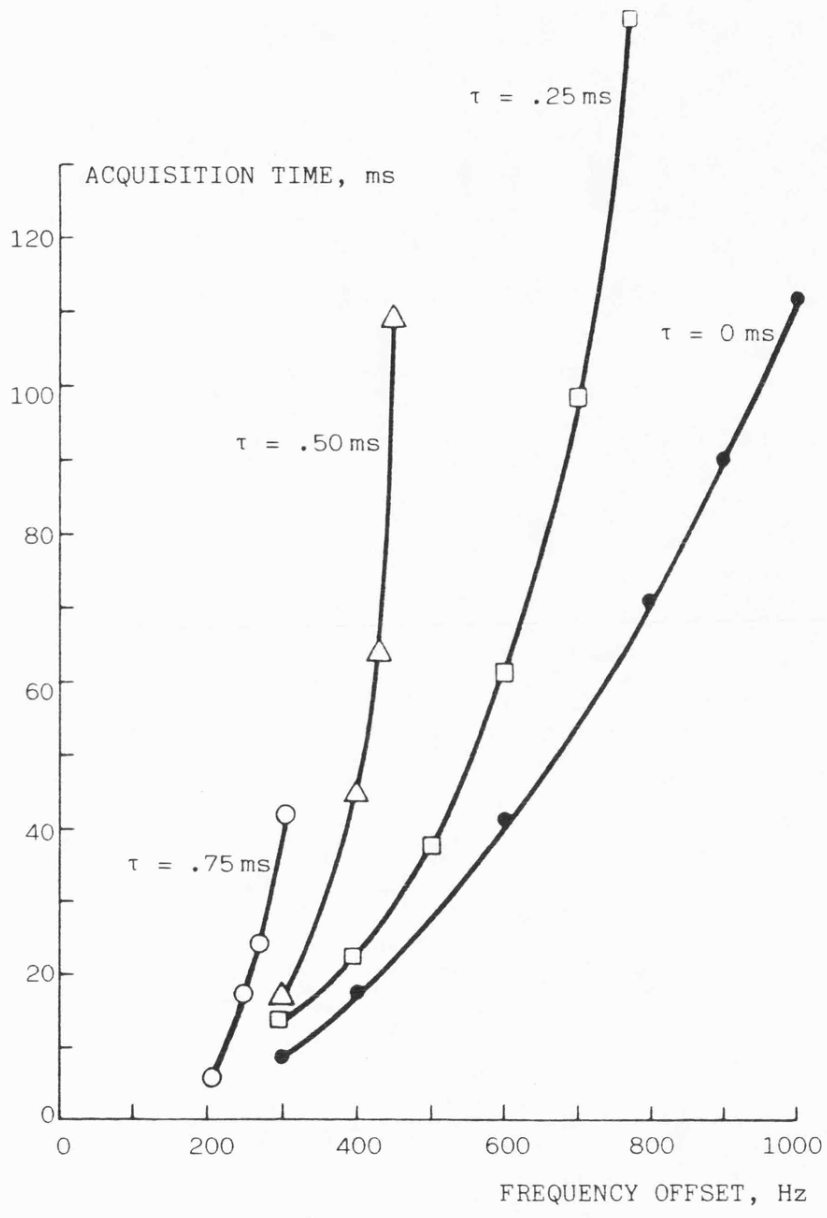

Figure 3.4 Acquisition performance of a PLL with time delay τ

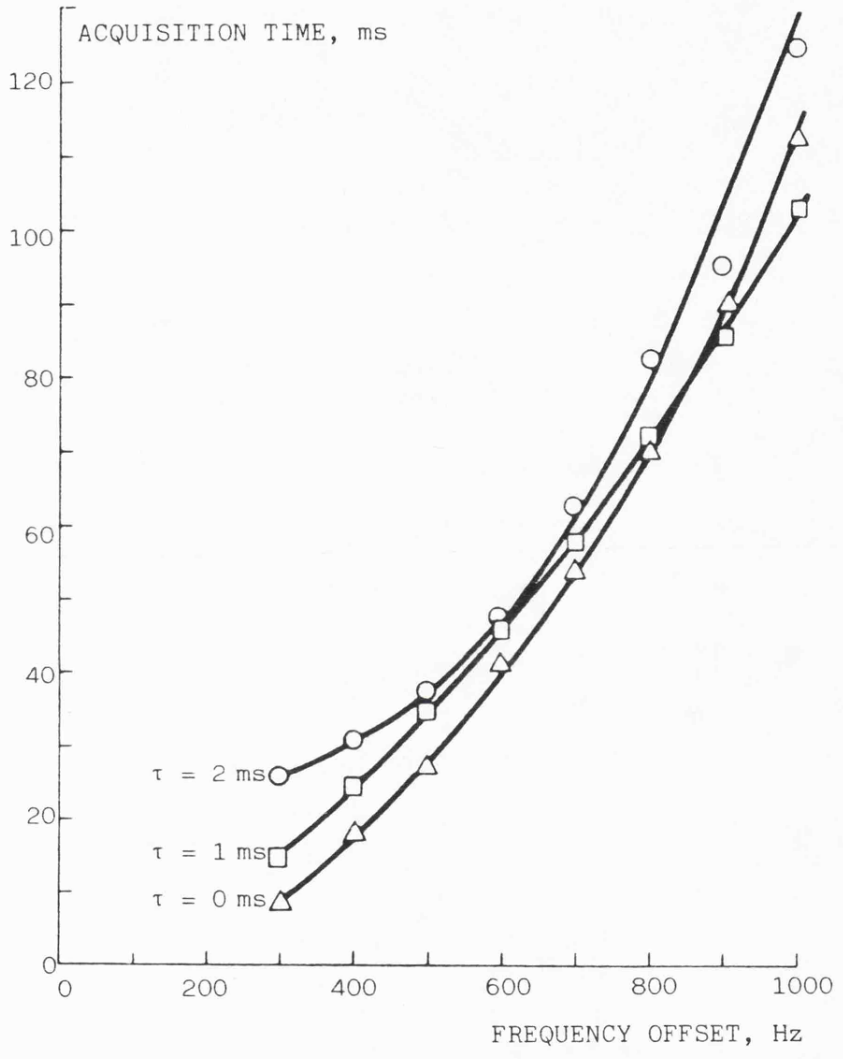

Figure 3.5 Acquisition performance of a split PLL with time delay τ present in the integrator path

the loop stability limit had negligible effect on the acquisition time.

3.4 Experimental study of the acquisition time of a phaselocked SSB receiver

The results of the previous section, using an equivalent audio PLL system, would suggest that the acquisition performance of a long loop receiver could be substantially improved by use of the split loop technique. In order to verify this, a phaselocked receiver with facilities for long, split and short loop oscillator control was constructed, and its acquisition performance investigated.

3.4.1 Experimental configuration

A 86.2875 MHz tone-in-band receiver was constructed with a single 10.7 MHz IF and a nominal demodulated pilot tone frequency of 1672 Hz. Although of similar form to that depicted in figure 2.5, it was possible to switch the loop filter between the first and second local oscillators to obtain short, split or long loop control. Excess phase shift was introduced into the split and long loops by the first local oscillator frequency synthesiser and the IF filter. The PLL synthesiser was based on the high performance LN123/LN124 integrated circuits and had a closed loop 3 dB bandwidth of 625 Hz. The design was typical for a synthesiser required for a multichannel receiver operating within narrow channel spacings. The IF crystal characteristic was measured with a Hewlett Packard type HP3575A gain/phase meter and the resulting group delay response is shown in figure 3.6. The filter amplitude response varied by only 1.0 dB over the 2 kHz frequency range of the acquisition

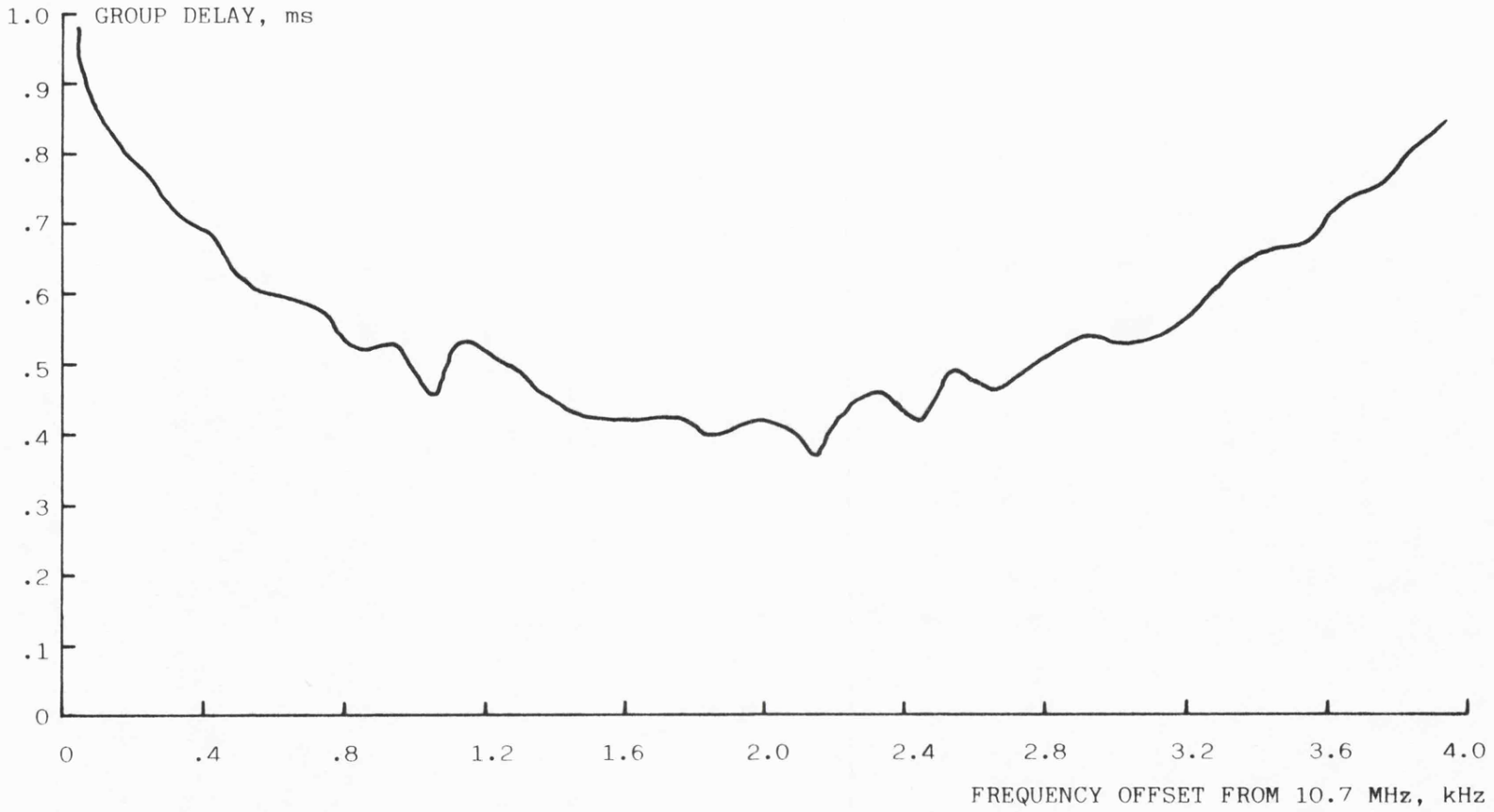

Figure 3.6 IF filter group delay

measurements, and is shown in figure 3.7. Again, the filter was typical of those required for a narrow channel spacing SSB system. Further details of the receiver design are given in Appendix 1.

The acquisition time measurement procedure was similar to that of section 3.3. Initially the receiver was phaselocked to an input tone of frequency 86.289172 MHz, which demodulated to a frequency of 1672 Hz when the local oscillator outputs were at centre frequency. Stepping the input frequency to the required offset triggered the acquisition time counter and, when phaselock was detected, the counter was inhibited. The tests were carried out at high signal to noise ratio, with the receiver's AGC fixed throughout and the correct demodulated tone level being set by manual adjustment of the gain controlled RF and IF amplifiers. A PLL natural frequency of 100 Hz and a damping factor of $1/\sqrt{2}$ were chosen, thus corresponding to the loop parameters of section 3.3. As well as to null any PSD and operational amplifier voltage offsets, it was also necessary to ensure that the local oscillator centre frequencies were correctly adjusted before each measurement.

3.4.2 Results

The acquisition time measurements for the long, split and short loops are compared in figure 3.8. Again, each point represents the average of ten measurements and similar results were obtained for negative frequency offsets. The poor performance of the long loop is evident. In fact, acquisition was not possible for frequency offsets over 300 Hz and false locking occurred. This value compares well with the theoretical pull-in limit of 331 Hz. As suggested in section 2.8, the theore-

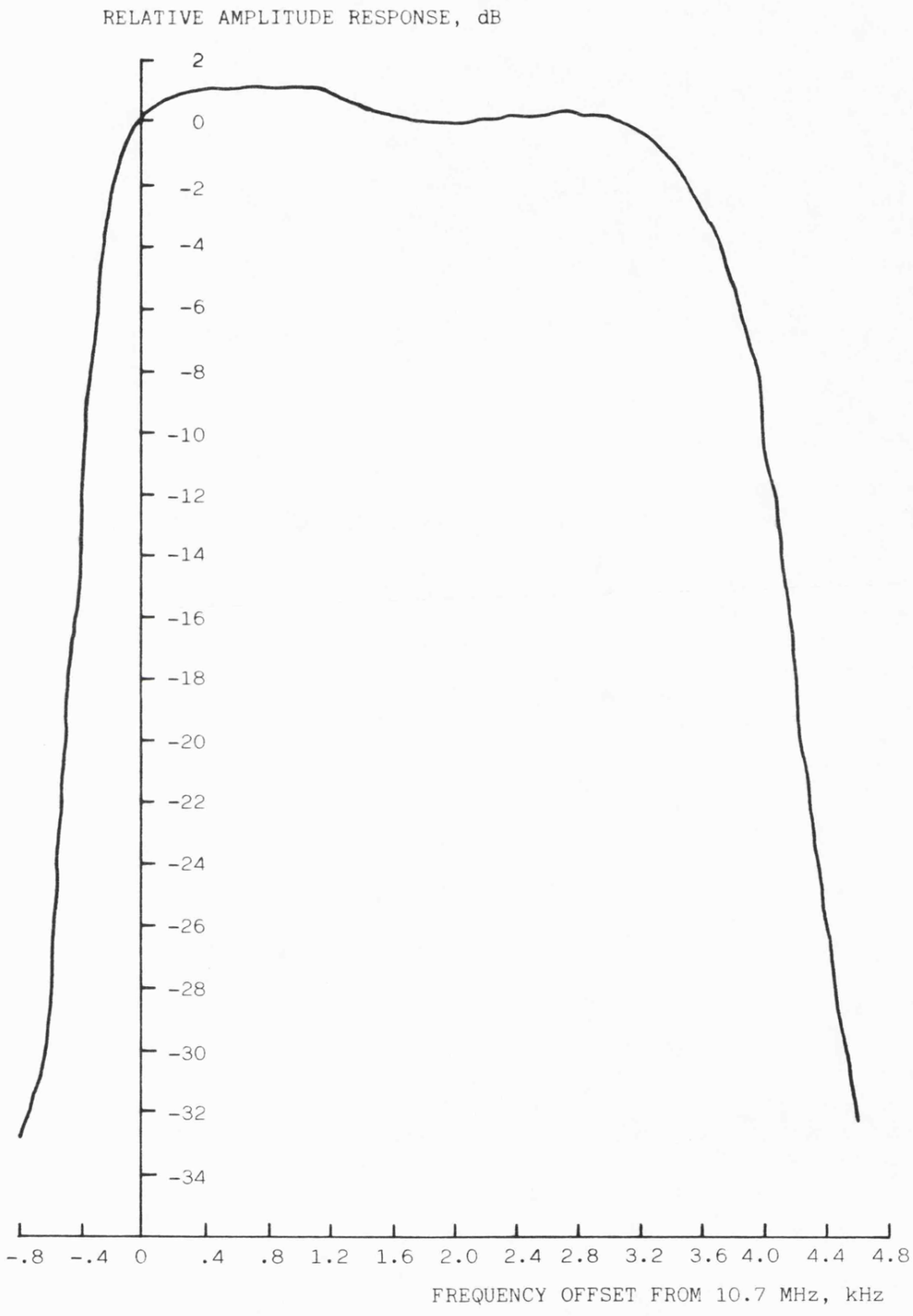

Figure 3.7 IF filter amplitude response

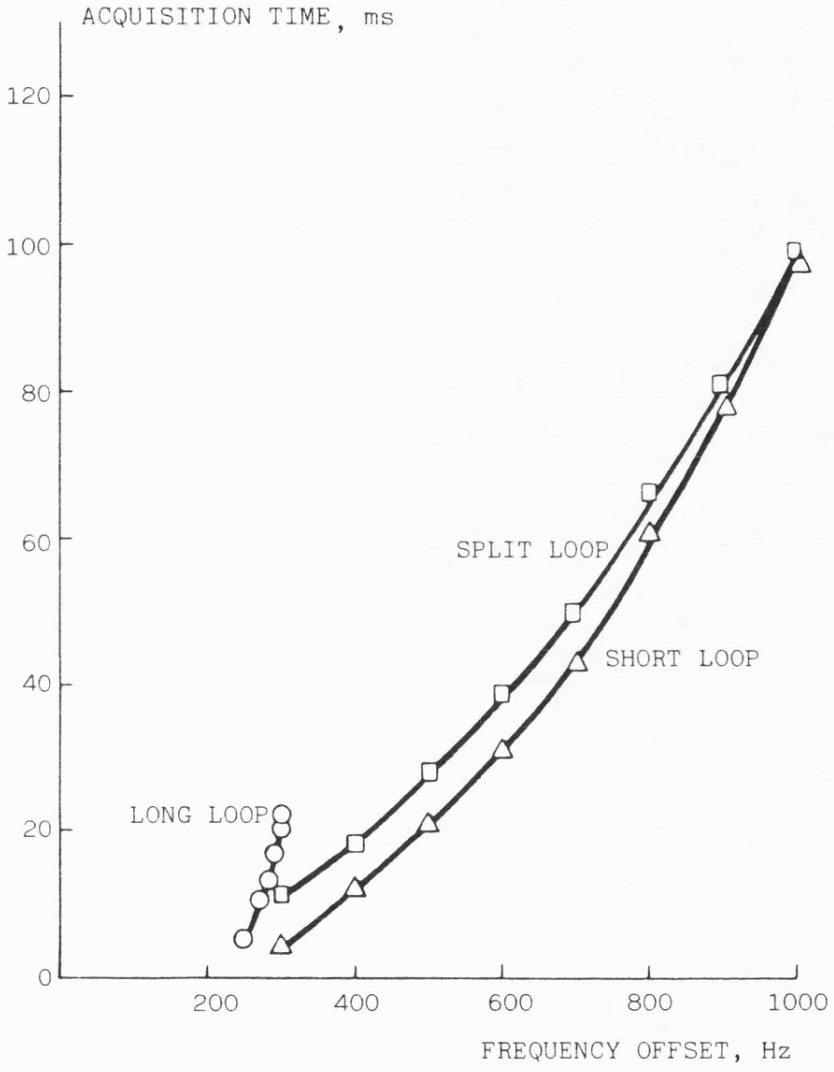

Figure 3.8 Comparative acquisition performance of long, split and short loop receivers

tical pull-in limit is reached when the loop beat frequency incurs an excess phase shift of 90 degrees. In this case, the theoretical limit was found by numerically solving the transcendental phase equation relating the offset frequency to the mid-band IF filter group delay and the synthesiser phase response.

For the short and split loops, acquisition occurred without difficulty. The split loop results are very similar to those of the short and clearly show that the receiver's first local oscillator can acquire from large frequency offsets irrespective of the excess loop phase shift.

3.5 The implementation of the split loop technique incorporating acquisition aids

Use of the split loop technique will only slightly, if at all, increase circuit complexity of any frequency acquisition aids which may be required. If the switched bandwidth technique is used, it will be necessary to switch loop parameters in both filter paths. However, in the VCO sweeping method, only the first local oscillator need be swept as this oscillator alone accommodates the frequency offsets. In the derived rate rejection technique (6,7) the proportional term in the loop filter is switched out whenever the cos θ_e signal, obtained from the quadrature PSD, is negative. Clearly, as the split loop receiver already contains a loop filter decomposed into its proportional and integral paths, implementation of this technique is achieved simply by switching out the control to the second local oscillator whenever cos θ_e is negative.

3.6 The effect of time delay on loop noise bandwidth

The noise bandwidth of a PLL is a useful measure of the loop's performance when the input signal is contaminated with additive white Gaussian noise. For example, minimisation of noise bandwidth, for constant loop natural frequency, is the first stage in the design of low threshold PLL FM demodulators (8) and, in AFC applications, the noise bandwidth gives a measure of the purity of the phaselocked local oscillator in terms of noise induced phase jitter.

The definition of loop noise bandwidth was given by equation 2.21 as:

$$B_n = \int_0^\infty |H(j2\pi f)|^2 df \text{ Hz} \qquad (3.14)$$

Here, the integral has been evaluated numerically for the second order type two split and long loops containing pure time delay. When the delay is contained in both filter paths H(s) is given by:

$$H(s) = \frac{\omega_n^2 + 2\zeta\omega_n s}{\omega_n^2 + 2\zeta\omega_n s + \exp(s\tau)s^2} \qquad (3.15)$$

and when the delay is restricted to the integrator path:

$$H(s) = \frac{\exp(-s\tau)\omega_n^2 + 2\zeta\omega_n s}{\exp(-s\tau)\omega_n^2 + 2\zeta\omega_n s + s^2} \qquad (3.16)$$

Simpson's rule was used to compute the integrals up to a maximum frequency of 300 ω_n. The results presented in figure 3.9 are for a fixed loop damping factor of $1/\sqrt{2}$, and show the noise bandwidth, normalized to ω_n, versus delay phase, $\omega_n\tau$ in degrees. The conventional long loop noise bandwidth increases steadily with time delay until the loop eventually becomes unstable. The split loop noise bandwidth,

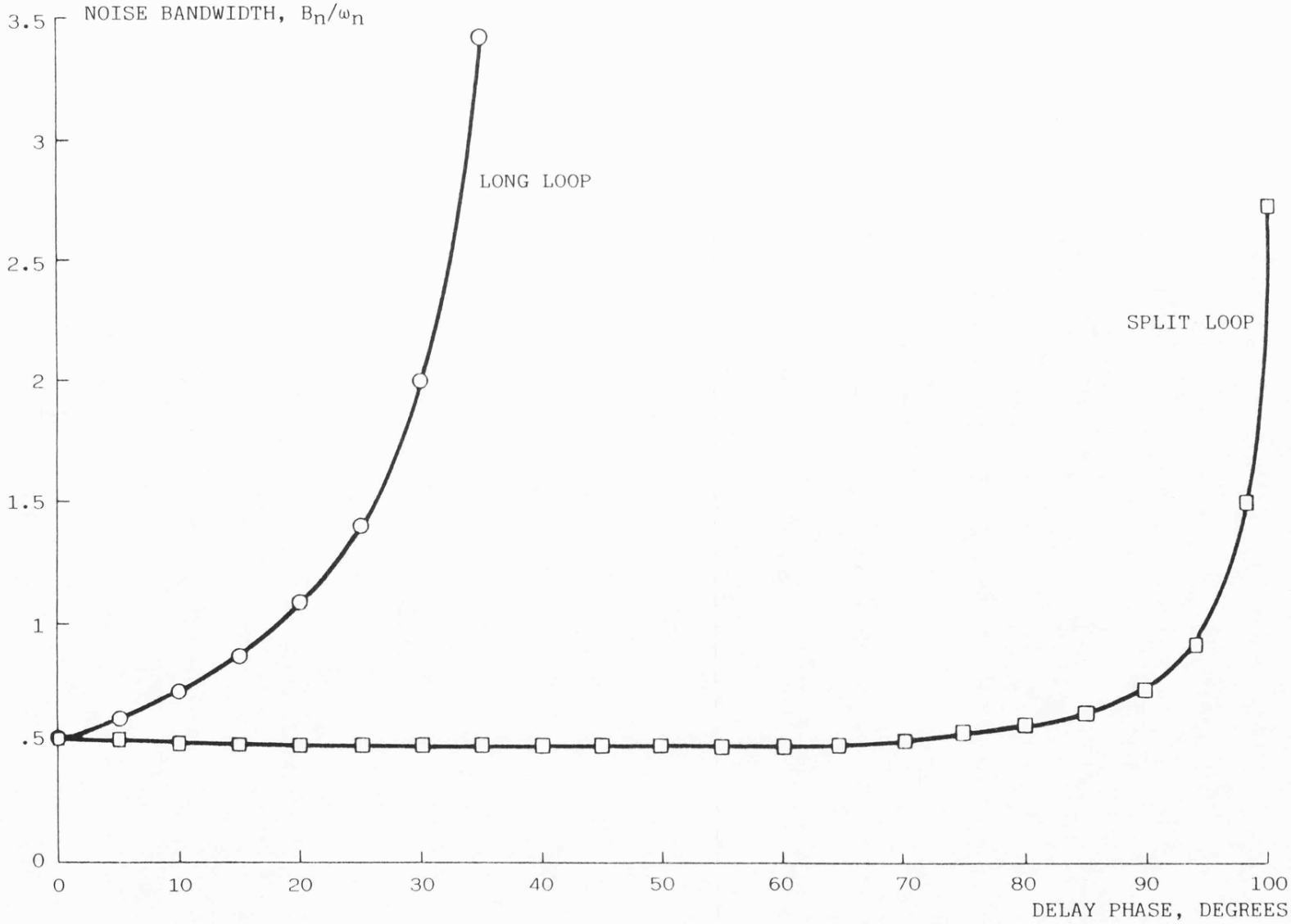

Figure 3.9 Effect of time delay on noise bandwidth for a damping factor of $1/\sqrt{2}$

however, is only negligibly effected for delay phases up to about 80 degrees. As mentioned in section 2.2, the delayless loop attains minimum noise bandwidth, for fixed ω_n, when the loop damping factor is set to 1/2. The minimization has been carried out here when time delay is included in the loop, and the results are presented in figure 3.10. The graph is similar in form to figure 3.9 but now includes the computed loop damping factor required to achieve the minimum noise bandwidth. For the long loop, the results are similar to those of Klapper and Frankle (9), the minimum noise bandwidth rising rapidly with increasing delay phase. The minimum noise bandwidth of the split loop, on the other hand, is hardly effected by the time delay. Figures 3.9 and 3.10 illustrate that, in comparison to the long loop, the effect of delay on the split loop noise bandwidth can be neglected.

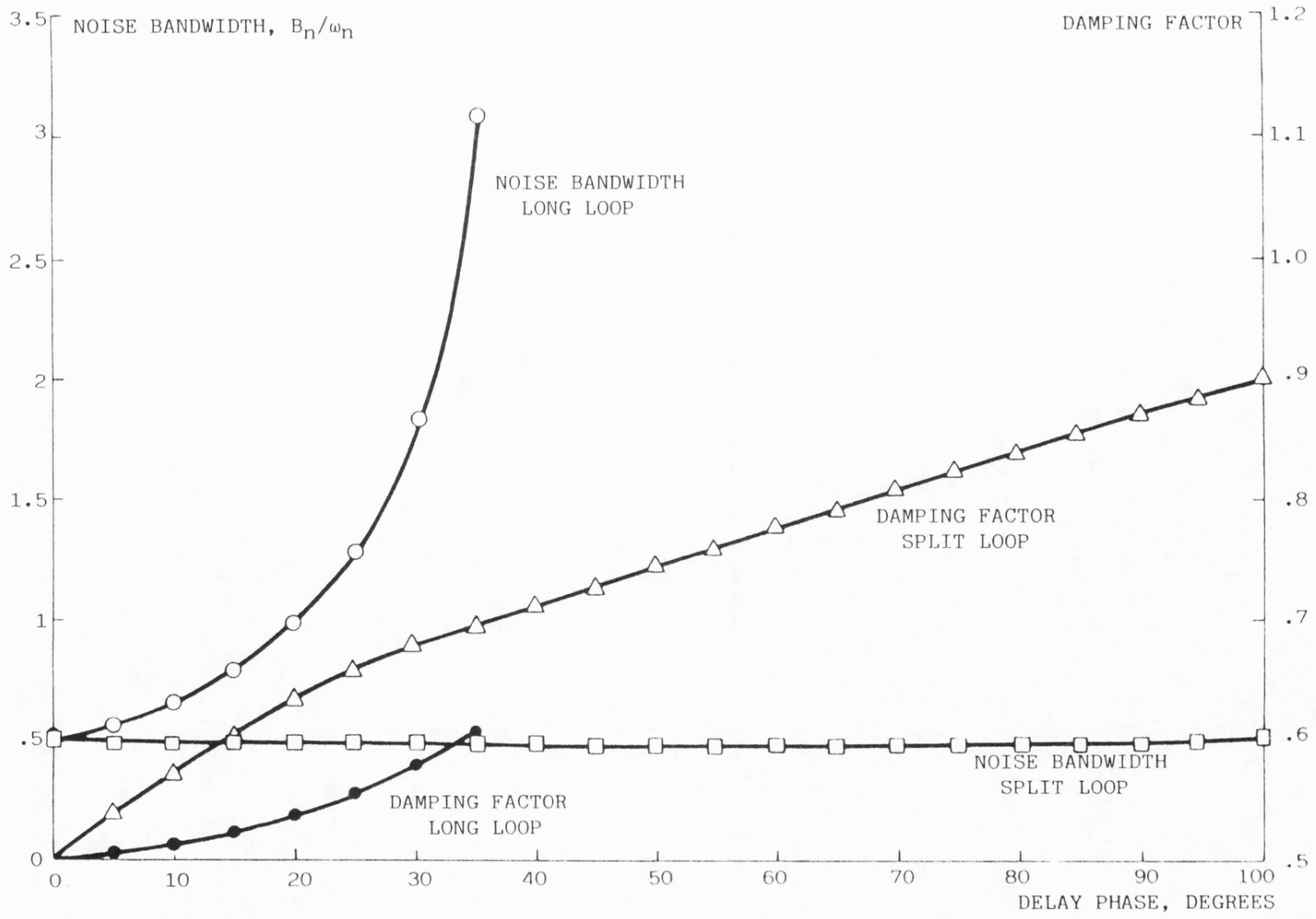

Figure 3.10 Effect of time delay on minimum noise bandwidth

REFERENCES

1) Richardson, J.H.: "Practical investigation of a phase-locked SSB receiver for VHF civil land mobile radio", M.Sc. thesis, University of Bath, 1979, chapter 5.

2) McGeehan, J.P., and Lymer, A.: "Acquisition performance of 2nd-order phase-locked loops in the presence of time delay for switched and swept signal conditions", Proc. IEE, August 1983, Vol. 130G, pp. 131-137.

3) Biswas, B.N., Banerjee, P., and Bhattacharya, A.K.: "Heterodyne phase locked loops - revisited", IEEE Trans., October 1977, Vol. COM-25, pp. 1164-1171.

4) Meer, S.A.: "Analysis of phase-locked loop acquisition: A quasi-stationary approach", IEEE international convention record, March 1966, Vol. 14, Part 7, pp. 85-106.

5) Burrows, D.F.: "Automatic gain control in mobile radio receivers", Ph.D. thesis, University of Bath, 1982, chapters 6 and 7.

6) Hiroshige, K.: "A simple technique for improving the pull-in capability of phase-lock loops", IEEE Trans., March 1965, Vol. SET-11, pp. 40-46.

7) McGeehan, J.P.: "Technique for improving the pull-in characteristics of phase-locked loops", Proc. IEE, August 1976, Vol. 123, pp. 761-764.

8) Klapper, J., and Frankle, J.T.: "Phase-locked and frequency feedback systems", (Academic, 1971), chapter 6.

9) Klapper, J., and Frankle, J.T.: "Phase-locked and frequency feedback systems", (Academic, 1971), chapter 5.

CHAPTER 4

THE ADJACENT CHANNEL PERFORMANCE OF A PHASELOCKED SSB RECEIVER

When the VHF land mobile radio service was first introduced into the UK in the 1940's, the channel spacing was 200 kHz. Successive halvings of this bandwidth have necessarily demanded a more stringent specification for system adjacent channel performance. The specification limits both transmitter emissions outside the wanted information bandwidth and, also, receiver response to the adjacent channels. Clearly, if SSB is going to be adopted in the land mobile service, it will have to be shown to meet adjacent channel specifications similar to those of current AM and FM equipment, albeit for narrower channel spacings. To date, most of the work in this area has concentrated on the problem of spurious adjacent channel emissions caused by non-linear distortion in the transmitter output stages. For instance, in the comparison of the adjacent channel selectivity performance of FM, AM and SSB systems given by Flett (1), the dominant interference effect was spurious radiation from the transmitters. However the Home Office has recently carried out adjacent channel selectivity measurements on a SSB transmitter and receiver independently (2) and has shown the selectivity of the SSB receiver operating in 5 kHz channel spacing was within the specified limits of current 12.5 kHz FM and AM receivers. Although the results of the Home Office trials were particularly encouraging for the proponents of SSB, the receiver used in the tests contained high stability local oscillators without

AFC. It is the purpose of this chapter to demonstrate that the use of a long loop for AFC can degrade the adjacent channel immunity of the receiver. This is essentially a result of the first local oscillator, which is exposed to the adjacent channel interference, being frequency modulated by filtered components of the PSD output.

In section 4.1, a definition of adjacent channel selectivity for a pilot tone SSB receiver is suggested and details of a tone-in-band receiver constructed in order to perform selectivity measurements are given in section 4.2. Two mechanisms which contribute to the degradation of a phaselocked receiver's selectivity are then described. The first is a previously unreported effect and has been termed adjacent channel induced instability. The second is simply due to reciprocal mixing caused by wanted information mixing with the reference frequency in the PSD, passing through the loop filter and modulating the receiver's first local oscillator. Finally, results of adjacent channel selectivity measurements on the tone-in-band receiver are given. They demonstrate that a long loop receiver can possess poor selectivity which can be substantially improved by use of the split loop technique. As a pilot tone design is used for illustration in this chapter, some of the analysis is necessarily only directly applicable to this case, although pilot carrier and tone-above-band designs can be treated in an almost identical manner. The use of a second order, type two, PLL is assumed throughout the chapter.

4.1 Adjacent channel selectivity definitions

In the absence of an official specification, the adjacent channel selectivity of a pilot tone SSB receiver is defined here so as to parallel the definition for full carrier AM equipment in the Home Office specification MPT1302 and the definition used in the Home Office SSB trials (2). To measure the adjacent channel selectivity in accordance with MPT1302, the wanted signal at the nominal frequency of the receiver and with normal test modulation (a modulation frequency of 1 kHz with a 30 % modulation depth) is applied to the receiver input via one path of a combining unit. The unwanted signal is applied through the second path at the frequency of the upper adjacent channel and modulated with a frequency of 400 Hz at a depth of 30 %. The audio output of the receiver is monitored by a distortion factor meter, and in the absence of the unwanted signal, the level of the wanted signal is adjusted until the ratio of signal plus noise plus distortion to noise plus distortion (SINAD ratio) is 12 dB. The unwanted signal is switched in and adjusted in level until the SINAD ratio is reduced to 6 dB. This measurement is then repeated with the unwanted signal at the frequency of the lower adjacent channel. The adjacent channel selectivity is expressed as the lower value of the ratios, in decibels, for the upper and lower adjacent channels, of the level of the unwanted signal to the level of the wanted signal. The selectivity must be not less than 60 dB.

For an SSB pilot tone receiver, the wanted signal consists of a pilot tone, set at the nominal receiver pilot tone frequency, and a second tone set at the nominal receiver frequency of a 1 kHz audio

tone at a voltage level 30 % of its maximum relative to the pilot. An RF tone at the upper or lower adjacent channel frequency constitutes the unwanted signal. The SINAD measurements are carried out as in the full carrier AM case and the adjacent channel selectivity is expressed as the lower value of the ratios, in decibels, for the upper and lower adjacent channels, of the level of the unwanted signal to the level of the wanted 1 kHz tone. A pilot tone is not transmitted together with the adjacent tone, primarily because it would increase the complexity of the measurement and add another low noise signal generator to the required test equipment. It is noteworthy that the Home Office (2) found that the presence of the unwanted pilot had no significant effect on the selectivity results.

Some difficulties arise in transferring the AM definition to the SSB case. For instance, the frequency of the adjacent channels refer to the carrier frequencies in the AM case. However, if upper and lower adjacent channel carrier frequencies were used in the SSB test, the result would not portray a fair comparison between upper and lower adjacent channel selectivity as a SSB signal is positioned to one side of the carrier. Upper and lower adjacent channel frequencies would best be chosen to be equidistant from the centre of the wanted RF information bandwidth. Also, at the chosen value of adjacent channel frequency, it is possible that the major spurious tone at the demodulator output falls close to the frequency of the demodulated pilot. It is consequently filtered out by the tone notch filter and does not appreciably degrade the SINAD ratio. This could give rise to an artificially high level of selectivity and would have to be overcome by measuring the

selectivity over a small band of adjacent channel frequencies to avoid any false nulls. In the selectivity tests described at the end of this chapter, measurements were taken over a wide range of adjacent channel frequencies and this difficulty was not encountered. The effect is therefore left out of the theoretical analysis in order to make it more generally applicable and easier to interpret.

4.2 Receiver characterisation

The receiver used for the adjacent channel measurements is described in Appendix 1, being almost identical to that used for the acquisition tests in the previous chapter, with facility for long, split or short loop oscillator control. The first local oscillator was not, however, derived from a PLL synthesiser, but by direct frequency multiplication of a crystal oscillator. This adjacent channel study was essentially designed to demonstrate the effect of a phaselocked AFC loop on receiver selectivity and inclusion of the synthesiser would have unnecessarily complicated the conclusions. Not only would the phase noise of the synthesiser output have limited the selectivity but also, the filtering action of the synthesiser's PLL on the frequency modulation of the first local oscillator would make the results less general. A peak speech tone to pilot tone ratio of 15 dB, a PLL natural frequency of 10 Hz and a damping factor of $1/\sqrt{2}$ were employed, thus conforming to the current Wolfson system.

The amplitude response of the IF filter is given in figure 4.1. The 3 dB bandwidth of 3.7 kHz is a little too large to accomodate a 300 Hz - 3 kHz information channel and it is believed that the filter

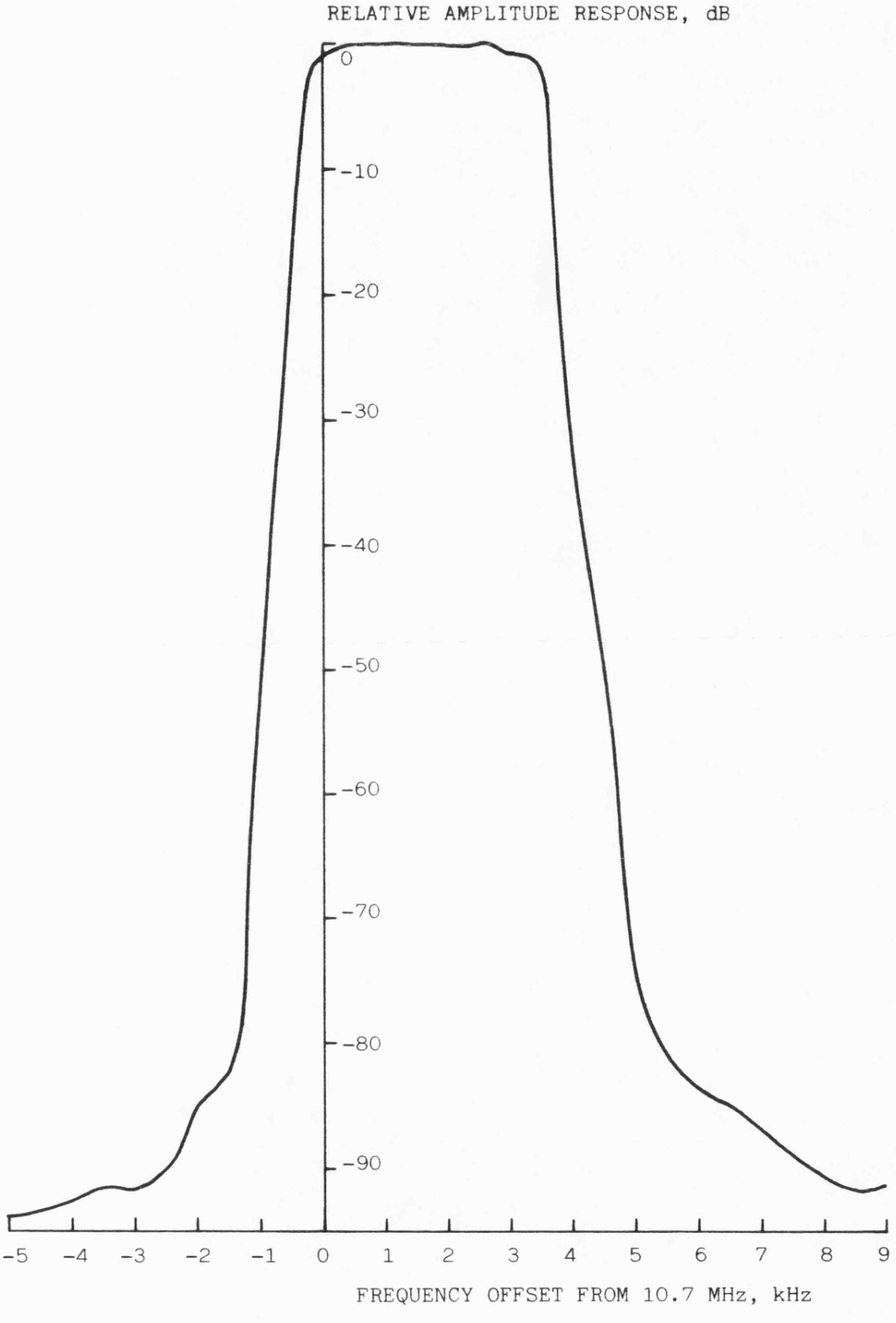

Figure 4.1 IF filter amplitude response

would present a pessimistic indication of the adjacent channel performance of an SSB receiver operating in 5 kHz channel spacing. As far as selectivity is concerned, the filter serves to limit lower sideband detection and feedthrough of adjacent channel frequencies above the wanted frequency band. Of course, it also ensures that the full adjacent channel power does not appear at the second local oscillator input so that it does not mix components of the second local oscillator frequency spectrum into the required audio band. Consequently, the purity of this oscillator's spectrum is unimportant compared to that of the first local oscillator.

Apart from the phaselocked AFC effects described presently, the only selectivity limitation was due to lower sideband detection and feedthrough caused by the imperfect IF filter response. Nonlinear distortion in the front end and first mixer were not evident. Blocking, which is the reduction of front end gain due to a large out of band signal, only occured for unwanted signal powers greater than -29 dBm (for 3 dB gain reduction). In the tests described later in this chapter, this level, corresponding to an adjacent channel selectivity of over 90 dB, was never reached. The sensitivity of the receiver, defined as the input modulation tone level for a 12 dB audio SINAD, was .19 μV into 50 Ω.

4.3 Adjacent channel induced instability

During a preliminary investigation of the effect of an adjacent channel tone on the performance of the long loop phaselocked receiver, it was observed that, for a small increase in adjacent channel tone

power above a particular level, an additional demodulated tone of large amplitude appeared at the SSB detector output, at a frequency seemingly unrelated to the adjacent channel frequency. At this level of adjacent channel interference, the receiver became unusable. The effect is due to instability in the PLL caused by the presence of the adjacent channel tone.

4.3.1 Theoretical Analysis

To demonstrate how this induced instability occurs, assume that the receiver is phaselocked to the reference tone input and that there is also a demodulated tone, $V_t \sin(\omega_t t + \theta_t)$, at the SSB detector output. This tone gives rise to two frequency components at the PSD output, owing to mixing with the reference frequency oscillator, which in turn modulate the first local oscillator. The resulting sidebands will mix with the adjacent channel tone and may produce a component within the IF passband which is subsequently demodulated to audio. If this tone is of the same amplitude, frequency and phase as the original tone, the oscillation will be maintained and the loop becomes unstable. The equations governing this instability are now derived, with reference to the receiver of figure 4.2. The receiver inputs consist of a wanted reference tone v_i, to which it is phaselocked, and an adjacent channel interferer, v_a, with the receiver oscillators denoted as in the previous two chapters. The phaselocked loop filter response is given by $F(\omega)$ and the VCO gain constant by K_1. The IF gain and filter response are A and $G(\omega)$ respectively. As well as the demodulated pilot, we will assume there is also a tone $v_t(t)$ at the SSB detector output, where:

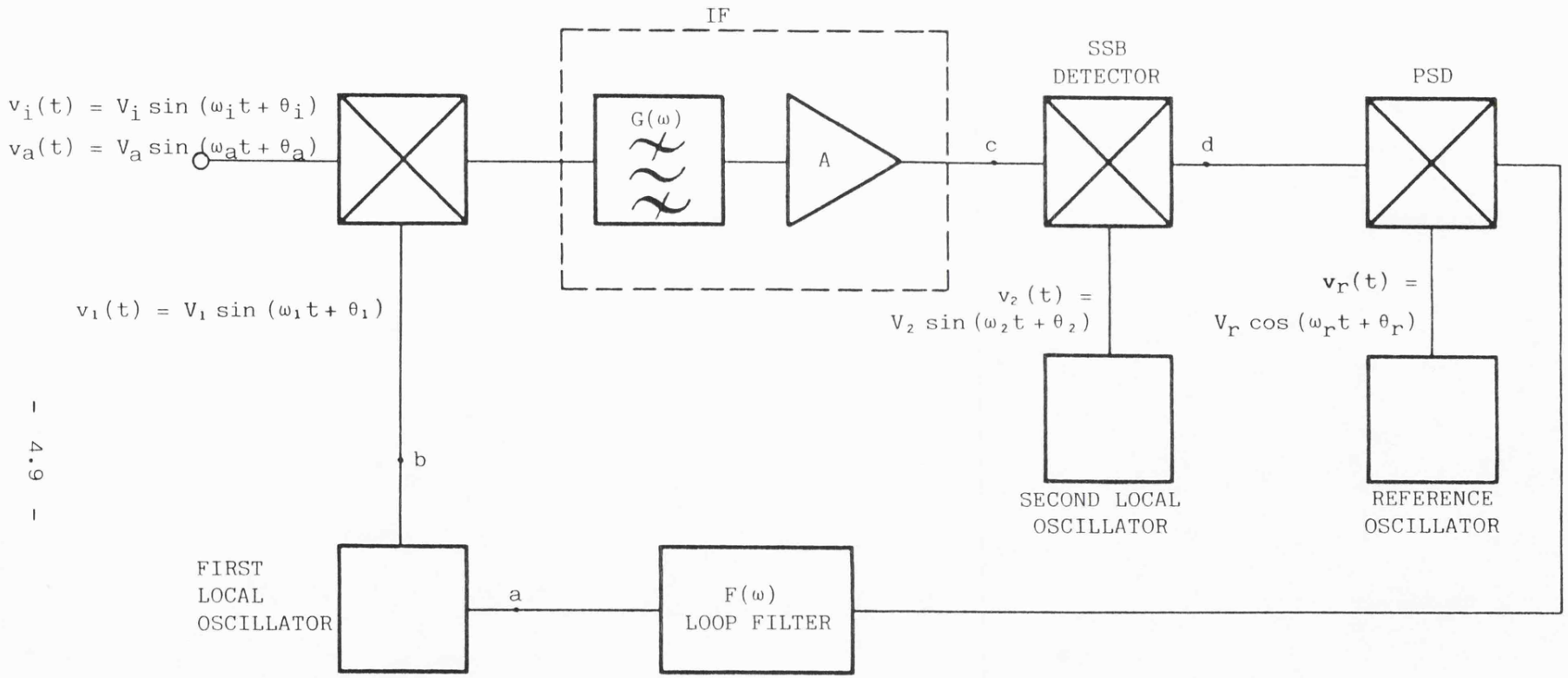

Figure 4.2 Block diagram of long loop pilot tone receiver

$$v_t = V_t \sin(\omega_t t + \theta_t) \tag{4.1}$$

We now trace the disturbances caused by this tone clockwise around the loop, eventually arriving back at the SSB detector output, and equating each resulting tone to the original tone.

$v_t(t)$ gives rise to the following voltages at the points labelled in figure 4.2:

a) $$|F(\omega_t - \omega_r)| \frac{V_t V_r}{2} \sin(\omega_t t - \omega_r t + \theta_t - \theta_r + \underline{/F(\omega_t - \omega_r)}) \tag{4.2}$$

and

$$|F(\omega_t + \omega_r)| \frac{V_t V_r}{2} \sin(\omega_t t + \omega_r t + \theta_t + \theta_r + \underline{/F(\omega_t + \omega_r)}) \tag{4.3}$$

b) Assuming narrowband frequency modulation, the four first order sidebands are:

(i) $$|F(\omega_t - \omega_r)| \frac{V_t V_r V_1 K_1}{4(\omega_t - \omega_r)} \sin[\omega_1 t + \omega_t t - \omega_r t + \theta_1 + \theta_t - \theta_r + \underline{/F(\omega_t - \omega_r)}] \tag{4.4}$$

(ii) $$|F(\omega_t - \omega_r)| \frac{V_t V_r V_1 K_1}{4(\omega_t - \omega_r)} \sin[\omega_1 t - \omega_t t + \omega_r t + \theta_1 - \theta_t + \theta_r - \underline{/F(\omega_t - \omega_r)}] \tag{4.5}$$

(iii) $$|F(\omega_t + \omega_r)| \frac{V_t V_r V_1 K_1}{4(\omega_t + \omega_r)} \sin[\omega_1 t + \omega_t t + \omega_r t + \theta_1 + \theta_t + \theta_r + \underline{/F(\omega_t + \omega_r)}] \tag{4.6}$$

(iv) $$|F(\omega_t + \omega_r)| \frac{V_t V_r V_1 K_1}{4(\omega_t + \omega_r)} \sin[\omega_1 t - \omega_t t - \omega_r t + \theta_1 - \theta_t - \theta_r - \underline{/F(\omega_t + \omega_r)}] \tag{4.7}$$

c) (i) $|F(\omega_t - \omega_r)||G(\omega_a - \omega_1 - \omega_t + \omega_r)| \frac{AV_tV_rV_1V_aK_1}{8(\omega_t - \omega_r)} \cos$

$[\omega_a t - \omega_1 t - \omega_t t + \omega_r t + \theta_a - \theta_1 - \theta_t + \theta_r - \underline{/F(\omega_t - \omega_r)}$

$+ \underline{/G(\omega_a - \omega_1 - \omega_t + \omega_r)}]$ (4.8)

(ii) $|F(\omega_t - \omega_r)||G(\omega_a - \omega_1 + \omega_t - \omega_r)| \frac{AV_tV_rV_1V_aK_1}{8(\omega_t - \omega_r)} \cos$

$[\omega_a t - \omega_1 t + \omega_t t - \omega_r t + \theta_a - \theta_1 + \theta_t - \theta_r + \underline{/F(\omega_t - \omega_r)}$

$+ \underline{/G(\omega_a - \omega_1 + \omega_t - \omega_r)}]$ (4.9)

(iii) $|F(\omega_t + \omega_r)||G(\omega_a - \omega_1 - \omega_t - \omega_r)| \frac{AV_tV_rV_1V_aK_1}{8(\omega_t + \omega_r)} \cos$

$[\omega_a t - \omega_1 t - \omega_t t - \omega_r t + \theta_a - \theta_1 - \theta_t - \theta_r - \underline{/F(\omega_t + \omega_r)}$

$+ \underline{/G(\omega_a - \omega_1 - \omega_t - \omega_r)}]$ (4.10)

(iv) $|F(\omega_t + \omega_r)||G(\omega_a - \omega_1 + \omega_t + \omega_r)| \frac{AV_tV_rV_1V_aK_1}{8(\omega_t + \omega_r)} \cos$

$[\omega_a t - \omega_1 t + \omega_t t + \omega_r t + \theta_a - \theta_1 + \theta_t + \theta_r + \underline{/F(\omega_t + \omega_r)}$

$+ \underline{/G(\omega_a - \omega_1 + \omega_t + \omega_r)}]$ (4.11)

d) Finally, at the SSB detector output, there are four demodulated tones. After making the following substitutions:

$$\omega_s = \omega_a - \omega_1 - \omega_2 \quad (4.12)$$

the frequency spacing between adjacent tone and and wanted carrier

$$\theta_s = \theta_a - \theta_1 - \theta_2 \quad (4.13)$$

$$K_d = \frac{AV_rV_1V_2V_i}{8} \quad (4.14)$$

the PSD gain

these tones become

$$\text{(i)}\ |F(\omega_t-\omega_r)||G(\omega_2+\omega_S-\omega_t+\omega_r)|\ \frac{V_tV_aK_1K_d}{V_i2(\omega_t-\omega_r)}\cos$$

$$[\omega_St-\omega_tt+\omega_rt+\theta_S-\theta_t+\theta_r-\underline{/F(\omega_t-\omega_r)}$$

$$+\underline{/G(\omega_2+\omega_S-\omega_t+\omega_r)}] \qquad (4.15)$$

$$\text{(ii)}\ |F(\omega_t-\omega_r)||G(\omega_2+\omega_S+\omega_t-\omega_r)|\ \frac{V_tV_aK_1K_d}{V_i2(\omega_t-\omega_r)}\cos$$

$$[\omega_St+\omega_tt-\omega_rt+\theta_S+\theta_t-\theta_r+\underline{/F(\omega_t-\omega_r)}$$

$$+\underline{/G(\omega_2+\omega_S-\omega_t+\omega_r)}] \qquad (4.16)$$

$$\text{(iii)}\ |F(\omega_t+\omega_r)||G(\omega_2+\omega_S-\omega_t-\omega_r)|\ \frac{V_tV_aK_1K_d}{V_i2(\omega_t+\omega_r)}\cos$$

$$[\omega_St-\omega_tt-\omega_rt+\theta_S-\theta_t-\theta_r-\underline{/F(\omega_t+\omega_r)}$$

$$+\underline{/G(\omega_2+\omega_S-\omega_t-\omega_r)}] \qquad (4.17)$$

$$\text{(iv)}\ |F(\omega_t+\omega_r)||G(\omega_2+\omega_S+\omega_t+\omega_r)|\ \frac{V_tV_aK_1K_d}{V_i2(\omega_t+\omega_r)}\cos$$

$$[\omega_St+\omega_tt+\omega_rt+\theta_S+\theta_t+\theta_r+\underline{/F(\omega_t+\omega_r)}$$

$$+\underline{/G(\omega_2+\omega_S+\omega_t+\omega_r)}] \qquad (4.18)$$

Comparing the frequencies and phases of the tones to those of v_t, the following equations are obtained for ω_t, θ_t and the voltage gain around the loop:

$$\text{(i)}\ 2\omega_t = \omega_S+\omega_r \qquad (4.19)$$

$$2\theta_t = \theta_S+\theta_r-\underline{/F(\omega_t-\omega_r)}+\underline{/G(\omega_2+\omega_t)}+\pi/2+2k\pi \qquad (4.20)$$

where k is an integer

$$\text{gain} = |F(\omega_t-\omega_r)||G(\omega_2+\omega_t)|\ \times\frac{V_aK_1K_d}{V_i2(\omega_t-\omega_r)} \qquad (4.21)$$

(ii) $2\omega_t = -\omega_s + \omega_r$ (4.22)

$$2\theta_t = -\theta_s + \theta_r - \underline{/F(\omega_t - \omega_r)} - \underline{/G(\omega_2 - \omega_t)} - \pi/2 + (2k-1)\pi \quad (4.23)$$

$$\text{gain} = |F(\omega_t - \omega_r)||G(\omega_2 - \omega_t)| \times \frac{V_a K_1 K_d}{V_i 2(\omega_t - \omega_r)} \quad (4.24)$$

(iii) $2\omega_t = \omega_s - \omega_r$ (4.25)

$$2\theta_t = \theta_s - \theta_r - \underline{/F(\omega_t + \omega_r)} + \underline{/G(\omega_2 + \omega_t)} + \pi/2 + 2k\pi \quad (4.26)$$

$$\text{gain} = |F(\omega_t + \omega_r)||G(\omega_2 + \omega_t)| \times \frac{V_a K_1 K_d}{V_i 2(\omega_t + \omega_r)} \quad (4.27)$$

(iv) $2\omega_t = -\omega_s - \omega_r$ (4.28)

$$2\theta_t = -\theta_s - \theta_r - \underline{/F(\omega_t + \omega_1)} - \underline{/G(\omega_2 - \omega_t)} - \pi/2 + (2k-1)\pi \quad (4.29)$$

$$\text{gain} = |F(\omega_t + \omega_r)||G(\omega_2 - \omega_t)| \times \frac{V_a K_1 K_d}{V_i 2(\omega_t + \omega_r)} \quad (4.30)$$

It can now be deduced that if the magnitudes of any of the gains given be equations 4.21, 4.24, 4.27 or 4.30, are greater than unity, then oscillations at a frequency and phase given by the corresponding equations will be maintained at the SSB detector output. In a lower sideband receiver, the gains given by equations 4.21 and 4.27 will be small because of the $G(\omega_2 + \omega_t)$ term. Similarly, for an upper sideband receiver the solutions containing a $G(\omega_2 - \omega_t)$ term can be neglected.

We continue by considering an upper sideband receiver, although

the lower sideband case could be treated similarly, and simplifying the gain equations of solutions (i) and (iii) for a second order type two long PLL with loop filter defined by equation 2.17. Provided the loop natural frequency, ω_n, is small enough such that $|\omega_s - \omega_t| \gg \omega_n$, which will invariably be the case, the gain of the loop filter can be well approximated by the constant τ_2/τ_1 term in the equation above. The two important solutions for the upper sideband receiver are then

$$\text{(i)} \quad 2\omega_t = \omega_s + \omega_r \tag{4.41}$$

$$\text{gain} = |G(\omega_2 + \omega_t)| \frac{V_a 2\zeta\omega_n}{V_i(\omega_s - \omega_r)} \tag{4.42}$$

$$\text{(iii)} \quad 2\omega_t = \omega_s - \omega_r \tag{4.43}$$

$$\text{gain} = |G(\omega_2 + \omega_t)| \frac{V_a 2\zeta\omega_n}{V_i(\omega_s + \omega_r)} \tag{4.44}$$

where equations 2.19 and 2.20 have been used so that equations 4.42 and 4.44 could be written in terms of loop damping factor, ζ, and natural frequency, ω_n. Equations 4.41 to 4.44 are shown in figure 4.3 for the receiver described in the previous section. The horizontal axis represents f_s, the frequency spacing between the wanted carrier and the adjacent channel interfering tone. There are two vertical axes, as the figure is a superposition of the frequency and gain equations. The straight, dotted, lines give the frequency of instability, f_t, and the full lines give the corresponding value of open loop gain when the ratio of adjacent channel tone power to reference tone power at the receiver input is unity. For instance, taking f_s to be 8 kHz, the gain is about -57 dB and f_t 3.3 kHz. In other words, at this value of adjacent channel frequency spacing, if the level of the adjacent channel tone relative to the wanted reference tone was greater than 57 dB, then

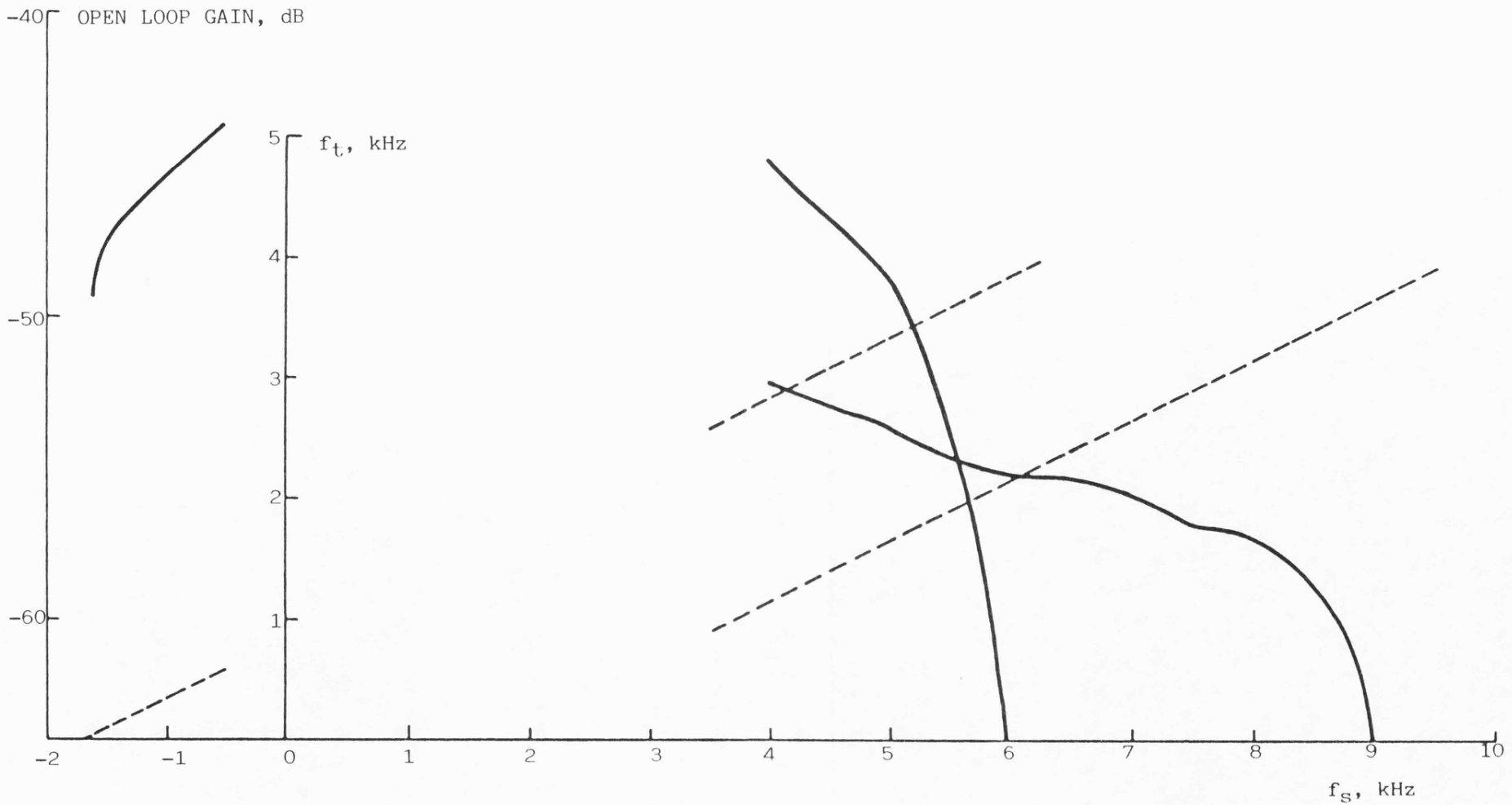

Figure 4.3 Variation of open loop gain and f_t with carrier to adjacent channel tone frequency spacing, f_s

induced instability would occur and oscillations at a frequency of 3.3 kHz would be maintained at the SSB detector output. The solutions are only shown over their significant regions and they are omitted for f_s between -0.5 kHz and 3.5 kHz as these frequencies are not in the adjacent channel. The sharp decline at the outer edges of the three gain curves is due to the IF filter characteristic. At some values of f_s, two solutions are shown for f_t, although, clearly, it would be expected that the one with the greater corresponding gain would limit the receiver selectivity. It should be noted that the term open loop gain, or simply gain, used throughout this section represents the voltage gain between a tone injected into the PSD audio input of a pilot tone receiver and the resulting tone of identical frequency at the SSB detector output, assuming there is no connection between the PSD audio input and the SSB detector output. It should not, therefore, be confused with the open loop gain of the actual receiver PLL.

The above analysis for adjacent channel induced instability was verified experimentally using the receiver described in the previous section. The measurements were in two stages. Firstly, open loop tests were made with the connection between the SSB detector output and PSD input broken and, secondly, the performance of the closed loop receiver was studied.

4.3.2 Open loop tests

The measurement configuration for the open loop tests is shown in figure 4.4. A wanted tone at the nominal frequency for the reference tone input and an adjacent channel interfering tone were summed at the

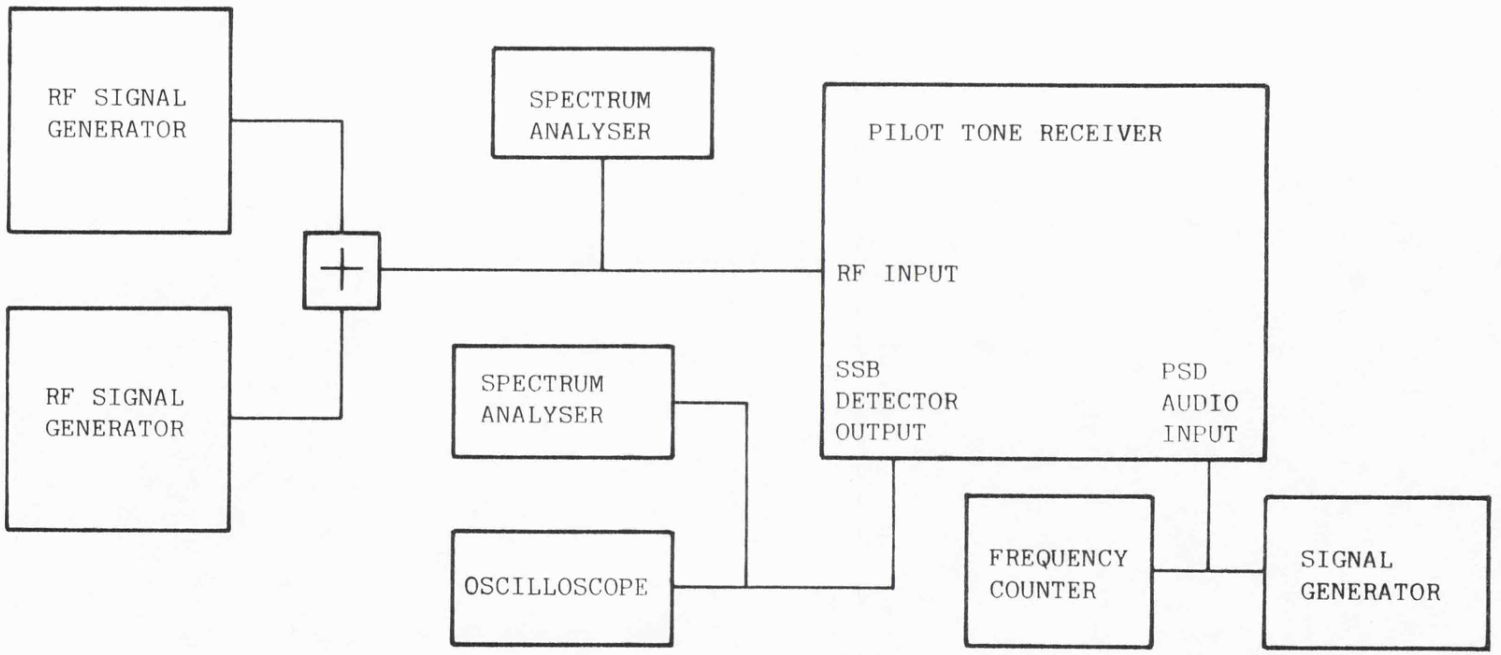

Figure 4.4 Adjacent channel induced instability open loop measurement configuration

receiver RF input. The wanted tone was set to -100 dBm at the RF input and the receiver AGC was adjusted manually to give the correct level of demodulated pilot. In the previous analysis, a tone, $v_t(t)$, was assumed to exist at the PSD input and its disturbance was traced around the loop, up to the SSB detector output. In these open loop measurements, a similar approach was taken. The connection between the SSB detector output and PSD audio input was broken and an audio signal generator was used to inject a tone into the PSD audio input. For a fixed adjacent channel tone frequency, the audio generator frequency was varied to search for one or more values which gave rise to a tone of identical frequency at the SSB detector output. When this occured, the level of the adjacent channel interferer was adjusted until the amplitudes of the audio generator output and the SSB detector output of identical frequency were equal. The frequency and amplitude of the adjacent channel tone and the frequency of the audio generator were then recorded. This whole procedure was repeated for several values of adjacent channel frequency. In this experiment, the receiver phaselocked loop was not actually locked to the input reference tone. Consequently, the first local oscillator frequency tended to drift due to integration of the PSD and loop filter voltage offsets. In order to maintain it at its centre frequency, the integrator path of the loop filter was disconnected throughout. This was acceptable since equations 4.42 and 4.44 were derived by ignoring propagation of the instability frequency through the integrator path.

The results are shown in figure 4.5 and compare well with the theoretical curves. Having verified the open loop gain equations, it

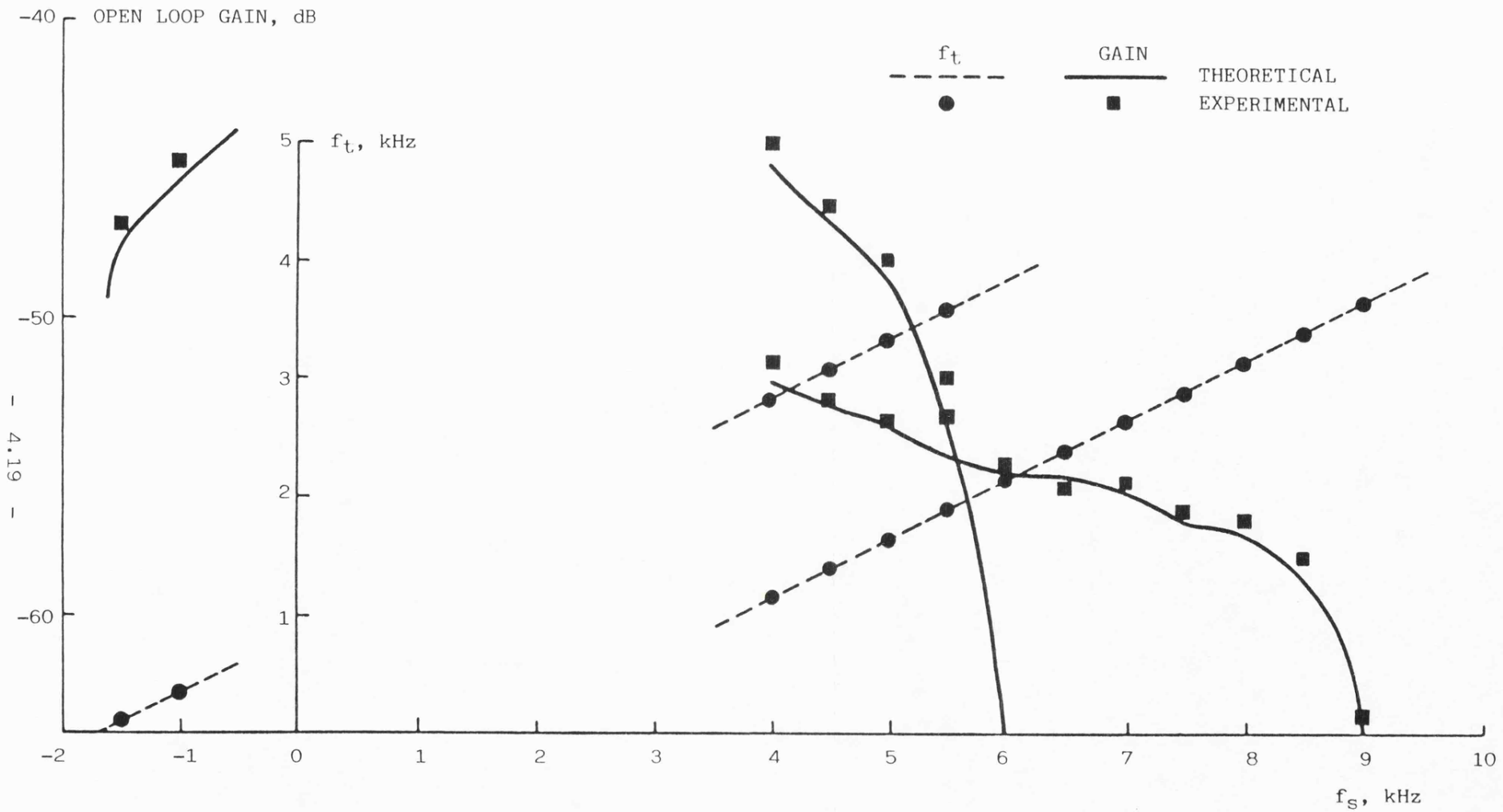

Figure 4.5 Open loop results

was then necessary to confirm that this phenomenon was responsible for instability in the closed loop receiver.

4.3.3 Closed loop tests

The measurement configuration for the closed loop tests was similar to that of the open loop described in the previous section and shown in figure 4.4. However, the SSB detector output was reconnected to the PSD audio input and the audio signal generator was removed. The integrator path of the loop filter was also reconnected. With the receiver locked to the reference tone input, the level of the adjacent channel tone was increased until instability occured, at which point the adjacent channel amplitude and the frequency of the large spurious tone appearing at the SSB detector output were recorded. The procedure was repeated for several values of adjacent channel frequency spacing. The experimental points are compared with the theoretical curves in figure 4.6, and they confirm that instability occurs when the open loop gain reaches unity. One anomalous result was found, however. For f_s equal to 6 kHz, two tones (at 1.22 kHz and 3.11 kHz) appeared at the SSB detector output. This observation can be explained as follows. A tone of frequency ω_t at the PSD audio input is fedback through the loop and appears at the SSB detector output at a frequency ω_t'. This tone is in turn fedback around the loop and appears at the SSB detector output at the original frequency, ω_t. An analysis of this type of solution is given in Appendix 2, using the same technique as that adopted in section 4.3.1. It is shown there that solutions requiring two tones at the SSB detector output are possible and, in fact, the single tone

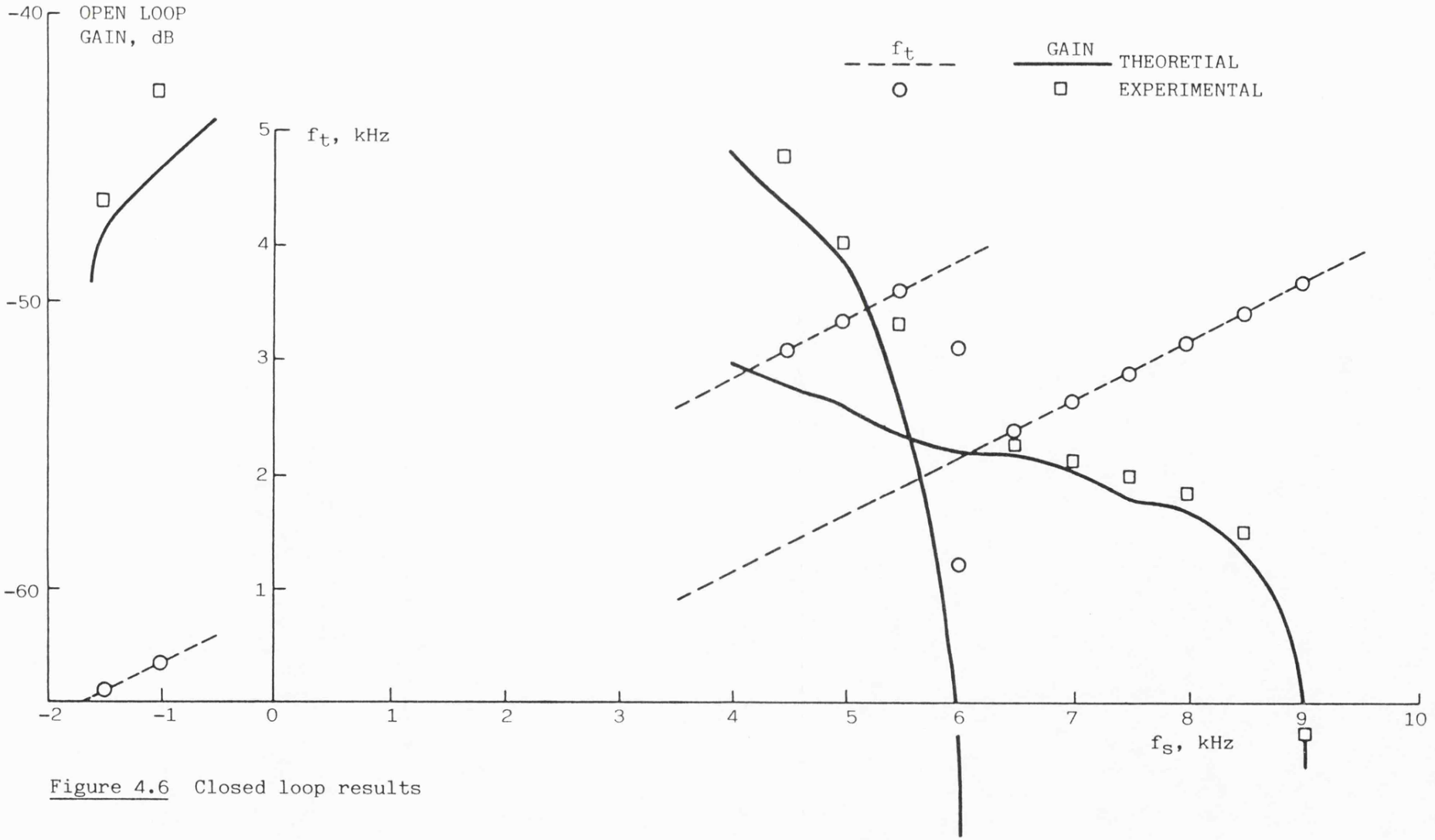

Figure 4.6 Closed loop results

equations derived above are special cases of two tone solutions for ω_t equal to ω_t'. Two tone solutions occur in preference to the single tone case if a lower level of adjacent channel tone is required to reach unity open loop gain. Solutions requiring more than two tones at the SSB detector output to be fed around the loop do not occur. For the Wolfson receiver, a comparison was made between the adjacent channel tone levels required for the single and two tone solutions and it is shown in Appendix 2 that, for fixed ω_s, the required level of the adjacent channel tone will only be a few dB's, at most, below that required for the corresponding single tone case. Consequently, the degradation of the receiver's adjacent channel selectivity due to instability could be predicted fairly accurately by using equations 4.42 and 4.44 alone.

4.3.4 Improvement by the use of the split loop technique

In a split loop receiver, the proportional path of the loop filter is used to feed the second local oscillator which, we can assume, is protected from the adjacent channel interference by the IF filter. The filter path to the first local oscillator is now an integrator term, $1/s\tau_1$. It is a simple matter to show that this reduces the open loop gains of equations 4.42 and 4.44 so that the upper sideband solutions now become:

(i) $2\omega_t = \omega_s + \omega_r$ (4.45)

$$\text{gain} = |G(\omega_2 + \omega_t)| \frac{V_a \omega_n^2}{V_i (\omega_s - \omega_r)^2} \quad (4.46)$$

(iii) $2\omega_t = \omega_s - \omega_r$ (4.47)

$$\text{gain} = |G(\omega_2 + \omega_t)| \frac{V_a \omega_n}{V_i(\omega_s + \omega_r)^2} \quad (4.48)$$

For example, for f_s equal to 5 kHz, the split loop gives an open loop gain reduction of 47 dB in the Wolfson receiver so that, for instability to occur, the ratio of the adjacent channel tone to the level of the wanted reference tone must be greater than 95 dB. In fact, the improvement achieved by the use of the split loop ensures that adjacent channel induced instability would not limit the selectivity of the Wolfson receiver. It is possible, however, that, if a larger loop bandwidth was employed, the split loop technique may not give sufficient gain reduction to meet a stringent selectivity requirement. Satisfactory performance could then possibly be achieved by placing additional filtering in the integrator path so as to lower the loop gain. Clearly this option would not be available in the long loop case without incurring the consequent penalties of the excess loop phase shift.

4.4 Reciprocal mixing

The demodulated signal at the SSB detector output enters the PSD and, after mixing and passing through the loop filter, modulates the first local oscillator of the long loop receiver. This degrades the spectrum of the oscillator, giving rise to the possibility of reciprocal mixing of the adjacent channel interferer into the IF channel by the oscillator's sidebands. To illustrate this degradation, the first local oscillator spectrum of the long loop version of the Wolfson receiver used for these adjacent channel selectivity tests is shown in

figure 4.7. A 1 kHz 'speech' tone is being received 5 dB above the pilot tone with a SINAD ratio of 12 dB. The six discrete sidebands are due to the PSD output terms at twice the reference frequency and at the reference frequency ± the speech tone frequency. Clearly, once the first local oscillator spectrum has been obtained, it is a straightforward matter to calculate the selectivity performance for a given adjacent channel tone frequency and amplitude and IF filter characteristic. A derivation of the discrete sidebands will now be undertaken, followed by an estimation of the sidebands caused by the noise voltage at the SSB detector output.

4.4.1 Discrete sidebands

Let the SSB detector output of the long loop receiver consist of a modulation term, $v_b(t)$ and a demodulated reference term, $v_g(t)$, which is phaselocked to the receiver reference, $v_r(t)$. These three tones are defined as:

$$v_b = V_b \sin(\omega_b t + \theta_b) \tag{4.49}$$

$$v_g = V_g \sin(\omega_r t + \theta_g) \tag{4.50}$$

$$v_r = V_r \sin(\omega_r t + \theta_r) \tag{4.51}$$

The PSD output then consists of a DC term and three AC terms which are:

$$\text{(i)} \quad \frac{V_g V_r}{2} \sin(2\omega_r t + \theta_g + \theta_r) \tag{4.52}$$

$$\text{(ii)} \quad \frac{V_b V_r}{2} \sin(\omega_b t - \omega_r t + \theta_b - \theta_r) \tag{4.53}$$

$$\text{(iii)} \quad \frac{V_b V_r}{2} \sin(\omega_b t + \omega_r t + \theta_b + \theta_r) \tag{4.54}$$

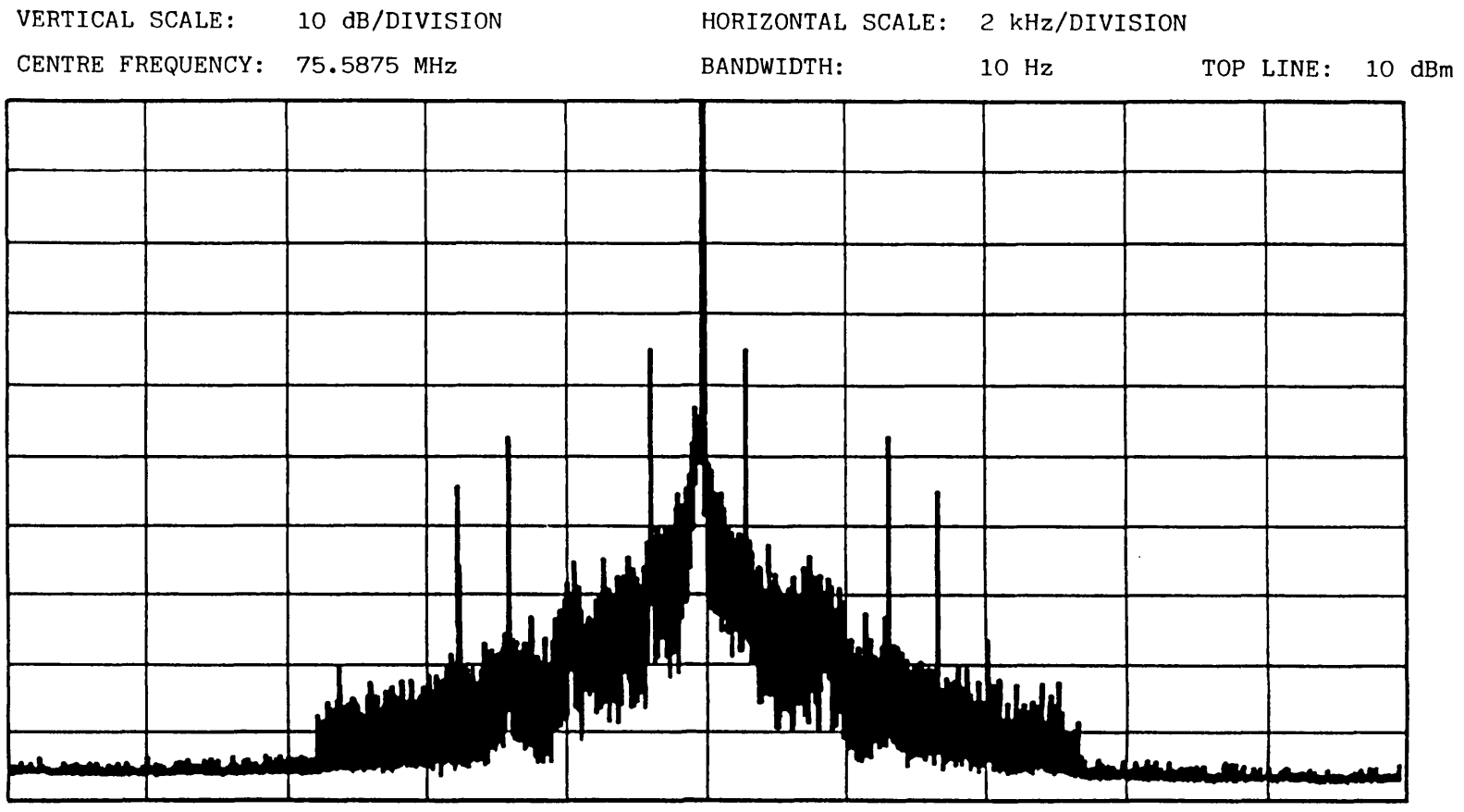

Figure 4.7 First local oscillator frequency spectrum of the long loop Wolfson receiver

If the reference frequency and the spacing between the demodulated modulation and pilot tone frequencies are both much greater than the PLL bandwidth, the three terms pass through the loop filter with a gain of τ_2/τ_1. Assuming, for the present, that the modulation on the first local oscillator is narrowband, it can simply be shown (3) that the oscillator output single sideband to carrier power ratios are given by:

$$\text{(i)} \quad 10 \log_{10} \left(\frac{V_g V_r \tau_2 K_1}{8 \tau_1 \omega_r} \right)^2 \text{ dB} \tag{4.55}$$

$$\text{(ii)} \quad 10 \log_{10} \left(\frac{V_b V_r \tau_2 K_1}{4 \tau_1 (\omega_b - \omega_r)} \right)^2 \text{ dB} \tag{4.56}$$

$$\text{(iii)} \quad 10 \log_{10} \left(\frac{V_b V_r \tau_2 K_1}{4 \tau_1 (\omega_b + \omega_r)} \right)^2 \text{ dB} \tag{4.57}$$

for each of the terms, respectively. If we define α as the ratio of the SSB detector output modulation tone level to reference tone level, i.e.:

$$\alpha = V_b/V_g \tag{4.58}$$

and note that $V_g V_r/2$ is the PSD gain constant, K_d, then the above expressions simplify to:

$$\text{(i)} \quad 10 \log_{10} \left(\frac{\zeta \omega_n}{2 \omega_r} \right)^2 \text{ dB} \tag{4.59}$$

$$\text{(ii)} \quad 10 \log_{10} \alpha^2 + 10 \log_{10} \left(\frac{\zeta \omega_n}{(\omega_b - \omega_r)} \right)^2 \text{ dB} \tag{4.60}$$

$$\text{(iii)} \quad 10 \log_{10} \alpha^2 + 10 \log_{10} \left(\frac{\zeta \omega_n}{(\omega_b + \omega_r)} \right)^2 \text{ dB} \tag{4.61}$$

where equations 2.19 and 2.20 have been employed in order that the results could be written in terms of loop damping factor and natural frequency.

In the above derivation, sidebands higher than first order have

been ignored and this is strictly only valid when the ratio of the local oscillator frequency deviation to modulating frequency, i.e. the modulation index, is much less than unity. For a single modulation tone and a modulation index of m, the VCO output sideband to carrier ratios are given exactly by (3):

$$\frac{\text{first order sideband}}{\text{carrier}} = 10 \log_{10} \left(\frac{J_1(m)}{J_0(m)} \right)^2 \text{ dB} \qquad (4.62)$$

$$\frac{\text{second order sideband}}{\text{carrier}} = 10 \log_{10} \left(\frac{J_2(m)}{J_0(m)} \right)^2 \text{ dB} \qquad (4.63)$$

$$\frac{\text{third order sideband}}{\text{carrier}} = 10 \log_{10} \left(\frac{J_3(m)}{J_0(m)} \right)^2 \text{ dB} \qquad (4.64)$$

.....*etc.*

where $J_k( )$ is the kth order Bessel function of the first kind. The extent of local oscillator modulation by speech terms must be limited in a pilot tone system as the resultant frequency variation of the local oscillator gives rise to distortion of the demodulated signal. It can even cause the PLL to jump out of lock with the pilot tone and to track a modulation component. The audio distortion caused by local oscillator frequency modulation is termed "speech pulling" and has been investigated by McGeehan and Lymer (4). For instance, in order to keep distortion products at a minimum of 20 dB below the wanted modulation at the SSB demodulator output, it is necessary to ensure that the local oscillator modulation index is no greater than 0.2. These authors have also derived an equation for the local oscillator modulation index due to a single 'speech' tone at a frequency spacing, ω_m, from the demodulated pilot:

$$m = \frac{\alpha}{\left[\left(\frac{\omega_m}{2\zeta\omega_n} \right)^2 + 1 \right]^{1/2}} \qquad (4.65)$$

The equation is a good approximation when m is much less than unity and ω_m is much greater than the PLL bandwidth. In the Wolfson system m is in fact limited to .2 in order to keep the audio distortion at an acceptable level. This value gives first, second and third order sideband to carrier ratios of -20 dB, -46 dB and -75 dB respectively. However, it would be pessimistic to take these levels of sidebands for all values of ω_m. The modulation index is limited by the use of a notch filter in the transmitter to remove modulation components close to the pilot, prior to the addition of the pilot to the modulation. It follows that, for a given value of α and for modulation frequencies far removed from the pilot which are not appreciably attenuated by the transmitter notch filter, then the resultant receiver modulation index decreases as ω_m increases. In other words, as ω_m increases and is consequently more likely to yield a sideband in the adjacent channel, then the levels of the sidebands decrease. This is illustrated in table 4.1 for the Wolfson system, which employs a transmitter notch filter with a 3 dB bandwidth of about 770 Hz. For each value of VCO modulating frequency, the value of modulation index obtained from equation 4.65 together with the resultant sideband levels are given. α is taken equal to 15 dB, ω_n to 20 π rad/s and ζ to $1/\sqrt{2}$. The effect of the second and third order sidebands on the adjacent channel selectivity is negligible compared with the sum and difference first order sidebands and with the adjacent channel induced instability effect. Furthermore, for values of

modulation index up to .2, the simple derivation of first order sideband to carrier level given previously is accurate to 1 % at worst.

MODULATING FREQUENCY, Hz	m	SIDEBAND TO CARRIER RATIO		
		FIRST ORDER	SECOND ORDER	THIRD ORDER
500	.159	-22	-50	- 81
750	.106	-26	-57	- 92
1000	.080	-28	-62	-100
1250	.064	-30	-66	-105
1500	.053	-32	-70	-110

Table 4.1 Local oscillator sidebands

In conclusion, it can be assumed that, as the extent of local oscillator modulation has to be limited in a pilot tone system to avoid excessive speech pulling, then it follows that the effect of second and higher order sidebands on adjacent channel selectivity will usually be small.

4.4.2 Noise sidebands

The effect of noise at the SSB detector output may be approximated as follows. Assume that the SSB detector output consists of the demodulated reference tone, given by equation 4.50, together with noise, of RMS voltage V_n and bandlimited to B rad/s (see figure 4.8 a). The PSD output will then be as shown in figure 4.8 b, the noise being mixed with the reference tone and folded over at 0 rad/s resulting in a 3 dB

(a) SSB detector output

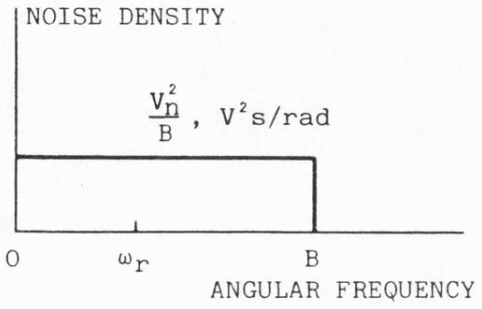

(b) PSD output

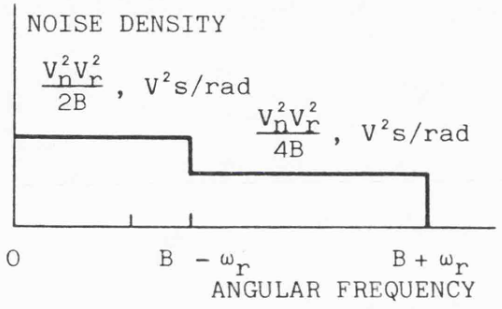

(c) VCO output

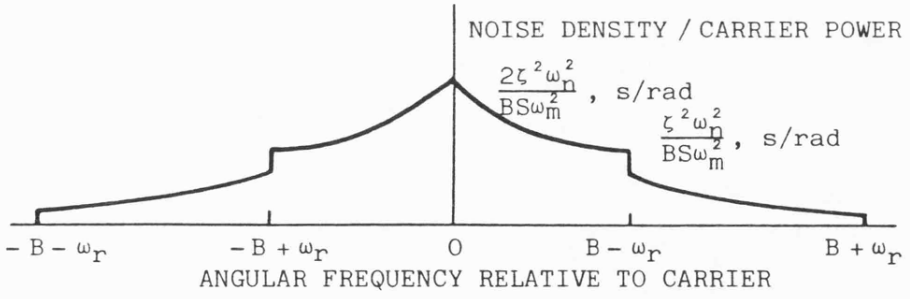

Figure 4.8 Degradation of VCO output spectrum due to SSB detector output noise

drop in noise power density at $(B - \omega_r)$. The RMS oscillator deviation (3) is then given by:

$$\Delta\omega_{rms}^2 = \frac{K_1^2\tau_2^2V_n^2V_r^2}{2\tau_1^2B} = \frac{4\zeta^2\omega_n^2}{SB} \qquad (4.66)$$

for $\omega_n \ll \omega_m < (B - \omega_r)$

and

$$\Delta\omega_{rms}^2 = \frac{2\zeta^2\omega_n^2}{SB} \qquad (4.67)$$

for $(B - \omega_r) < \omega_m < (B + \omega_r)$

where S is the reference tone signal to noise ratio, defined by:

$$S = \frac{V_g^2}{2V_n^2} \qquad (4.68)$$

At the local oscillator output, the ratio of the noise power density to the carrier power is given by:

$$\frac{\text{noise power density}}{\text{carrier power}} = \frac{\Delta\omega_{rms}^2}{2\omega_m^2} \qquad (4.69)$$

and is shown in figure 4.8 c. By integrating this expression over the appropriate region for a given adjacent channel frequency, the noise power mixed into the IF passband can be estimated.

4.4.3 Improvement by use of the split loop technique

The improvement in adjacent channel selectivity using the split loop configuration is similar to that of the adjacent channel induced instability case. It is easily shown that the technique reduces the levels of the sidebands given in equations 4.59 to 4.61 by a factor of

$10 \log_{10}(2\zeta\omega_m/\omega_n)^2$, provided that ω_m is much greater than the loop bandwidth. For example, in the Wolfson receiver, the sum and difference terms due to a 1 kHz speech tone are reduced by 52 dB and 40 dB respectively. The first local oscillator spectrum of the split loop receiver is shown in figure 4.9 for comparison with figure 4.7. It too was measured when the SSB demodulator output consisted of a 1 kHz tone 5 dB above the received pilot and with a SINAD ratio of 12 dB.

4.5 Overall adjacent channel selectivity performance of the Wolfson receiver

To conclude this chapter, measurements of the adjacent channel selectivity performance of the Wolfson receiver are described, with the definition of pilot tone receiver selectivity given in section 4.1 being used as the basis of the tests. Results are given for the long, short and split loop configurations. The experimental configuration is shown in figure 4.10 and the measurement procedure was as follows. The wanted signal was summed with the adjacent channel tone at the receiver input. In the Wolfson system a peak speech to pilot level of 15 dB is employed and consequently the input RF tone which demodulated to a frequency of 1 kHz was set at 5 dB relative to the pilot RF input. With the adjacent channel signal switched out, the attenuator was adjusted to give a SINAD ratio of 12 dB at the receiver output. The adjacent channel tone was then applied and adjusted in level until the SINAD ratio fell to a value of 6 dB. The test was repeated for several values of adjacent channel frequency.

Figure 4.11 shows a graph of the experimental points obtained for

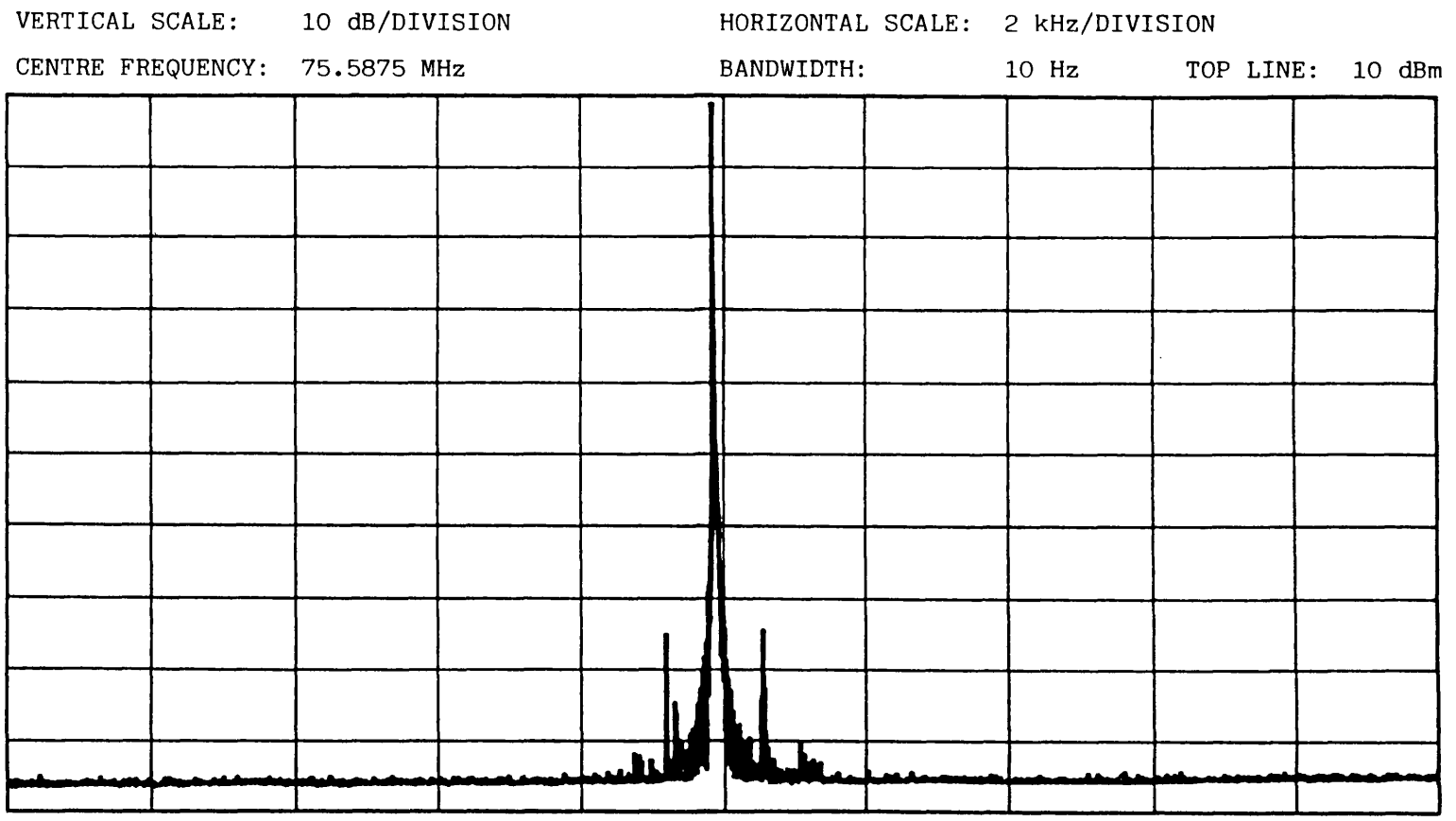

Figure 4.9 First local oscillator frequency spectrum of the split loop Wolfson receiver

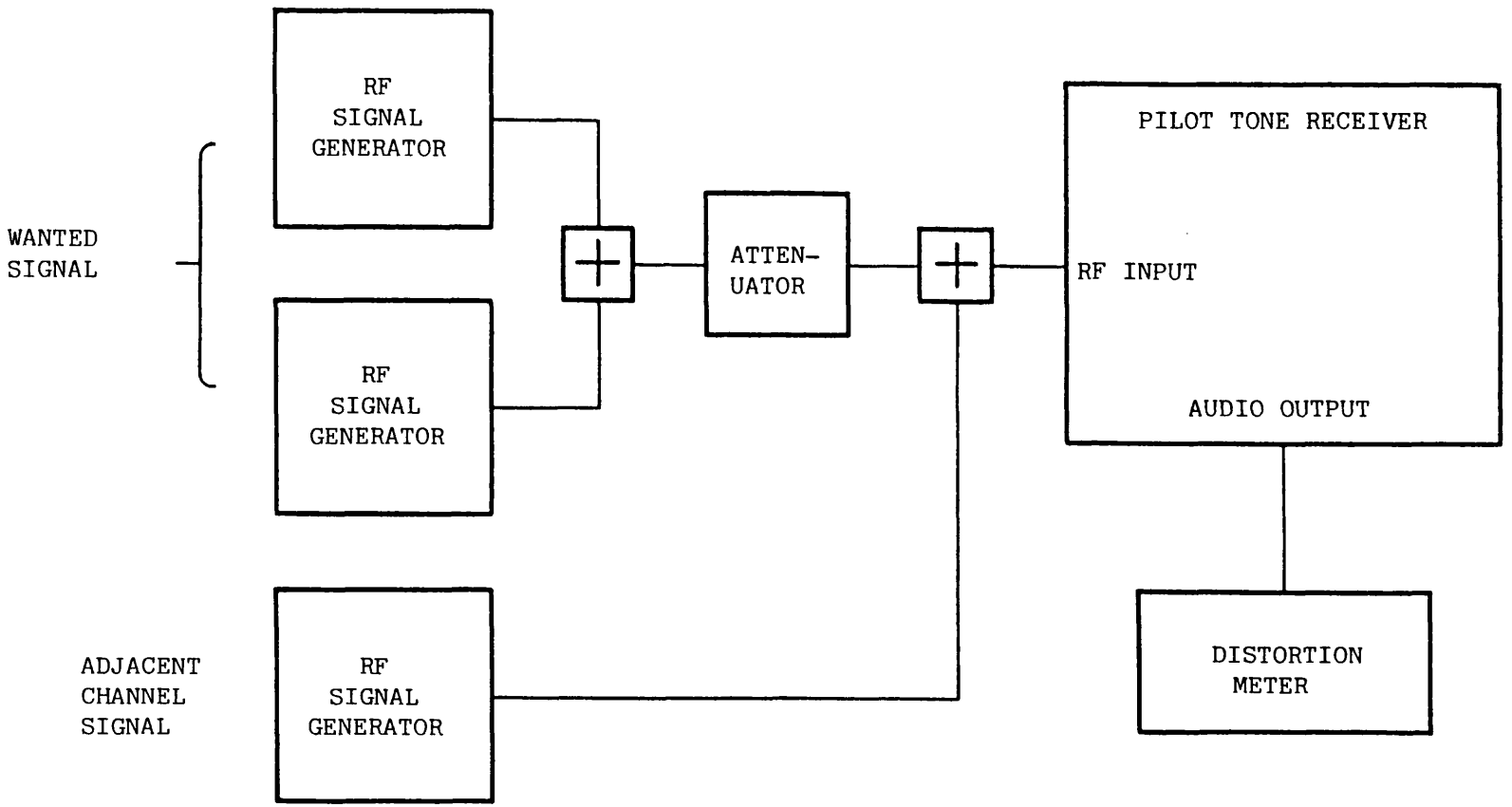

Figure 4.10 Adjacent channel selectivity test configuration

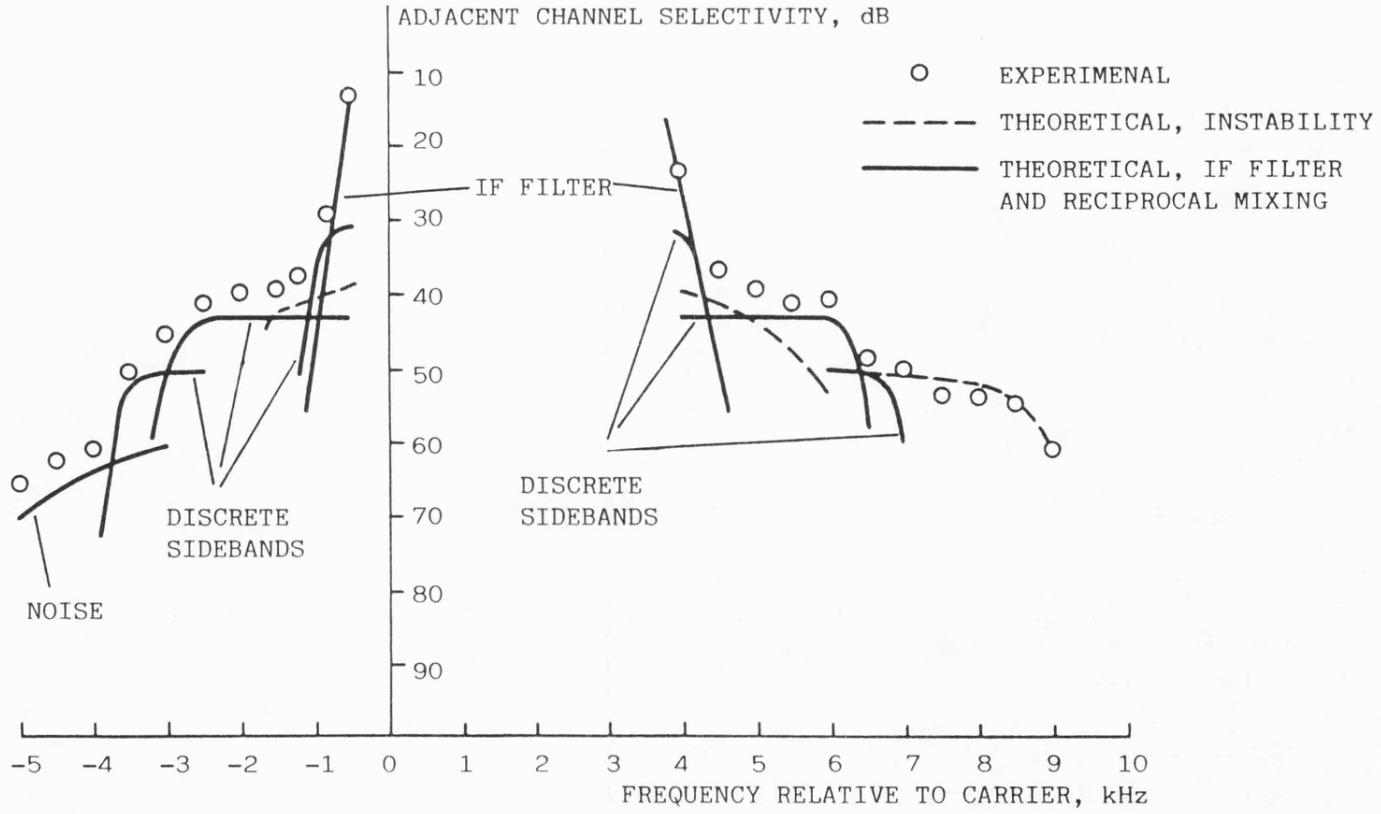

Figure 4.11 Theoretical and experimental selectivity of the long loop Wolfson receiver

the long loop, together with theoretical curves illustrating the performance resulting from IF filter limitations, adjacent channel induced instability and reciprocal mixing. Only the significant portions of these curves which effectively form a selectivity boundary are shown. Figures 4.12 and 4.13 show the experimental points obtained for the split and short loop configurations, together with the expected performance resulting from the IF filter characteristic which is now the only significant limitation of adjacent channel selectivity. The results in figures 4.11 to 4.13 compare favourably with the theoretical curves, although the long loop curves appear to be optimistic in predicting the receiver's selectivity. However, it should be noted that the theoretical selectivity is always above the worst case line (3 dB above when two continuous lines intersect).

The results demonstrate how a long loop receiver can possess poor selectivity, limited by the mechanisms of reciprocal mixing and adjacent channel induced instability. Satisfactory performance can be achieved, however, while still maintaining control of the first local oscillator, provided that the split loop technique is used.

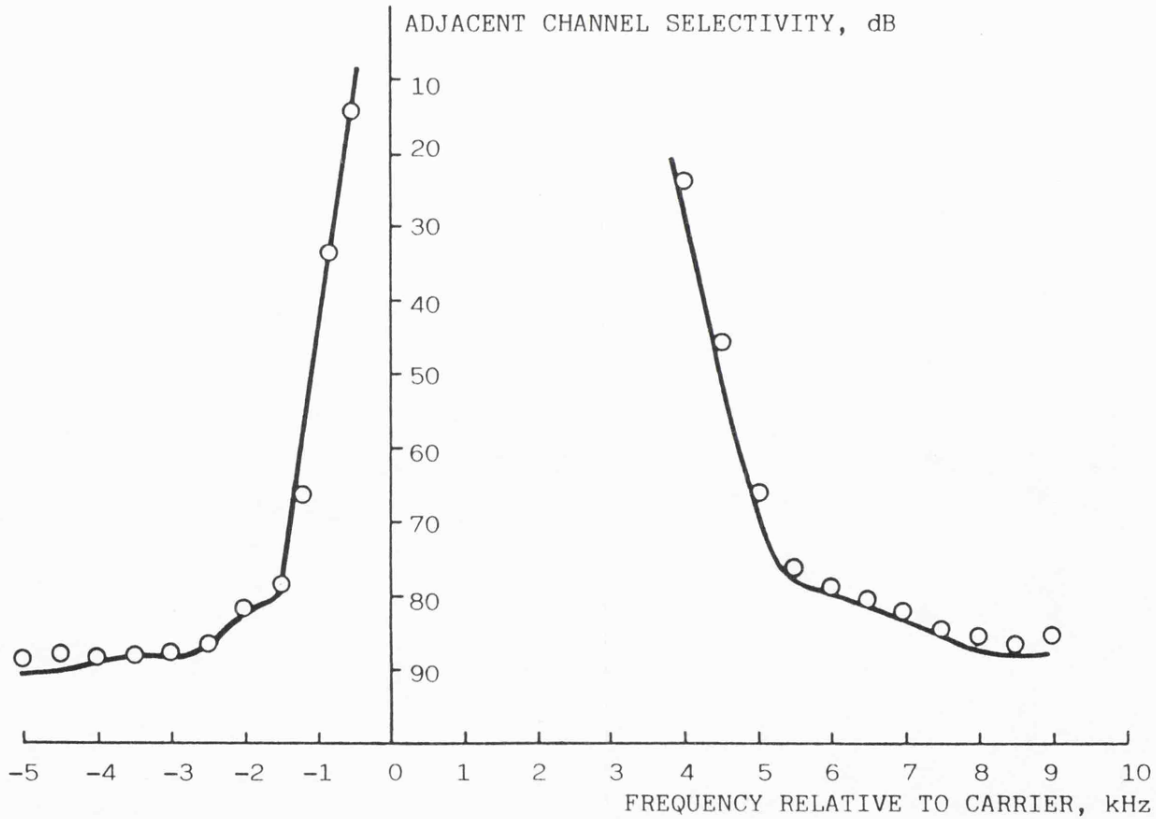

Figure 4.12 Theoretical and experimental selectivity of the split loop Wolfson receiver

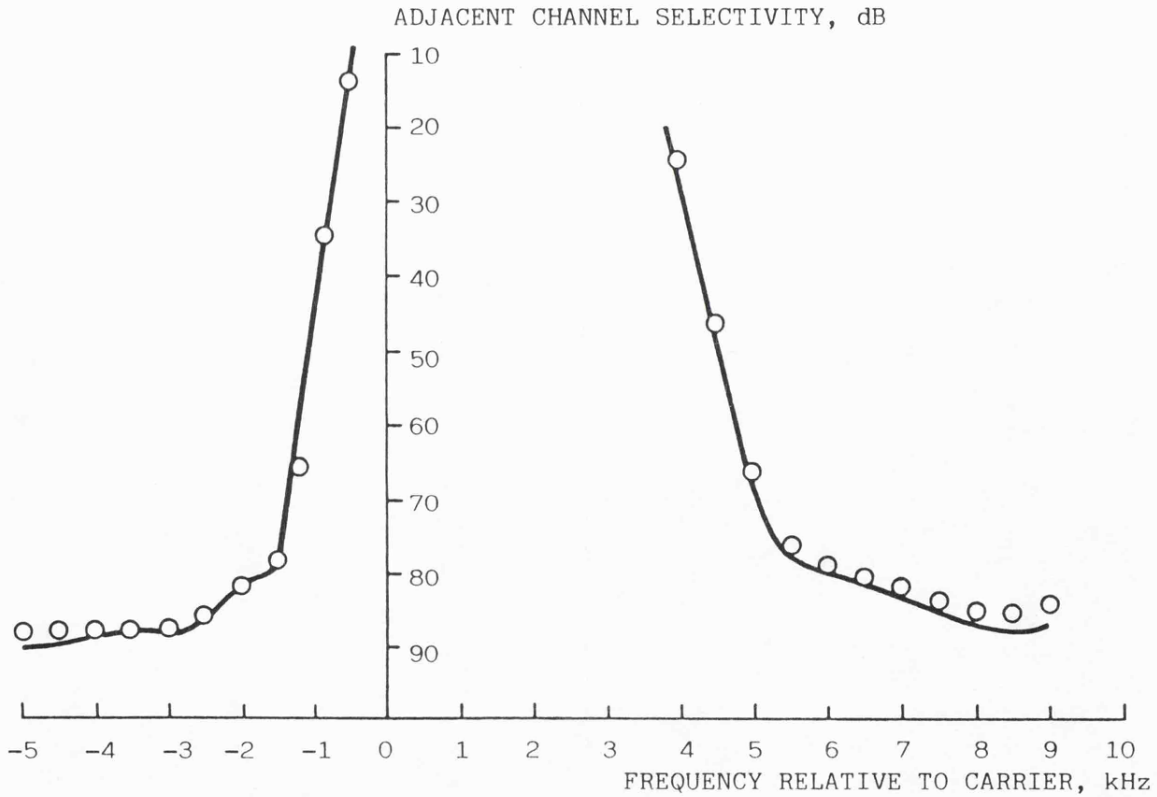

Figure 4.13 Theoretical and experimental selectivity of the short loop Wolfson receiver

REFERENCES

1) Flett, A.: "Adjacent channel performance of FM, AM and SSB at VHF", IEE conference on communications equipment and systems, April 1978, pp. 137-139.

2) "Report on comparative tests of modulation methods for private mobile radio", Home Office Radio Regulatory Department, April 1982.

3) Manassewitsch, V.: "Frequency synthesizers, theory and design", (Wiley, 1976), chapter 2.

4) McGeehan, J.P., and Lymer, A.: "The problem of speech pulling and its implications for the design of phase-locked SSB radio systems", Proc. IEE, November 1981, Vol. 128F, pp. 361-369.

CHAPTER 5

LAND MOBILE RADIO PROPAGATION

The pilot tone received by the moving vehicle will have random amplitude and phase variations impressed upon it, due to propagation through the mobile radio communication medium. As the variations will hinder the ability of the receiver's PLL to track the pilot tone, their characteristics must be studied. This chapter considers some received signal variations that occur in the mobile communications medium and a distinction is made between long and short term fading. Various receiver correction schemes devised to improve the demodulated signal quality in fading conditions are then discussed. Finally, the implications of the propagation medium for receiver PLL design are introduced, leading to the investigations described in chapters 6 and 7.

Unless otherwise stated, chapters 5 to 7 consider communication to take place via the electric radiation field between two antennas using vertical polarisation, at a single transmitted frequency.

5.1 The land mobile radio communications medium

Short and long term fading are two phenomena, usually considered as seperable, which occur in communications between a land mobile vehicle and a fixed base station (1,2). Short term fading is also known as multipath or fast fading and results in rapid phase and amplitude variations of a signal received by a moving vehicle. Successive fades occur about every half wavelength, with fade depths of 30 dB or more

being common. Short term fading is caused by the mobile travelling through a quasi-stationary interference pattern set up, typically, by multiple reflections from nearby obstacles. When the received signal strength is averaged out over tens of wavelengths, the short term fading is effectively removed and only the large scale signal variations remain. These large scale variations are known as long term or slow fading and are caused by variation of the terrain profile and the general nature of the environment.

Because the signal variations due to long term fading occur relatively slowly, it is reasonable to assume that they give rise to much less severe PLL tracking problems, compared to those caused by the short term fading. Consequently, the remainder of this chapter and the following two chapters will concentrate on short term fading with the assumption that the receiver's feedback AGC maintains the average level of the demodulated pilot constant, effectively removing the long term fading. In the next two sections, various models which have been proposed for short term fading will be described.

5.2 Short term fading - multiple path case

A brief description of the widely quoted model of multipath fading of Jakes (1) will now be given. Some of the more significant properties of the received signal that it predicts will also be presented. Other similar models of multipath fading have been proposed (3) and lead to comparable statistical properties of the field.

It is assumed (1) that, at any point, the field received at the mobile is made up of a large number of horizontally polarized plane

waves arriving from all directions via nearby stationary scatterers. The incident waves have random amplitudes and angles of arrival for different locations, and phases which are independent of the amplitudes and are uniformly distributed from 0 to 2π. This model can be used to predict many of the observed characteristics of the received signal. In particular, it predicts a Rayleigh distribution for the envelope of the received signal. Measurements at frequencies from the VHF to the microwave ranges have confirmed this result (1). The received signal can be written as a phase and amplitude modulated carrier of nominal frequency ω_c:

$$v_i(t) = r(t) \sin (\omega_c t + \theta(t)) \qquad (5.1)$$

where $r(t)$ is the envelope of the received signal and $\theta(t)$ is its phase, uniformly distributed from 0 to 2π. The probability density of r is then given by:

$$p(r) = \begin{cases} \frac{r}{b} \exp(-r^2/2b) & r \geq 0 \\ 0 & r < 0 \end{cases} \qquad (5.2)$$

where b is the mean received power. $p(r)$ is illustrated in figure 5.1a. The level crossing rate, N_r, gives an indication of how often particular fade depths are likely to be encountered. It is defined as the expected rate at which the envelope crosses a specified level, r, in the positive direction, and is derived by Jakes (*ibid*) as:

$$N_r = \left(\frac{2\pi}{3b}\right)^{1/2} \omega_d r \exp(-r^2/3b) \qquad (5.3)$$

where ω_d is the maximum Doppler shift, given by:

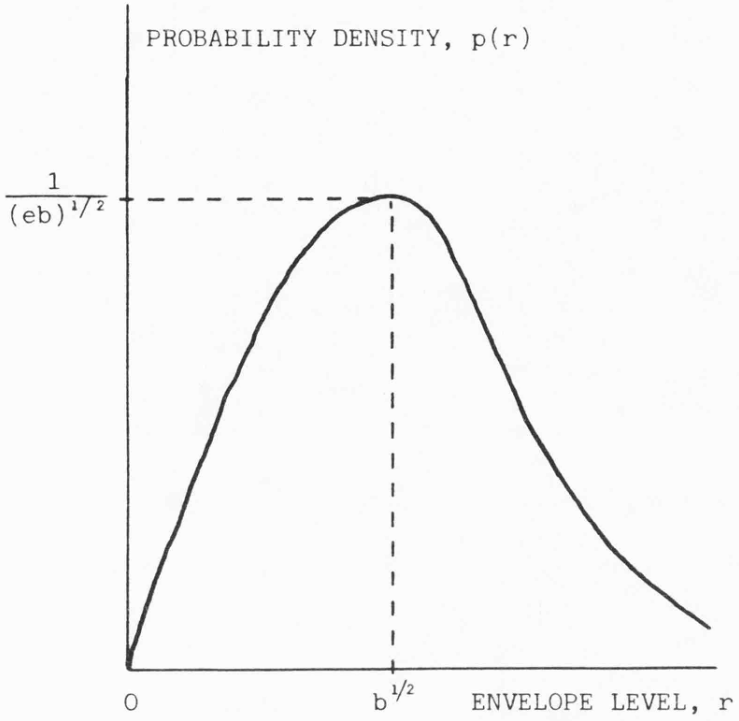

(a) Envelope modulation

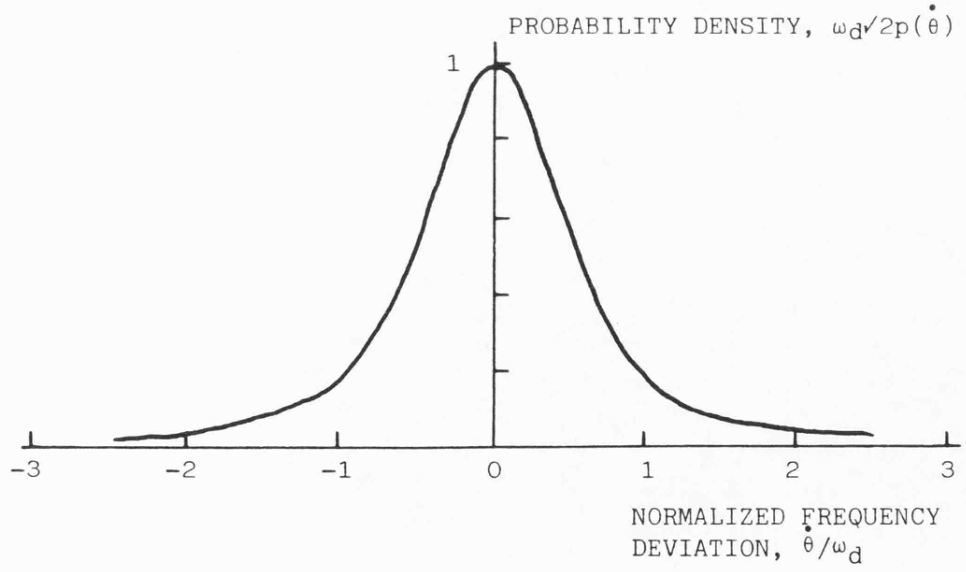

(b) Frequency modulation

Figure 5.1 Post-detection multipath probability densities

$$\omega_d = 2\pi \left(\frac{\text{vehicle speed}}{\text{wavelength}} \right) \qquad (5.4)$$

N_r is shown in figure 5.2, together with T, the average time spent below the level r, or the duration of fade. T is given by Jakes (*ibid*) as:

$$T = \frac{\exp(r^2/3b) - 1}{\left(\frac{2\pi}{3b}\right)^{1/2} \omega_d r} \qquad (5.5)$$

The power spectra of the received signal before and after detection are of interest. Jakes (*ibid*) gives the power spectrum of the received electric field as:

$$S_e(\omega) = \frac{3b}{\omega} \left(1 - \left(\frac{\omega - \omega_c}{\omega_d}\right)\right)^{-1/2} \qquad (5.6)$$

for $(\omega_c - \omega_d) \leq \omega \leq (\omega_c + \omega_d)$, zero otherwise. This is a "U" shaped spectrum , bandlimited to $2\omega_d$, and is illustrated in figure 5.3. In an ideal SSB receiver, this signal would undergo a series of linear frequency translations and, if demodulated to an audio frequency, the shape of the spectrum would be preserved. In contrast to the well defined bandwidth of this signal, the random amplitude modulation, r(t), and frequency modulation, $d\theta/dt$ or $\dot{\theta}$, are infinitely wideband processes. The value of the envelope power spectrum, $S_r(\omega)$, over the complete range of ω, has not been obtained. Jakes (*ibid*) gives the following result which is only valid for frequencies up to $2\omega_d$:

$$S_r(\omega) = \frac{b}{4\omega_d} K\left(\left(1 - \left(\frac{\omega}{2\omega_d}\right)^2\right)^{1/2} \right) \qquad (5.7)$$

where K( ) is the complete elliptical integral of the first kind. This approximation is shown in figure 5.4a. More success has been obtained

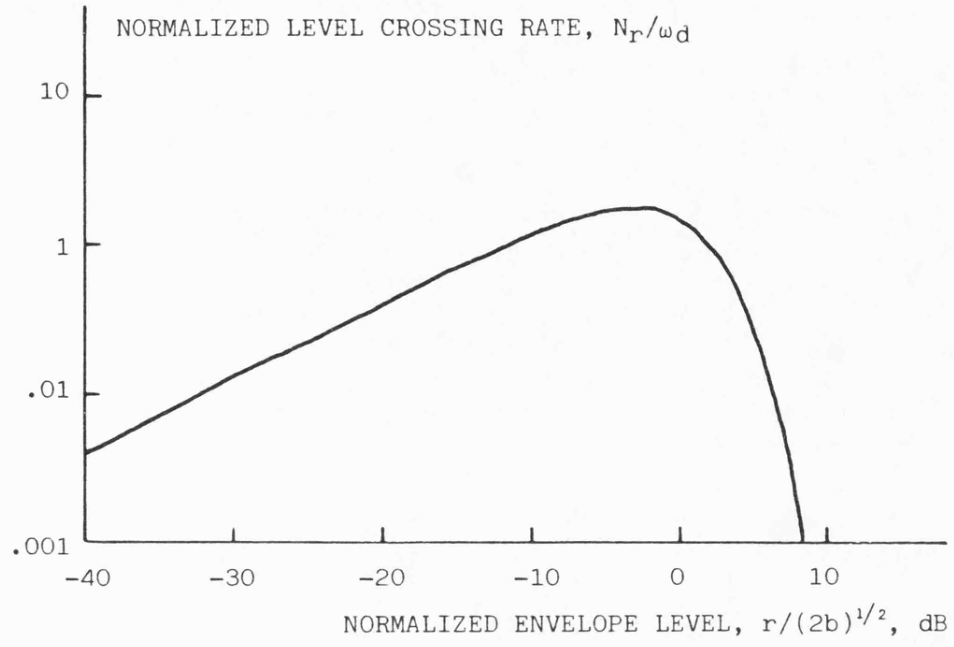

(a) Level crossing rate

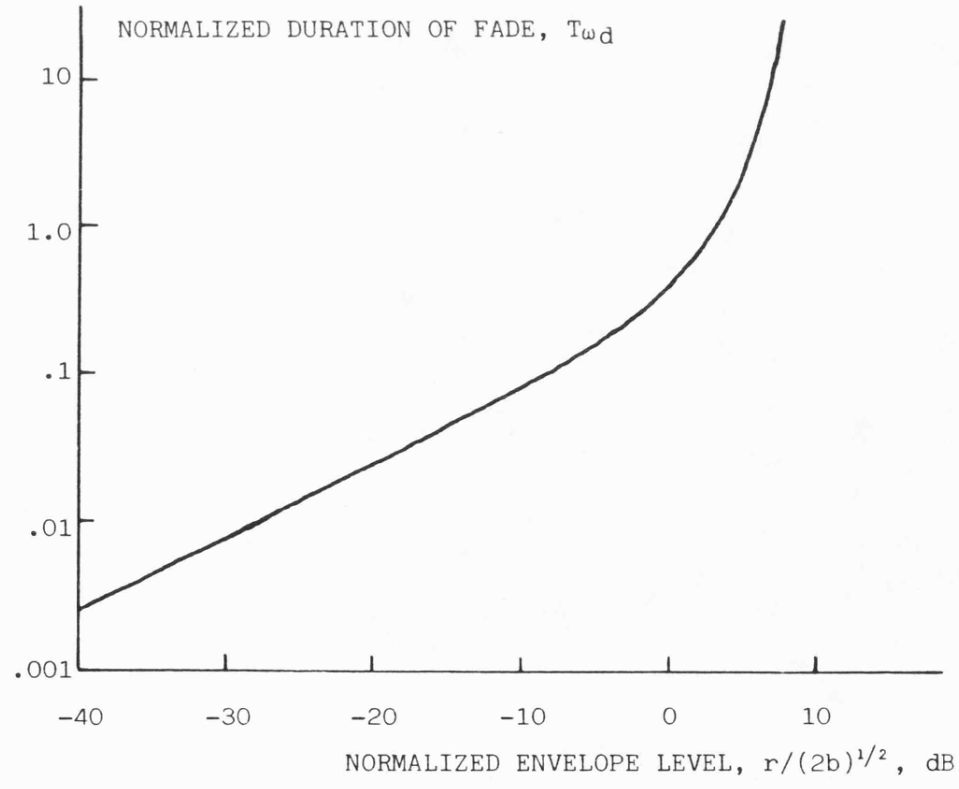

(b) Duration of fade

Figure 5.2 Multipath envelope level crossing rate and duration of fade

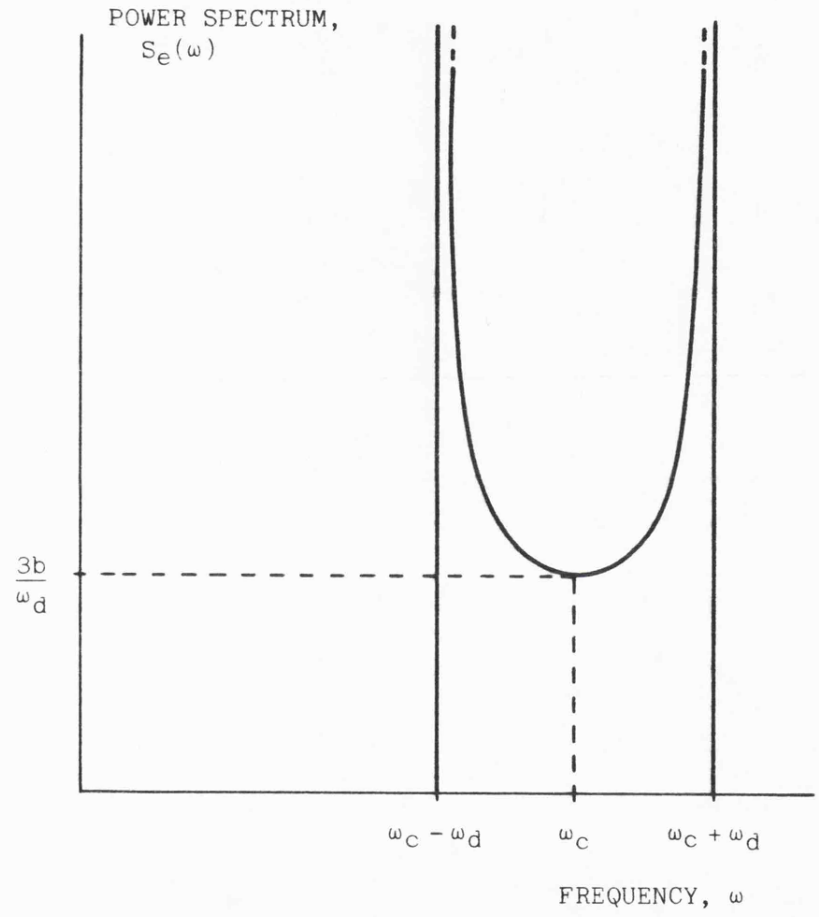

Figure 5.3 Pre-detection multipath power spectrum

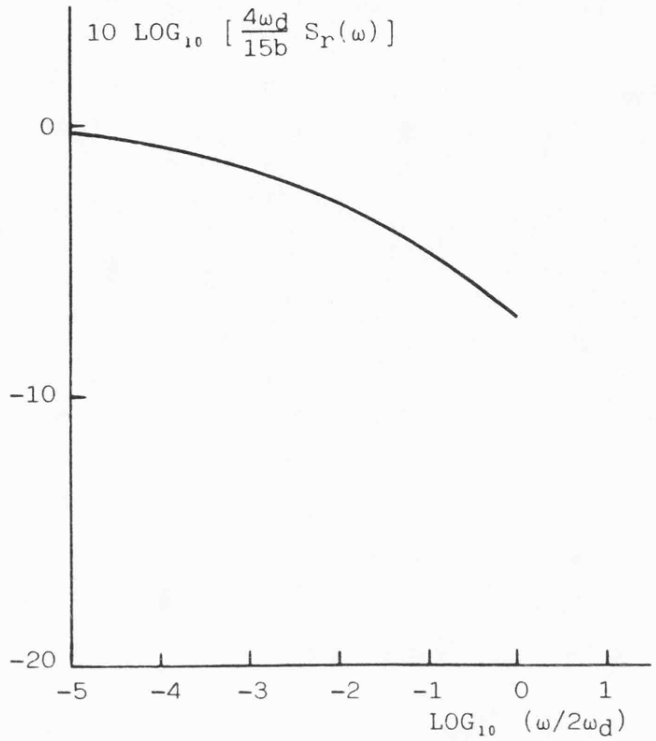

(a) Envelope modulation

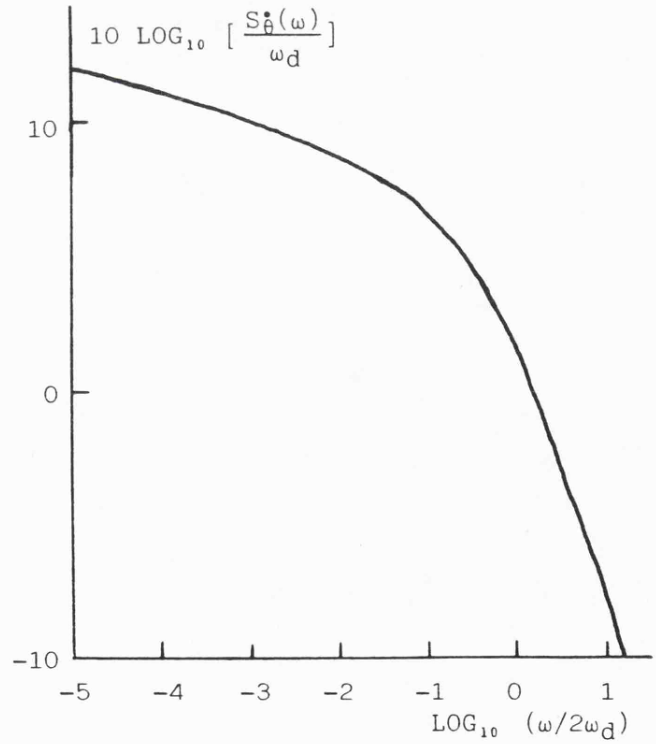

(b) Frequency modulation

Figure 5.4 Post-detection multipath power spectra

in estimating the power spectrum of the random frequency modulation, $S_{\dot{\theta}}(\omega)$, over a wide frequency range. Figure 5.4b shows the spectrum obtained by Jakes (*ibid*) via numerical integration.

The probability density function of the random frequency modulation is given by (1):

$$p(\dot{\theta}) = \frac{1}{\omega_d \sqrt{2}} \left(1 + \frac{2\dot{\theta}^2}{\omega_d}\right)^{-3/2} \qquad (5.8)$$

and is illustrated in figure 5.1b. It is interesting to note that the larger frequency excursions are associated with the deeper fades of the signal. This can be seen by examining the probability density function of $\dot{\theta}$ conditioned on the envelope level, r (1):

$$p(\dot{\theta}|r) = \left(\frac{2}{3\pi b}\right)^{1/2} \frac{r}{\omega_d} \exp\left(-2r^2\dot{\theta}^2/3b\omega_d^2\right) \qquad (5.9)$$

For fixed r, this is a Gaussian distribution with standard deviation $(\omega_d/2r)\,(3b)^{1/2}$. Consequently, as the fade depth increases, the frequency deviations increase proportionally.

Fuller details of the signal statistics for this model are given by Jakes (*ibid*) who also considers the special case of the model when the received scattered waves are accompanied by a direct, line of sight, component.

5.3 Short term fading - twin path case

In 1964 Ossana proposed a model for suburban mobile radio propagation based on the reception of one direct and one reflected component (4). Although largely superseded by models similar to those of Jakes (1), it is of importance because of its relative simplicity

and because it has been partially substantiated by experimental results. The model is based on the assumption that, over short lengths of time, the signal received at the mobile consists of a direct component and not more than one component of equal amplitude, reflected from the side of a building. To analyse the received signal properties over a reasonable length of time, it is necessary to consider the vehicle passing through a number of these distinct interference areas. The received envelope power spectrum, which Ossana (*ibid*) obtained by assuming all reflector angles equally likely, agreed fairly well with field data.

The final model of short term fading to be described is that given by Burrows (5) and was derived from the air-to-air fading communications model of Reed and Russel (6). It is similar to the model of Ossana (*ibid*), in that twin path propagation is assumed. However, it is a scattering model and does not include the restriction of equal amplitude received tones. Burrows (*ibid*) has successfully used the model as a means of predicting receiver AGC performence in the field. The model is illustrated in figure 5.5. The power received by the mobile is assumed to originate from two nearby fixed scatterers, with the mean power from each remaining constant over the distance travelled. The mobile travels along the x axis with speed U. At time t = 0, the positions of the two scattering sources, SS1 and SS2, relative to the vehicle are X_1 , Y_1 and X_2 , Y_2 respectively. δ_1 and δ_2 are the angles between the vehicle and the respective scatterers, given by:

$$\cos \delta_1 = \frac{X_1 - Ut}{((X_1 - Ut)^2 + Y_1^2)^{1/2}} \qquad (5.10)$$

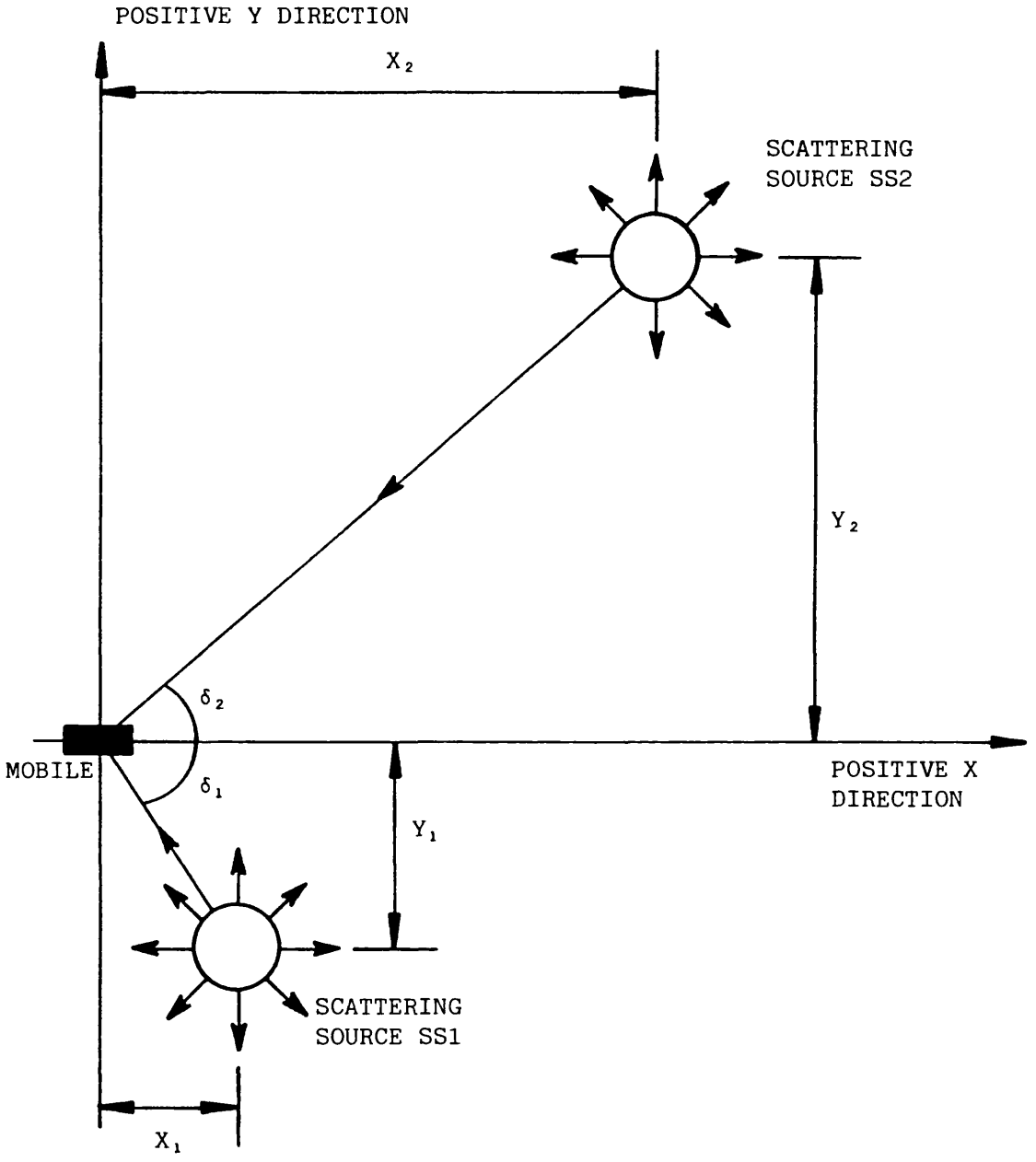

Figure 5.5 Twin path scattering model

$$\cos \delta_2 = \frac{X_2 - Ut}{((X_2 - Ut)^2 + Y_2^2)^{1/2}} \qquad (5.11)$$

If the signal amplitude at the receiver's input from SS1 is E and that from SS2 is RE, with $0 < R < 1$, then the total received signal is:

$$v_i(t) = E\,(\sin(\omega_c t + \omega_d t \cos \delta_1) + R \sin(\omega_c t + \omega_d t \cos \delta_2)) \qquad (5.12)$$

where ω_c is the carrier frequency and ω_d is the maximum Doppler frequency defined by equation 5.4. The frequency spectrum of $v_i(t)$ is thus formed by two components that vary in instantaneous frequency as the vehicle approaches and passes the scattering sources. The maximum frequency separation between the two components is equal to $2\omega_d$ and occurs when one source is directly in front of the vehicle and the other is directly behind. Again writing the received signal as a phase and amplitude modulated carrier wave in the form of equation 5.1, we obtain:

$$r(t) = E\,(1 + R^2 + 2R \cos \omega_f t)^{1/2} \qquad (5.13)$$

$$\tan \theta(t) = \frac{\sin(\omega_d t \cos \delta_1) + R \sin(\omega_d t \cos \delta_2)}{\cos(\omega_d t \cos \delta_1) + R \cos(\omega_d t \cos \delta_2)} \qquad (5.14)$$

where ω_f is the fade rate given by:

$$\omega_f = \omega_d (\cos \delta_2 - \cos \delta_1) \qquad (5.15)$$

Further details of this model and a comparison between some of the received signal properties predicted by this model and that of Jakes (*ibid*) are given by Burrows (*ibid*). Using the above equations for the input envelope and phase, receiver performance analysis can continue without reference to any particular position of the scattering sources,

assuming δ_1 and δ_2 constant wherever necessary. By using this deterministic expression for r(t), Burrows (*ibid*) was able to analyse receiver AGC performance, when results using the more complex statistical models could not be obtained. Consequently, the following chapter, which considers the impairment of AGC performance caused by phaselocked AFC, will also make use of this model.

5.4 Multipath distortion correction techniques

As mentioned in chapter 1, the purpose of transmitting a pilot tone together with the SSB signal is to facilitate receiver AGC and AFC. In particular, pilot based correction systems are required to counteract the unwanted modulation effects of multipath propagation. Unless suppressed, these random fluctuations cause considerable distortion of speech communications at high band VHF and UHF (7).

Although feedback AGC is able to remove the slow, long term fading from the received signal, it is unable to suppress the short term fading at these frequencies. This is essentially because of the inherent time delay within the AGC feedback loop (8). However, a new form of AGC has been proposed and shown to overcome this problem, satisfactorily suppressing the fast unwanted envelope variations (9). The technique has been termed feedforward AGC (FFAGC) and is shown in block diagram form in figure 5.6. This correction system operates entirely on the demodulated signal which is assumed to be of the form x(t)r(t), where r(t) is the fading envelope and x(t) is the required FFAGC output. A linear phase bandpass filter, of bandwidth at least equal to $2\omega_d$, is used to extract the demodulated pilot tone from the information

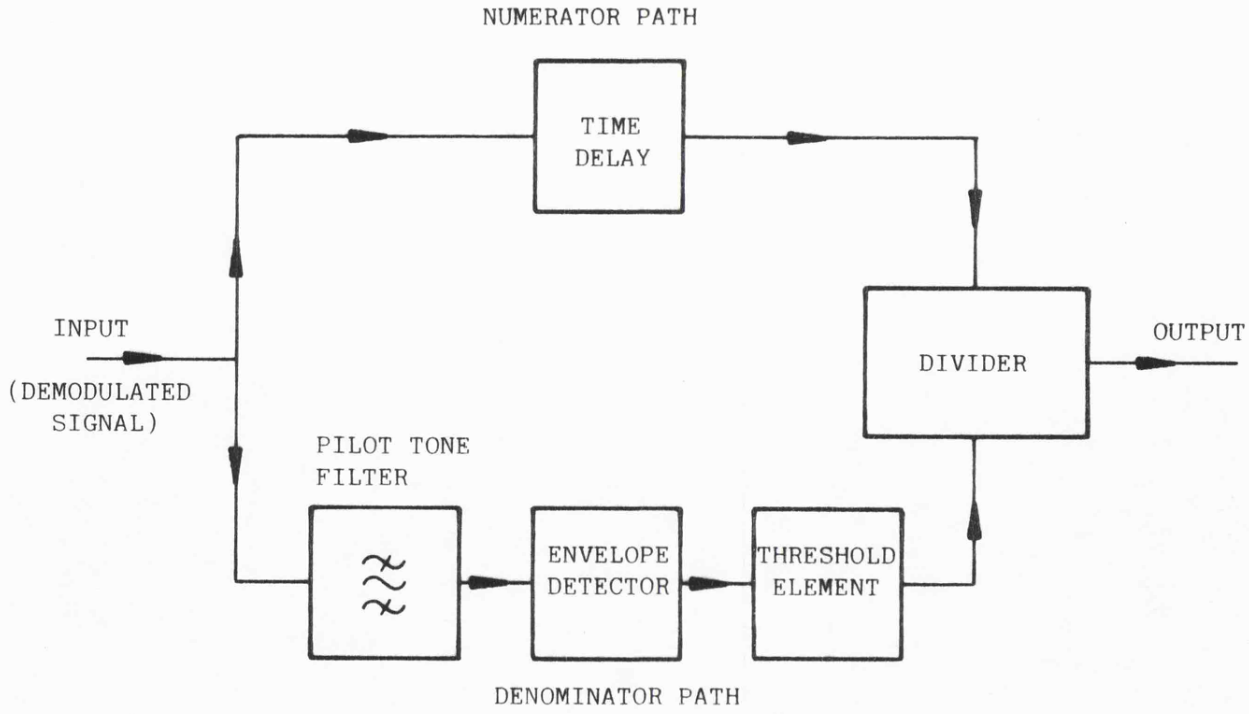

Figure 5.6 FFAGC circuit configuration

components. The envelope of the pilot tone, which is proportional to r(t), is then obtained. By dividing x(t)r(t) by r(t), the multipath envelope variations are removed to give the required output, x(t). A time delay unit is required in the numerator path to match the delays of the denominator processing. Also, a threshold circuit is often employed in the denominator path to limit the lowest level of denominator input. This reduces output noise bursts in deep fades.

While providing adequate suppression of the multipath induced amplitude fluctuations, FFAGC has no effect on reducing the distortion due to the remaining phase fluctuations. Because of this, a more comprehensive feedforward technique, termed feedforward signal regeneration, has been developed (7). It is similar to FFAGC, in that it operates on the demodulated signal and employs a bandpass filter to extract the pilot tone. However, both multipath phase and amplitude information are obtained from the pilot. Using this information, the corresponding multipath phase and amplitude variations are removed simultaneously from the demodulated output.

A well documented technique for reducing the effects of multipath fading is that of diversity (10,11). It offers a partial solution to the problem by reducing the dynamic range of the envelope fluctuations and improving the signal to noise ratio. Diversity requires that a number of independently fading transmission paths are available, all carrying the same message. Proper combination of the signals from these paths can yield a resultant with greatly reduced severity of fading, since the chance of having simultaneous deep fades from uncorrelated signals is rare. However, implementation of such systems normally

involves the use of multiple transmitter or multiple receiver aerial systems, together with special combining circuitry, and can be prohibitively expensive. A technique combining the advantages of diversity and feedforward signal regeneration has also been developed (12). It consists of a dual diversity SSB receiver in which the combining of the two signals takes place after demodulation. Firstly the multipath phase variations are removed from the two demodulated signals, using the phase information from the respective demodulated pilot tones. The two co-phased signals are then combined and FFAGC is used to remove the remaining multipath envelope variations.

5.5 Implications of fading for phaselocked AFC design

The rapid phase and amplitude variations impressed upon the received pilot tone in the land mobile multipath environment have serious consequences for the design of phaselocked AFC. In the derivation of equation 2.4 it was assumed that K_d, which is proportional to the pilot amplitude at the PSD input, was a constant. However, if the multipath envelope variations, r(t), are not removed by feedback AGC, then K_d becomes proportional to r(t). Consequently the gain of the PLL becomes time variant and, in particular, the instantaneous loop bandwidth reduces during fades, when the most rapid phase changes usually occur. The loop, unless very wideband, will therefore have great difficulty tracking the phase of the received pilot. Nevertheless, it could be argued that, for an AFC system, it is not required, or even desirable, that the loop should track the multipath induced phase variations of the pilot. Instead, it is necessary for the loop to

estimate the pilot's centre frequency. The performance of a PLL for such a purpose is investigated in chapter 7.

A further problem is that, in attempting to track the random phase variations of the received pilot, the PLL will widen the frequency spectrum of the demodulated pilot tone. This leads to a possible degradation of the performance of subsequent multipath distortion correction systems. For example, if FFAGC is employed, and unless the pilot tone extraction bandpass filter is much wider than $2\omega_d$, then the filter will distort the pilot's envelope. The extent of the performance degradation is studied in the following chapter.

REFERENCES

1) Jakes, W.C.: "Microwave mobile communications" (Wiley, 1974), chapter 1.

2) Jakes, W.C.: "Microwave mobile communications" (Wiley, 1974), chapter 2.

3) Clarke, R.H.: "A statistical theory of mobile radio reception", Bell System Technical Journal, July 1968, Vol. 47, pp. 957-1000.

4) Ossana, J.F.: "A model for mobile radio fading due to building reflections: theoretical and experimental fading waveform power spectra", Bell System Technical Journal, November 1964, Vol. 43, pp. 2935-2971.

5) Burrows, D.F.: "Automatic gain control in mobile radio receivers", Ph.D. thesis, University of Bath, 1982, chapters 2 and 3.

6) Reed, H.R., and Russel, C.M.: "Ultra high frequency propagation" (Chapman and Hall, 1965), chapter 10.

7) McGeehan, J.P., and Bateman, A.J.: "Theoretical and experimental investigation of feedforward signal regeneration as a means of combating multipath propagation effects in pilot-based SSB mobile radio systems,", IEEE Trans., February 1983, Vol. VT-32, pp. 106-120.

8) Burrows, D.F., and McGeehan, J.P.: "Time delay in receiver AGC systems", Clerk Maxwell Commemorative Conference on Radio Receivers and Associated Systems, IERE, July 1981, pp. 73-78.

9) McGeehan, J.P., and Burrows, D.F.: "Performance limits of feed-forward automatic gain control in mobile radio receivers", Proc. IEE, November 1981, Vol. 128F, pp. 385-392.

10) Jakes, W.C.: "Microwave mobile communications" (Wiley, 1974), chapters 5 and 6.

11) Parsons, J.D., Henze, M., Ratliff, P.A., and Withers, M.J.: "Diversity techniques for mobile radio reception", Radio and Electronic Engineer, July 1975, Vol. 45, pp. 357-367.

12) Kanso, A., Griffiths, J., and McGeehan, J.P.: "An FFSR diversity combining system for pilot based SSB mobile radio schemes at UHF", Colloquium on the Characterisation and Mitigation of Multipath Interference Effects, IEE, May 1983, pp. 7/1-7/3.

CHAPTER 6

FEEDFORWARD AGC PERFORMANCE IN A PHASELOCKED RECEIVER

This chapter deals with the degradation of receiver FFAGC performance caused by the presence of phaselocked AFC. Results of a computer simulation of a coupled PLL/FFAGC system with a twin path fading input are described. These illustrate the FFAGC effectiveness in terms of residual output envelope modulation and are verified experimentally. Finally, the results of field trials obtained using a coupled PLL/FFAGC system are presented.

The computer simulation was undertaken since it has not been possible to obtain a complete analytic solution to the nonlinear PLL equation when no restrictions are made on the ratio of loop bandwidth to fading bandwidth (twice the maximum Doppler frequency). Weber (1) has analysed the tracking performance of first order PLLs in the presence of Rayleigh fading channels. He characterizes their performance in terms of the steady state phase error and has shown that the loop bandwidth must be considerably greater than the fading bandwidth for the signal to be tracked with low phase error. However his analysis is restricted to the case when the loop bandwidth is much greater than the fading bandwidth. Blanchard (2) has studied second order PLL performance in the presence of two tones, although not from the standpoint of twin path fading. He has investigated loop behaviour when tracking a wanted component in the presence of an interfering tone, and his analysis makes use of the assumption that the tone frequency spacing is much greater than the loop bandwidth. For a comprehensive study of the performance

of coupled PLL/FFAGC system operation, it is not possible to place these restrictions on the ratio of loop bandwidth to fading bandwidth.

6.1 AGC in land mobile SSB receivers

Feedback AGC is required in SSB receivers to suppress unwanted output signal variations and to prevent stages from being overloaded or underdriven. It is generally implemented by first filtering the speech components from the demodulated pilot, subtracting the pilot's envelope from a reference level and then filtering this signal to control the RF and IF amplifier gains. Although capable of suppressing the slow, long term fading, feedback AGC has been shown to be unable to suppress the fast short term fading, occurring at rates up to twice the maximum Doppler frequency, for carrier frequencies above the low band VHF range (3). This is because a limit is placed on the maximum AGC bandwidth which can be employed before performance is severely degraded by the time delay introduced into the loop by the pilot tone extraction bandpass filter. Attempts to suppress the fast fading by increasing the loop bandwidth can, in the presence of time delay, lead to a worsening of the feedback AGC's fade suppression ability. It can even cause loop instability and the enhancement of unwanted envelope modulation. Taking a typical value of pilot tone bandpass filter delay to be 1 ms, then the maximum fade rate the feedback AGC can satisfactorily suppress is only of the order of a few Hertz (3). This fade rate is considerably less than that encountered at UHF. For example, for a carrier frequency of 457 MHz and a vehicle speed of 60 mph, twice the maximum Doppler frequency is 82 Hz. FFAGC is required to suppress this fast fading. It

allows the use of a filter of very high order to separate the fading pilot from the required signal, without introducing any stability problems (4). The basic circuit diagram for FFAGC was given in figure 5.6 and the operating principle was described in section 5.4. The performance limits have been analysed elsewhere for a twin path fading input (4), and only a brief résumé will be given here. A stringent requirement is placed on the specification of the pilot tone bandpass filter, which is designed to be just wide enough to pass the incoming pilot reference spectrum with negligible amplitude or phase distortion. Accurate time delay matching between the numerator and denominator paths is essential and, consequently, a linear phase filter must be employed. Furthermore, for the circuit to accurately estimate the depths of fade, a filter with very low passband ripple is required. For instance, in order to suppress a 30 dB input fade to 3 dB or less residual output modulation, then the maximum allowable passband ripple is .16 dB (4). Noise entering the denominator path of the FFAGC circuit causes random envelope modulation of the output signal and output noise bursts when the signal fades into the noise at the circuit input. For a noisy input signal, there is a subjective improvement in incorporating a denominator threshold circuit. This results in the deepest parts of the fades passing through the circuit and reduces the corresponding noise bursts. A threshold level of 20 dB below the mean FFAGC input pilot level has been found suitable.

Amplitude and phase distortion in receiver filtering prior to the FFAGC circuit can, unless compensated for, seriously impair its performance. In particular, the group delay variation across the IF filter passband causes decorrelation between fading of the pilot and

fading of wanted information. The problem is particularly acute for signals positioned at the edges of the IF filter passband since, for such positioning, the group delay suffered by the signal can typically be twice as much as that experienced by a signal near the centre of the passband. Decorrelation between fades of the pilot and fades of the required modulation is also caused by the time delay spread in the multipath propagation medium (5). However, evidence suggests that, for the time delay spreads encountered in the field, there is little degradation of FFAGC peformance for all practical values of pilot tone to modulation component frequency spacing (4, 6).

Past analysis of FFAGC performance (4) is only strictly applicable to non-phaselocked receivers, where the pilot tone can be fully extracted from the speech information. The following section identifies a mechanism for FFAGC degradation due to the presence of phaselocked AFC and the remainder of this chapter considers the limitations this places on a FFAGC system which is perfect in other respects. Therefore, unless otherwise stated, the following assumptions will be made. Perfect time delay matching between the numerator and denominator paths of the FFAGC circuit is assumed and the bandpass filter is taken to be a 'brickwall' type with zero passband ripple and a centre frequency equal to the nominal frequency of the demodulated pilot, ω_r. Amplitude and phase distortion of the IF filter are ignored, as is any decorrelation between fades of the pilot and fades of the modulation. A noiseless fading input is assumed and no FFAGC threshold is incorporated.

6.2 The behaviour of a coupled PLL/FFAGC system in fading

A block diagram of the PLL/FFAGC receiver system considered in this chapter is shown in figure 6.1. It is similar to the phaselocked receivers discussed in chapter 2, with the addition of the FFAGC circuit at the demodulator output. Although the feedback AGC circuitry is not shown for clarity, its use is essential in maintaining the mean envelope level of the demodulated pilot constant. In this respect, it is assumed that the receiver's feedback AGC has no effect on the short term fading envelope.

Firstly, let us neglect the effect of the PLL by considering the control to the first local oscillator to be disconnected, with both local oscillators running at their correct centre frequencies. The demodulated pilot tone at the SSB detector output, $v_g(t)$, is then of the form:

$$v_g = Cr(t) \sin(\omega_r t + \theta(t)) \qquad (6.1)$$

where $r(t)$ and $\theta(t)$ represent the multipath induced envelope and phase variations respectively, and C is a constant. Figure 6.2 shows a typical spectrum of the demodulated pilot in the presence of neighbouring modulation, the spectrum of each component being spread to a well defined width of twice the maximum Doppler frequency. Provided the pilot is correctly positioned in the linear phase FFAGC bandpass filter, it can be extracted from the information components without distortion and $r(t)$ can be obtained. As described in section 5.4, the demodulated output, $x(t)r(t)$, is then divided by $r(t)$ to give the required FFAGC output, $x(t)$.

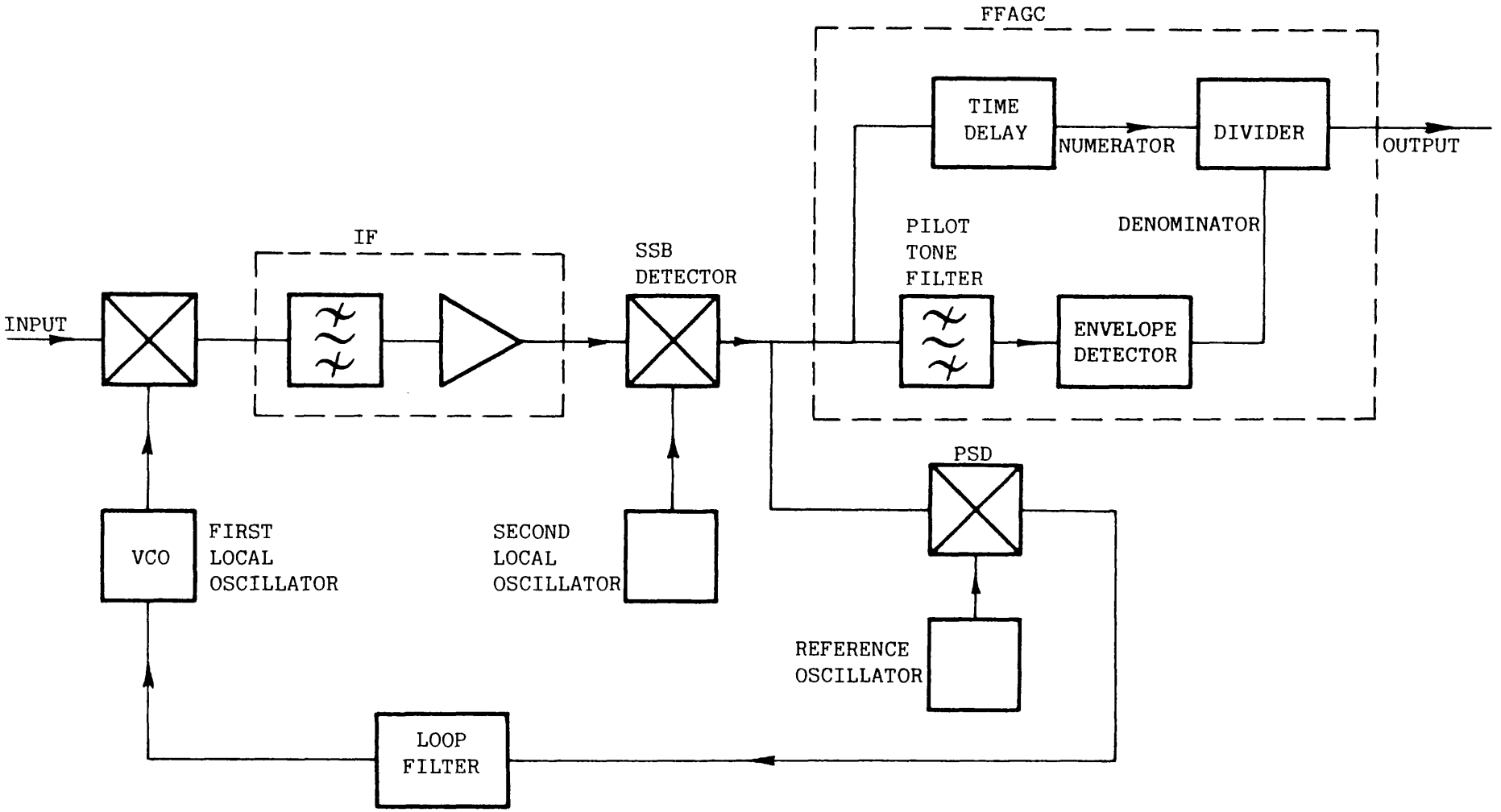

Figure 6.1 Phaselocked SSB receiver with FFAGC

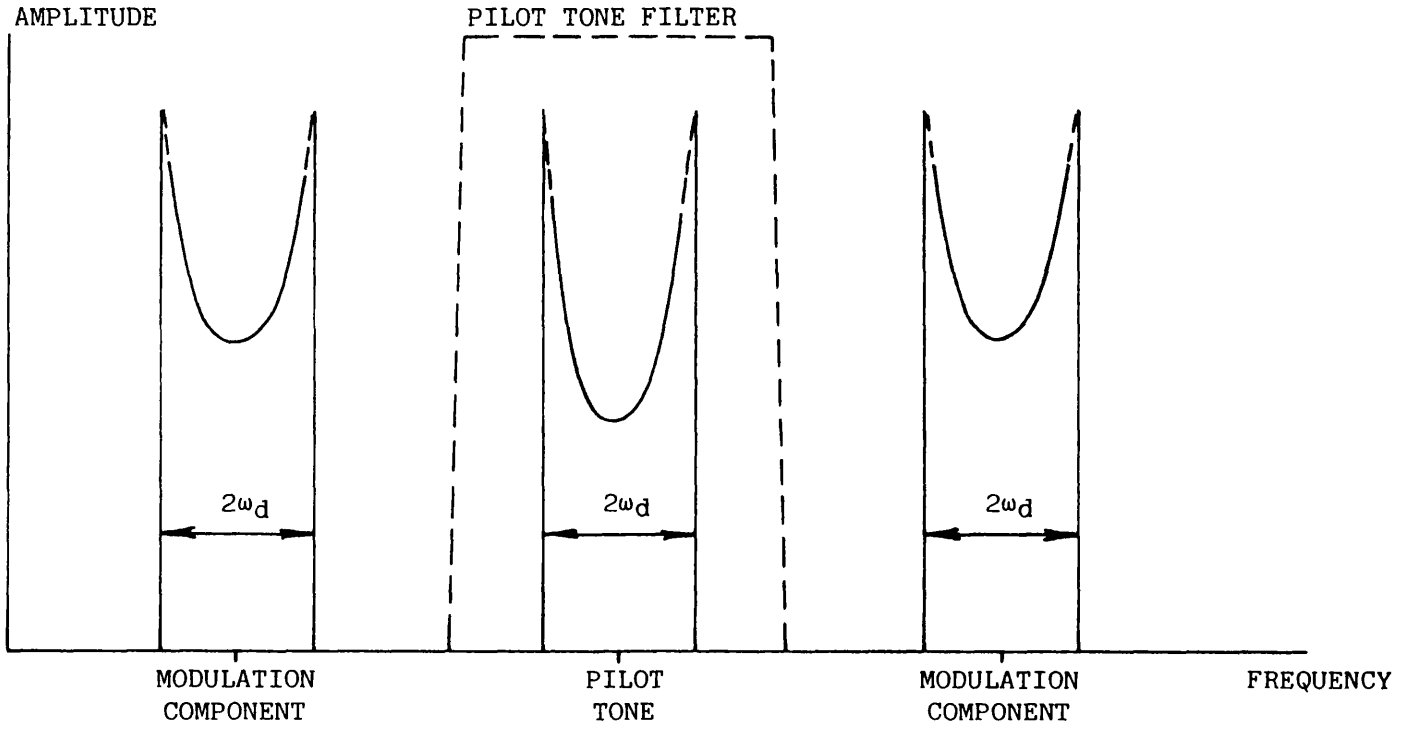

Figure 6.2 Demodulated spectrum

It is clearly the purpose of an AFC system to ensure that the demodulated pilot is correctly positioned within the FFAGC bandpass filter, so we now consider the PLL to be reconnected and tracking the received pilot. The demodulated pilot is now of the form:

$$v_g' = Cr(t) \sin(\omega_r t + \theta_e(t)) \qquad (6.2)$$

where $\theta_e(t)$ is dependent or $r(t)$, $\theta(t)$ and the PLL parameters. The spectrum of the demodulated pilot is no longer confined to twice the maximum Doppler frequency and the FFAGC bandpass filter now distorts the pilot's envelope to, say, $r'(t)$. The FFAGC output is now $r(t)x(t)/r'(t)$ and multipath envelope distortion remains. In order to ascertain the magnitude of this degradation, a computer simulation of a combined PLL/FFAGC system was undertaken and is now described.

6.3 Computer simulation of a coupled PLL/FFAGC system

For the purposes of this simulation, the received signal was taken to consist solely of the pilot. The twin path scattering model described in section 5.3 was employed, such that the received pilot was of the form:

$$v_i(t) = E(\sin \omega_i t + R \sin \omega_i' t)$$
$$0 < R < 1 \qquad (6.3)$$

where ω_i and ω_i' are the frequencies of the two received components. Expressing $v_i(t)$ as a phase and amplitude modulated carrier in the form:

$$v_i(t) = r(t) \sin(\omega_i t + \theta_i(t)) \qquad (6.4)$$

we obtain:

$$r(t) = E(1 + R^2 + 2R\cos\omega_f t)^{1/2} \qquad (6.5)$$

$$\theta_i(t) = \tan^{-1}\left(\frac{R\sin\omega_f t}{1 + R\cos\omega_f t}\right) \qquad (6.6)$$

where ω_f is the frequency spacing between the two tones, variable up to twice the maximum Doppler frequency, $2\omega_d$. These input amplitude and phase variations are depicted in figure 6.3 for values of R of .698, .818 and .894. These correspond to fade depths of 15 dB, 20 dB and 25 dB respectively.

The PLL natural frequency and damping factor are dependent on the input amplitude. For the purpose of this chapter and the next, these parameters are defined as the values obtained with a single tone input which has the same mean envelope level as the fading input signal. The nonlinear equation for a second order type two loop was solved using the Runge-Kutta-Nystrom method (7). The effect of the IF filter characteristic on the loop equation was ignored. The solution continued until a steady state was reached, i.e. until the loop phase and frequency errors became periodic. This involved comparing the values of loop phase and frequency error at the end of each input period with those at the beginning. If the corresponding values coincided to within a given degree of accuracy, then this period was assumed to contain the steady state solution. The degree of accuracy was chosen so as to give negligible error in the final outcome of the simulation. In other words, the simulation was run repeatedly until further accuracy had little effect on the results. A similar approach was taken in choosing the number of steps which were computed over one input period. The step size was reduced until further reduction had negligible effect on the outcome of the simulation.

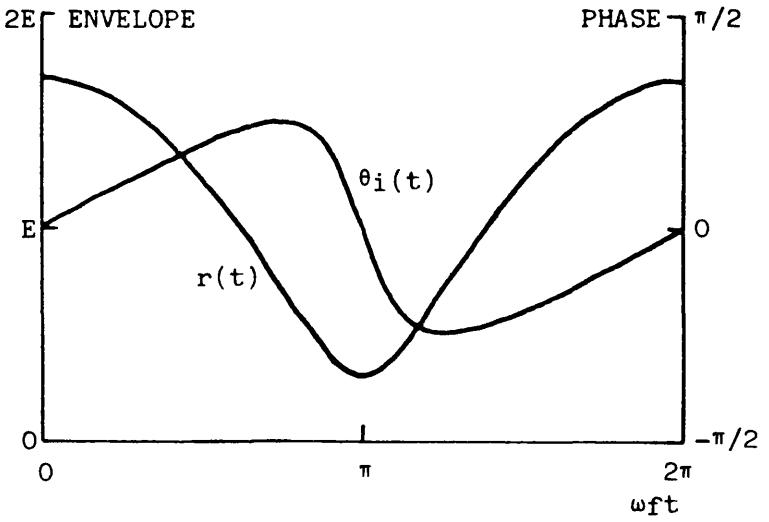

(a)
15 dB fade

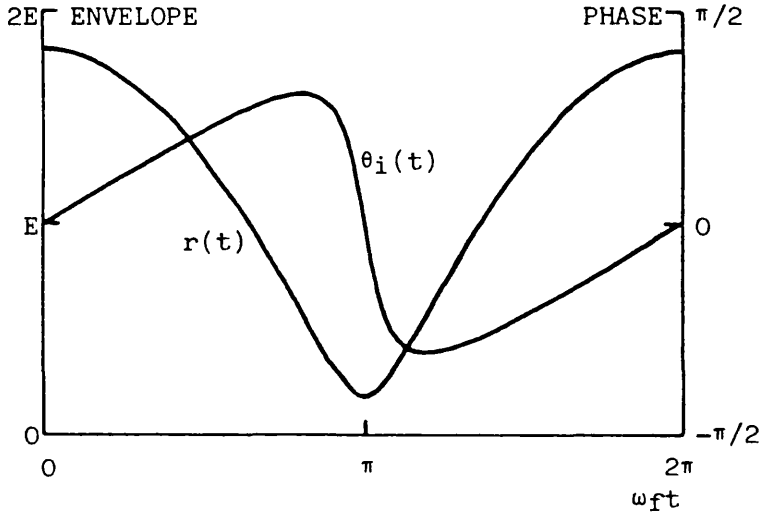

(b)
20 dB fade

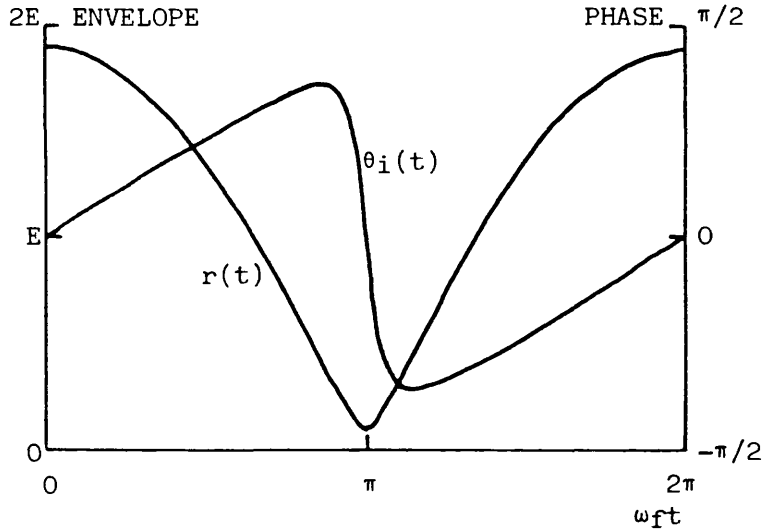

(c)
25 dB fade

Figure 6.3 Twin path envelope and phase variations

Referring to figure 6.2, if the PLL behaved as an ideal AFC loop and, in the steady state, centred the demodulated pilot within the FFAGC bandpass filter without spreading its spectrum, then the minimum permissable width of the bandpass filter would be $2\omega_d$. However, it is known from preliminary work in the field that even very low bandwidth PLLs, which do not appreciably spread the fading spectrum, do not centre the spectrum within the bandpass filter. In fact, the loop tends to track individual components of the fading signal and, in order for the whole spectrum to be contained within the filter, the minimum bandwidth required is $4\omega_d$. Therefore, this filter bandwidth was used in the simulation. The brickwall bandpass filter was modelled by its equivalent lowpass filter (8) of bandwidth equal to half that of the bandpass filter. The filter was simulated by a fast Fourier transform (FFT), followed by removal of outlying harmonics and an inverse FFT. The number of samples used in the FFT was equal to the number of steps computed over one input period by the Runge-Kutta-Nystrom routine. FFTs were performed on $r(t) \cos\theta_e$ and $r(t) \sin\theta_e$. Having removed the appropriate harmonics, $r'(t) \cos\theta_e$ and $r'(t) \sin\theta_e$ could be obtained. These were then squared, added and squarerooted to yield $r'(t)$, the distorded envelope. In the final stage of the simulation, the original envelope, $r(t)$, was divided by $r'(t)$. The maximum and minimum values of $r(t)/r'(t)$ over one period were found and their ratio is the required residual output modulation. The simulation was written in FORTRAN on a Honeywell 68 computer running the Multics operating system.

The main results are presented in figures 6.4 to 6.6. Each figure represents a single fade depth and illustrates the residual output modulation as a function of the normalized tone frequency spacing,

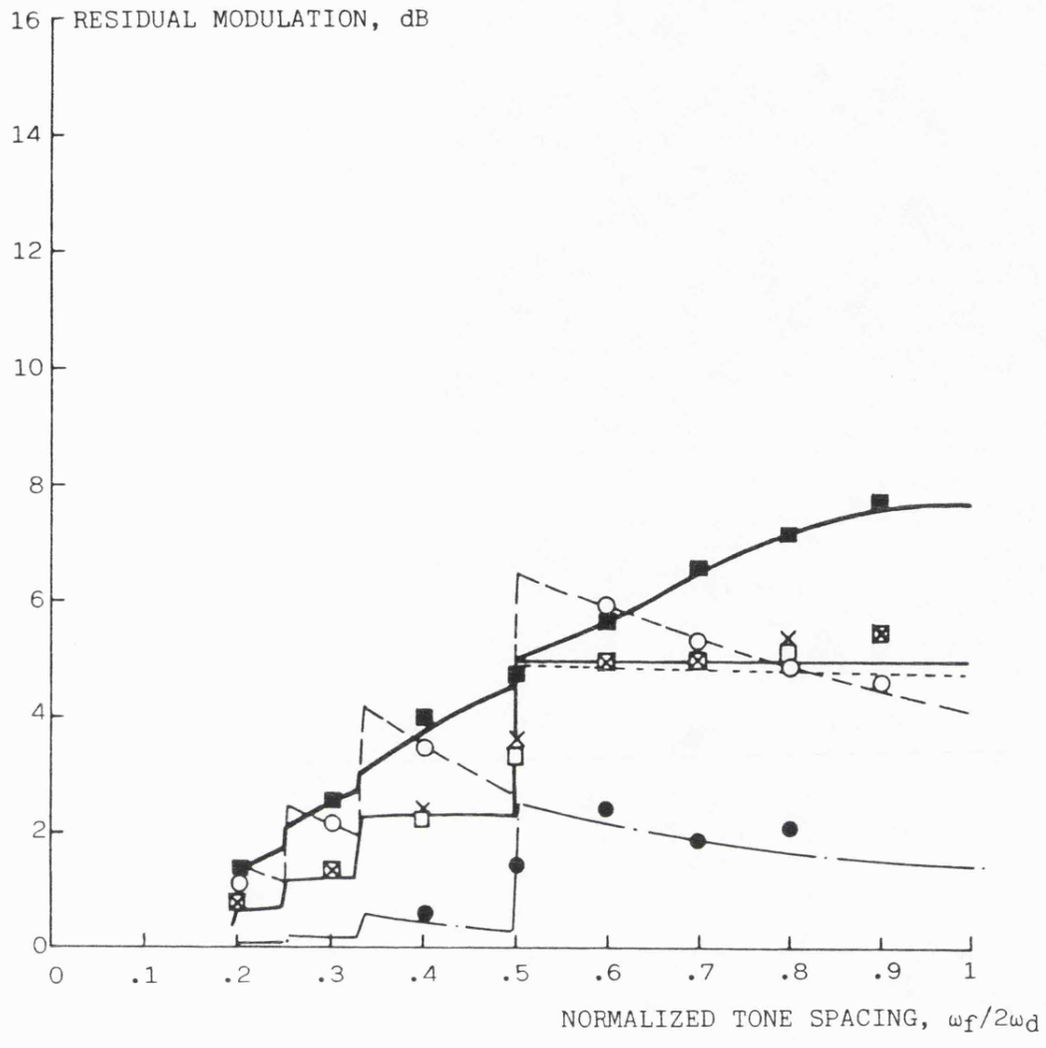

$\omega_n/2\omega_d$	SIMULATION RESULTS	EXPERIMENTAL RESULTS
.1	- ——— -	●
.33	— — — —	○
1	———	■
3.3	- - - - - - -	□
10	———	×

Figure 6.4 Residual output modulation, 15 dB input fade

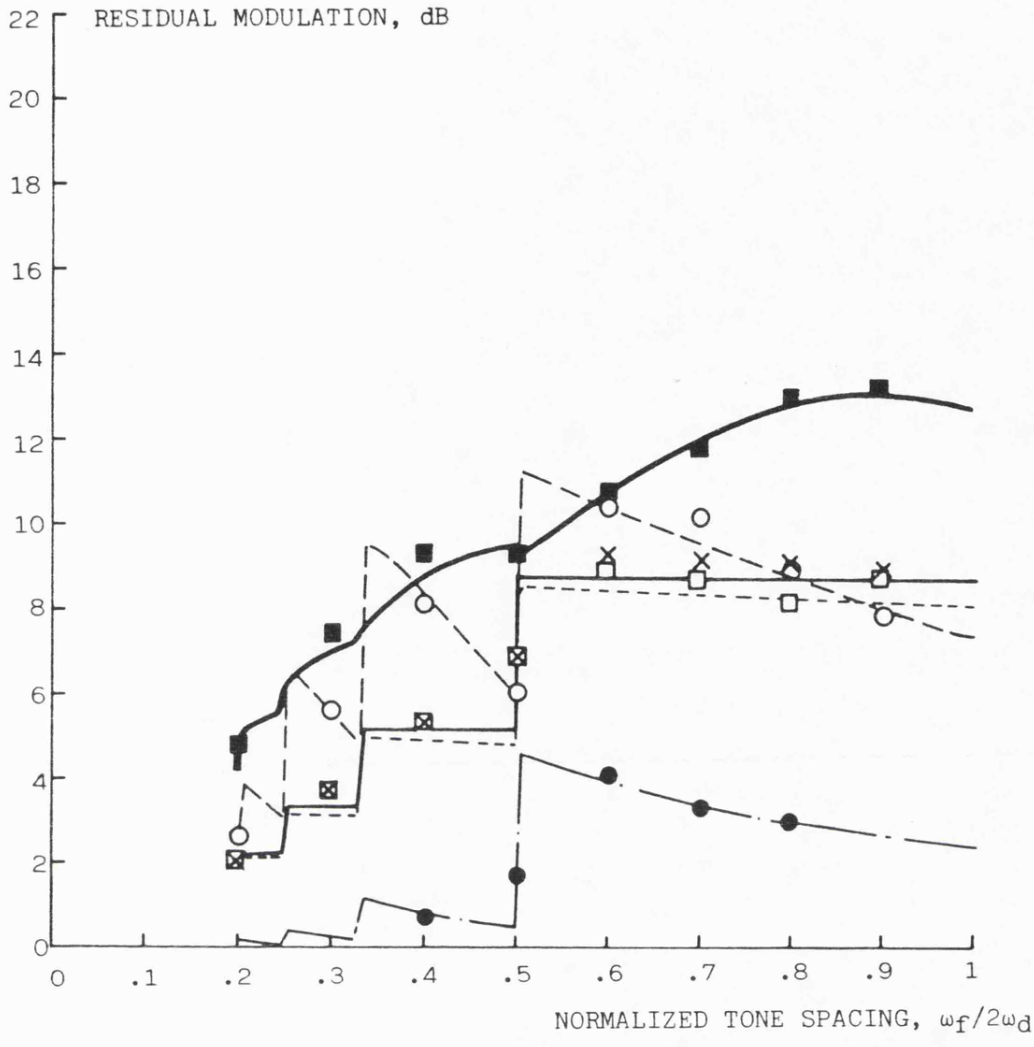

$\omega_n/2\omega_d$	SIMULATION RESULTS	EXPERIMENTAL RESULTS
.1	- ——— -	●
.33	— — — —	○
1	———	□
3.3	- - - - - - - -	□
10	———	×

Figure 6.5 Residual output modulation, 20 dB input fade

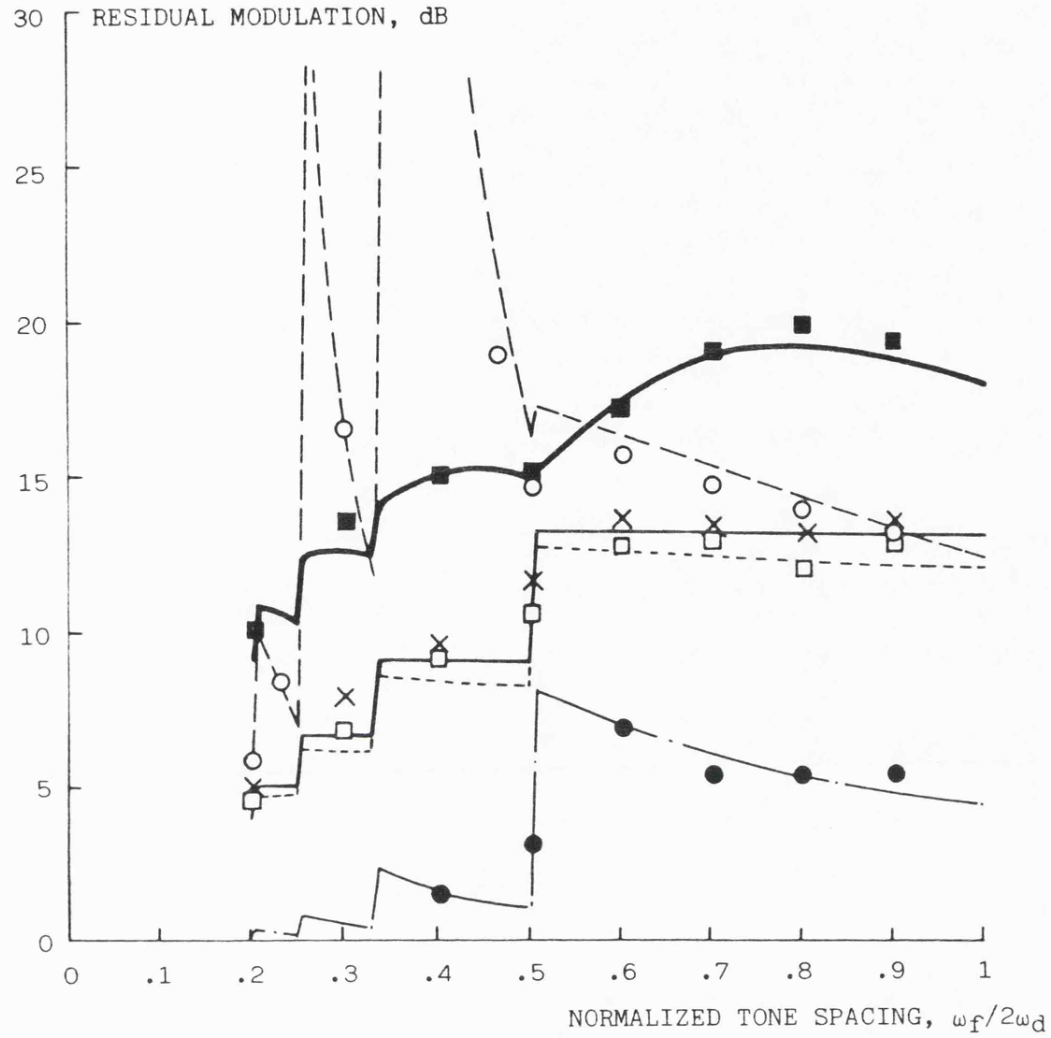

$\omega_n/2\omega_d$	SIMULATION RESULTS	EXPERIMENTAL RESULTS
.1	———	●
.33	– – – –	○
1	———	■
3.3	·····	□
10	———	×

Figure 6.6 Residual output modulation, 25 dB input fade

$\omega_f/2\omega_d$, for various values of normalized PLL natural frequency, $\omega_n/2\omega_d$. The PLL damping factor was fixed at $1/\sqrt{2}$. For low values of $\omega_f/2\omega_d$, there is little output modulation. This is because most of the significant harmonics of the demodulated pilot are contained within the bandpass filter which, consequently, has little effect on the pilot's envelope. However, as $\omega_f/2\omega_d$ is increased, harmonics of the demodulated pilot are removed and the envelope is distorted giving rise to high residual modulation at the FFAGC output. For instance, for $\omega_f/2\omega_d$ between .5 and 1, there are only three components within the bandpass filter, at frequencies of ω_r and $\omega_r \pm \omega_f$. The step changes in the curves are due to the assumption of a perfect brickwall bandpass filter. A somewhat surprising result is that the residual modulation is generally greatest for the case $\omega_n/2\omega_d = 1$ and reduces for larger PLL bandwidths. This trend was observed for other fade depths. In figure 6.6 the possibility of modulation enhancement is shown when $\omega_n/2\omega_d = .33$. Figure 6.7 illustrates the shape of some simulated FFAGC output envelope variations for three values of $\omega_n/2\omega_d$. These plots are for an input fade depth of 20 dB and with ω_f set to $2\omega_d$.

6.4 Experimental verification

Experimental measurements, with a two tone test signal, were made so as to verify the simulation results. For this purpose the circuit shown in figure 6.8 was constructed. To avoid the necessity of using an IF within the PLL, and a tone extraction bandpass filter, the equivalent lowpass circuit was implemented (8). The two lowpass filters at the PSD and quadrature PSD outputs, with cut-off frequencies of $2\omega_d$, are the

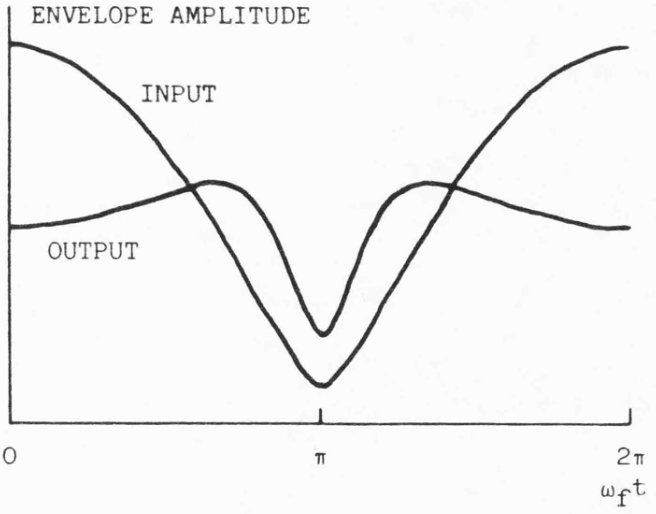

(a)
$\omega_n/2\omega_d = 10$

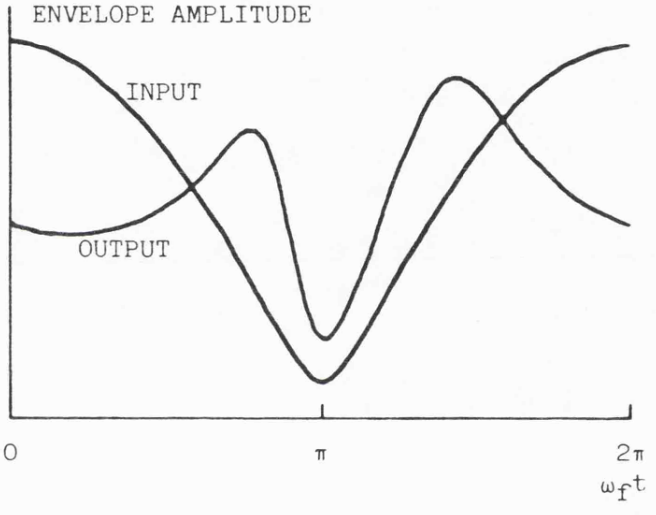

(b)
$\omega_n/2\omega_d = 1$

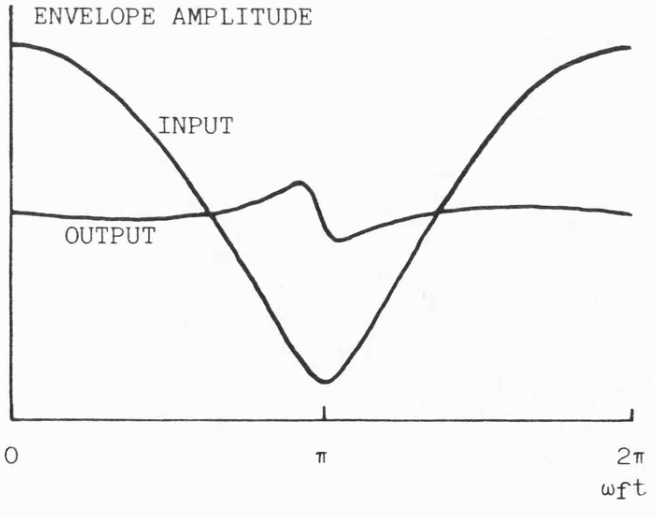

(c)
$\omega_n/2\omega_d = .1$

Figure 6.7 PLL/FFAGC simulation response for 20 dB input fade depth and $\omega_f = 2\omega_d$

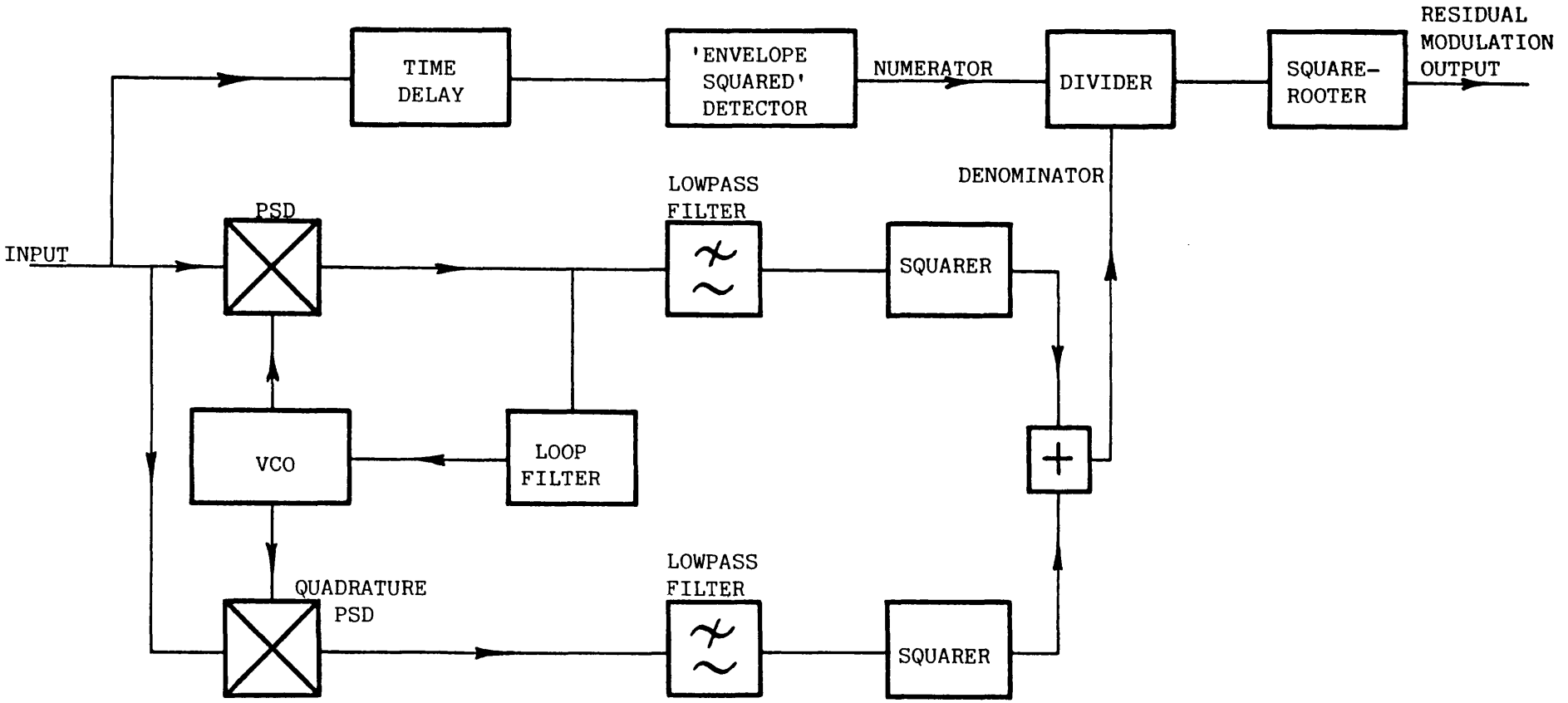

Figure 6.8 Experimental PLL/FFAGC system

lowpass equivalents of a symmetrical bandpass filter of bandwidth $4\omega_d$ centred at the IF. The PLL input consisted of the summed signal from two audio signal generators. The frequency of one was set to 1.67 kHz, the nominal VCO centre frequency, and the frequency of the second was variable, up to a maximum spacing of $2\omega_d$ from 1.67 kHz. The input signal was passed through a time delay element and then its squared envelope, $r^2(t)$ was obtained. This signal fed the numerator input of an analogue divider. Signals proportional to $r(t) \sin\theta_e$ and $r(t) \cos\theta_e$ were produced at the outputs of the PSD and quadrature PSD respectively. These were lowpass filtered to produce $r'(t) \sin\theta_e$ and $r'(t) \cos\theta_e$. When these signals were squared and added, the square of the distorted envelope was obtained and became the divider's denominator input. The divider output was therefore proportional to $r^2(t)/r'^2(t)$, and the FFAGC output residual modulation could be observed at the squarerooter output.

The PLL circuitry has been described previously in section 3.3.1. The linear phase lowpass filters were implemented using type R5602-1 transversal charge transfer devices, each with a 3 dB bandwidth of $2\omega_d$ equal to 30 Hz. The filters possessed a passband ripple of less than .2 dB and their response was 1 dB down at 28 Hz and 20 dB down at 36 Hz. They were clocked at 1 kHz via a variable ratio divider from a 4.13 MHz master crystal oscillator. These filters were preceded and followed by 100 Hz fourth order Butterworth anti-aliasing filters. The squarers were implemented with type AD534JD analogue multipliers. A bucket brigade analogue delay line, type SAD4096, was incorporated in the numerator path to match the delay between the numerator and denominator processing. Its clock frequency was also derived from the 4.13 MHz master oscillator, and it was preceded and followed by 6 kHz fourth

order Butterworth filters. The 'envelope squared' detector consisted of a type AD534JD analogue multiplier followed by a 250 Hz fourth order Butterworth filter. The divider was implemented by a type 436B precision analogue divider and another type AD534JD was used to perform the squareroot operation. The Butterworth filters and the remaining circuitry were designed using standard operational amplifier techniques.

The overall dynamic range of the circuit was about 30 dB. Figure 6.9 illustrates the measured circuit performance with no PLL. For this purpose, the connection between the VCO and the loop filter was broken and the VCO was maintained at its nominal centre frequency of 1.67 kHz. The frequency of the larger input tone was also fixed at this value. The measurements were taken for fade depths of 15 dB, 20 dB and 25 dB, and for several values of normalized tone spacing, $\omega_f/2\omega_d$. The rapid deterioration in performance for normalized tone spacings above about .9 is due to the roll-off of the transversal lowpass filters. The experimental results obtained with the PLL reconnected and tracking the input are shown in figures 6.4 to 6.6, for comparison with the simulation results. It can be seen that there is good agreement between the two sets. The experimental points are not shown when the roll-off of the lowpass filters contributed largely to the residual output modulation.

6.5 Field trials of the coupled PLL/FFAGC system

A series of field trials were undertaken so as to investigate the performance of the coupled PLL/FFAGC system in the true multipath environment. A pilot tone was transmitted at UHF from a fixed location

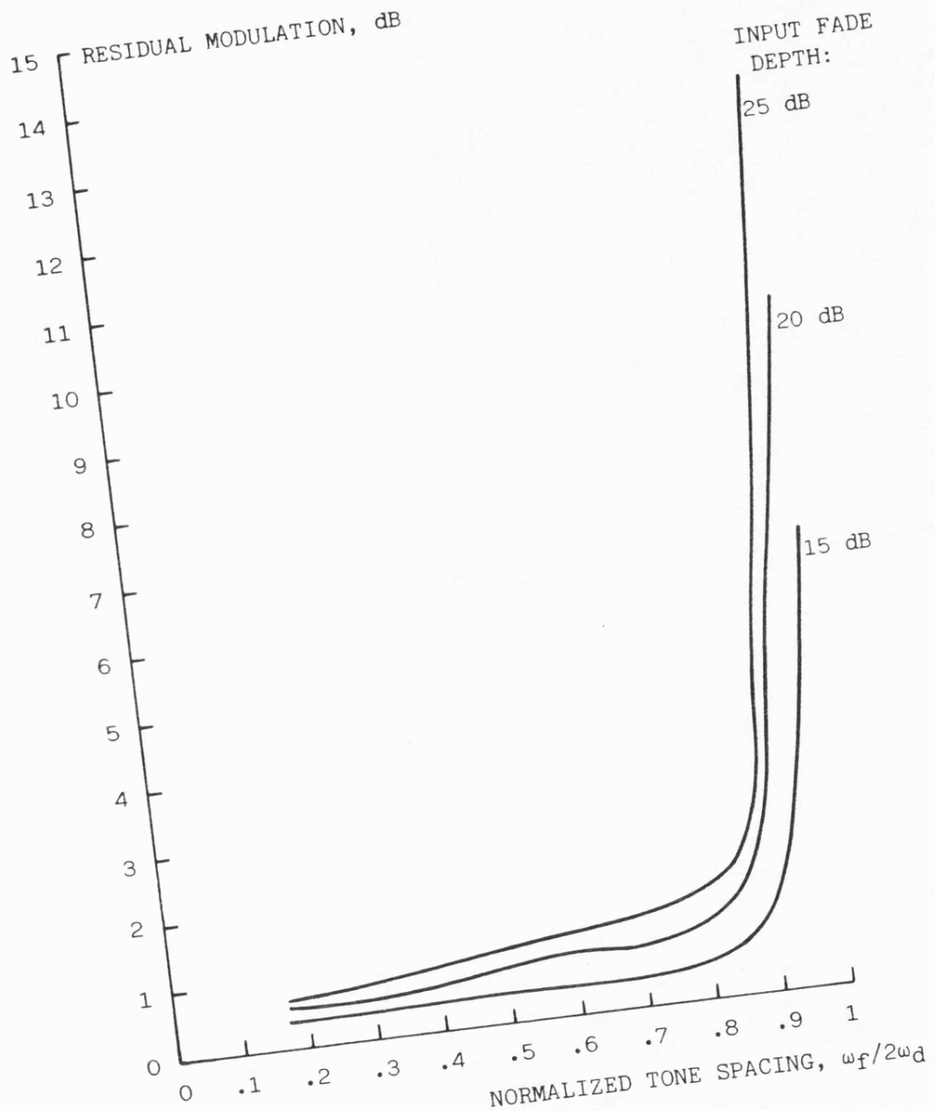

Figure 6.9 FFAGC circuit performance, without PLL

and audio recordings of the tone were obtained by means of a mobile frequency translating receiver. A non-phaselocked SSB receiver could be used for this purpose as the demodulated output consists of the frequency translated input signal with the multipath amplitude and phase information preserved. The recordings could then be played back through the coupled PLL/FFAGC system in the laboratory. A description is now given of the UHF radio system used for the trials and this is followed by details of the field trial recording procedure. Finally, the laboratory tests are described and results illustrating the PLL/FFAGC system performance are presented.

6.5.1 UHF system

The UHF system employed has been fully described elsewhere (9) and, consequently, only brief details will be given here. It essentially comprised of a SSB tone-in-band transmitter and receiver operating at 456.925 MHz. The transmitted signal consisted solely of a pilot tone of high frequency stability. The transmitter aerial was a 6 dB collinear mounted on the roof of the Wolfson laboratory, University of Bath. A similar aerial was used for receiving and was mounted on the roof of a Volvo estate car. The receiver was placed inside the car and contained a single 10.7 MHz IF with a bandwidth of 3.65 kHz. The nominal frequency of the demodulated pilot tone was 1672 Hz. The receiver's first local oscillator was a voltage controlled ovened type, while the second was temperature compensated. The long loop phaselocked AFC system incorporated in the receiver was disconnected for these trials and the local oscillator frequencies were adjusted manually to their nominal values. There was negligible frequency drift of the local oscillators over the

period of each trial.

Receiver feedback AGC of the input-signal-level-invariant type (10) was employed with a loop bandwidth set at 1 Hz. This low value of bandwidth was chosen so that the feedback AGC would have negligible effect on suppressing the multipath fading (10).

6.5.2 Field trial recording procedure

The field trial route chosen was in a suburban area of Bath, near to the University and is shown in figure 6.10. The receiver's demodulated output was recorded on an FM channel of a Tandberg, series 115D, instrumentation tape recorder. The recorder's direct input channel was used to record a running commentary of the field trial and a series of marker blips. The mean signal to noise ratio at the demodulator output was in the region of 50 dB or greater. This value was estimated from signal strength measurements obtained by Burrows (9) along the same route.

The field trial tapes were recorded with the vehicle travelling as near as possible to constant speed over the entire route. Recordings were made at speeds of 20 mph, 22 mph and 24 mph. These give values of twice the maximum Doppler frequency of 27 Hz, 30 Hz and 33 Hz respectively.

6.5.3 Coupled PLL/FFAGC performance

The field trial recordings were played back through the experimental PLL/FFAGC system described in section 6.4. However, in order to

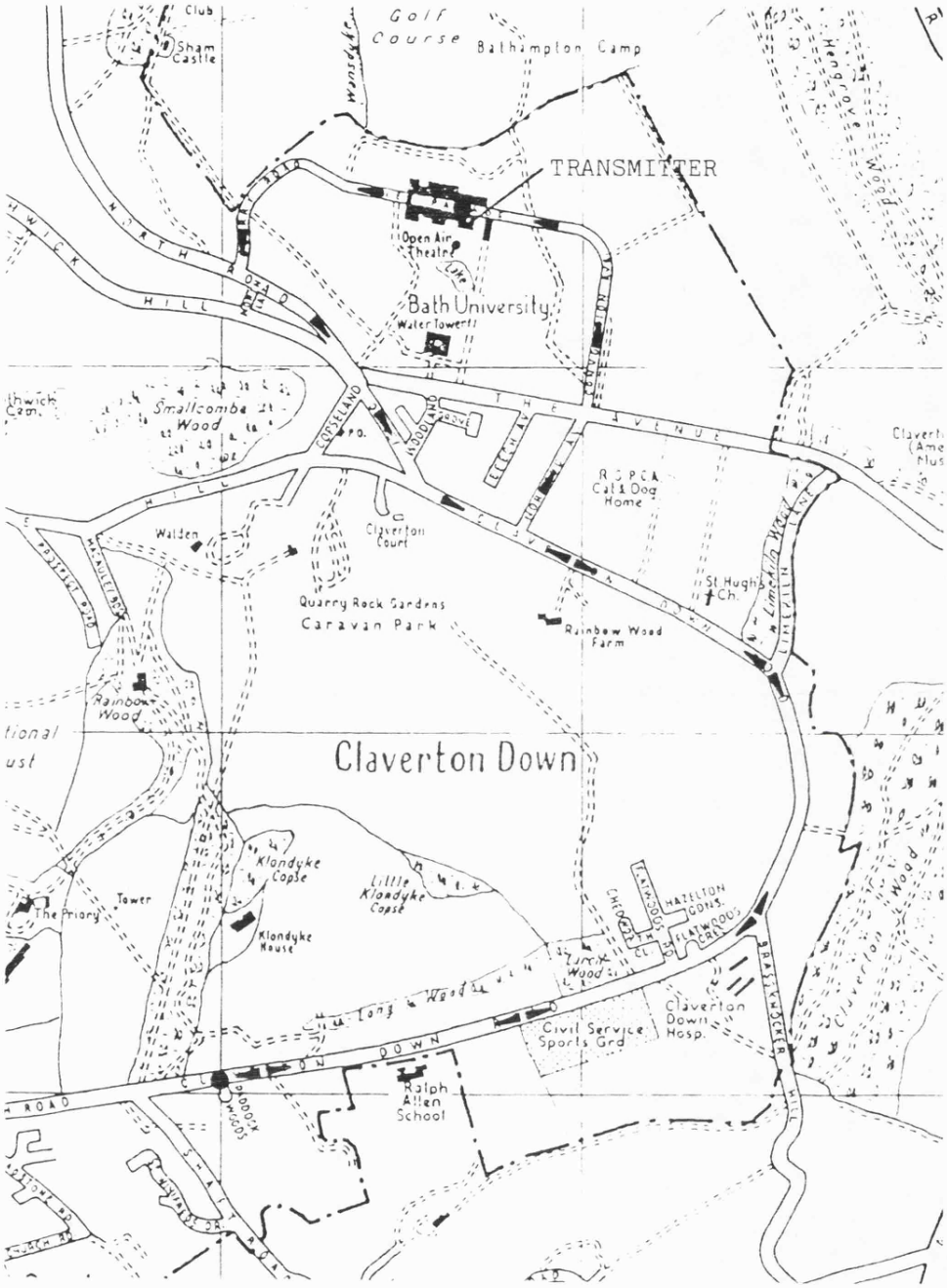

Figure 6.10 Field trial route, scale 1 : 15,000

ensure the mean level of the fading input was at the correct level for the PLL, it was first passed through an audio feedback AGC system with a 1 Hz bandwidth. This circuit was of the input-signal-level-invariant type and has been described elsewhere (11). For input signal levels ranging from .1 V to 10 V, the circuit maintained the mean level of the output envelope at .2 V. This was the correct level to feed the PLL input.

The results of four typical two second runs are shown in figures 6.11 to 6.14, each being obtained with a vehicle speed of 22 mph. The bottom curve of each figure shows the envelope of the received pilot. Above this is the FFAGC output envelope with the PLL disconnected and the demodulated tone remaining correctly positioned within the FFAGC filter. It can be seen that the multipath envelope variations are successfully removed by the FFAGC circuit. The top five curves on each of the figures show the PLL effect on the FFAGC output envelope. Values of .1, .33, 1, 3.3 and 10 were chosen for the PLL natural frequency normalized to twice the maximum Doppler frequency and the loop damping factor was fixed at $1/\sqrt{2}$. The results clearly indicate the severity of the degradation caused by the PLL and confirm the conclusion of the two tone simulation that the poorest fade suppression generally occurs for the case $\omega_n/2\omega_d = 1$.

As the speed of the vehicle could not be measured very accurately, it was necessary to ensure that the field trial results were not seriously effected by any error in measurement or slight changes of speed. To do this, the field trial recordings obtained at 20 mph and 24 mph were also played through the experimental PLL/FFAGC system. It was found that there was little noticeable variation of circuit

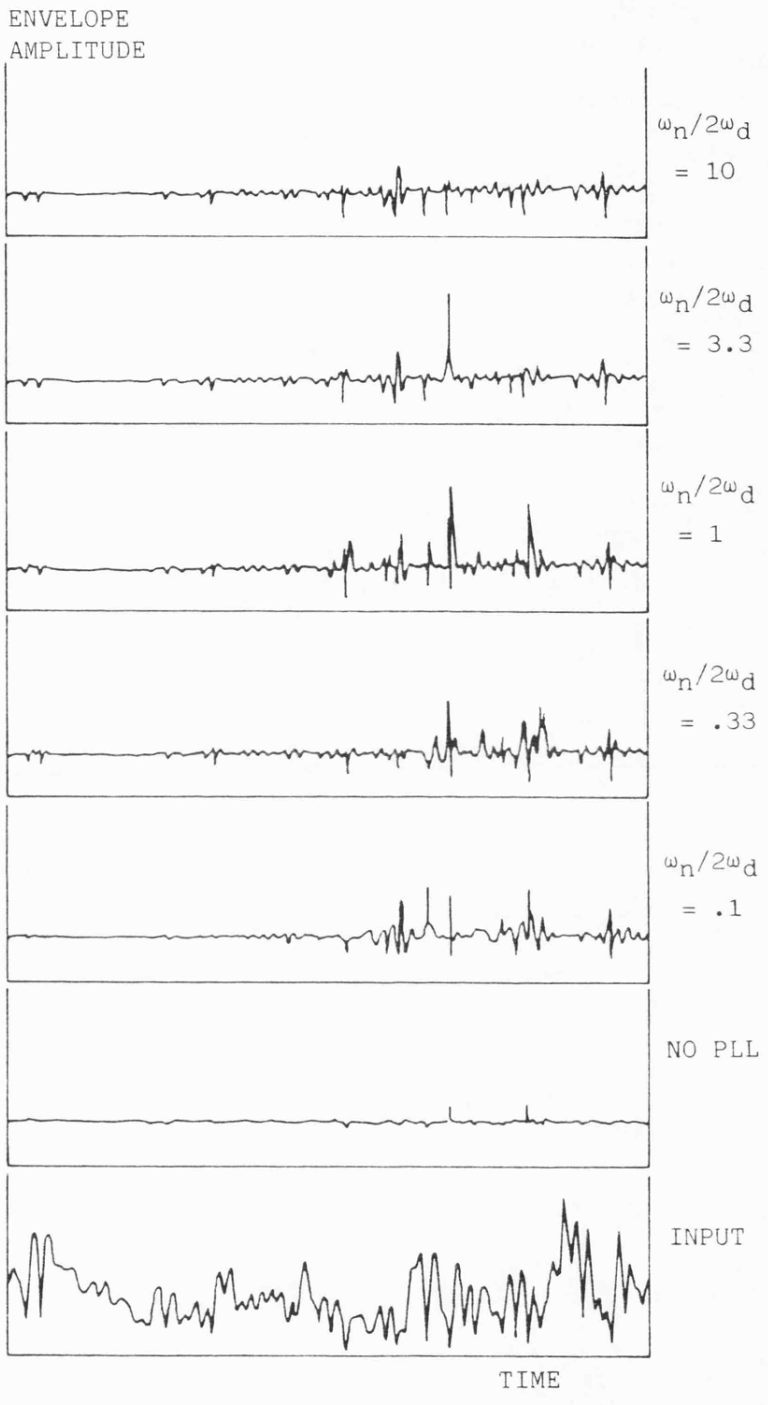

Figure 6.11 PLL/FFAGC field trial results

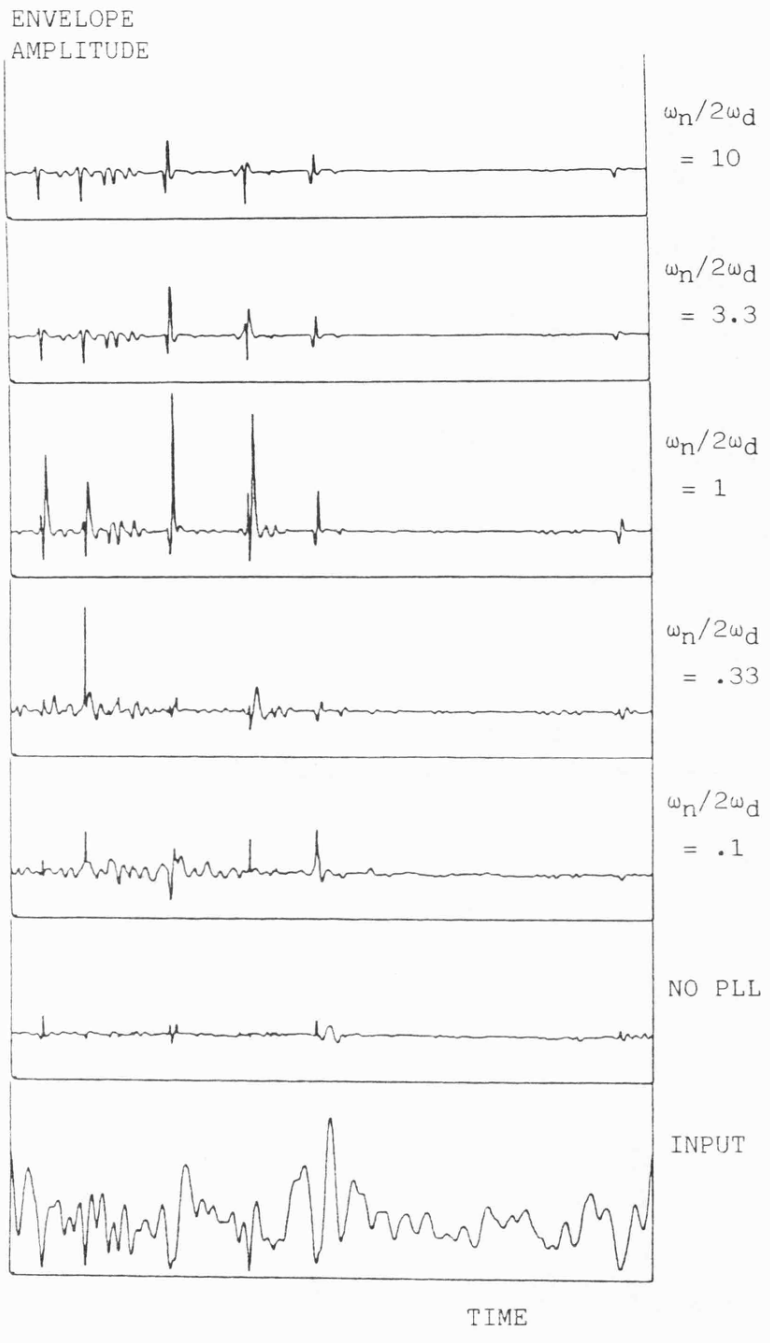

Figure 6.12 PLL/FFAGC field trial results

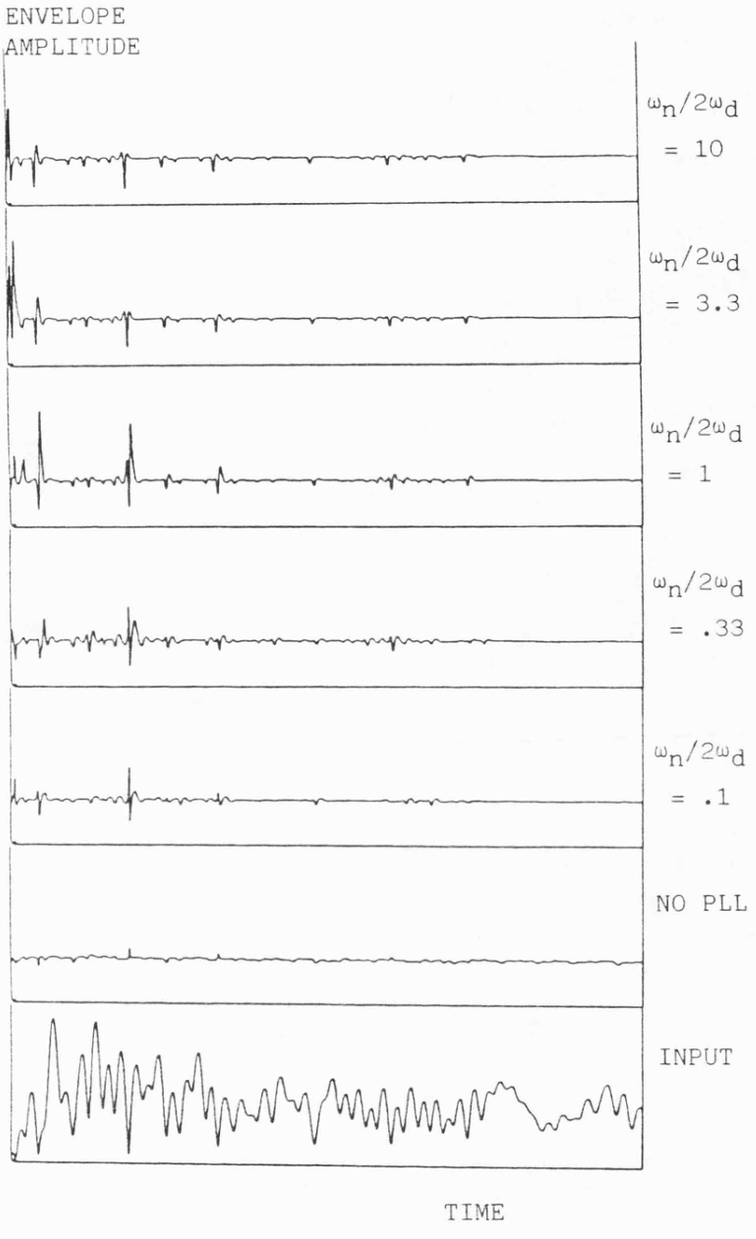

Figure 6.13 PLL/FFAGC field trial results

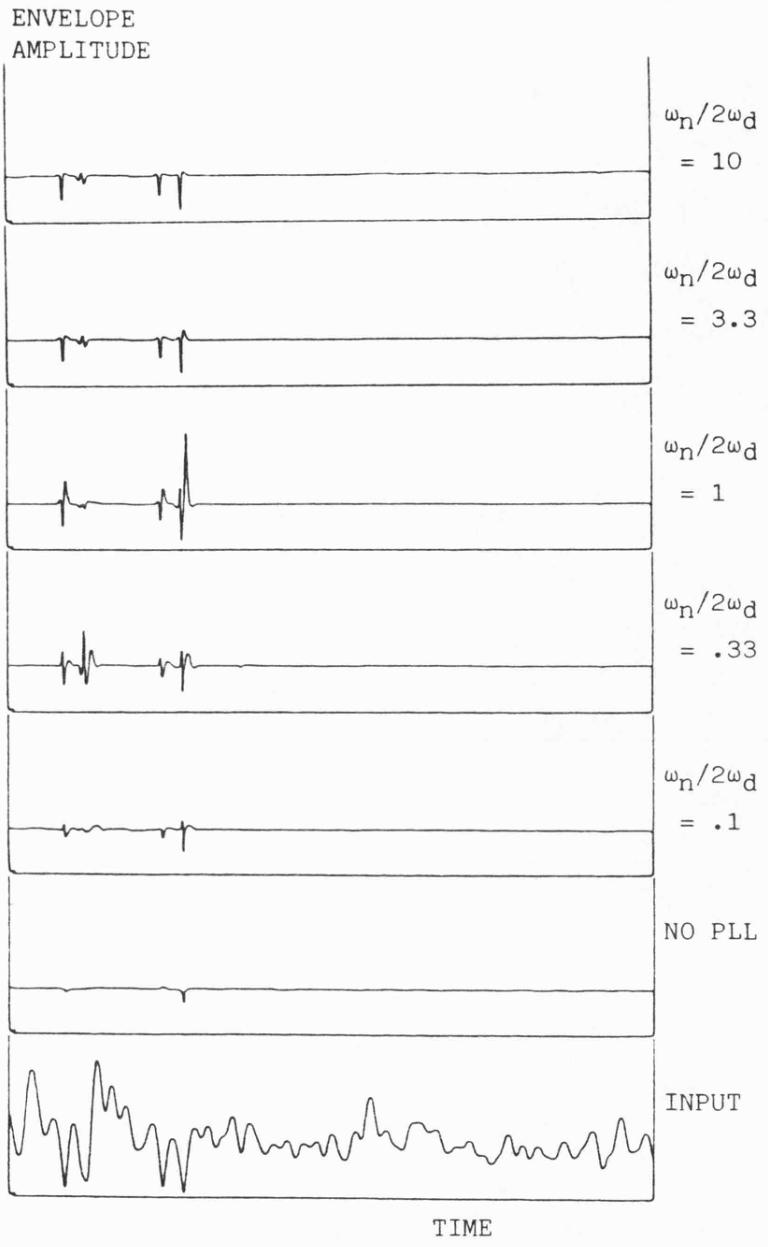

Figure 6.14 PLL/FFAGC field trial results

performance between the three tapes.

REFERENCES

1) Weber, W.J.: "Performance of phase-locked loops in the presence of fading communication channels", IEEE Trans., May 1976, Vol. COM-24, pp. 487-499.

2) Blanchard, A.: "Interferences in phase-locked loops", IEEE Trans., September 1974, Vol. AES-10, pp. 686-697.

3) Burrows, D.F., and McGeehan, J.P.: "Time delay in receiver AGC systems", Clerk Maxwell commemorative conference on radio receivers and associated systems, IERE, July 1981, pp. 73-78.

4) McGeehan, J.P., and Burrows, D.F.: "Performance limits of feedforward automatic gain control in mobile radio receivers", Proc. IEE, November 1981, Vol. 128F, pp. 385-392.

5) Jakes, W.C.: "Microwave mobile communications" (Wiley, 1974), chapter 5.

6) Leland, K.W., and Sollenberger, N.R.: "Impairment mechanisms for SSB mobile communications at UHF with pilot-based Doppler/fading correction", Bell System Technical Journal, December 1980, Vol. 59, pp. 1923-1942.

7) Kreysig, E.: "Advanced engineering mathematics" (Wiley, 1972), chapter 18.

8) Viterbi, A.J.: "Principles of coherent communication" (McGraw-Hill, 1966), chapter 2.

9) Burrows, D.F.: "Automatic gain control in mobile radio receivers", Ph.D. thesis, University of Bath, 1982, chapter 4.

10) McGeehan, J.P., and Burrows, D.F.: "Large signal performance of feedback automatic gain control systems", Proc. IEE, April 1981, Vol. 128F, pp. 110-117.

11) Burrows, D.F.: "Automatic gain control in mobile radio receivers", Ph.D. thesis, University of Bath, 1982, chapter 5.

CHAPTER 7

THE TRACKING PERFORMANCE OF NARROWBAND PHASELOCKED LOOPS IN A LAND MOBILE RECEIVER

In the previous chapter, it was shown that the use of phaselocked AFC could seriously impair the performance of receiver AGC. In order to obtain acceptable AGC performance it was necessary to employ a PLL with a bandwidth much narrower than twice the maximum Doppler frequency. However, if such a loop is used in a mobile receiver, it still remains to study its performance in tracking the nominal frequency of the received pilot. This subject has been alluded to by Burrows (1). His experimental observations indicate that the loop has difficulty in performing the task and gives frequency errors up to $\pm \omega_d$. However he gives no explanation of the loop's behaviour. In this chapter, insight is gained into the PLL's response by obtaining the Doppler frequency spectrum of the fading pilot. An experimental approach is taken throughout, with field trial data being collected for laboratory analysis.

Cox (2) has presented samples of the Doppler spectrum of a 910 MHz signal propagated to a vehicle moving through a suburban mobile radio environment. His results suggest that the received spectrum would often consist of a few major components which would persist for a significant length of time. With a fading pilot tone input of this form, it is not unlikely that a narrowband PLL would track individual components spaced up to $\pm \omega_d$ from the nominal pilot frequency. The experiment described below was designed so this behaviour could be demonstrated.

7.1 Field trial recording procedure

Recordings of a pilot tone demodulated in a mobile non-phaselocked SSB receiver were obtained. The equipment, technique and route used were the same as those described in section 6.5. However, the recordings were obtained with faster vehicle speeds. The results presented at the end of this chapter are for vehicle speeds of around 30 mph and 35 mph. These correspond to values of twice the maximum Doppler frequency of 41 Hz and 48 Hz respectively. The nominal frequency of the demodulated pilot was manually adjusted at the start of each recording. The frequency drift over the route was less than .5 Hz.

7.2 Experimental configuration for tracking study

The field trial recordings were played back through the 1 Hz feedback AGC circuit described in section 6.5.3 and into the audio PLL circuit described in section 3.3.1. The VCO input was monitored to give an indication of the VCO instantaneous frequency. This signal was passed through a 1 kHz fourth order Butterworth lowpass filter (to remove the PSD output sum term) and into the input of a digital storage oscilloscope sampling at 5 ms per point. Spectrum analysis of the fading pilot was obtained by means of a Bruel and Kjaer, type 2033, FFT analyser. The instrument has an input memory of 10240 time samples and can perform an FFT on any selected 1024 sample section in this memory. It is therefore well suited to the analysis of non-stationary signals. Before entering the analyser, the PLL input signal was mixed down to a nominal frequency of 100 Hz using a stable signal generator and a type

AD534JD analogue multiplier. This enabled an analyser sampling frequency of 512 Hz to be chosen. The total time covered by 10240 samples was therefore 20 s and the FFT frequency line spacing was .5 Hz. For each 20 s of sampled data, 19 spectra were obtained by stepping the analyser's 1024 sample long Hanning time window by 512 samples. The oscilloscope and analyser were triggered simultaneously by marker blips on the commentary channel of the field trial tapes.

Storage and analysis of data were facilitated by means of a Hewlett Packard, type 9826, desk top computer, connected to both the oscilloscope and analyser through a HP-IB bus system. For each of the 20 s lengths of data, the computer was used to form a composite picture from the 19 spectra. One of these is shown in figure 7.1. Each spectrum covers a duration of 2 s with 1 s overlap. The linear amplitude scale is normalized to the voltage obtained from a non-fading signal with the same mean envelope level. The frequency scale is relative to the nominal frequency of the demodulated pilot. The multipath nature of the signal is evident, as is the existence of discrete components.

7.3 PLL tracking performance

Figures 7.2 to 7.9 illustrate the response of a 3 Hz PLL to 20 s duration sections of the field trial data. The upper diagrams depict the Doppler spectra and are similar in form to figure 7.1, with the addition of stars indicating the average of the VCO's instantaneous frequency for the 2 s duration of the FFT. An amplitude axis with a non-zero origin was chosen so that the VCO frequency indication would appear more clearly and so that the noise and distortion introduced by

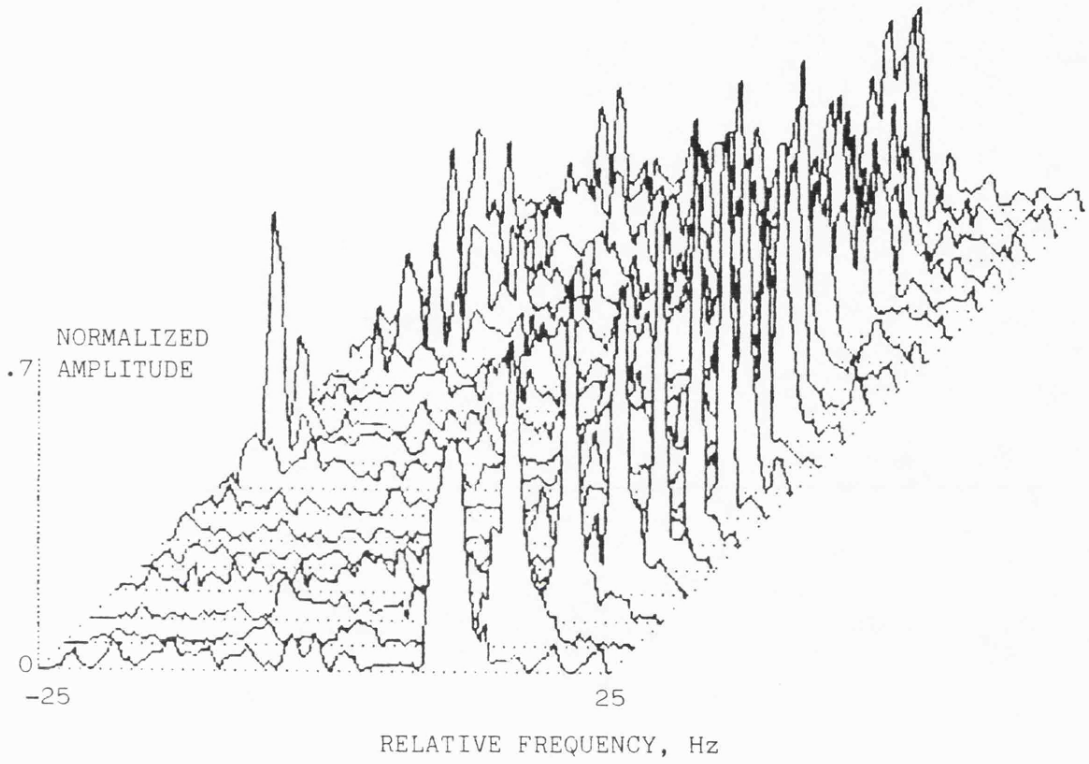

Figure 7.1 Doppler spectrum, 35 mph

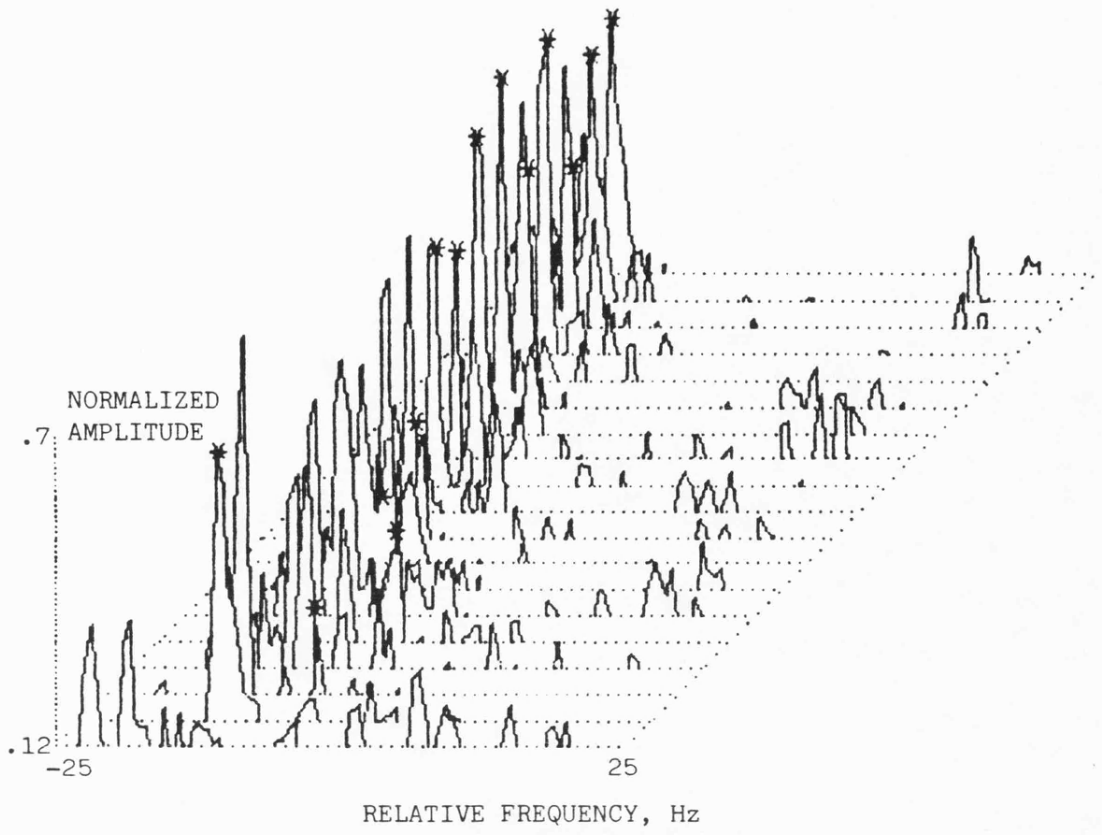

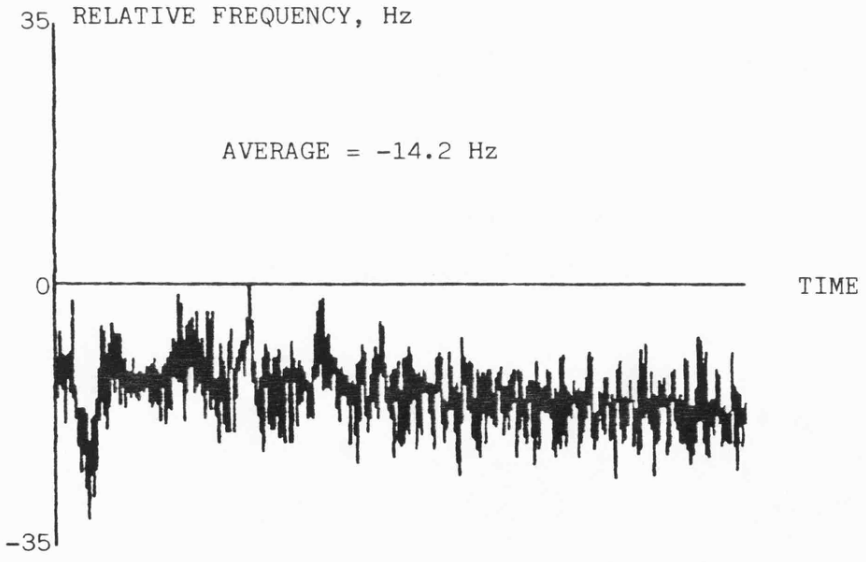

Figure 7.2 Tracking performance, 3 Hz loop, 30 mph

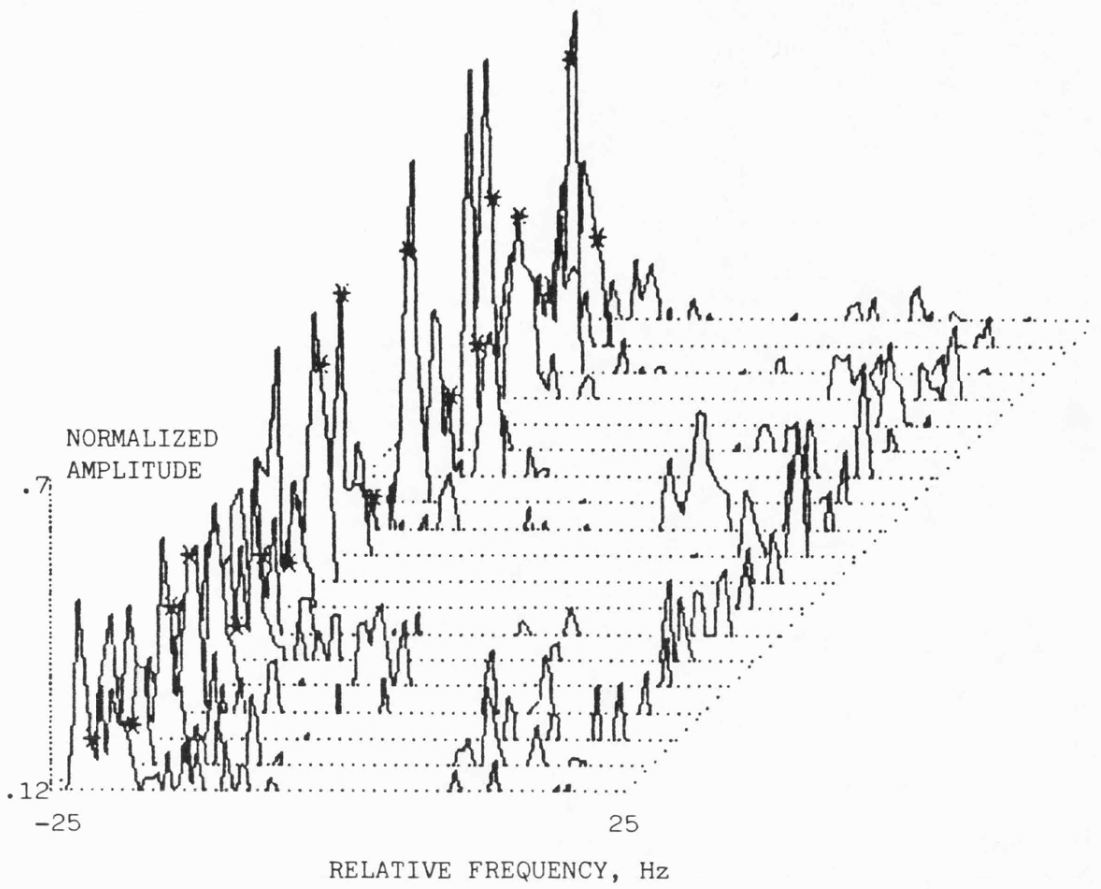

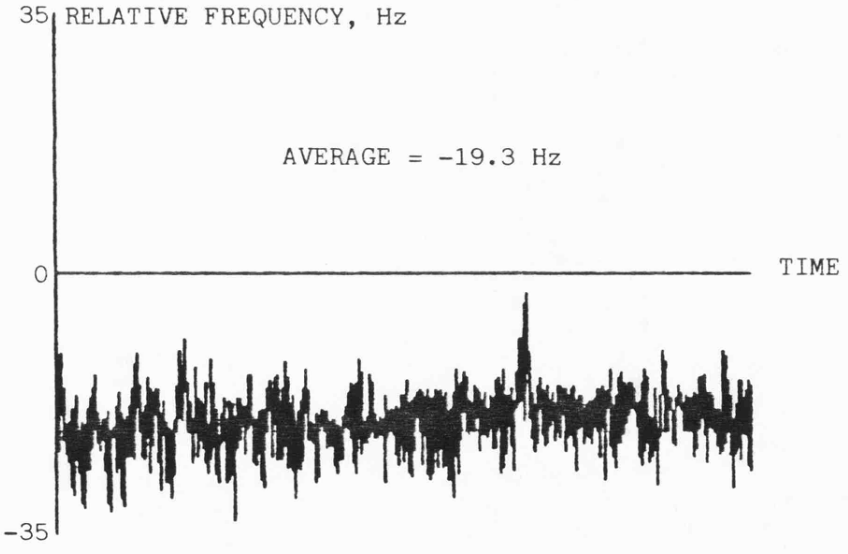

Figure 7.3 Tracking performance, 3 Hz loop, 30 mph

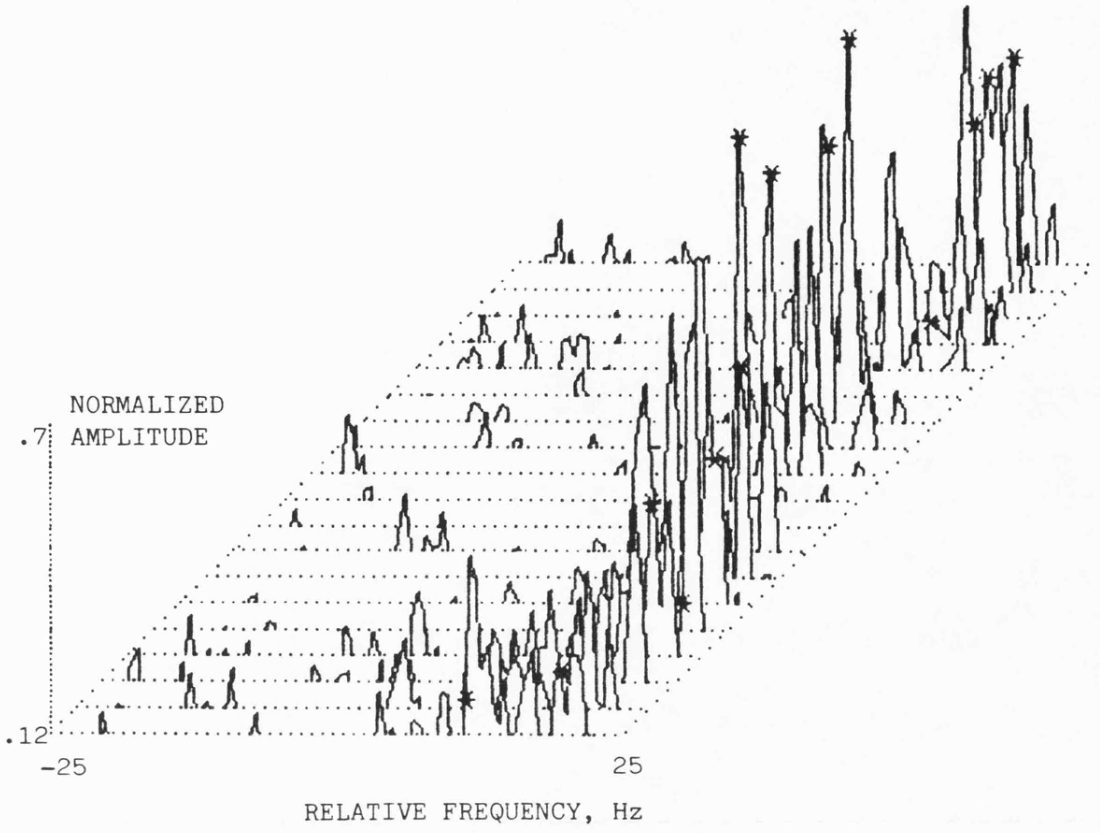

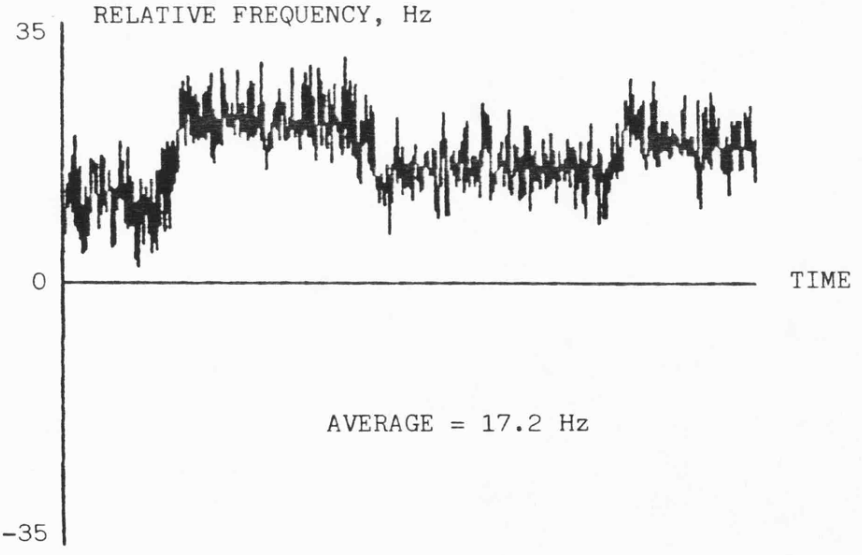

Figure 7.4 Tracking performance, 3 Hz loop, 35 mph

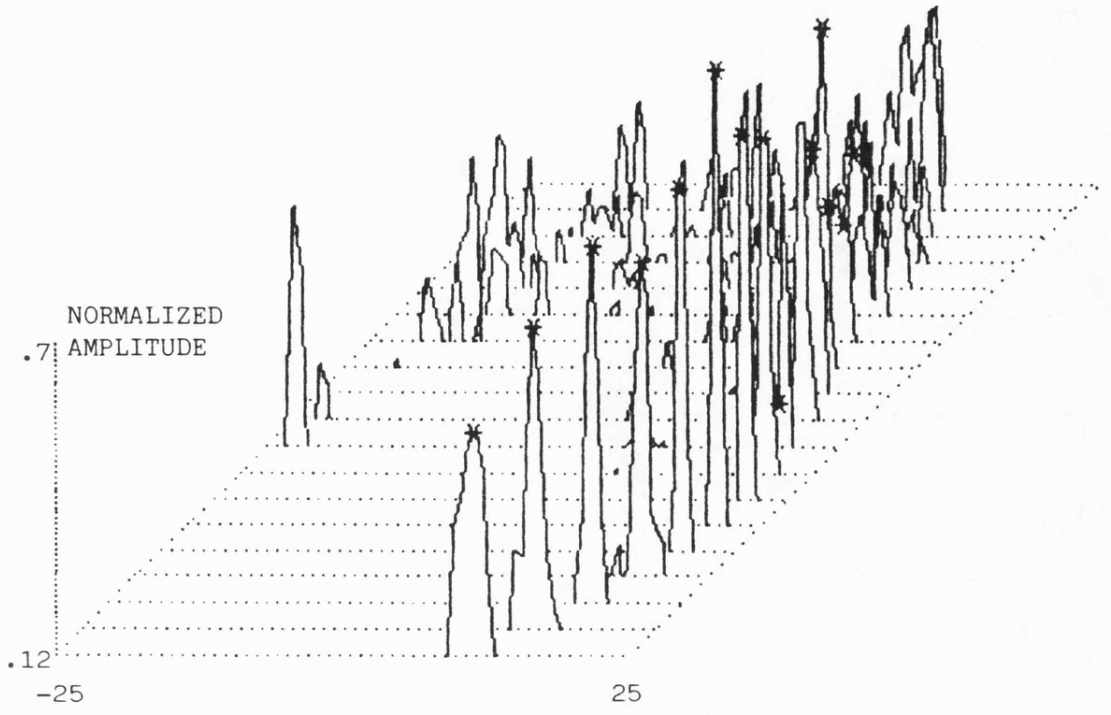

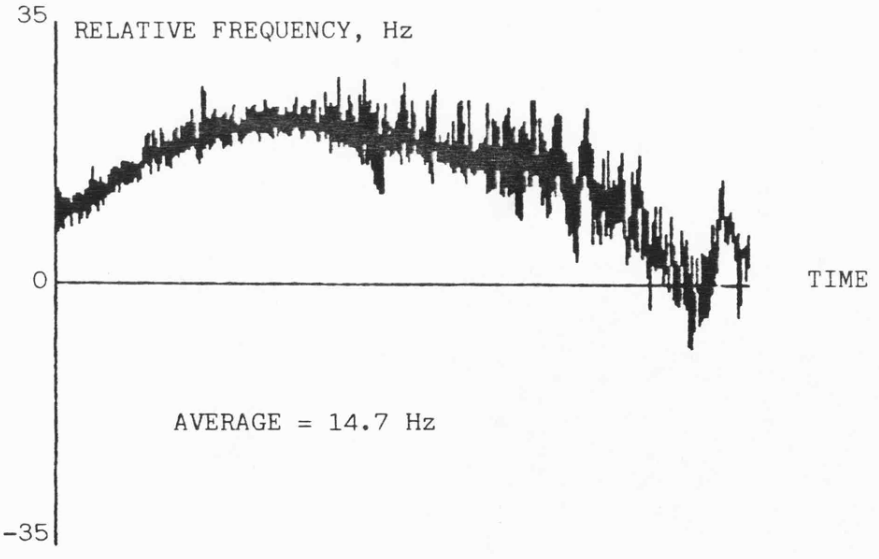

Figure 7.5 Tracking performance, 3 Hz loop, 35 mph

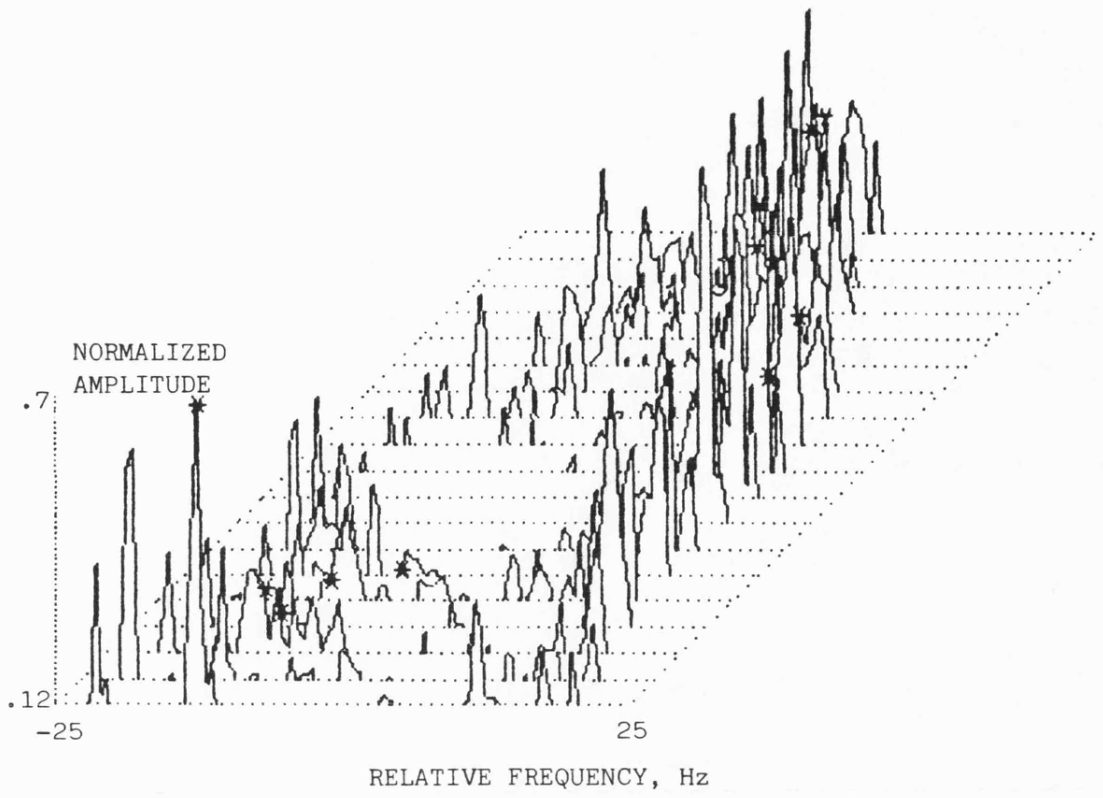

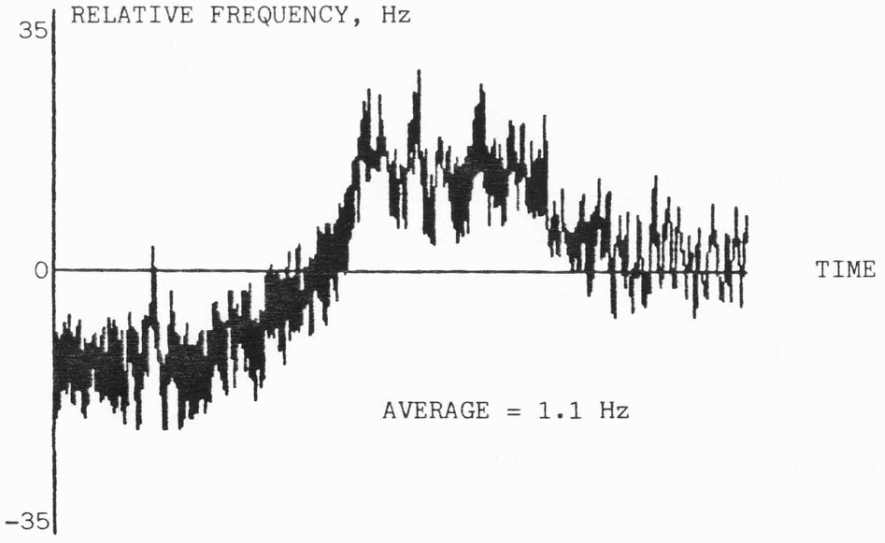

Figure 7.6 Tracking performance, 3 Hz loop, 30 mph

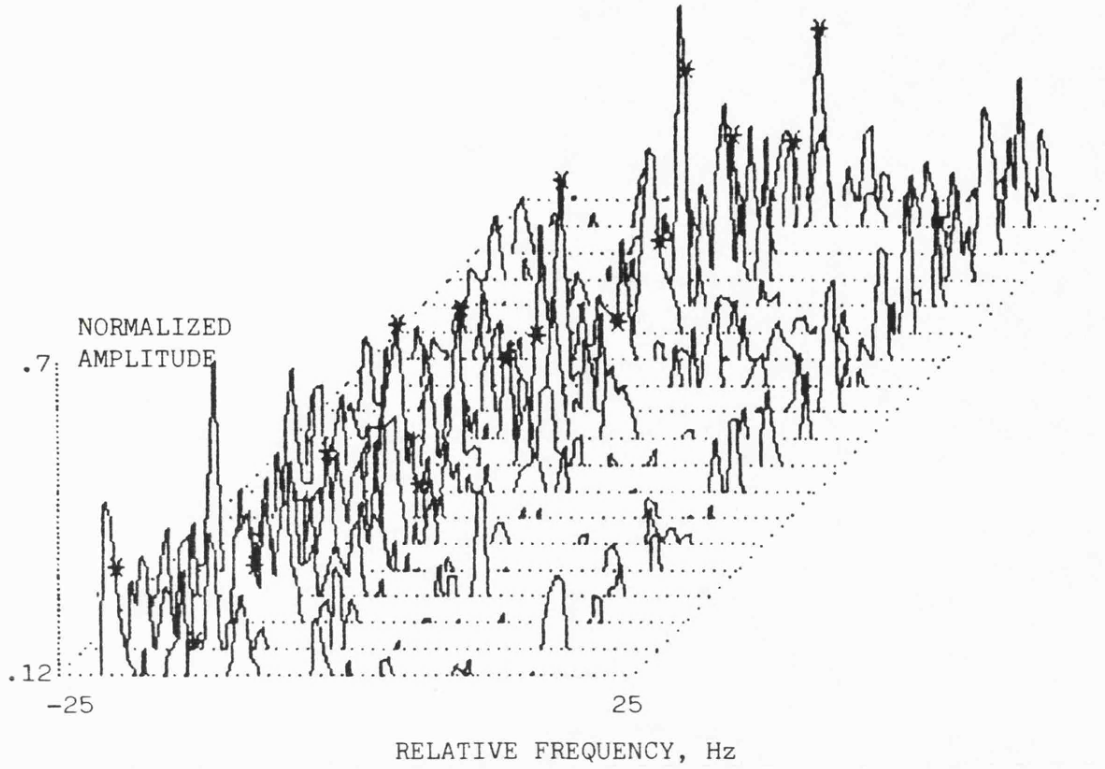

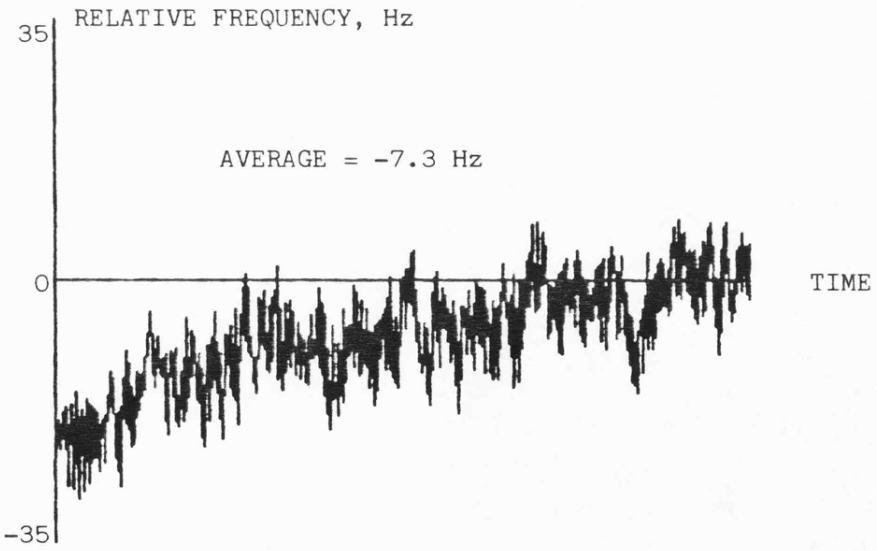

Figure 7.7 Tracking performance, 3 Hz loop, 30 mph

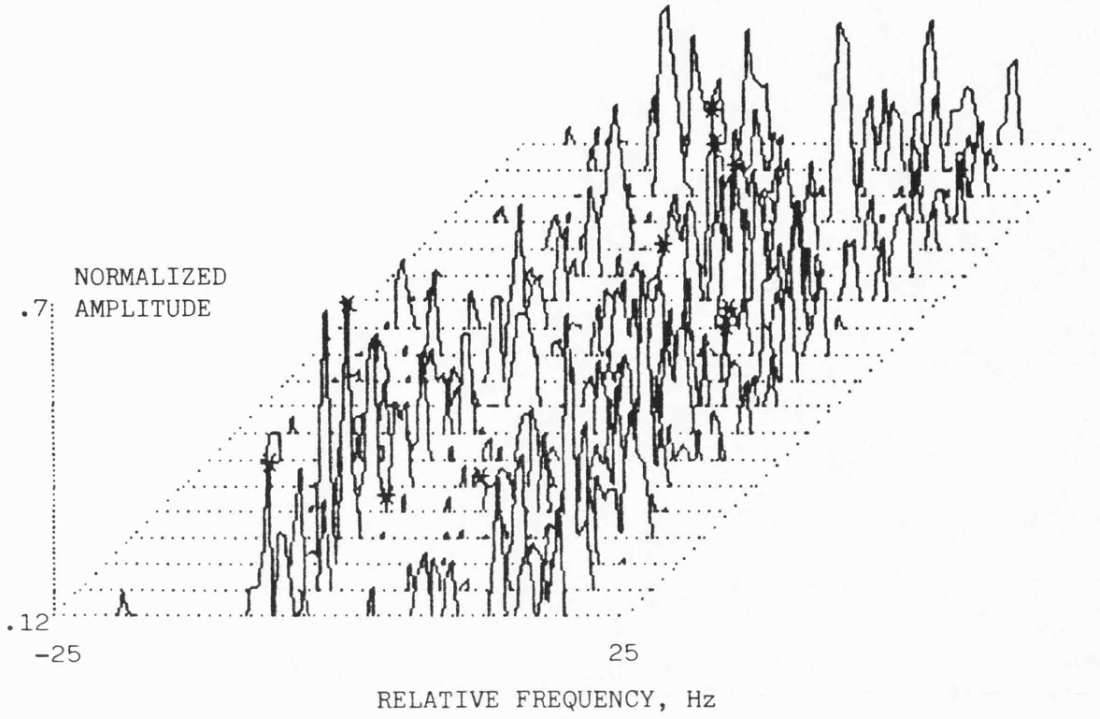

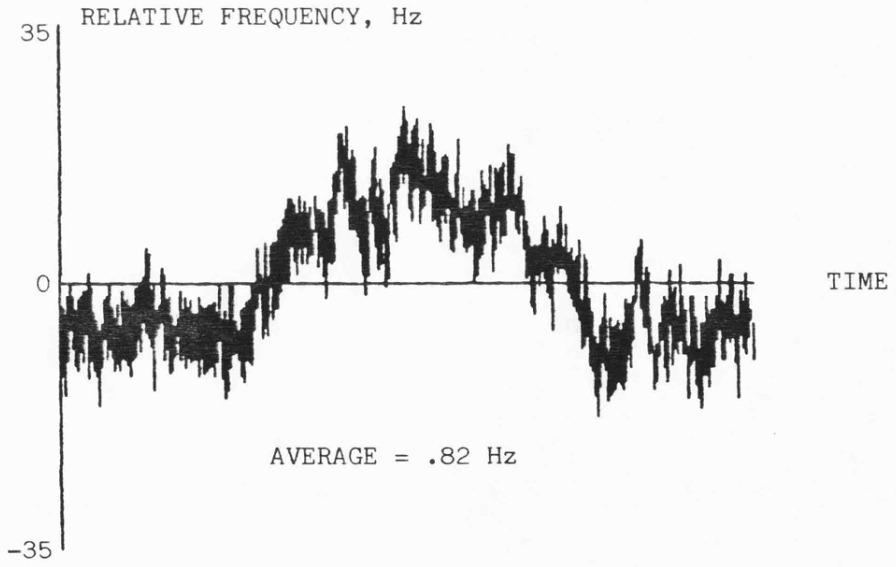

Figure 7.8 Tracking performance, 3 Hz loop, 30 mph

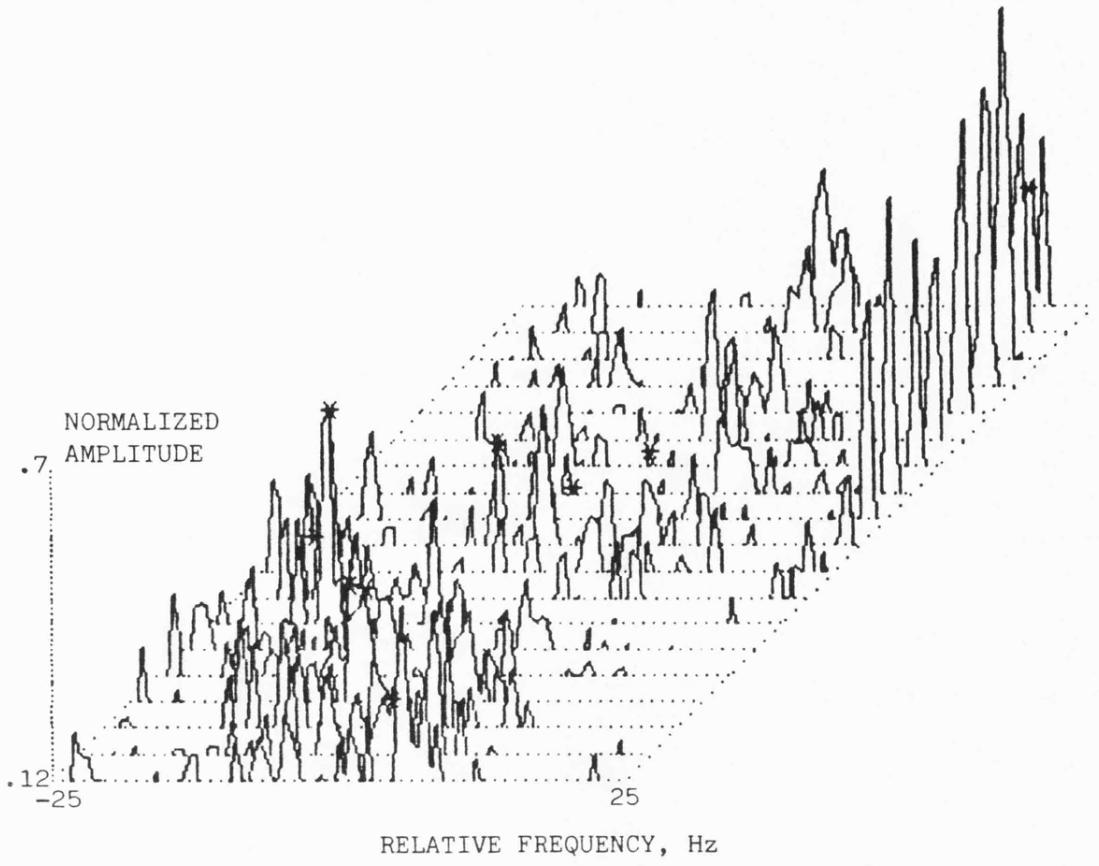

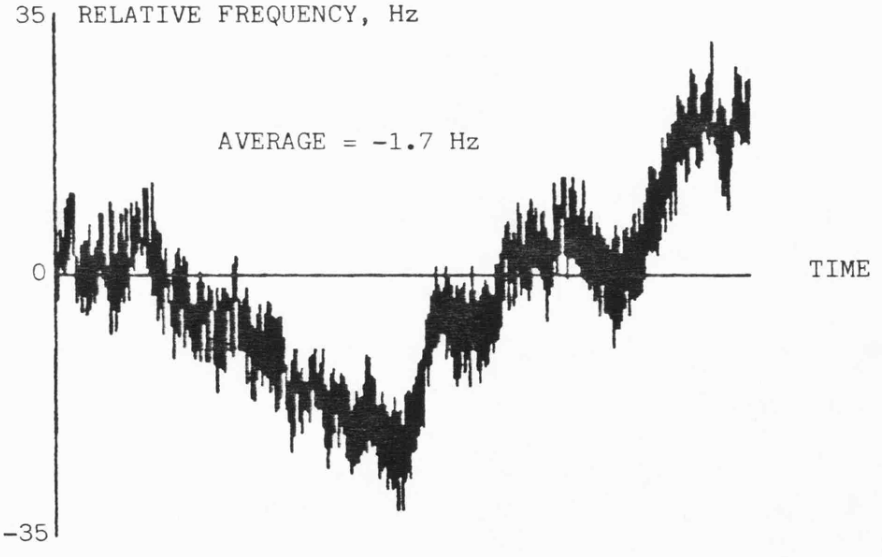

Figure 7.9 Tracking peformance, 3 Hz loop, 30 mph

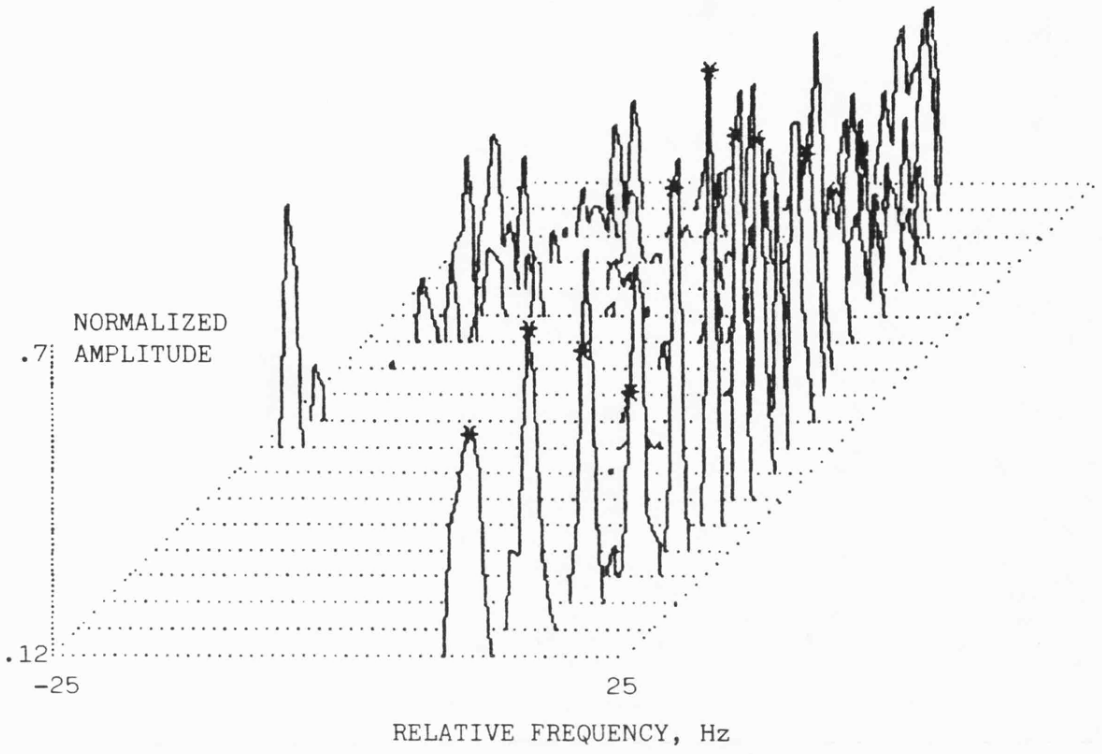

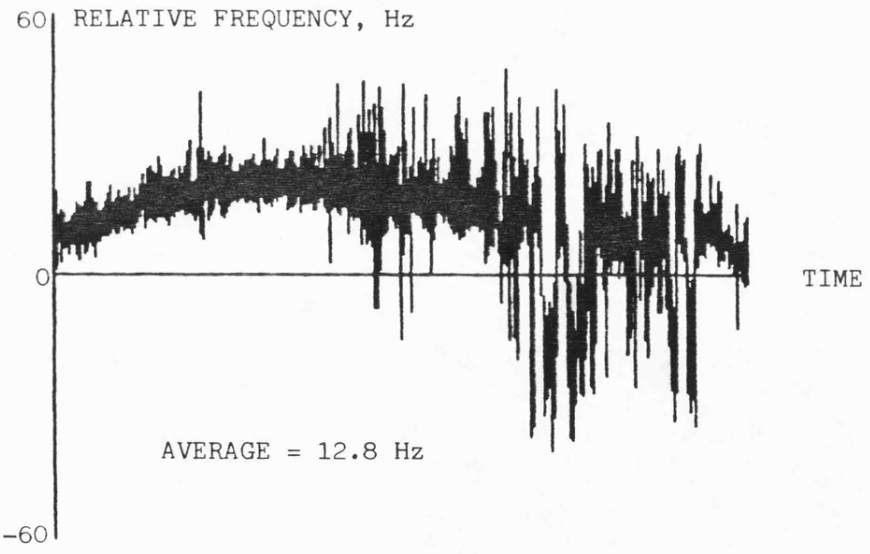

Figure 7.10 Tracking peformance, 10 Hz loop, 35 mph

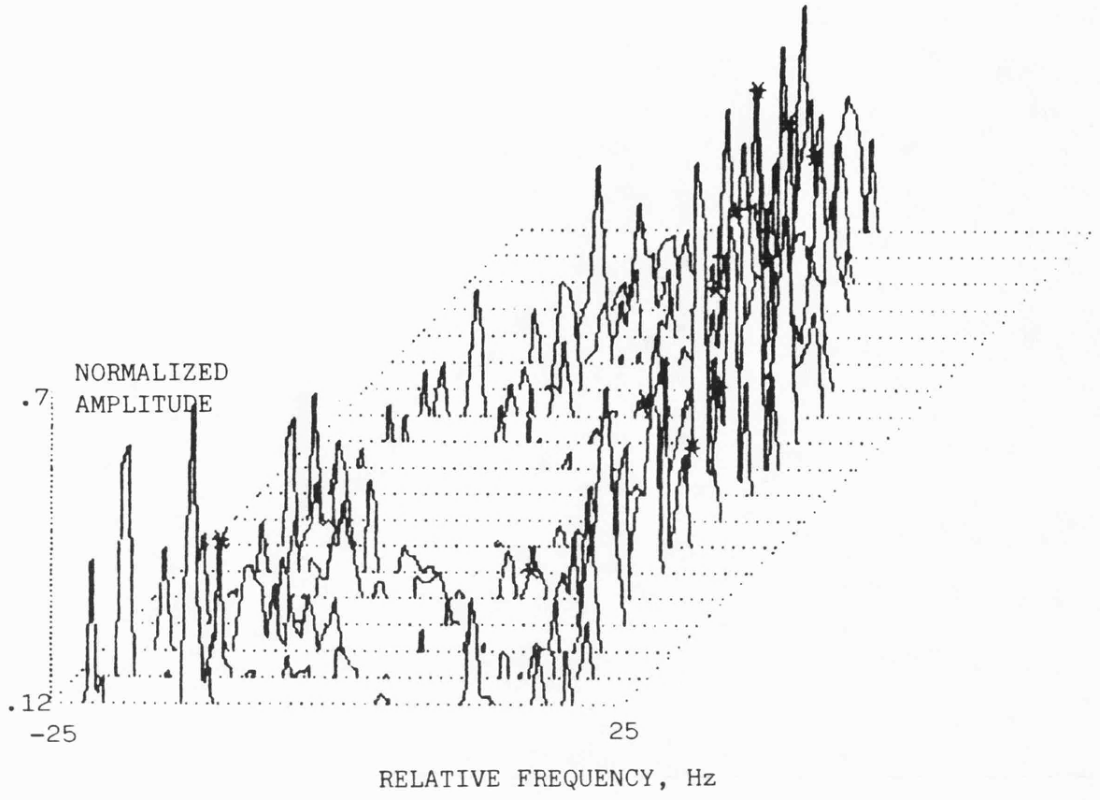

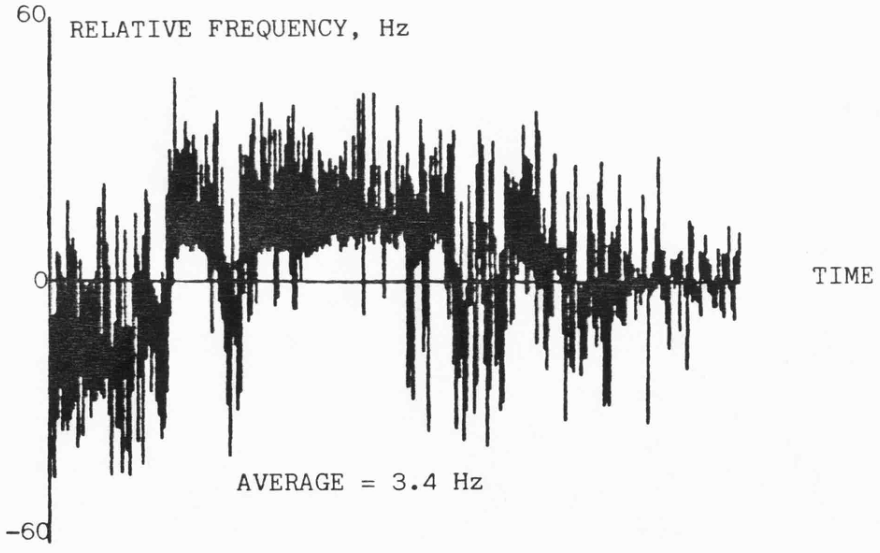

Figure 7.11 Tracking performance, 10 Hz loop, 30 mph

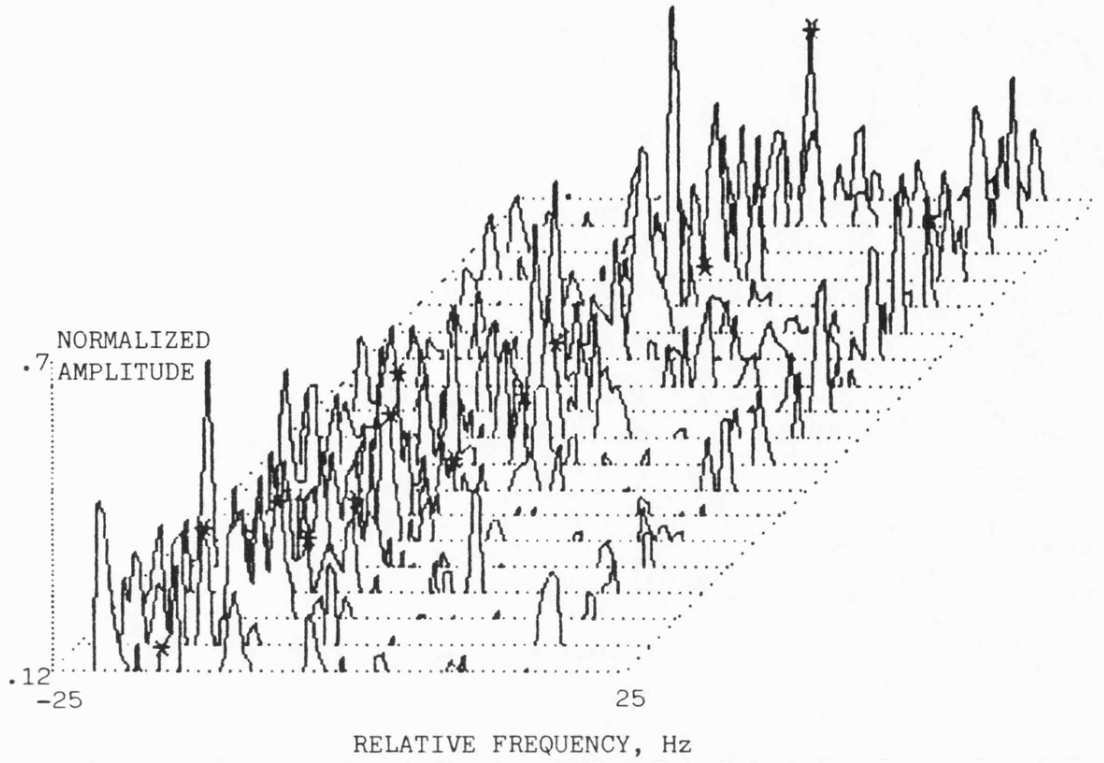

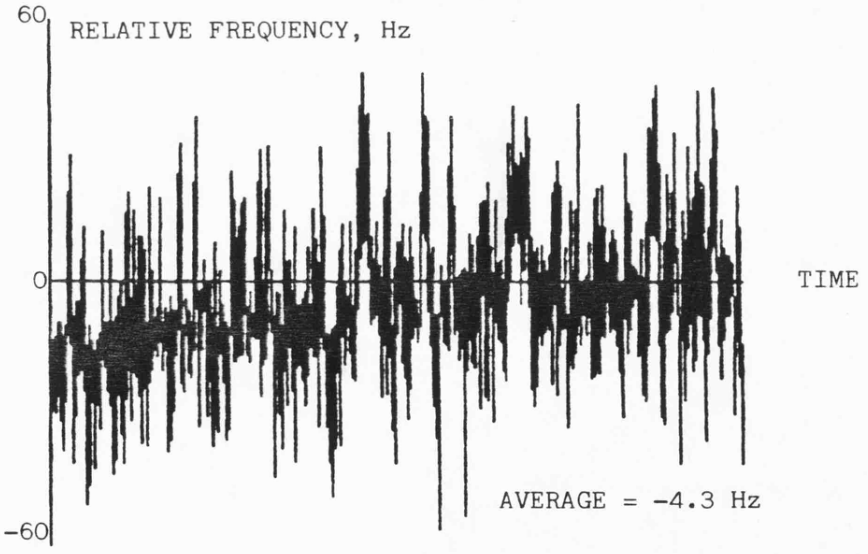

Figure 7.12 Tracking performance, 10 Hz loop, 30 mph

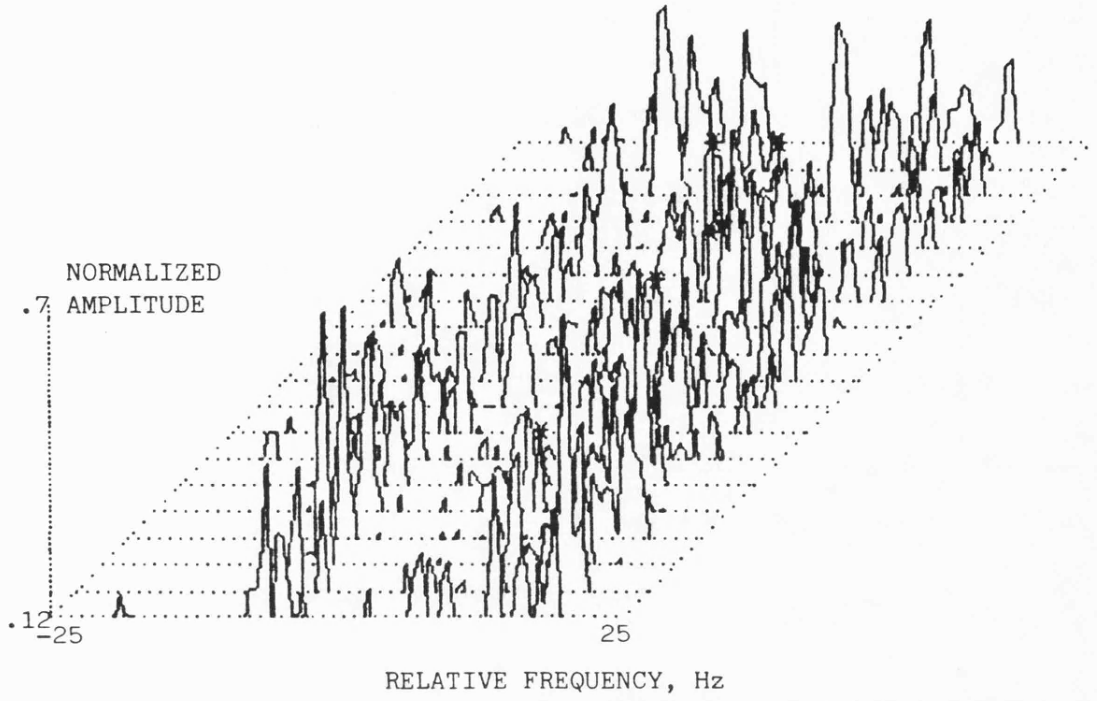

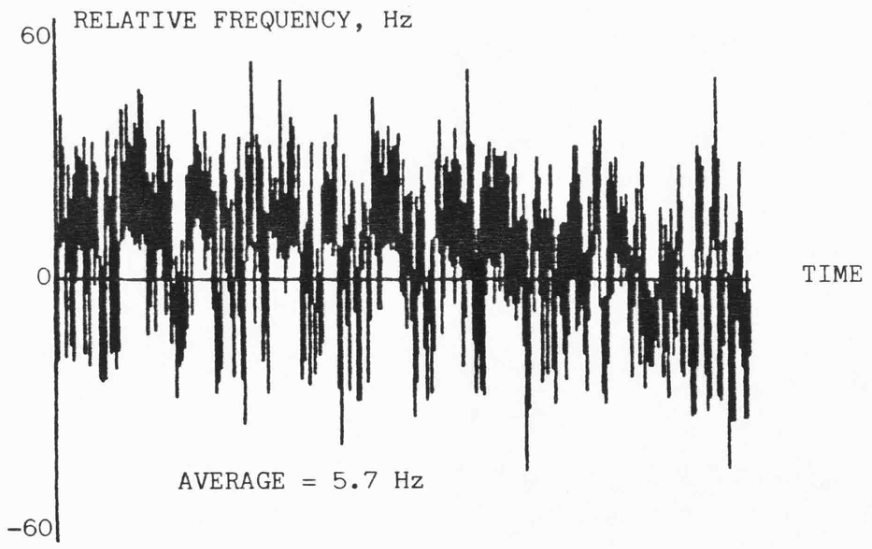

Figure 7.13 Tracking performance, 10 Hz loop, 30 mph

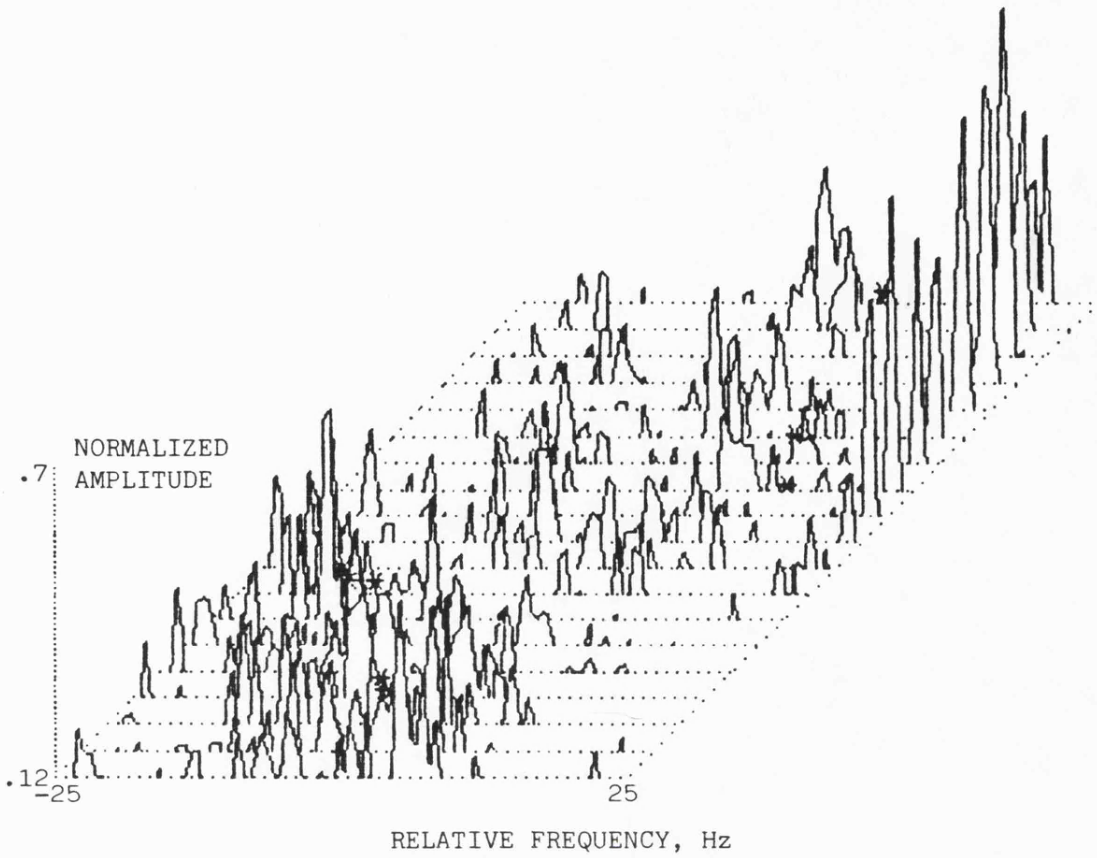

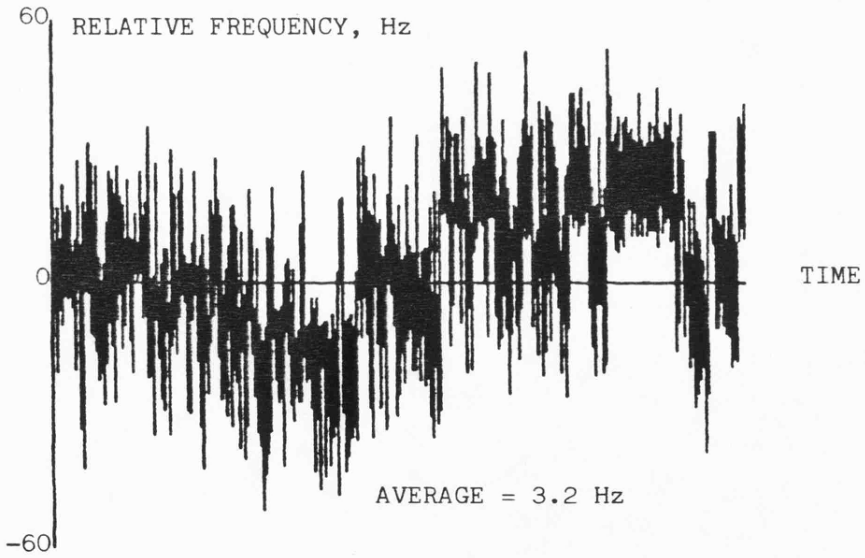

Figure 7.14 Tracking performance, 10 Hz loop, 30 mph

the recording procedure are removed. The lower diagrams depict the instantaneous VCO frequency over the 20 s duration. The frequency scale is relative to the nominal frequency of the demodulated pilot. The average of the instantaneous frequency, over the 20 s duration, is also given.

There are several interesting features illustrated in these figures. The VCO frequency indicators are usually on or close to a major component of the Doppler spectrum. When the signal essentially consists of one large component, its frequency is tracked by the VCO. This behaviour is demonstrated in figures 7.2 to 7.4. In figure 7.5 it is seen that the introduction of a second major component, spaced well away from the first, has little effect on the loop response. Figures 7.6 to 7.9 show sections of data with a more multiple path nature. For these, the VCO frequency tends to wander within the $\pm \omega_d$ limits. However the relation between the VCO frequency and the Doppler spectra is still evident. For instance, in figure 7.9 the VCO frequency is initially near its correct value and then moves lower to track a component being received from behind the vehicle. About half way through the run, a strong component appears from in front of the vehicle and by the end is tracked by the loop.

Results using a 10 Hz PLL are shown in figures 7.10 to 7.14. They represent the loop's response to the same sections of input data as illustrated in figures 7.5 to 7.9. The observations noted for the 3 Hz loop tend to apply here, although the increase in loop bandwidth results in the rapid VCO frequency fluctuations being greater.

The full implications of this study for the design of phaselocked

SSB systems will be discussed in the following chapter. However, it is apparent that the principal conclusion is that the PLL can give rise to errors of up to $\pm \omega_d$ in estimating the nominal frequency of the tracked pilot.

REFERENCES

1) Burrows, D.F.: "Automatic gain control in mobile radio receivers", Ph.D. thesis, University of Bath, 1982, chapter 10.

2) Cox, D.C.: "Doppler spectrum measurements at 910 MHz over a suburban mobile radio path", Proc. IEEE, June 1971, Vol. 59, pp. 1017-1018.

CHAPTER 8

CONCLUSIONS AND SUGGESTIONS FOR FUTURE WORK

Three problems concerning the use of PLLs for AFC in land mobile SSB receivers have been studied in this thesis. They are excess loop time delay, adjacent channel interference and the effect of the multipath propagation medium. Having presented background information on the PLL and its use in SSB receiver design, a novel loop implementation, termed the split loop technique, was introduced and shown to minimize the effects of incorporating time delay within the loop. An analysis of the adjacent channel selectivity of a phaselocked SSB receiver was then presented. The conventional long loop receiver was shown to possess poor selectivity, limited by the mechanisms of reciprocal mixing and loop instability. Use of the split loop technique led to a greatly improved selectivity performance, comparable to that of current full carrier AM equipment. Attention was then turned to the multipath propagation medium and its consequences for loop design. A computer simulation was described, illustrating the degradation of receiver AGC performance due to the spreading of the received pilot's Doppler spectrum by the PLL. In order to minimize the effect, it was necessary to choose a loop bandwidth much narrower than $2\omega_d$, the width of the received pilot's Doppler spectrum. An experimental study of the tracking performance of such a loop in the field revealed that the loop would track individual components of the incoming Doppler spectrum. This resulted in frequency errors of up to $\pm \omega_d$.

The second order PLL has found application in performing AFC in

SSB land mobile radio receivers. In particular, the long loop configuration has often been employed, with the superheterodyne receiver's IF stage (providing the main selectivity) being incorporated within the loop. The advantage of this configuration is that frequency drifts of the input and first local oscillator are tracked out prior to the IF stage and a narrower IF filter can be specified. However, the inclusion of additional filtering within the loop degrades its performance in both the acquisition and tracking modes. Long loop control of the receiver's first local oscillator can also lead to the degradation of the receiver's adjacent channel selectivity performance. This is because PSD output components passing through the loop filter modulate the first local oscillator and lower the purity of its frequency spectrum. The first local oscillator is exposed to adjacent channel transmissions which can mix with spurious components of the oscillator's spectrum and give rise to components within the IF bandwidth. In chapter 4, two mechanisms were analysed which limit the adjacent channel selectivity of a phaselocked SSB receiver. They were reciprocal mixing of modulation components entering the control loop and a previously unreported effect termed adjacent channel induced instability. The latter gave rise to instability within the PLL in the presence of an adjacent channel tone. These two mechanisms were shown to reduce the receiver's adjacent channel selectivity to well below the level required in a mobile radio system operating in narrow channel spacings. Good agreement was obtained between theoretical and experimental results.

In the split loop technique, it is recognized that the loop filters of many second and higher order loops are comprised of a constant gain

term and a lowpass term with a gain decaying to zero for frequencies outside the loop noise bandwidth. The split loop receiver is configured by controlling the first local oscillator with the lowpass term and the second local oscillator with the constant gain term. For example, for the important second order type two loop, the first local oscillator is controlled by an integrator term which tracks out frequency errors prior to the IF stage. The advantage of the technique is due to the existence of a high frequency path bypassing the first local oscillator and the excess loop time delay. PSD output frequency components well outside the loop bandwidth are heavily attenuated by the lowpass filter term and propagate through the second local oscillator. The aberration of the long loop's frequency acquisition performance, known as false locking, is due to the excess phase shift incurred by the PSD output beat frequency component outside the loop bandwidth. As the beat frequency path in the split loop receiver bypasses the excess time delay, the possibility of false locking is eliminated. This conclusion has been confirmed by experimental measurement. Excess time delay also degrades the linear tracking performance of a PLL by increasing the loop noise bandwidth. However, the effect on the noise bandwidth is greatly reduced when the delay is restricted to the integrator path in a second order split loop receiver. Use of the split loop technique also greatly improves the spectral purity of the first local oscillator as the degradation was mainly caused by components passing through the constant gain section of the loop filter. Evidence has been presented to show that the adjacent channel selectivity of a split loop SSB receiver will not be limited by the presence of the PLL. In conclusion, the split loop technique satisfactorily overcomes the first two problems of phaselocked

receivers (namely time delay and adjacent channel interference) studied in this thesis. It is believed that it will have wide application in coherent receiver design, outside the SSB field.

Random phase and amplitude variations are impressed upon a signal transmitted through the land mobile multipath environment and have important consequences for the design of the phaselocked receiver. Several models of the propagation medium have been discussed as well as a need to counteract the multipath distortion by means of pilot based feedforward correction schemes. However, in a phaselocked receiver it can be difficult to extract the demodulated pilot from modulation components since the width of its spectrum is spread well beyond $2\omega_d$. This gives rise to a degradation in the performance of subsequent correction schemes as has been demonstrated by a computer simulation of a coupled PLL/FFAGC system. The simulation made use of a twin path model of the propagation channel and system effectiveness was judged in terms of the residual output envelope modulation of the feedforward processing. A pilot tone bandpass filter bandwidth of $4\omega_d$ was chosen since, although twice the width of the incoming pilot's spectrum, it is the minimum acceptable with phaselocked AFC. The results indicated that, unless the PLL bandwidth was substantially less than $2\omega_d$, the FFAGC gave poor fade suppression. The worst fade suppression tended to occur when the loop natural frequency was equal to $2\omega_d$. These conclusions were confirmed experimentally with field trial data. Of course, the system performance could be improved by sufficiently widening the tone extraction bandpass filter. However this solution is unlikely to be acceptable. To ensure modulation components do not enter the tone extraction bandpass filter, it requires a widening of the frequency

spacing between the transmitted pilot and the nearest modulation component. It is therefore wasteful of the available bandwidth, particularly at UHF and microwave frequencies. Unless the transmitted pilot power was increased, it would also lead to a worsening in performance of any pilot based correction schemes due to a lowering of the signal to noise ratio at the pilot tone extraction filter output.

The tracking performance of narrowband PLLs has been studied using field trial data and the results have confirmed that the loop would often track individual frequency components of the pilot's Doppler spectrum. The loop can therefore give rise to a frequency error of up to $\pm \omega_d$ and a bandpass filter of bandwidth at least equal to $4\omega_d$ is required to extract the demodulated pilot. Consequently, a transmitter pilot notch bandwidth of at least $8\omega_d$ must be employed to avoid modulation components entering the receiver's tone extraction filter. It should be noted that these bandwidths are stated assuming perfect, brickwall, filtering and would have to be increased to allow for non-ideal characteristics.

For a vehicle speed of 70 mph, a frequency error of $\pm \omega_d$ is equivalent to an absolute error of about 1×10^{-7} in the frequency of the incoming signal. Assuming high stability in the base station transmitter, the PLL becomes superfluous if the frequency error introduced by the receiver's local oscillators is less than this value. At present, a stability of $\pm 1 \times 10^{-7}$ over a temperature range of $0^{\circ}C$ to $70^{\circ}C$ can only be achieved with expensive temperature compensated or ovened oscillators which have a typical aging specification in the region of 1×10^{-6} /year. However recent developments in digitally compensated crystal oscillators (1) with excellent temperature

stability seem promising. Although these devices are presently expensive, it is likely that their price will fall when production quantities become available. If inexpensive oscillators with sufficient temperature stability can be obtained, then the AFC loop is only required to compensate for the crystal aging.

The following areas of study are suggested for future research into PLLs and mobile radio AFC:

(i) *Frequency acquisition.* The frequency acquisition performance of PLLs in the fading environment, both with and without acquisition aids, requires further study. The acquisition performance of the split loop receiver incorporating acquisition aids is also worthy of investigation.

(ii) *Computer simulation.* Valuable information on phaselocked receiver systems could be obtained by extending the computer simulation described in chapter 6. The performance of feedforward signal regeneration circuitry in a phaselocked receiver could be gauged in a similar manner. In this respect, the degradation of the envelope correction performance of feedforward signal regeneration is identical to the results presented for FFAGC. A more comprehensive simulation could include many additional factors. For instance, the interaction between feedback AGC and the PLL could be studied as well as the effects of co-channel interference, noise and a feedforward threshold circuit. A more advanced model of the multipath medium, such as that described by Gladstone and McGeehan (2), could also be employed.

(iii) *Subjective tests.* A definition of the adjacent channel selectivity of a pilot tone SSB receiver was given in chapter 4, paralleling the full carrier AM definition. However, it would be worthwhile to carry out tests to compare the subjective effects of adjacent channel interference in AM and SSB receivers. It would also be instructive to study the subjective effects of residual distortion in feedforward multipath correction systems, particularly distortion created by the AFC loop.

(iv) *Alternative AFC schemes.* Past applications of PLLs can be broadly classified into loops which track a particular frequency component of a signal and those which track the signal's modulation. A problem of using the PLL for AFC in a land mobile receiver is that the loop function does not fit into either of these categories. It is neither required to track the random frequency modulation of the received pilot nor to lock onto a particular component of its Doppler spectrum. In fact, it is required to track the nominal frequency of the received pilot. As there is unlikely to be a received component at the centre of the pilot's Doppler spectrum, it is not surprising that the PLL has difficulty in performing this task. The question of the suitability of the PLL for this application therefore arises. In turn, this leads to a requirement to study alternative AFC systems in the multipath environment. There are many other well known AFC schemes, for example, those employing frequency discriminators or FFT techniques (3). However, if the temperature

stability of the receiver's oscillators is acceptable, then less conventional systems may be more suitable. Frequency corrections need then only take place occasionally, preferably when the vehicle is stationary. Certainly, alternative schemes for mobile radio AFC should be investigated. By using much of the material contained within this thesis, their performance can be compared to that of the PLL.

REFERENCES

1) Hughes aircraft company, solid state products division: Private communication, October 1982.

2) Gladstone, K.J., and McGeehan, J.P.: "Computer simulation of multipath fading in the land mobile radio environment", Proc. IEE, December 1980, Vol. 127G, pp. 323-330.

3) Natali, F.D.: "AFC tracking algorithms for satellite links", IEEE international conference on communications, June 1983, pp. D1.7.1-D1.7.13.

APPENDIX 1

VHF RECEIVER

This appendix gives details of the tone-in-band receiver used for the acquisition and adjacent channel measurements described in chapters 3 and 4 respectively. It was designed for upper sideband detection of an input carrier frequency of 86.2875 MHz, incorporating one, 10.7 MHz, IF. Although similar to the Wolfson VHF receiver, there was a facility for long, split or short loop oscillator control and the option of a synthesised first local oscillator. Circuit boards from the Wolfson VHF receiver were used wherever possible to simplify construction. A block diagram of the receiver is given in figure A1.1.

(i) *RF and IF stages.* The front end was conventional and was taken from a Pye type W30 full carrier AM land mobile receiver. It consisted of two tuned, voltage controlled, RF amplifier stages followed by a transistor mixer. A Seiwa type YF-107H3.6 IF filter was employed with a nominal 3.6 kHz bandwidth and 1 dB passband ripple. It was found that the particular filter used for the acquisition measurements possessed a stop band attenuation below the maker's specification and was replaced for the adjacent channel measurements by one of identical type which performed satisfactorily. Details of the IF filter characteristics are given in the relevant chapters. The filter was followed by an IF amplifier consisting of three cascaded SL1612 gain controlled amplifiers. The output fed a

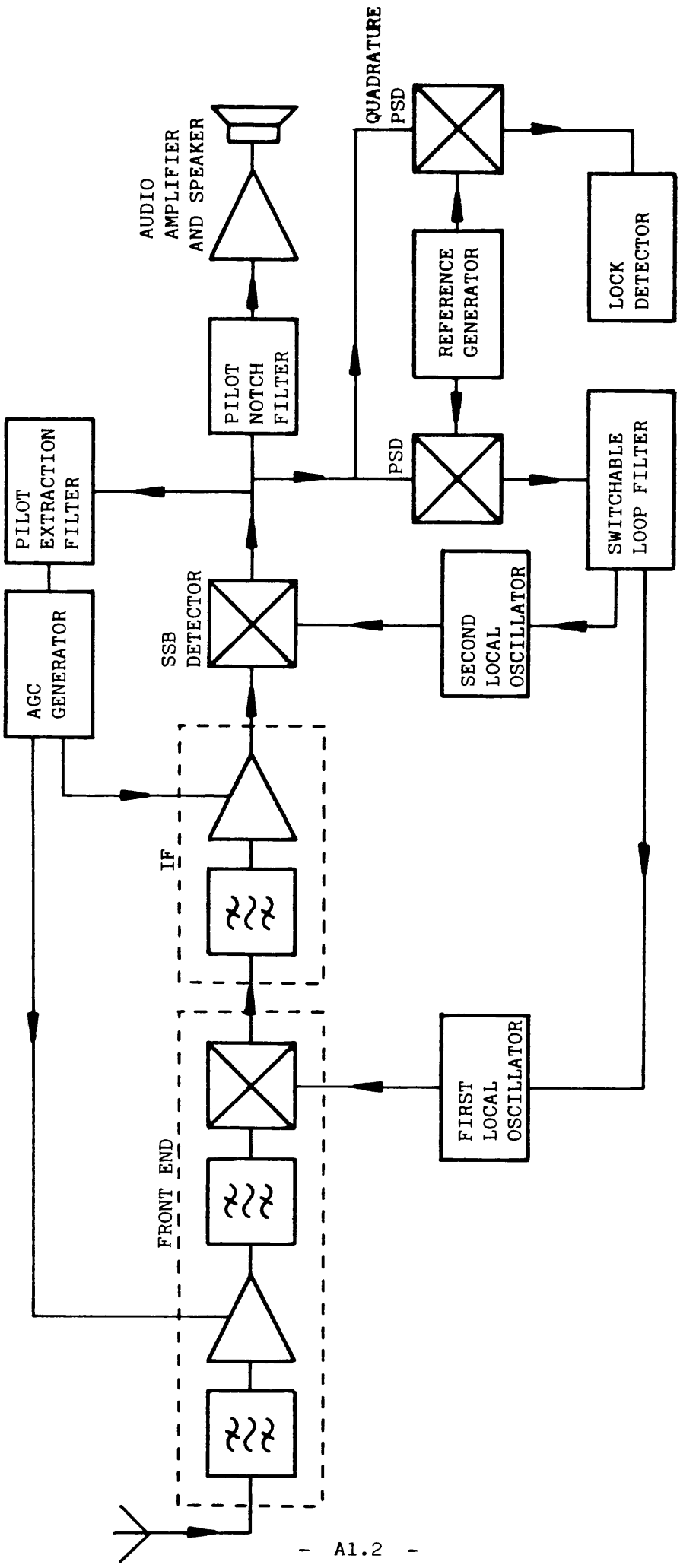

Figure A1.1 VHF pilot tone receiver

double balanced mixer, type TL442 which performed SSB detection.

(ii) *Local oscillators.* There was a choice of two 75.5875 MHz first local oscillators. The first comprised of a 18.896875 MHz voltage controlled temperature compensated crystal oscillator, ITT type TCX08, and a times four frequency multiplier. The rated temperature stability of the crystal was $\pm 5 \times 10^{-8}$ (0°C to 60°C). The unit was designed for a VCO gain of 174 Hz/V and the measured characteristic, given in figure A1.2, yields a centre frequency gain of 169 Hz/V.

The alternative first local oscillator, consisting of a PLL frequency synthesiser, is shown in figure A1.3 and was based on the high performance LN123/LN124 integrated circuits. In a multichannel system the synthesiser would enable the receiver to operate on many channels in a given band using a single common reference crystal. Although in this research application only a single channel was required, the synthesiser was designed to operate in a 6.25 kHz channel spacing system. Referring to figure A1.3, the output of the varactor controlled Colpitts oscillator is frequency divided by a fast ECL ÷10/11 prescaler followed by the LN124 universal divider. The channel selector serves to fix the correct division ratio and here consisted of a diode read only memory. The phase comparator and reference oscillator divider are both contained within the LN123. The reference frequency was derived from a voltage controlled, temperature compensated crystal oscillator, Toyo

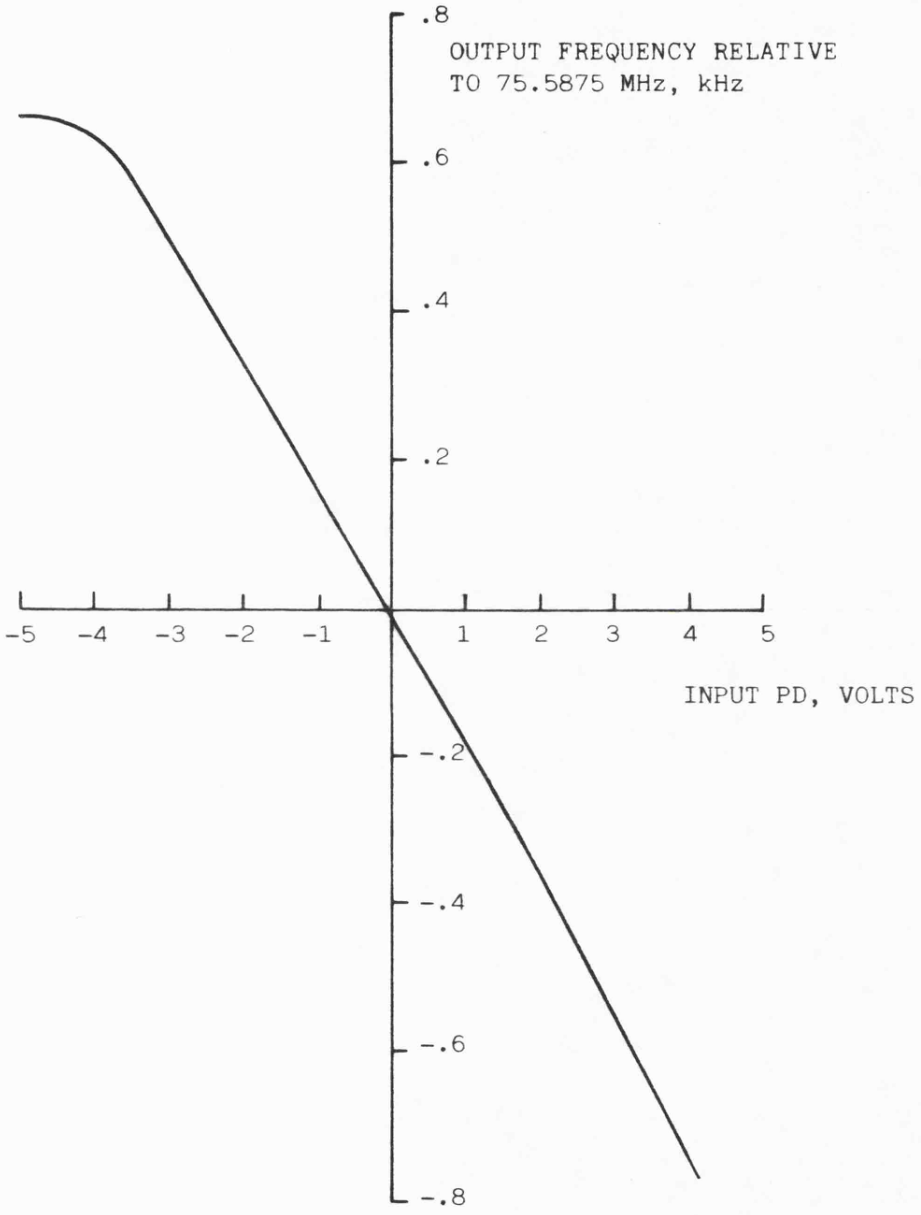

Figure A1.2 TCXO8 first local oscillator characteristic

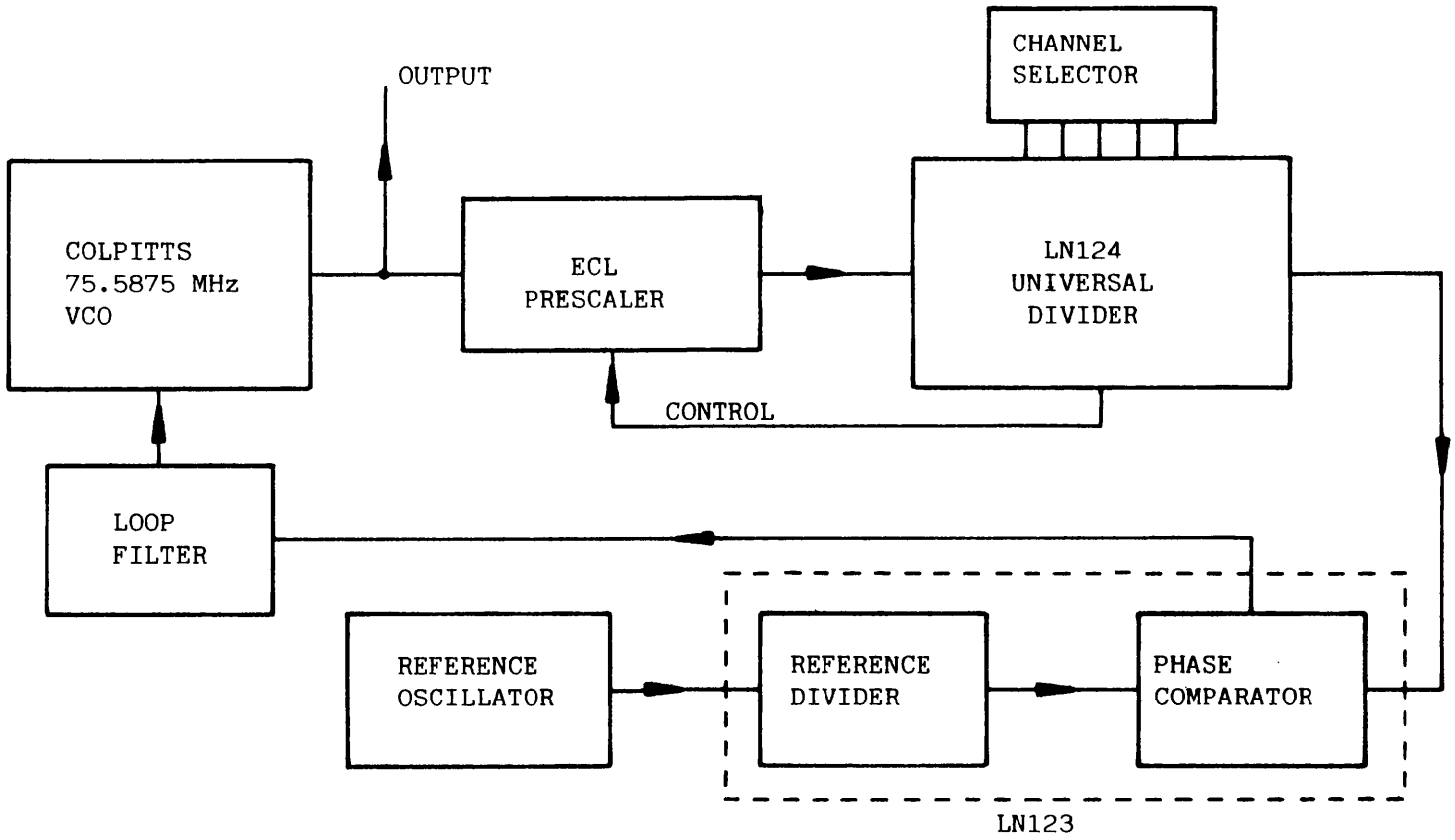

Figure A1.3 First local oscillator frequency synthesiser

type TC0952B, with a rated temperature stability of $\pm 3 \times 10^{-6}$(-30°C to 60°C) and a centre frequency of 10.7 MHz. Fine adjustment of the centre frequency could be achieved by means of a trimming tool. The PLL parameters chosen were those recommended in the manufacturer's data for the LN123/LN124. The loop is essentially second order type two, with the addition of a RC lowpass filter at the loop filter output to reduce the level of spurious outputs. The loop natural frequency was set at 1/20 of the channel spacing (313 Hz), with a damping factor of $1/\sqrt{2}$, and the RC cut-off frequency was set at ten times the loop natural frequency (3130 Hz). The overall 'VCO' characteristic between the reference oscillator input voltage and the loop VCO output frequency is shown in figure A1.4. The centre frequency gain was designed to be 174 Hz/V and the measured value was 172 Hz/V.

The 10.7 MHz second local oscillator, Toyo type TC0952B, was identical to the synthesiser reference oscillator and its characteristic is shown in figure A1.5. The mid-band VCO gain was 174 Hz/V. The in-phase and quadrature 1672 Hz reference tones were also derived from this 10.7 MHz crystal oscillator. The two 1672 Hz quadrature square waves, formed by frequency division, passed through switched capacitor bandpass filters, type R5604, to obtain pure quadrature sinewaves, before being applied to the PSDs.

(iii) *Audio and control circuitry.* A fourth order notch filter was used to remove the pilot tone from the demodulated signal prior

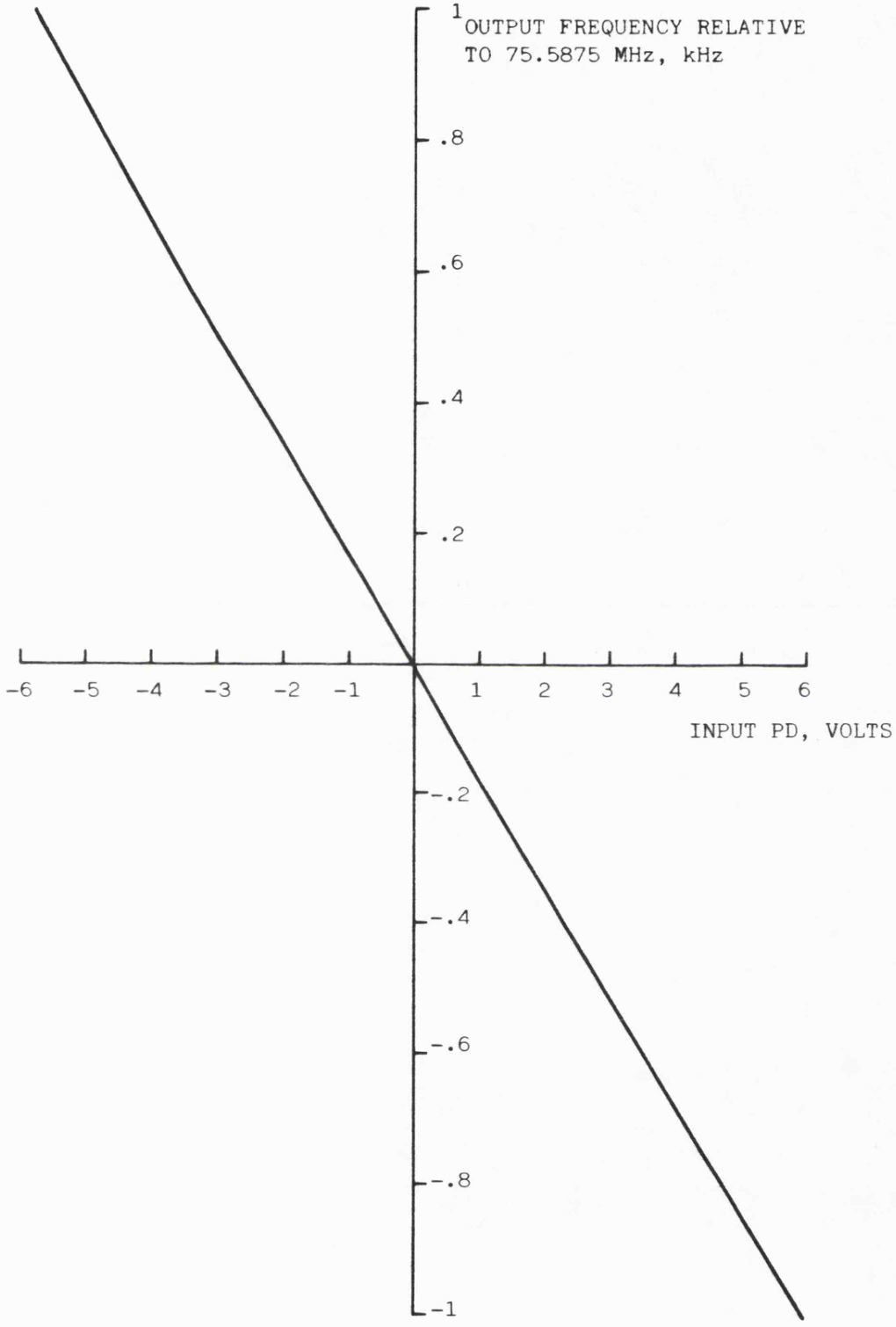

Figure A1.4 Synthesised first local oscillator characteristic

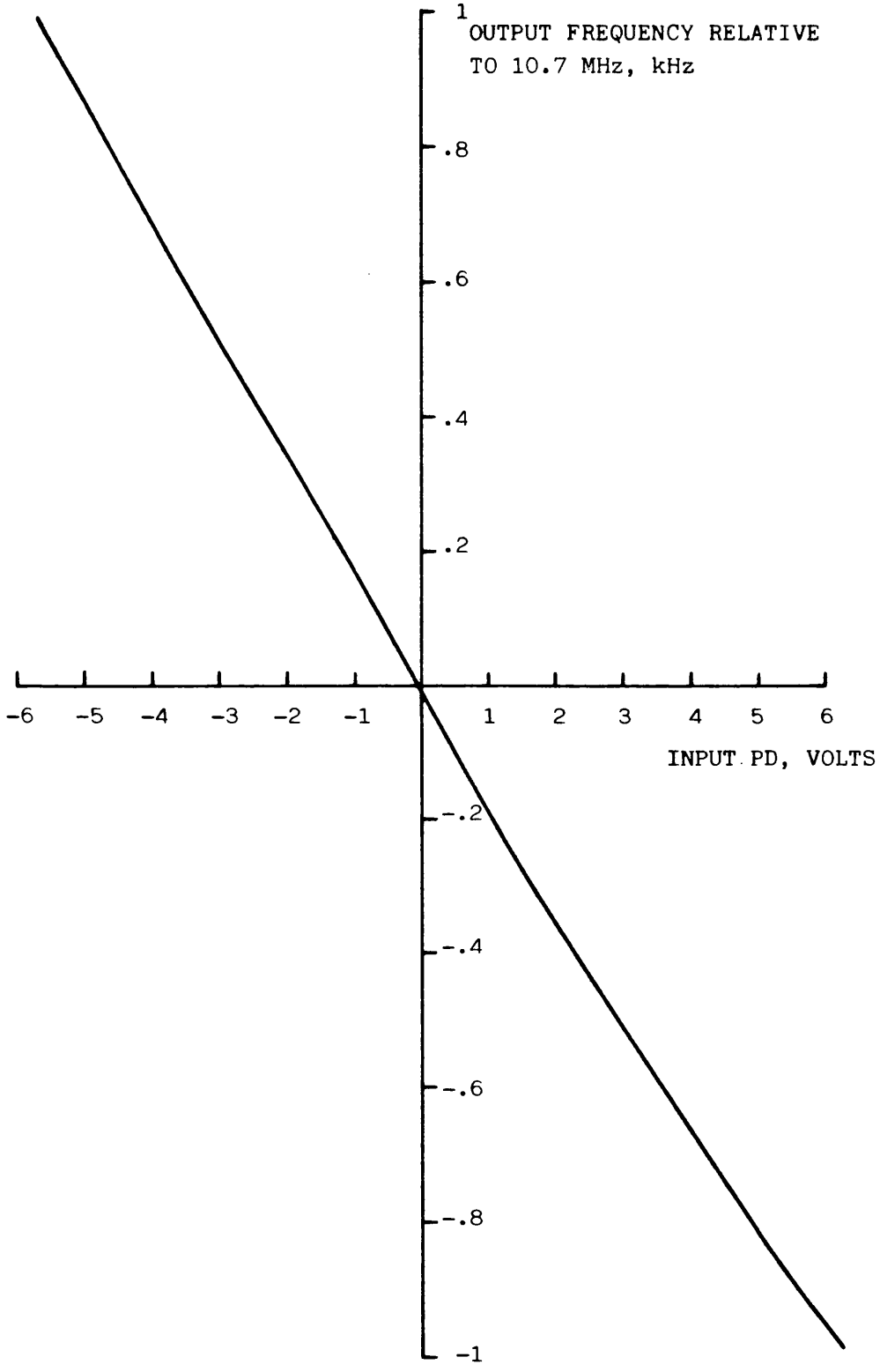

Figure A1.5 Second local oscillator characteristic

to audio amplification. The filter had a 10 dB bandwidth of 210 Hz, a 40 dB bandwidth of 34 Hz and a centre frequency of 1671 Hz. The audio amplifier output fed a loudspeaker with the audio volume being controlled by a potentiometer at the amplifier input.

For AGC purposes, the demodulated pilot tone was extracted from the audio information by a fourth order bandpass filter with a 3 dB bandwidth of 420 Hz and a centre frequency of 1690 Hz. Feedback AGC of the input-signal-level-invariant type, described by McGeehan and Burrows (1), was used and the closed loop bandwidth was set at 10 Hz. The AGC maintained the demodulated pilot at an average level of 300 mV RMS at the SSB detector output.

Both the in-phase and quadrature PSD's were implemented by analogue multipliers, type AD534JD, with K_d set at 0.212 V/rad. The active loop filter was built as seperate proportional and integral sections which could be summed together to feed one local oscillator or connected for split loop control. The lock detector consisted of an RC low pass filter and a voltage comparator.

References

1) McGeehan, J.P., and Burrows, D.F.: "Large signal performance of feedback automatic gain control", Proc. IEE, April 1982, Vol. 128F, pp. 110-117.

APPENDIX 2

TWO TONE ADJACENT CHANNEL INDUCED INSTABILITY SOLUTIONS

In section 4.3.1, two adjacent channel induced instability solutions for an upper sideband receiver were derived, namely:

$$2\omega_t = \omega_s + \omega_r \qquad \text{(A2.1)}$$

with

$$\text{gain} = |G(\omega_z + \omega_t)| \frac{V_a \zeta \omega_n}{V_i(\omega t - \omega_r)} \qquad \text{(A2.2)}$$

$$2\omega t = \omega_s - \omega_r \qquad \text{(A2.3)}$$

with

$$\text{gain} = |G(\omega_z + \omega t)| \frac{V_a \zeta \omega_n}{V_i(\omega t + \omega_r)} \qquad \text{(A2.4)}$$

These solutions were derived by assuming a tone, vt, of frequency, ωt, existed at the PSD audio input, tracking the tone around the loop and equating each resultant SSB detector output component to the original tone. Using a similar technique, but now assuming that the original tone results in a tone of frequency $\omega t'$ at the SSB detector output and that tone, in turn being fed around the loop, gives rise to a tone of frequency $\omega t''$ at the SSB detector output, then the following equations apply:

$$\omega t' = \omega_s + \omega_r - \omega t \qquad \text{(A2.5)}$$

$$\text{or } \omega t' = \omega_s - \omega_r - \omega t \qquad \text{(A2.6)}$$

$$\omega t'' = \omega_s + \omega_r - \omega t' \qquad \text{(A2.7)}$$

$$\text{or } \omega t'' = \omega_s - \omega_r - \omega t' \qquad \text{(A2.8)}$$

By equating ω_t'' to ω_t, two solutions are obtained relating the instability frequencies ω_t and ω_t', namely:

$$\omega_t' + \omega_t = \omega_s + \omega_r \qquad \text{(A2.9)}$$

$$\omega_t' + \omega_t = \omega_s - \omega_r \qquad \text{(A2.10)}$$

These equations demonstrate that an adjacent channel induced instability mode can occur which requires two tones to be fed around the loop. It can also be deduced from equations A2.5 to A2.8 that solutions requiring more than two tones are not possible. As any two instability frequencies, for instance ω_t' and ω_t'', can be written as a function of only ω_s and ω_r, then it is not possible to form a similar equation relating three or more instability frequencies to ω_s and ω_r.

The open loop gains relating to equations A2.9 and A2.10 can easily be derived and are given by:

$$\text{gain} = |G(\omega_2 + \omega_t)||G(\omega_2 + \omega_t')| \frac{V_a^2 \zeta^2 \omega_n^2}{V_i^2 (\omega_t' - \omega_r)(\omega_t - \omega_r)} \qquad \text{(A2.11)}$$

and

$$\text{gain} = |G(\omega_2 + \omega_t)||G(\omega_2 + \omega_t')| \frac{V_a^2 \zeta^2 \omega_n^2}{V_i^2 (\omega_t' + \omega_r)(\omega_t + \omega_r)} \qquad \text{(A2.12)}$$

It can be seen that equations A2.2 and A2.4 are special cases of the above solutions when ω_t is equal to ω_t'. Furthermore, ignoring the IF filter characteristic, it can simply be shown that equations A2.11 and A2.12 have a minimum, with respect to ω_t and ω_t', when ω_t and ω_t' are equal, and the gains increase as the two frequencies separate. However

a strict limit is placed on the increase in gain by the IF filter which will attenuate values of ω_t and ω_t' outside the receiver audio passband. To illustrate the extent of the increase in loop gain, consider a receiver similar to the Wolfson, with a reference frequency of 1672 Hz,

ADJACENT CHANNEL TONE FREQUENCY SPACING, kHz	REDUCTION IN ADJACENT TONE LEVEL REQUIRED FOR INSTABILITY, dB	
	$\omega_t + \omega_t' = \omega_s + \omega_r$	$\omega_t + \omega_t' = \omega_s - \omega_r$
-1.5	0.0	
-1	0.3	
-0.5	1.5	
4.5	2.4	1.0
5	0.8	1.2
5.5	0.2	1.5
6	0.0	1.1
6.5		0.7
7		0.4
7.5		0.2
8		0.1
8.5		0.1
9		0.0

Table A2.1 Comparison of adjacent channel tone levels for single and two tone instability

but with an IF filter possessing unity gain for frequencies from that

of the second local oscillator to 4 kHz above, and zero gain elsewhere. For several values of adjacent channel tone frequency spacing, the maximum decrease in V_a/V_i required for instability, compared to the value for the corresponding single tone solution (i.e. $\omega_t = \omega_t'$) is shown in table A2.1. The results for this receiver indicate that, although two tone solutions can occur, the level of adjacent channel tone power required is, at most, only a few dBs below that required for the corresponding single tone solution. Consequently, the single tone gain equations can be used for predicting the adjacent channel selectivity performance with a fair amount of accuracy.

As a further example, consider the actual Wolfson receiver and the two tone instability case observed at an adjacent channel frequency spacing of 6 kHz. Equations A2.10 and A2.12 relate to this case and are plotted in figure A2.1, with the ratio V_a/V_i set equal to unity. The experimentally observed instability frequencies and gain are also shown. It is interesting to note that, as expected, the oscillations occured at the peaks of the gain curve, and that the gain at $\omega_t = \omega_t'$ is only fractionally lower. For comparison, figure A2.2 shows curves of the same equations, except, this time, for an adjacent channel frequency spacing of 6.5 kHz. The peak in the gain curve around $\omega_t = \omega_t'$ explains why no two tone solution was observed at this value of frequency offset.

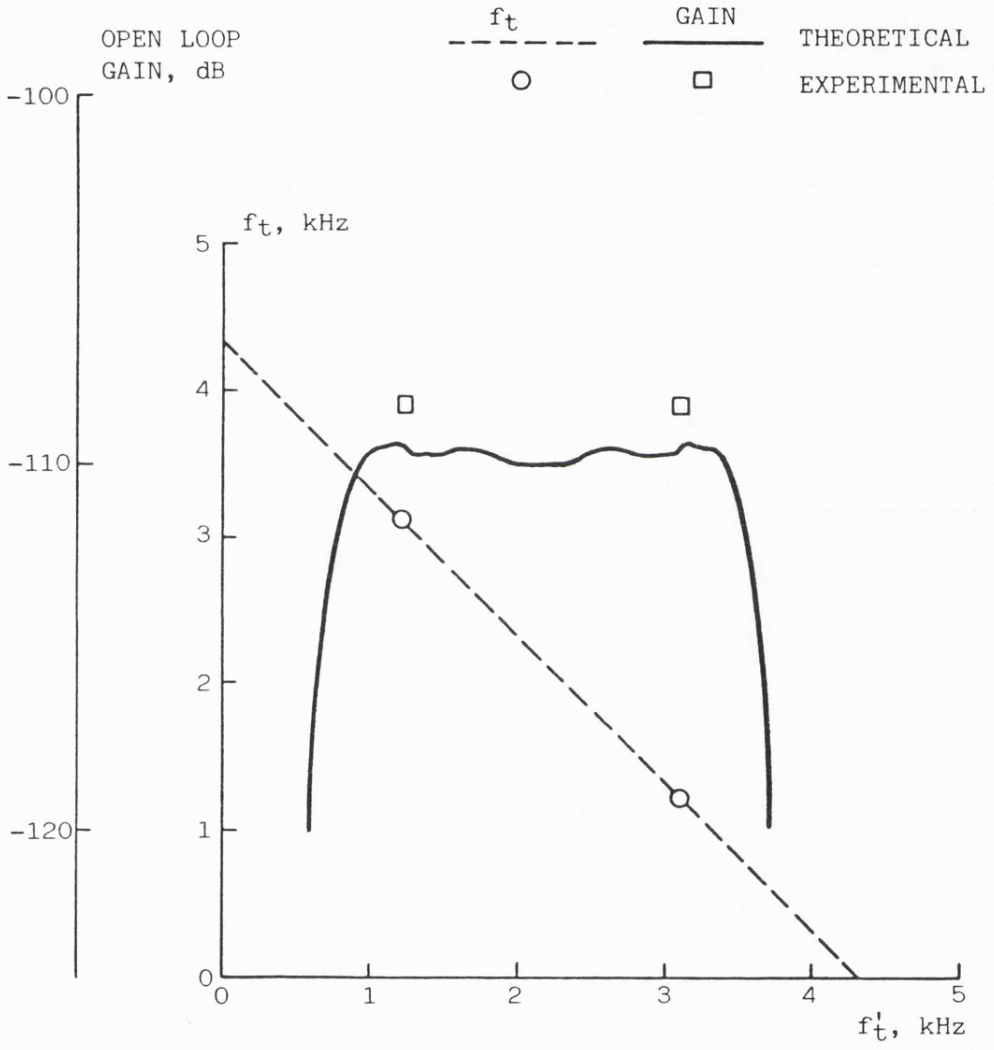

Figure A2.1 Variation of open loop gain and f_t with f_t' for a carrier to adjacent channel tone frequency spacing, f_s, of 6 kHz and for $f_t + f_t' = f_s - f_r$

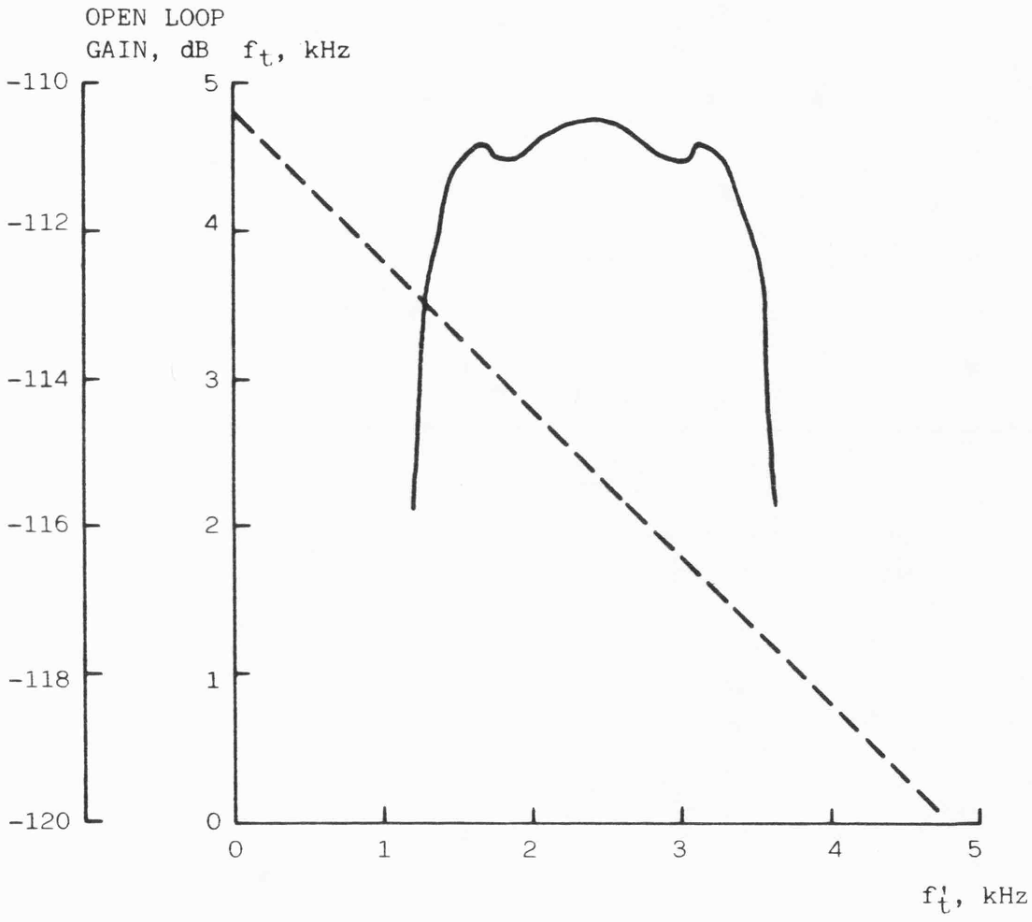

Figure A2.2 Variation of open loop gain and f_t with f_t' for a carrier to adjacent channel tone frequency spacing, f_s, of 6.5 kHz and for $f_t + f_t' = f_s - f_r$

Elimination of False-Locking in Long Loop Phase-Locked Receivers

JOSEPH P. McGEEHAN AND JONATHAN P. H. SLADEN

Abstract—**Although long-loop phase-locked techniques are finding increasing application in the fields of mobile radio and satellite communications, their use has several drawbacks. Time delay associated with filtering processes within the loop gives rise to a degradation in acquisition capability, and information components entering the control loop cause a reduction in adjacent channel performance. In this paper, a split-loop technique is described, which eliminates false-locking, substantially improves the acquisition characteristics to that associated with a loop with zero time delay, and "cleans up" the first local oscillator spectrum. Furthermore, the technique is simple to implement.**

I. INTRODUCTION

In recent years, phase-locked techniques have found wide application in receiver design, for example, in satellite [1] and land mobile [2] communication systems. It has often been necessary to incorporate the intermediate frequency (IF) amplifier stages of a superheterodyne receiver within the phase-locked loop, thereby allowing frequency control of the first local oscillator. This configuration is called a long-loop receiver [3] and is shown in the simplified block diagram form of Fig. 1. For such a system, once phase-lock is achieved, $\omega_r = (\omega_i - \omega_0)$ and the received information is correctly positioned within the narrow IF crystal filter. Furthermore, it should be possible to track out frequency changes due to Doppler or oscillator drift. Unfortunately, the excess phase shift introduced into the loop by the IF filter can cause a significant deterioration in the loop's acquisition and tracking characteristics. In particular, a phenonemon known as false-locking [4] may occur whereby synchronization is never achieved and incorrect signal demodulation results.

Although some fundamental work in this area has been undertaken, notably by Develet [5] and Jelonek *et al.* [6], little published work exists in its application to long-loop superheterodyne receivers with the exception of that by Biswas *et al.* [7]. These authors suggest a technique by which false-locking may be eliminated which will be discussed more fully in the next section. Although somewhat complex, the method is nonetheless significant in that it is a positive design response for radio frequency engineers attempting to use long-loop phase-locked receivers. At this time, such work is particularly relevant because of the renewed interest in using 5 kHz single sideband modulation in the land mobile services of North America and the United Kingdom. The three methods presently under investigation differ essentially in the positioning of the pilot tone (required for automatic frequency control and automatic gain control) within the audio band. They are pilot carrier SSB [8], [9], tone-in-band SSB [10], and tone-above-band SSB [11]. Although each system has advantages and disadvantages, it is now generally accepted that each receiver type requires the use of a long-loop phase-locked receiver if correct demodulation and an economically viable receiver design are to be achieved. Failure to incorporate the first local oscillator within the loop can lead to "sideband cutting" by the IF crystal filter. Since it is also likely that each receiver system will be multichannel, the first local oscillator will use a frequency synthesizer with its own inherent and considerable time delay. This will, of course, degrade further the acquisition and tracking performance of the loop. In addition, any noise or modulation components appearing on the control line of the first local oscillator will spread its output spectrum and, thus, reduce the adjacent channel performance of the receiver, a problem which has been discussed in some detail by McGeehan and Lymer [12].

In this paper, a novel approach to the design of long-loop phase-locked receivers is described whereby both the first and second local oscillators are controlled in a split-loop configuration. Use of this method will be shown, not only to eliminate false-locking, allowing pull-in from much larger frequency offsets, but also to improve the spectral purity of the first local oscillator. The technique has wide application, for example, in satellite and land mobile receivers, and here it is applied to the design of a phase-locked single sideband mobile radio receiver. Finally, the effect of excess time delay on the noise bandwidth of both a conventional and a split-loop receiver is investigated.

II. EFFECT OF TIME DELAY ON PHASE-LOCKED LOOP ACQUISITION

Insight into the false-lock problem may be gained by first considering a commonly used explanation for phase-locked loop pull-in. When out of lock, the output voltage of a phase-locked loop phase detector (neglecting higher frequency terms) consists of a beat note and a dc voltage. The dc voltage causes a gradual reduction in the beat frequency until the lock-in limit is reached and the loop quickly achieves phase-lock. This dc voltage is a product of the input and a VCO sideband of the same frequency. Gardner [13] obtains an accurate expression for the pull-in time of a second-order type-two loop by assuming that the beat frequency passes only through the proportional filter term while the slowly changing dc voltage passes solely through the integrator.

Manuscript received August 3, 1981; revised February 11, 1982. This work was supported in part by the U.K. Science and Engineering Research Council.

The authors are with the School of Electrical Engineering, University of Bath, Bath, England.

0090-6778/82/1000-2391$00.75

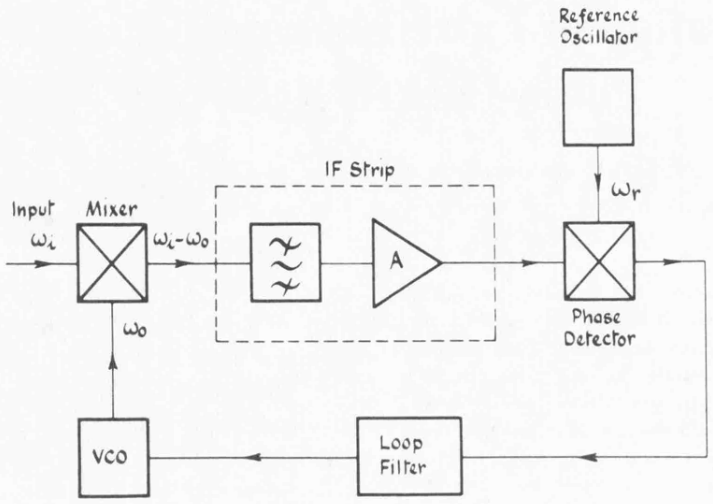

Fig. 1. The long-loop phase-locked receiver.

Now, when considering the effect of additional filtering within the loop, Gardner [4] shows that the increased pull-in times and false-locking are due to excess phase shift in the beat frequency path. Similarly, Develet [5] considers the effect of pure time delay τ on the acquisition performance of a second-order loop and obtains an important result. For a high-gain second-order loop he concludes that the loop will fail to acquire correctly if the initial frequency offset is greater than $1/4\tau$ Hz. Subsequent workers [14], [15] have confirmed this result.

In a method proposed by Biswas *et al.* [7] for avoiding false-locking, an electronic phase shifter is connected between the IF output and phase detector input in Fig. 1. The phase shifter introduces a phase shift δ proportional to the rectified output of the loop filter. If the excess loop phase shift is equal and opposite to δ, its effect is removed. However, if this is not the case, the loop analysis is greatly complicated by the additional circuitry and no explanation of its behavior has been given. The technique to be described in the next section is easier to implement and does not complicate the loop analysis. Throughout this paper it is assumed that the excess time delay is small compared to the reciprocal of the loop noise bandwidth so that a stable locked condition exists.

III. THE SPLIT-LOOP TECHNIQUE

Several authors have found considerable advantage in "splitting" the filter of a phase-locked loop. Richman [16] originated the method for analysis of loop acquisition. Biswas and Banerjee [17] propose a hybrid-locked loop which includes two VCO's controlled by independent low-pass filters. More recently, Ward [18] has reported improvement in the locking range of a first-order loop by splitting a loop filter into high and low frequency paths. The split-loop technique applied to a phase-locked superheterodyne receiver is shown in schematic form in Fig. 2. It can be seen that the phase detector output controls both the first and second local oscillators through the filters $F_1(s)$ and $F_2(s)$, respectively. Neglecting mixer output sum term components and, for the present, the effect of any excess loop phase shift, it can simply be shown that

$$\frac{d\phi}{dt} = \Omega + \frac{d\theta i}{dt} - [K_1F_1(s) + K_2F_2(s)]K_d \sin\phi \tag{1}$$

where

$$\Omega = \omega_i - \omega_0 - \omega_r, \qquad \text{the frequency offset}$$

$$\phi = (\omega_i - \omega_0 - \omega_r)t + \theta_i - \theta_0 - \theta_r,$$

the phase error

and

$$K_d = \frac{V_iV_0V_rA}{4}.$$

If we now write

$$F(s) = \frac{K_2}{K_1}F_2(s) + F_1(s) \tag{2}$$

then (1) reduces to that of a phase-locked loop, with loop filter of transfer function $F(s)$, VCO gain K_1, and phase detector constant K_d. Meer [19] states that for a loop filter with equal numbers of poles and zeros it is reasonable to consider the filter as composed of a constant high frequency term and a low-pass term which decays to zero for frequencies outside the loop noise bandwidth. All order filters which are Wiener-optimized for tracking or demodulation in the presence of additive white noise possess this property. Therefore, it is permissible to rewrite (2) as

$$F(s) = \frac{K_2}{K_1}F_2 + F_1(s) \tag{3}$$

where F_2 is independent of s and $F_1(s)$ is the low-pass term with zero high frequency gain.

The advantage of employing the split-loop technique is apparent when the excess phase shift introduced into the long

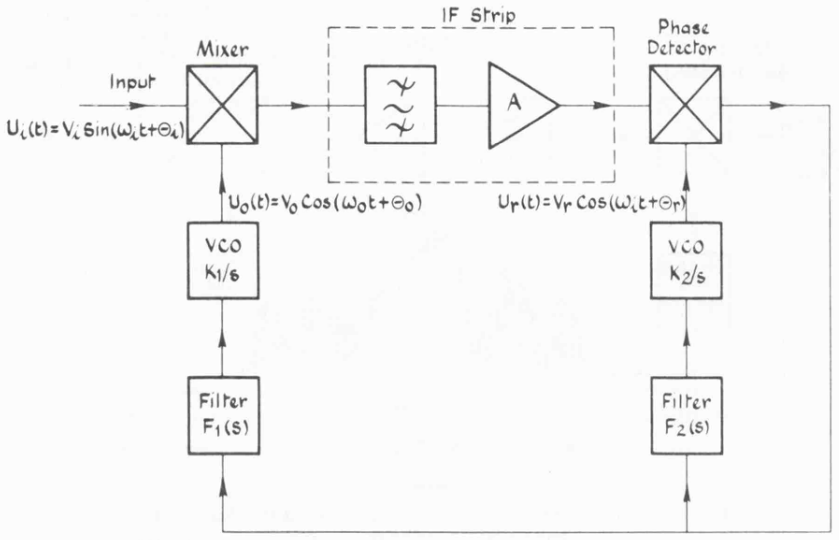

Fig. 2. Configuration of the split-loop phase-locked receiver.

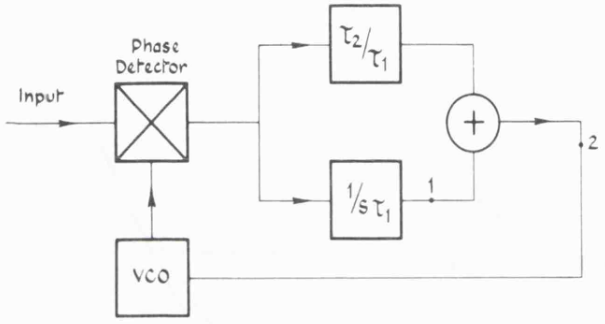

Fig. 3. Equivalent model of a second-order, type-two phase-locked loop.

loop by the IF stages is taken into account. During the acquisition stage of the long loop, the beat frequency from the phase sensitive detector propagates around the F_2 path, bypassing the IF stages, and, thus, eliminating the possibility of false-locking. To confirm the validity of the method, acquisition time measurements were conducted on an audio second-order type-two phase-locked loop, a block diagram of which is shown in Fig. 3. Here, the loop filter is described by the relationship

$$F(s) = \frac{1 + s\tau_2}{s\tau_1} \tag{4}$$

where, using (3), $F_2 = \tau_2/\tau_1$ and $F_1(s) = 1/s\tau_1$. By inserting a variable CCD delay line at either points 1 or 2 in Fig. 3, it was possible to simulate either the split or conventional long loop. The loop had a natural frequency of 100 Hz and a damping factor of $1/\sqrt{2}$. The resulting acquisition time-frequency offset measurements for the conventional and split-loops are shown in Figs. 4 and 5, respectively. As expected, Fig. 4 illustrates the dramatic reduction in pull-in range caused by the presence of time delay. However, when the time delay is restricted to the integrator path of the filter, the effect of delay is substantially reduced and false-locking is eliminated. In fact, for large frequency offsets, increasing the time delay up to the stability limit shows negligible effect on acquisition time.

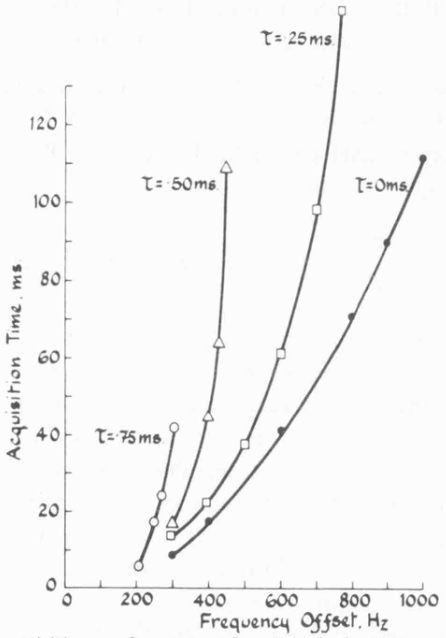

Fig. 4. Acquisition performance of a phase-locked loop with time delay τ.

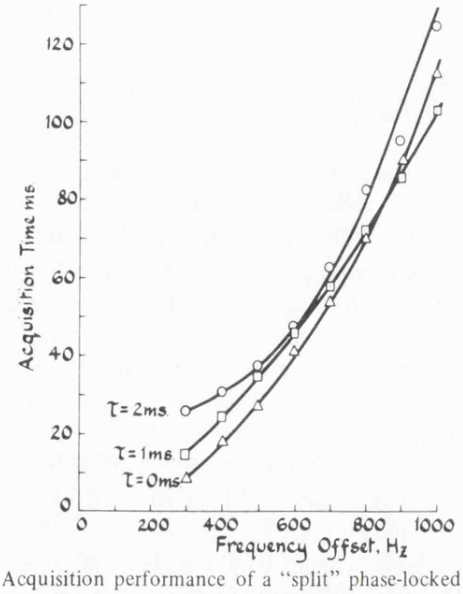

Fig. 5. Acquisition performance of a "split" phase-locked loop with time delay τ present in the integrator path.

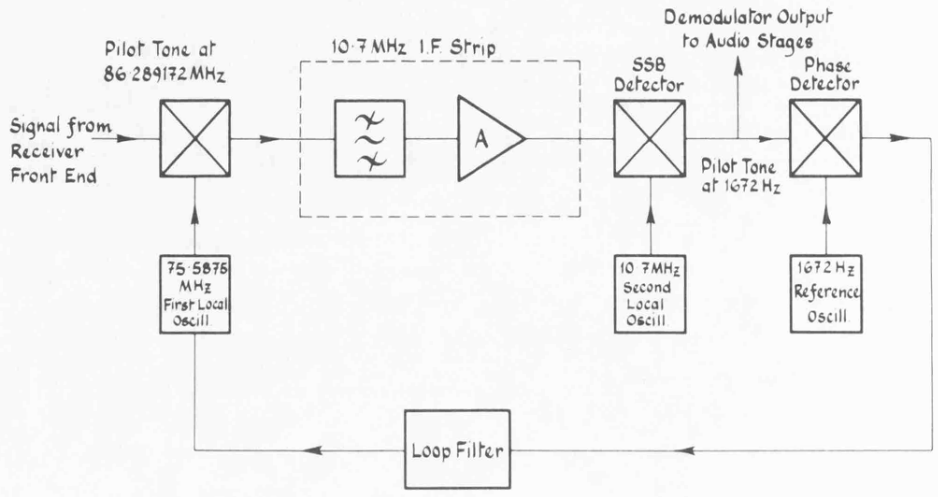

Fig. 6. Conventional long phase-locked loop in the Wolfson tone-in-band VHF single sideband receiver.

IV. APPLICATION OF SPLIT-LOOP TECHNIQUE TO A VHF SSB MOBILE RADIO

In this section, the split-loop technique is applied to the design of the Wolfson tone-in-band VHF SSB land mobile radio receiver developed at the University of Bath. The technique is equally applicable to the pilot carrier and tone-above-band systems.

A. Acquisition Performance

In the Wolfson pilot tone SSB system [10], a tone some 15 dB down on peak envelope power is transmitted in a notch in the midband region of the audio spectrum. The choice of tone frequency is somewhat arbitrary, but frequencies in the range of 1.2-2.5 kHz are acceptable. The tone is used in the receiver for AGC and AFC purposes. In this research work, a tone frequency of 1.672 kHz was used, such that when the received signal was demodulated to audio, the received tone is compared in frequency and phase to an internally generated 1.672 kHz precise reference. A simplified block diagram showing a low-band VHF phase-locked receiver is given in Fig. 6. Additional filtering within the loop, for instance, the IF filter or a tone bandpass filter, has been shown [20] to severely degrade pull-in performance characteristics even when a derived rate rejection acquisition aid [21] is used. The problem is further exacerbated if the first local oscillator frequency is derived from a narrow bandwidth synthesizer.

An 86.2875 MHz receiver, which allowed control of the first or second oscillators or split control with integral control of the first oscillator and proportional control of the second, was constructed. Acquisition measurements were taken for a 100 Hz loop with a damping factor of $1/\sqrt{2}$, thus corresponding to the loop parameters of Section III. The receiver AGC was fixed throughout the experiment. Excess phase shift was introduced into the loop by the SSB IF filter and the first local oscillator channel synthesizer. The IF filter had a measured midband group delay of 0.41 ms at 10.70167 MHz. The phase-locked loop synthesizer was based on the Philips LN123/LN124 integrated circuits with a closed-loop, 3 dB bandwidth of 625 Hz, as recommended in the manufacturer's specification for 6.25 kHz channel spacing. The experimental results are shown in Fig. 7. For the conventional long-loop receiver, false-locking occurred and acquisition was only possible at frequency offsets up to 300 Hz. For the short (i.e., fixed first local oscillator) and split-loop configurations, acquisition occurred without difficulty. The split-loop results clearly illustrate that the receiver's first local oscillator can acquire large frequency offsets irrespective of the excess loop phase shift.

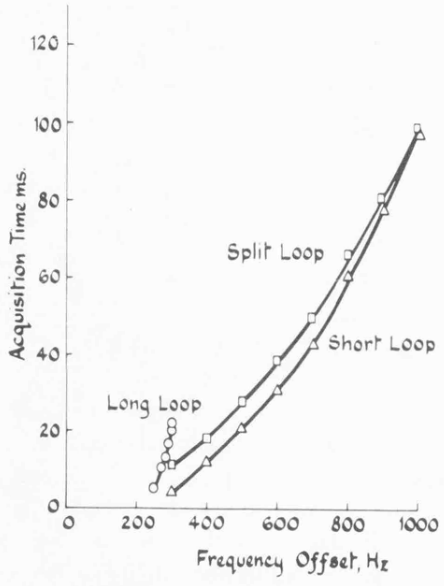

Fig. 7. Comparative acquisition performance of a VHF single sideband receiver for the long-, short-, and split-loop configurations.

B. Improvement in Output Spectrum of First Local Oscillator

Modulation components at the SSB detector output, Fig. 6, mix with the reference tone in the phase sensitive detector. The resulting sum and difference phase sensitive detector outputs give rise to sidebands on the first local oscillator. McGeehan and Lymer [12] indicate that this could result in poor adjacent channel protection caused by reciprocal mixing. This form of spurious reception occurs when a side-

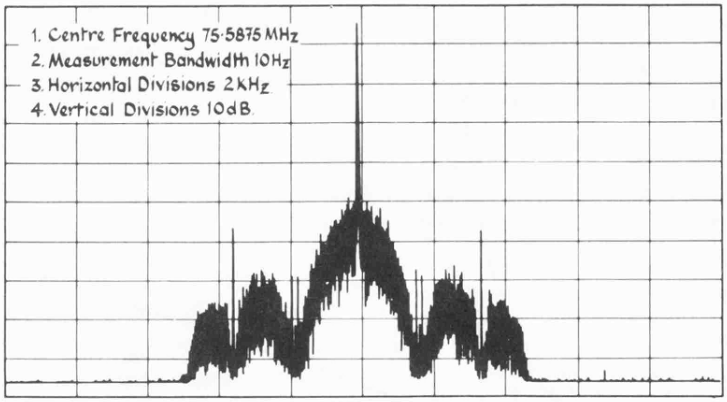

Fig. 8. First local oscillator spectrum of a tone-in-band long-loop SSB receiver.

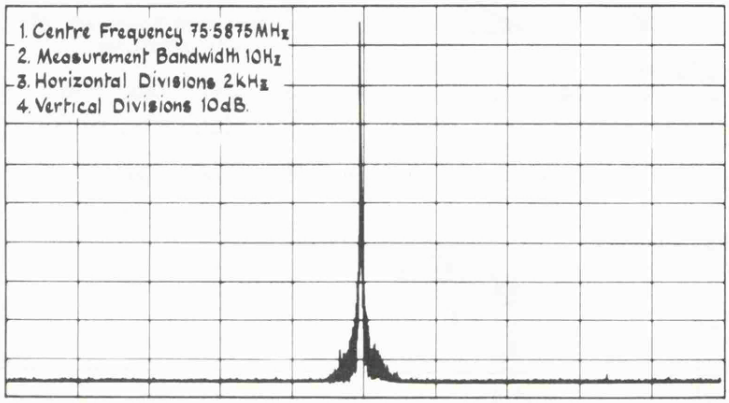

Fig. 9. First local oscillator spectrum of a tone-in-band split-loop SSB receiver.

band on the first local oscillator mixes with an unwanted adjacent channel tone producing a component within the IF crystal filter passband. However, when the split-loop is used, the modulation components mainly degrade the second local oscillator which is protected from the adjacent channel by the IF filter. In the conventional long loop, a tone at frequency ω rad/s, at the phase detector output, frequency modulates the VCO after passing through a low-pass filter described by (4). In the split-loop case the proportional term to the first local oscillator is removed and the filter becomes $F_1(s) = 1/s\tau_1$. It is easily shown that the resultant reduction in the tone level at the first local oscillator input is given by $10 \log_{10} [1 + 4\zeta^2\omega^2/\omega_n{}^2]$ dB where ω_n is the loop natural frequency and ζ is the loop damping factor. In the current Wolfson SSB system [22], the peak envelope power is limited at 15 dB above the pilot tone in the transmitter and ω_n is set at 2π 10 rad/s. Figs. 8 and 9 depict the output spectra of the first local oscillator of the receiver with conventional and split-long-loop control, respectively, when receiving random noise. The noise was transmitted to simulate speech modulation. The conventional long-loop controlled oscillator spectrum of Fig. 8 shows that the first-order sidebands are evident with terms at ±3.34 kHz offset, twice the pilot tone reference frequency. In Fig. 9, which shows the split-loop controlled first local oscillator, the modulation induced phase noise is only visible up to about 1 kHz offset, 105 dB/Hz below carrier. This performance would not limit the adjacent channel protection ratio that is required for a land mobile radio system.

V. LOOP NOISE BANDWIDTH

The noise bandwidth of a phase-locked loop is given by

$$B_n = \int_0^\infty |H(j2\pi f)|^2 \, df \text{ Hz} \tag{5}$$

where $H(s)$ is the closed loop transfer function. For a second-order type-two loop with fixed natural frequency ω_n rad/s, the integral has a minimum value at $\omega_n/2$ Hz [23] when ζ is set equal to 0.5. In this paper, the minimization has been computed when the loop contains a pure time delay τ, initially in both filter paths, and second, when the delay is restricted to the integrator path alone. In the first case $H(s)$ is given by

$$H(s) = \frac{\omega_n{}^2 + 2\zeta\omega_n s}{\omega_n{}^2 + 2\zeta\omega_n s + e^{s\tau}s^2} \tag{6}$$

and when the delay is restricted to the integrator path

$$H(s) = \frac{e^{-s\tau}\omega_n{}^2 + 2\zeta\omega_n s}{e^{-s\tau}\omega_n{}^2 + 2\zeta\omega_n s + s^2}. \tag{7}$$

The integrals were evaluated numerically to a frequency of 300 ω_n rad/s and the resulting curves are given in Fig. 10. Here, the minimum normalized noise bandwidth and the corresponding damping factors required are plotted against delay phase $\omega_n\tau$. For the conventional long loop, the minimum

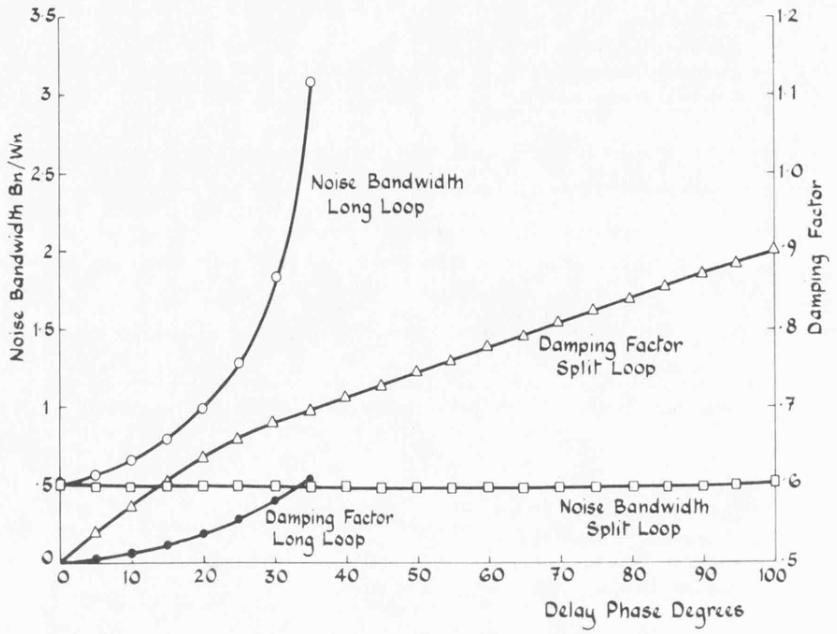

Fig. 10. Effect of time delay on minimum noise bandwidth.

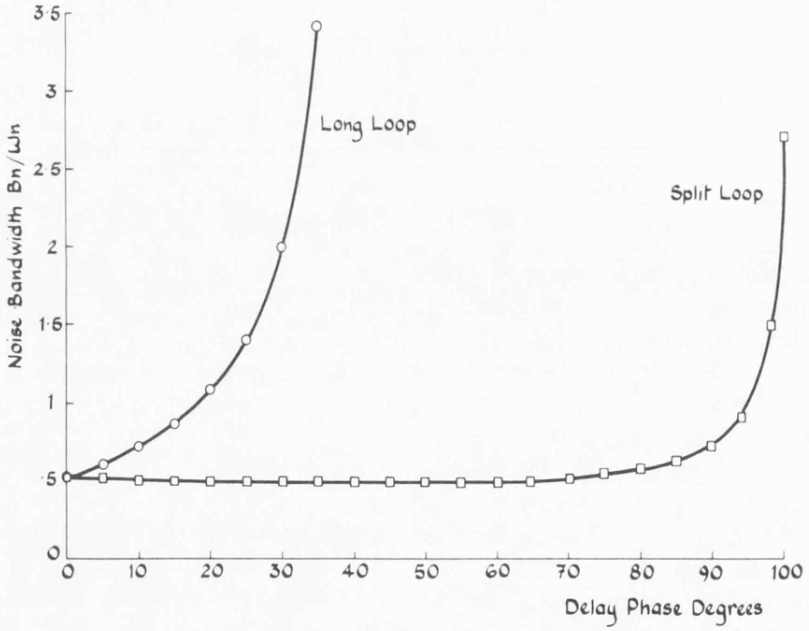

Fig. 11. Effect of time delay on noise bandwidth for a loop damping ratio ζ of $1/\sqrt{2}$.

noise bandwidth steadily increases with the time delay until the loop eventually becomes unstable. The results are similar to those obtained by Frankle and Klapper [24]. However, when the delay is restricted to the integrator path, the minimum noise bandwidth is affected to a negligible extent by the excess delay. Phase-locked receivers are usually designed with a damping factor of $1/\sqrt{2}$, and for this case the variation of noise bandwidth with delay is illustrated in Fig. 11. It can be seen again that the split-loop tolerates large delays before the noise performance is severely degraded.

VI. CONCLUSIONS

In this paper a split-loop technique which overcomes many of the problems associated with conventional long-loop phase-locked radio receivers has been described. It was shown to eliminate the problem of false-locking and result in a similar acquisition performance to that expected without time delay. The technique is extremely simple to implement in that the only additional circuitry required is a split-loop filter and a low deviation voltage-controlled second local oscillator. Furthermore, the degradation of the first local oscillator spectrum caused by modulation and noise components entering the loop has been shown to be substantially reduced, resulting in an improved adjacent channel performance. When the phase-locked loop contained pure time delay, the noise bandwidth performance was also improved by the use of the split-loop technique.

It is felt that the technique will find immediate application

in the current VHF SSB mobile radios being developed. It should be noted that the time delay generally associated with the pilot carrier and tone-above-band systems is somewhat greater than that for the midband tone system as a consequence of the increased group delay at the edges of IF crystal filter.

ACKNOWLEDGMENT

The authors wish to thank Prof. J. F. Eastham, Head of the School of Electrical Engineering, for the provision of laboratory facilities, and the second author is grateful to the U.K. Science and Engineering Research Council for the award of a research studentship.

REFERENCES

[1] M. H. Brockman, H. R. Buchanan, R. L. Choate, and L. R. Malling, "Extraterrestrial radio tracking and communication," *Proc. IRE*, vol. 48, pp. 643–655, Apr. 1960.

[2] J. P. McGeehan, "Design and characterization of a phaselocked VHF land mobile radio receiver," in *Proc. IERE Conf. Civil Land Mobile Radio*, London, England, Nov. 1975, pp. 37–46.

[3] F. M. Gardner, *Phaselock Techniques*. New York: Wiley, 1979, p. 144.

[4] ——, *Phaselock Techniques*. New York: Wiley, 1979, pp. 151–156.

[5] J. A. Develet, "The influence of time delay on second-order phase-lock loop acquisition range," in *Proc. Int. Telem. Conf.*, London, England, 1963, pp. 432–437.

[6] Z. J. Jelonek and C. I. Cowan, "Synchronized systems with time delay in the loop," *Proc. Inst. Elec. Eng.*, vol. 104C, pp. 388–397, 1957.

[7] B. N. Biswas, P. Banerjee, and A. K. Bhattacharya, "Heterodyne phase locked loops—revisited," *IEEE Trans. Commun.*, vol. COM-25, no. 10, pp. 1164–1171, 1977.

[8] R. Wells, "SSB for VHF mobile radio at 5 kHz channel spacing," in *Proc. IERE Conf. Radio Receivers, Associated Syst.*, London, England, 1978, pp.29–36.

[9] J. R. Ball and D. W. J. Holmes, "An SSB with pilot receiver for mobile radio," in *Proc. IERE Clerk Maxwell Commemorative Conf. Radio Receivers, Associated Syst.*, Leeds, England, July 1981, pp. 429–435.

[10] W. Gosling, J. P. McGeehan, and P. G. Holland, "Receivers for the Wolfson single sideband VHF land mobile radio system," *Radio Electron. Eng.*, vol. 49, pp. 321–325, 1979.

[11] B. B. Lusignan, "AGC, AFC, tone select circuits for narrow-band mobile radio," presented at the Int. Telecommun. Expo., Dallas, TX, Feb. 1979.

[12] J. P. McGeehan and A. Lymer, "The problem of speech pulling and its implications for the design of phaselocked SSB radio systems," *Proc. Inst. Elec. Eng.*, vol. 128, part F, no. 6, pp. 361–369, 1981.

[13] F. M. Gardner, *Phaselock Techniques*. New York: Wiley, 1979, p. 75.

[14] K. Daikoku, "Analysis of phase-locked loop acquisition with delay time," *Rev. Elec. Commun. Lab.*, vol. 23, no. 7–8, pp. 976–983, 1975.

[15] Y. Ueda, Y. Akamata, and T. Nanahara, "Phase-locked loop with delay time–Computer experiment on pull in range," *Trans. IECE Japan*, vol. E.61, no. 6, pp. 471–472, 1978.

[16] D. Richman, "Color carrier reference phase synchronization accuracy in NTSC color television," *Proc. IRE*, vol. 42, pp. 106–133, Jan. 1954.

[17] B. N. Biswas and P. Banerjee, "Range extension of a phase-locked loop," *IEEE Trans. Commun.*, vol. COM-21, pp. 293–296, 1973.

[18] C. J. Ward, "Delay reduction techniques in phase-locked loop amplifiers," *Electron. Lett.*, vol. 17, pp. 253–255, Apr. 1981.

[19] S. A. Meer, "Analysis of phase-locked loop acquisition: A quasi-stationary approach," in *IEEE Conv. Rec.*, vol. 14, pt. 7, 1966, pp. 85–106.

[20] J. H. Richardson, "Practical investigation of a phase-locked SSB receiver for VHF civil land mobile radio," M.Sc. thesis, Univ. Bath, Bath, England, 1979.

[21] J. P. McGeehan, "Technique for improving the pull-in characteristics of phase-locked loops," *Proc. Inst. Elec. Eng.*, vol. 123, pp. 761–764, Aug. 1976.

[22] J. P. McGeehan, G. Lightfoot, A. Lymer, and W. Gosling, "Optimisation of the Wolfson SSB radio receiver," in *Proc. IERE Clerk Maxwell Commemorative Conf. Radio Receivers, Associated Syst.*, Leeds, England, July 1981, pp. 417–428.

[23] F. M. Gardner, *Phaselock Techniques*. New York: Wiley, 1979, p. 31.

[24] J. Klapper and J. T. Frankle, *Phase-Locked and Frequency-Feedback Systems*. New York: Academic, 1971, p. 111.

★

Joseph P. McGeehan was born in Bootle, Merseyside, England, on February 15, 1946. He received the B.Eng. and Ph.D. degrees in electrical engineering from the University of Liverpool, Liverpool, England, in 1967 and 1972, respectively.

From 1970 to 1972 he held the position of Senior Scientist at the Allen Clark Research Centre, The Plessey Company Ltd., where he was primarily concerned with research into solid-state microwave devices and their applications. In September 1972, he was appointed Lecturer in the School of Electrical Engineering at the University of Bath, Bath, England, and has led a project team conducting research into the application of signal processing techniques to single sideband mobile radio communication systems. He is the author or co-author of 40 scientific papers.

In recent years, Dr. McGeehan has served as a member of the U.K. Home Office (Directorate of Radio Technology) Working Group on single sideband land mobile radio and is a member of U.K. Study Group 8A of CCIR. He is a Chartered Engineer and a member of the Institution of Electrical Engineers and the Institute of Electronic and Radio Engineers.

★

Jonathan P. H. Sladen was born in Bath, England, on February 9, 1957. He received the B.Sc. degree in electrical engineering from the University of Bristol, Bristol, England, in 1978.

From 1978 to 1980 he was employed by Racal (Slough) Limited, Tewkesbury, England, working on the design of specialized HF and VHF radio communications equipment. Since 1980 he has been undertaking research into phase-locked radio receivers at the University of Bath, Bath.

Comparative adjacent-channel selectivity performance of phase-locked pilot-tone SSB mobile radio receivers with particular reference to the long-, short- and split-loop configurations

J.P. McGeehan, B.Eng., Ph.D., C.Eng., M.I.E.R.E., M.I.E.E., and J.P.H. Sladen, B.Sc.

Indexing terms: *Radiocommunication, Mobile radio systems*

Abstract: There has been considerable interest, both in the USA and in the UK, in the use of 5 kHz pilot-tone single-sideband modulation for the VHF and UHF civil land mobile radio service. However, if single sideband (SSB) is going to be a commercially viable proposition, it will be necessary to use some form of automatic frequency control to reduce the specification and hence the cost of reference oscillators. The use of such techniques has the added advantage that system frequency drifts will be tracked out. To date, 'long-loop' phase-locked receiver configurations have been employed to achieve this aim. Unfortunately, this long-loop technique has several drawbacks, including a possible large degradation in adjacent-channel immunity. This problem was alluded to in a recent publication by McGeehan and Lymer, and these authors have indicated several ways of reducing the problem. In the paper, a technique is described which overcomes many of the drawbacks associated with long-loop receivers, notably the problem of poor adjacent-channel performance. To this end, the results of laboratory tests comparing the adjacent-channel performance of conventional long-loop, short-loop (equivalent to a fixed oscillator receiver) and the new split-loop technique are presented, together with an analysis of the receiver mechanisms which limit adjacent-channel selectivity. It is shown that satisfactory control of the first local oscillator may be obtained with the split-loop configuration.

List of principal symbols

$v(t)$	=	instantaneous value of voltage
V	=	peak value of voltage
ω	=	angular frequency ($2\pi f$)
θ	=	phase
A	=	IF gain
$G(\omega)$	=	IF filter characteristic
$F(\omega)$	=	loop filter characteristic
K_0	=	VCO gain
K_d	=	phase detector gain constant
ζ	=	loop damping factor
ω_n	=	loop natural frequency
τ_1, τ_2	=	time constants of loop filter
$F(s)$	=	loop filter transfer function
s	=	Laplacian operator
V_n	=	RMS noise voltage
B	=	bandwidth of noise voltage
$\Delta\omega_{RMS}$	=	RMS oscillator deviation
ω_m	=	angular modulation frequency
S	=	reference-tone signal/noise ratio
k	=	an integer

Subscripts for v(t), V, ω and θ

a	=	adjacent-channel RF input tone
i	=	wanted reference RF input tone
0	=	first local oscillator output
1	=	second local oscillator output
r	=	reference-tone oscillator output
t	=	demodulated tone induced by adjacent-channel RF tone
s	=	frequency spacing between adjacent-channel tone and wanted carrier
b	=	demodulated speech term
c	=	received reference tone at SSB detector output

Paper 2228F, first received 5th May and in revised form 23rd August 1982

The authors are with the School of Electrical Engineering, University of Bath, Claverton Down, Bath BA2 7AY, England

1 Introduction

Since the mid-1970s, there has been increasing interest both in the UK and in the USA in the use of single-sideband (SSB) modulation in the civil land mobile radio service. Recently, the UK Home Office Directorate of Radio Technology has conducted a series of comparative field trials at VHF involving uncompanded 5 kHz SSB, 12.5 kHz FM, 25 kHz FM and 12.5 kHz AM and published a report on their findings [1]. A similar series of trials comparing companded 5 kHz SSB with 25 kHz FM has recently begun in the USA under the auspices of the Federal Communication Commission [2, 3]. Although the results of the Home Office trials were particularly encouraging for the proponents of SSB, the receiver used in the tests was of the double superheterodyne type with high-stability fixed-frequency oscillators. It is now generally accepted that, for SSB to be a viable proposition in the private mobile and hand portable radio marketplace, some form of automatic frequency control is required. However, recent work [4, 5] has highlighted the fact that the use of such techniques may degrade the receiver's adjacent-channel performance through reciprocal mixing, caused by information components modulating the first local oscillator.

All three SSB systems currently under investigation transmit a constant-amplitude pilot tone, together with the speech information, for AFC and AGC reference purposes and essentially differ in the positioning of the reference tone within the transmitted audio bandwidth. The three systems are pilot carrier [6, 7], tone in band [8] and tone above band [9]. In the Wolfson tone-in-band system, the reference tone is placed in a notch in the audio spectrum prior to transmission. The reference frequency used is somewhat arbitrary and in the present system is fixed at 1.672 kHz. A simplified block diagram of the receiver is shown in Fig. 1. The demodulated reference tone is phase compared with an internally generated 1.672 kHz reference tone, and the resulting error signal is used to control the first local oscillator in a long-loop configuration. Control of the first local oscillator is advantageous since it ensures that the modulation is correctly positioned with in the narrow IF crystal filter, thereby preventing sideband cutting [10]. However, the received speech information mixes with the

0143–7070/82/060439 + 08 $01.50/0

reference tone in the phase detector, passes through the loop filter and frequency modulates the first local oscillator, thus spreading its output spectrum. Clearly, significant components of the oscillator spectrum spaced sufficiently far from the oscillator's centre frequency can cause frequency components in the adjacent channel to be received within the passband of the IF crystal filter. This effect is absent in a short-loop receiver (i.e. a receiver with fixed first local oscillator and voltage-controlled second local oscillator) as the SSB detector input is protected from the adjacent channel by the IF filter. In this respect, McGeehan and Sladen [5] have recently published a paper detailing a new phase-locked-loop receiver configuration which substantially reduces the spreading of the first local oscillator spectrum but retains the advantages of long-loop control. This 'split-loop' technique recognises the fact that the loop filter of a second-order type-two loop can be separated into an integrator path and a proportional path. The integrator path is used to control the first local oscillator, while the proportional path controls the second oscillator. The information components, which are outside the loop bandwidth, pass through the proportional term but are heavily attenuated by the integrator controlling the first local oscillator. This results in a considerable reduction in the spreading of the first local oscillator's spectrum. Use of the split-loop technique was also shown to substantially improve the dynamic behaviour of the loop. The usual problems of low frequency acquisition range, false locking and increased noise bandwidth which are associated with the conventional long-loop receiver are eliminated.

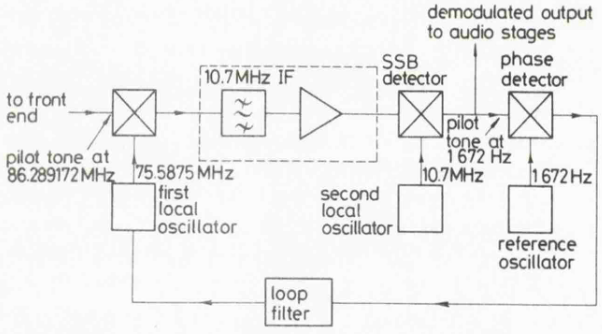

Fig. 1 *Long-loop configuration in Wolfson VHF tone-in-band receiver*

From the foregoing discussion, it is apparent that there is an urgent need for adjacent-channel selectivity measurements in phase-locked pilot-tone SSB receiver configurations, together with an understanding of the mechanisms which limit the selectivity. In this paper, these mechanisms will be detailed so that the adjacent-channel performance of the various loop types may be predicted theoretically. Although the analysis will be developed for a tone-in-band receiver, the tone-above-band and pilot carrier systems can be treated in a similar manner. The adjacent-channel selectivities of the conventional long- and short-loop tone-in-band SSB receivers, and the newly developed split-loop receiver, will then be measured and compared with the theoretically determined values. Finally, the results will be compared with those obtained in the Home Office SSB trials.

2 Adjacent-channel performance limitations of a phase-locked SSB pilot-tone receiver

This Section describes two mechanisms peculiar to a phase-locked design which limit the adjacent-channel selectivity of an SSB receiver. They are reciprocal mixing due to speech information entering the control loop and a previously unreported effect which causes instability within the phase-locked loop.

2.1 *Adjacent-channel induced instability*

During a preliminary investigation of the effect of an adjacent-channel tone on the performance of a long-loop phase-locked receiver, see Fig. 1, it was observed that, for a small increase in adjacent-channel tone power above a particular level, an additional demodulated tone of large amplitude appeared at the SSB detector output at a frequency seemingly unrelated to the adjacent-channel frequency. At this level of adjacent-channel interference, the receiver became unusable. The effect is due to instability in the phase-locked loop caused by the presence of the adjacent-channel tone. To demonstrate how this induced instability occurs, assume that the receiver is locked to the reference-tone input and that there is also a demodulated tone $V_t \sin(\omega_t t + \theta_t)$ at the SSB detector output. This tone gives rise to two frequency components at the phase detector output, owing to mixing with the reference oscillator frequency, which in turn modulate the first local oscillator. The resulting sidebands will mix with the adjacent-channel tone and may produce a component within the IF passband which is subsequently demodulated to audio. If this audio tone is of the same amplitude, frequency and phase as the original tone, the oscillation will be maintained and the loop becomes unstable. It is shown in Appendix 7.1 that, for an upper-sideband receiver and given values for the frequency spacing between the adjacent-channel tone and the wanted signal carrier frequency ω_s and the reference tone oscillator frequency ω_r, there are two solutions to the value of ω_t:

$$2\omega_t = \omega_s + \omega_r \tag{1}$$

and

$$2\omega_t = \omega_s - \omega_r \tag{2}$$

with corresponding open-loop gains given by

$$|G(\omega_1 + \omega_t)| \frac{V_a 2\zeta\omega_n}{V_i(\omega_s - \omega_r)} \tag{3}$$

and

$$|G(\omega_1 + \omega_t)| \frac{V_a 2\zeta\omega_n}{V_i(\omega_s + \omega_r)} \tag{4}$$

respectively, where

ζ = phase-locked-loop damping factor
ω_n = phase-locked-loop natural frequency
V_a = adjacent-channel-tone level at the receiver input
V_i = wanted reference-tone level at the receiver input
ω_1 = second local oscillator frequency

To summarise, if the adjacent-channel level V_a is sufficiently high that the magnitude of the gain given by either of exprs. 3 or 4 is greater than unity, then oscillations at a frequency given by either eqns. 1 or 2 will be maintained at the SSB detector output.

Fig. 2 illustrates the two solutions and the corresponding open-loop gains (with $V_a/V_i = 1$) for the receiver used for the selectivity tests in Section 3 of this paper. The tone-in-band receiver had a reference oscillator frequency of 1.672 kHz and phase-locked-loop parameters $\zeta = 1/\sqrt{2}$ and $\omega_n = 2\pi\,10$ rad/s. The upper-sideband IF crystal filter had a 3 dB bandwidth of 3.7 kHz. Although this bandwidth is a little too large to accommodate 5 kHz channelling, the filter nonetheless presented a stringent and overly pessimistic interpretation of the adjacent-channel performance of 5 kHz SSB mobile radio receivers. Measurements were carried out to verify eqns. 1 and 2 and exprs. 3 and 4. An adjacent-channel tone and the wanted

pilot tone were summed at the RF input of the receiver. The adjacent-channel-tone level was increased until the loop became unstable, at which point ω_s, ω_t and V_a/V_i were recorded. The test was then repeated for different values of carrier to adjacent-channel-tone frequency spacing ω_s. The open-loop gains at $V_a/V_i = 1$ were then calculated and these, together with the measured values of ω_t, are compared with the theoretical curves in Fig. 2. The results show good agreement except at an adjacent-channel tone to carrier spacing of 6 kHz, where two tones (1.22 and 3.11 kHz) appeared at the SSB detector output. This 'anomalous' result can be explained as follows.

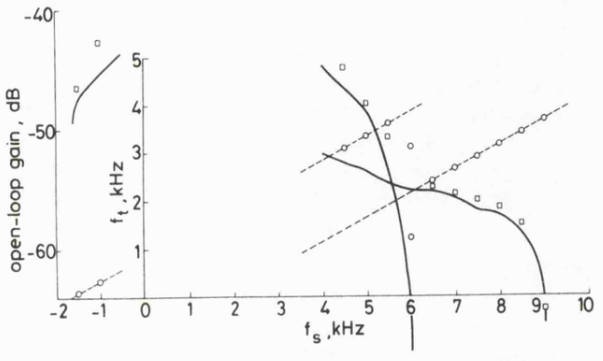

Fig. 2 *Variation of open-loop gain and f_t with carrier to adjacent-channel-tone frequency spacing f_s*

- – – – theoretical f_t
- ○ experimental f_t
- ——— theoretical gain
- □ experimental gain

A tone of frequency ω_t at the phase detector input is fedback through the loop and appears at the SSB detector output at a frequency ω_t'. This tone is in turn fedback around the loop and appears for a second time at the SSB detector output but at a frequency ω_t. Using the same technique as that adopted in Appendix 7.1, the following equations can be shown to apply for the case observed at $\omega_s = 2\pi\, 6 \times 10^3$ rad/s:

$$(\omega_t + \omega_t') = (\omega_s - \omega_r) \tag{5}$$

$$\text{open-loop gain} = \zeta^2 \omega_n^2 \frac{V_a^2}{V_i^2} \frac{1}{(\omega_t' + \omega_r)} \frac{1}{(\omega_t + \omega_r)}$$

$$\times |G(\omega_t + \omega_1)|\,|G(\omega_t' + \omega_1)| \tag{6}$$

The theoretical curves computed from eqns. 5 and 6 are shown in Fig. 3, together with the experimental results. As expected, the oscillations occur at the peaks of the gain curve, although the gain at $\omega_t = \omega_t'$ is only fractionally lower. This result observed at an adjacent-channel-tone offset frequency of 6 kHz indicates that eqns. 1 and 2 do not give the only possible values of the instability frequencies induced by an adjacent-channel interferer. Solutions which require more than one demodulated tone at the SSB detector output to be fedback around the loop are possible and will occur if their open-loop gains are sufficiently high. These solutions can be found by using a similar analysis to that contained in Appendix 7.1. However, for the receiver tested in this paper, only exprs. 3 and 4 are required to predict the degradation of the receiver's adjacent-channel selectivity due to instability.

For a split-loop receiver, the filter inserted between the phase detector and the first local oscillator is an integrator with transfer function $1/s\tau_1$. It is a simple matter to show that this filter reduces the magnitudes of the open-loop gains in exprs. 3 and 4 by $10\log_{10}(2\zeta\omega/\omega_n)^2$ dB, where ω is the tone frequency at the phase detector output [i.e. either $(\omega_t - \omega_r)$ or $(\omega_t + \omega_r)$]. For example, at $\omega_s = 2\pi\, 5 \times 10^3$ rad/s, the split loop gives an open-loop gain reduction of 47 dB in the Wolfson receiver so that, for oscillations to occur, the ratio of V_a/V_i must be greater than 95 dB.

2.2 *Reciprocal mixing*

Speech information at the SSB detector output enters the phase detector and, after mixing and passing through the loop filter, modulates the first local oscillator of the long-loop receiver. This degrades the spectrum of the oscillator, giving rise to the possibility of reciprocal mixing of the adjacent-channel interferer into the IF channel by the oscillator sidebands. The spectrum of the Wolfson receiver's first local oscillator is shown in Fig. 4 when a 1 kHz 'speech' tone is received 5 dB above the pilot tone with a SINAD ratio of 12 dB. The six discrete sidebands are due to the phase detector output terms at twice the reference frequency, and at the reference frequency ± the speech-tone frequency.

In Appendix 7.2, it is shown that the levels of these discrete sidebands are given by:

$$(a) \quad 10\log_{10}\left(\frac{\zeta\omega_n}{2\omega_r}\right)^2 \text{dB} \qquad \text{for } \pm 2\omega_r \text{ terms}$$

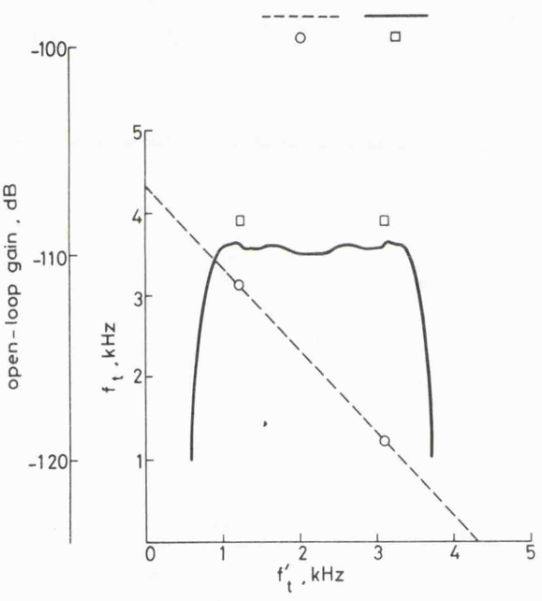

Fig. 3 *Variation of open-loop gain and f_t with f_t' for a carrier to adjacent-tone frequency spacing $f_s = 6$ kHz and for $(f_t + f_t') = (f_s - f_r)$*

- – – – theoretical $f_t + f_t'$
- ○ experimental $f_t + f_t'$
- ——— theoretical gain
- □ experimental gain

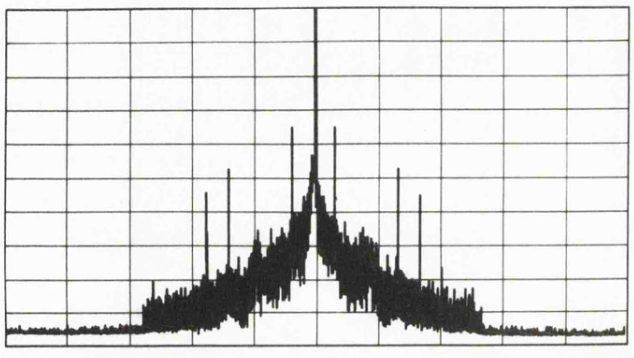

Fig. 4 *Frequency spectrum of first local oscillator for long-loop phase-locked receiver*

Vertical scale: 10 dB/division — Top line: + 10 dBm
Horizontal scale: 2 kHz/division — Centre frequency: 75.5875 MHz
Bandwidth = 10 Hz

$$(b)\quad 10\log_{10}\left(\frac{\text{speech tone power}}{\text{reference tone power}}\right)$$

$$+ 10\log_{10}\left(\frac{\zeta\omega_n}{\omega_b-\omega_r}\right)^2 \qquad \text{for } \pm(\omega_b-\omega_r) \text{ terms}$$

$$(c)\quad 10\log_{10}\left(\frac{\text{speech tone power}}{\text{reference tone power}}\right)$$

$$+ 10\log_{10}\left(\frac{\zeta\omega_n}{\omega_b+\omega_r}\right)^2 \qquad \text{for } \pm(\omega_b+\omega_r) \text{ terms}$$

where ω_b is the frequency of the demodulated speech tone. Each sideband will mix with an adjacent-channel tone and possibly give rise to a spuriously received tone within the IF passband.

Noise appearing at the SSB detector output will also give rise to modulation of the first local oscillator. For noise band-limited to B rad/s at the SSB detector output, the first local oscillator noise-power-density/carrier-power ratio is derived in Appendix 7.2 as

$$\frac{2\zeta^2\omega_n^2}{SB\omega_m^2}\ \text{s/rad} \qquad \text{for } \omega_n \ll \omega_m < (B-\omega_r)$$

and

$$\frac{\zeta^2\omega_n^2}{SB\omega_m^2}\ \text{s/rad} \qquad \text{for } (B-\omega_r) < \omega_m < (B+\omega_r)$$

where ω_m is the modulation frequency and S is the reference-tone signal/noise ratio. By integrating this expression over the appropriate region for a given adjacent-channel frequency, the noise power mixed into the IF passband can be estimated.

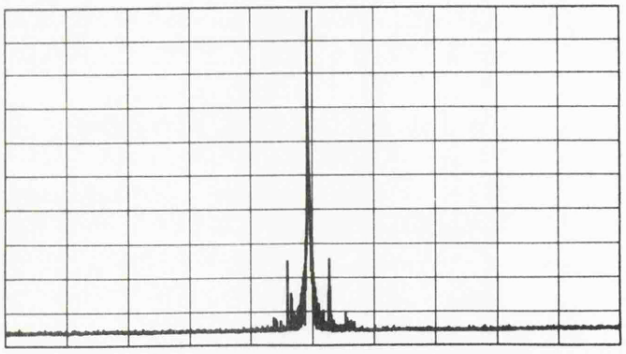

Fig. 5 *Frequency spectrum of first local oscillator for split-loop phase-locked receiver*

Vertical scale: 10 dB/division Top line: + 10 dBm
Horizontal scale: 2 kHz/division Centre frequency: 75.5875 MHz
Bandwidth = 10 Hz

The improvement in adjacent-channel selectivity using a split-loop configuration is similar to that of the instability case and, for modulation frequencies outside the loop bandwidth, the sideband levels are reduced by $10\log_{10}(2\zeta\omega_m/\omega_n)^2$. For example, in the Wolfson receiver, the sum and difference terms due to a 1 kHz speech tone are reduced by 52 and 40 dB, respectively. The first local oscillator spectrum of the split-loop receiver is shown in Fig. 5 for comparison with Fig. 4.

3 Adjacent-channel selectivity measurements

In this Section, measurements of the adjacent-channel performance of the Wolfson VHF SSB receiver will be described and results will be given for the long-, short- and split-loop configurations. In the absence of an official specification, the adjacent-channel selectivity of a pilot-tone SSB receiver is defined here so as to parallel the definition for full-carrier AM equipment in the Home Office specification MPT1302. To measure the adjacent-channel selectivity in accordance with this specification, the wanted signal at the nominal frequency of the receiver and with normal test modulation (a modulation frequency of 1 kHz with a 30% modulation depth) is applied to the receiver input via one path of a combining unit. The unwanted signal is applied through the second path at the frequency of the upper adjacent channel and modulated with a frequency of 400 Hz at a depth of 30%. The audio output of the receiver is monitored by a distortion-factor meter, and in the absence of the unwanted signal the level of the wanted signal is adjusted until the SINAD ratio is 12 dB. The unwanted signal is switched in and adjusted in level until the SINAD ratio is reduced to 6 dB. This measurement is then repeated with the unwanted signal at the frequency of the lower adjacent channel. The adjacent-channel selectivity is expressed as the lower value of the ratios, in decibels, for the upper and lower adjacent channels of the level of the unwanted signal to the level of the wanted signal.

For an SSB pilot-tone receiver, the wanted signal consists of a pilot tone, set at the nominal receiver pilot-tone frequency, and a second tone set at the nominal receiver frequency of a 1 kHz audio tone at a voltage level 30% of its maximum relative to the pilot. An RF tone at the upper or lower adjacent-channel frequency constitutes the unwanted signal. The SINAD measurements are carried out as in the full-carrier AM case,

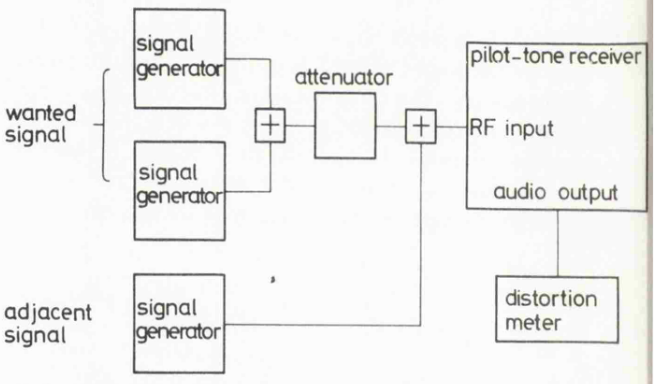

Fig. 6 *Adjacent-channel selectivity test configuration*

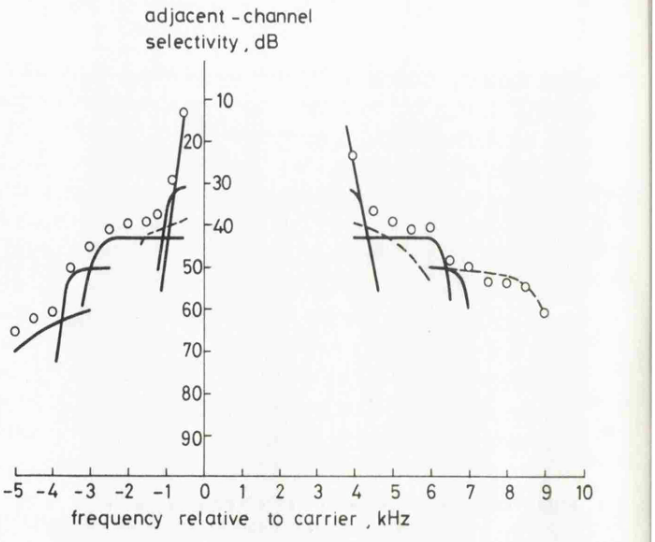

Fig. 7 *Theoretical and experimental adjacent-channel selectivity for a long-loop phase-locked receiver*

o experimental
– – – – theoretical, instability
——— theoretical, IF filter limitations and reciprocal mixing

and the adjacent-channel selectivity is expressed as the lower value of the ratios, in decibels, for the upper and lower adjacent channels of the level of the unwanted signal to the level of the wanted 1 kHz tone. The experimental set-up used to perform this test is shown in Fig. 6, and the measurement procedure was as follows. The wanted signal was summed with the adjacent tone at the receiver input. In the current Wolfson system a peak speech to pilot level of 15 dB is employed, and consequently the input RF tone which demodulated to a frequency of 1 kHz was set at + 5 dB relative to the pilot RF input. With the adjacent-channel signal switched out, the precision variable attenuator was adjusted to give a SINAD of 12 dB at the receiver output. The adjacent-channel tone was then applied and adjusted in level until the SINAD fell to a value of 6 dB. The test was repeated for several values of adjacent-channel frequency.

Fig. 7 shows a graph of the experimental points obtained for the long loop, together with theoretical curves illustrating the performance resulting from IF filter limitations, instability and reciprocal mixing. Only the significant portions of these curves which effectively form a selectivity boundary are shown. Figs. 8 and 9 show the experimental points obtained for the split- and short-loop receiver configurations, together with the expected performance resulting from the IF filter characteristic which is now the only significant limitation of adjacent-channel selectivity. The results in Figs. 7–9 compare

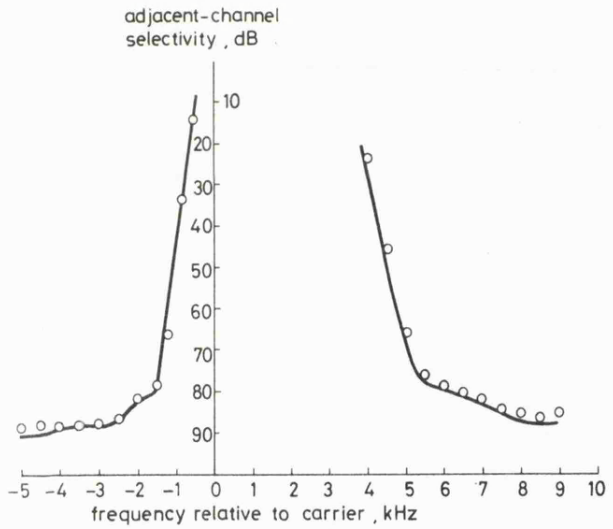

Fig. 8 *Theoretical and experimental adjacent-channel selectivity for a split-loop phase-locked receiver*

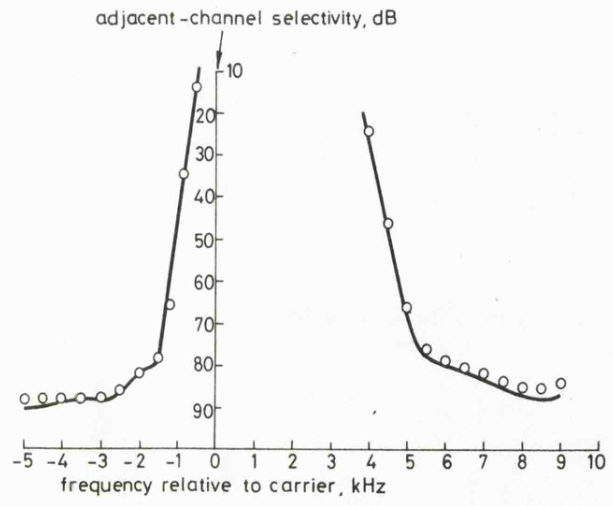

Fig. 9 *Theoretical and experimental adjacent-channel selectivity curves for a short-loop phase-locked receiver*

Table 1: Adjacent-channel selectivity comparison

	System		
	Wolfson long	Wolfson split/short	Home Office
IF bandwidth	3.7 kHz	3.7 kHz	3 kHz
Upper adjacent channel (+ 5 kHz)	39 dB	66 dB	68 dB
Lower adjacent channel (− 5 kHz)	65 dB	88 dB	70 dB

favourably with the theoretical curves, although the long-loop curves appear to be optimistic in predicting the receiver's selectivity. However, it should be noted that the theoretical selectivity is always above the worst-case line (3 dB above when two continuous lines intersect).

Table 1 compares the Wolfson receiver results with those obtained for a non-phase-locked receiver in the Home Office tests. In interpreting the results contained in this Table, it should be borne in mind that the IF crystal filter bandwidth between the − 3 dB points for the Home Office trial receiver was 3 kHz and was 3.7 kHz for the Wolfson tone-in-band system. The adjacent-channel-tone position is ± 5 kHz relative to the wanted carrier. Although this Table does not portray a fair comparison between upper and lower adjacent-channel selectivity (as an SSB signal is positioned to one side of the carrier), it does show the relative performance of the Wolfson and Home Office receivers. To obtain acceptable selectivity and first local oscillator control, the Wolfson phase-locked receiver requires a split-loop configuration.

4 Conclusions

In this paper, adjacent-channel selectivity tests for a tone-in-band SSB receiver have been described. The long-loop receiver was shown to possess poor selectivity, limited by the mechanisms of reciprocal mixing and loop instability. To overcome these problems and maintain control of the receiver's first local oscillator, a split-loop configuration was used. The only additional circuitry required is a split-loop filter and a low-deviation voltage-controlled second local oscillator. In this case, adjacent-channel selectivity performance comparable with current 12.5 kHz AM and 12.5 kHz FM equipment was obtained. However, it is believed that the selectivity of the Wolfson VHF receiver used in this particular series of tests could be further improved by using a narrower IF crystal filter more suited to 5 kHz channelling.

5 Acknowledgments

The authors wish to express their thanks to Prof. T.E. Rozzi, Head of the Electronics Group, for the provision of laboratory facilities, and one of us, J.P.H. Sladen, is grateful to the UK Science & Engineering Research Council for the award of a research studentship.

6 References

1 'Report on comparative tests of modulation methods for private mobile radio'. Home Office Directorate of Radio Technology, April 1982
2 'Sideband Technology conducts ACSB field trials with Standard Oil', *Mobile Times*, 1981, Oct., pp. 29–30
3 SNYDER, R.: 'ACSB – Our best hope for the future', *ibid.*, 1981, Oct., p. 34
4 McGEEHAN, J.P., and LYMER, A.: 'The problem of speech pulling and its implications for the design of phase-locked SSB radio systems', *IEE Proc. F, Commun., Radar & Signal Process.*, 1981, **128**, (6), pp. 361–369
5 McGEEHAN, J.P., and SLADEN, J.P.H.: 'Elimination of false locking in long loop phase-locked receivers', *IEEE Trans.*, 1982, **COM-30**, (10)

6 WELLS, R.: 'SSB for VHF mobile radio at 5 kHz channel spacing'. Proceedings of Conference on radio receivers and associated systems, IERE, London, 1978, pp. 29–36
7 BALL, J.R., and HOLMES, D.W.J.: 'An SSB with pilot receiver for mobile radio'. Clerk Maxwell conference on radio receivers and associated systems, IERE, Publication 50, 1981, pp. 429–435
8 GOSLING. W., McGEEHAN, J.P., and HOLLAND, P.G.: 'Receivers for the Wolfson single sideband VHF land mobile radio system', *Radio & Electron. Eng.*, 1979, **49**, pp. 321–325
9 LUSIGNAN, B.B.: 'AGC, AFC, tone select circuits for narrow-band mobile radio'. International telecommunications exposition, Dallas, Texas, USA, Feb., 1979
10 McGEEHAN, J.P.: 'Design and characterisation of a VHF phase-locked land mobile radio receiver', *Radio & Electron. Eng.*, 1977, **47**, pp. 67-73
11 MANASSEWITSCH, V.: 'Frequency synthesizers, theory and design' (Wiley, 1976), chap. 2

7 Appendixes

7.1 *Derivation of loop induced instability equations*

With reference to Fig. 10, let

$v_a(t)$ = $V_a \sin(\omega_a t + \theta_a)$ = RF adjacent tone
$v_i(t)$ = $V_i \sin(\omega_i t + \theta_i)$ = wanted reference-tone RF input
$v_0(t)$ = $V_0 \cos(\omega_0 t + \theta_0)$ = first local oscillator output
$v_1(t)$ = $V_1 \cos(\omega_1 t + \theta_1)$ = second local oscillator output
$v_r(t)$ = $V_r \cos(\omega_r t + \theta_r)$ = reference-tone oscillator output
A = IF gain
$G(\omega)$ = IF filter characteristic
K_0 = VCO gain (rad/Vs)
$F(\omega)$ = loop filter characteristic

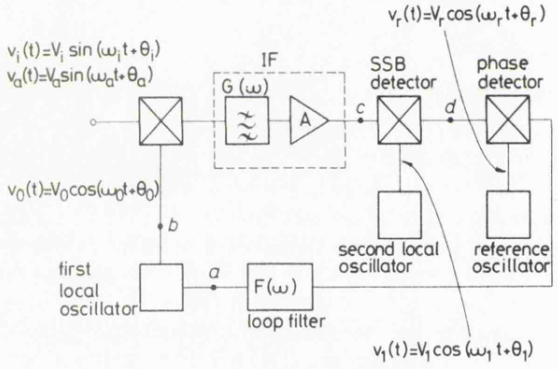

Fig. 10 *Block diagram of long-loop pilot-tone receiver*

Assume there is a voltage $v_t(t) = V_t \sin(\omega_t t + \theta_t)$ at the phase detector input. This gives rise to the following voltages at the points labelled in Fig. 10:

$$(a) \quad |F(\omega_t - \omega_r)| \frac{V_t V_r}{2} \sin(\omega_t t - \omega_r t + \theta_t - \theta_r + \underline{/F(\omega_t - \omega_r)})$$

and

$$|F(\omega_t + \omega_r)| \frac{V_t V_r}{2} \sin(\omega_t t + \omega_r t + \theta_t + \theta_r + \underline{/F(\omega_t + \omega_r)})$$

(*b*) Assuming narrowband frequency modulation, the four first-order sidebands are:

$$\text{(i)} \quad |F(\omega_t - \omega_r)| \frac{V_t V_r V_0 K_0}{4(\omega_t - \omega_r)} \sin[\omega_0 t + \omega_t t - \omega_r t + \theta_0 + \theta_t - \theta_r + \underline{/F(\omega_t - \omega_r)}]$$

$$\text{(ii)} \quad |F(\omega_t - \omega_r)| \frac{V_t V_r V_0 K_0}{4(\omega_t - \omega_r)} \sin[\omega_0 t - \omega_t t + \omega_r t + \theta_0 - \theta_t + \theta_r - \underline{/F(\omega_t - \omega_r)}]$$

$$\text{(iii)} \quad |F(\omega_t + \omega_r)| \frac{V_t V_r V_0 K_0}{4(\omega_t + \omega_r)} \sin[\omega_0 t + \omega_t t + \omega_r t + \theta_0 + \theta_t + \theta_r + \underline{/F(\omega_t + \omega_r)}]$$

$$\text{(iv)} \quad |F(\omega_t + \omega_r)| \frac{V_t V_r V_0 K_0}{4(\omega_t + \omega_r)} \sin[\omega_0 t - \omega_t t - \omega_r t + \theta_0 - \theta_t - \theta_r - \underline{/F(\omega_t + \omega_r)}]$$

$$(c) \quad \text{(i)} \quad |F(\omega_t - \omega_r)|\,|G(\omega_a - \omega_0 - \omega_t + \omega_r)| \frac{AV_t V_r V_0 V_a K_0}{8(\omega_t - \omega_r)} \cos[\omega_a t - \omega_0 t - \omega_t t + \omega_r t + \theta_a - \theta_0 - \theta_t + \theta_r - \underline{/F(\omega_t - \omega_r)} + \underline{/G(\omega_a - \omega_0 - \omega_t + \omega_r)}]$$

$$\text{(ii)} \quad |F(\omega_t - \omega_r)|\,|G(\omega_a - \omega_0 + \omega_t - \omega_r)| \frac{AV_t V_r V_0 V_a K_0}{8(\omega_t - \omega_r)} \cos[\omega_a t - \omega_0 t + \omega_t t - \omega_r t + \theta_a - \theta_0 + \theta_t - \theta_r + \underline{/F(\omega_t - \omega_r)} + \underline{/G(\omega_a - \omega_0 + \omega_t - \omega_r)}]$$

$$\text{(iii)} \quad |F(\omega_t + \omega_r)|\,|G(\omega_a - \omega_0 - \omega_t - \omega_r)| \frac{AV_t V_r V_0 V_a K_0}{8(\omega_t + \omega_r)} \cos[\omega_a t - \omega_0 t - \omega_t t - \omega_r t + \theta_a - \theta_0 - \theta_t - \theta_r - \underline{/F(\omega_t + \omega_r)} + \underline{/G(\omega_a - \omega_0 - \omega_t - \omega_r)}]$$

$$\text{(iv)} \quad |F(\omega_t + \omega_r)|\,|G(\omega_a - \omega_0 + \omega_t + \omega_r)| \frac{AV_t V_r V_0 V_a K_0}{8(\omega_t + \omega_r)} \cos[\omega_a t - \omega_0 t + \omega_t t + \omega_r t + \theta_a - \theta_0 + \theta_t + \theta_r + \underline{/F(\omega_t + \omega_r)} + \underline{/G(\omega_a - \omega_0 + \omega_t + \omega_r)}]$$

(*d*) Finally, at the SSB detector output, there are four demodulated tones. After making the following substitutions:

$\omega_s = \omega_a - \omega_0 - \omega_1$ = frequency spacing between adjacent tone and wanted carrier

$\theta_s = \theta_a - \theta_0 - \theta_1$

$K_d = \frac{AV_r V_0 V_1 V_i}{8}$ = phase detector gain

these tones become

$$\text{(i)}\quad |F(\omega_t-\omega_r)||G(\omega_1+\omega_s-\omega_t+\omega_r)|\frac{V_tV_aK_0K_d}{V_i2(\omega_t-\omega_r)}\cos[\omega_st-\omega_tt+\omega_rt+\theta_s-\theta_t+\theta_r-\underline{/F(\omega_t-\omega_r)}+\underline{/G(\omega_1+\omega_s-\omega_t+\omega_r)}]$$

$$\text{(ii)}\quad |F(\omega_t-\omega_r)||G(\omega_1+\omega_s+\omega_t-\omega_r)|\frac{V_tV_aK_0K_d}{V_i2(\omega_t-\omega_r)}\cos[\omega_st+\omega_tt-\omega_rt+\theta_s+\theta_t-\theta_r+\underline{/F(\omega_t-\omega_r)}+\underline{/G(\omega_1+\omega_s-\omega_t+\omega_r)}]$$

$$\text{(iii)}\quad |F(\omega_t+\omega_r)||G(\omega_1+\omega_s-\omega_t-\omega_r)|\frac{V_tV_aK_0K_d}{V_i2(\omega_t+\omega_r)}\cos[\omega_st-\omega_tt-\omega_rt+\theta_s-\theta_t-\theta_r-\underline{/F(\omega_t+\omega_r)}+\underline{/G(\omega_1+\omega_s-\omega_t-\omega_r)}]$$

$$\text{(iv)}\quad |F(\omega_t+\omega_r)||G(\omega_1+\omega_s+\omega_t+\omega_r)|\frac{V_tV_aK_0K_d}{V_i2(\omega_t+\omega_r)}\cos[\omega_st+\omega_tt+\omega_rt+\theta_s+\theta_t+\theta_r+\underline{/F(\omega_t+\omega_r)}+\underline{/G(\omega_1+\omega_s+\omega_t+\omega_r)}]$$

Comparing the frequencies and phases of the tones to those of v_t, the following equations are obtained for ω_t, θ_t and the voltage gain around the loop:

$$\text{(i)}\quad 2\omega_t = \omega_s+\omega_r$$
$$2\theta_t = \theta_s+\theta_r-\underline{/F(\omega_t-\omega_r)}+\underline{/G(\omega_1+\omega_t)}+\pi/2+2k\pi$$

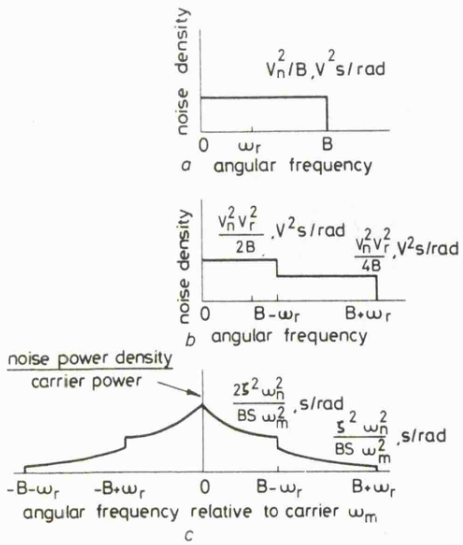

Fig. 11 *Degradation of VCO spectrum due to noise at SSB detector output*

a SSB detector output
b Phase detector output
c VCO output

where k is an integer

$$\text{gain} = |F(\omega_t-\omega_r)||G(\omega_1+\omega_t)|\times\frac{V_aK_0K_d}{V_i2(\omega_t-\omega_r)} \tag{7}$$

$$\text{(ii)}\quad 2\omega_t = -\omega_s+\omega_r$$
$$2\theta_t = -\theta_s+\theta_r-\underline{/F(\omega_t-\omega_r)}-\underline{/G(\omega_1-\omega_t)}-\pi/2+(2k-1)\pi$$
$$\text{gain} = |F(\omega_t-\omega_r)||G(\omega_1-\omega_t)|\times\frac{V_aK_0K_d}{V_i2(\omega_t-\omega_r)}$$

$$\text{(iii)}\quad 2\omega_t = \omega_s-\omega_r$$
$$2\theta_t = \theta_s-\theta_r-\underline{/F(\omega_t+\omega_r)}+\underline{/G(\omega_1+\omega_t)}+\pi/2+2k\pi$$
$$\text{gain} = |F(\omega_t+\omega_r)||G(\omega_1+\omega_t)|\times\frac{V_aK_0K_d}{V_i2(\omega_t+\omega_r)} \tag{8}$$

$$\text{(iv)}\quad 2\omega_t = -\omega_s-\omega_r$$
$$2\theta_t = -\theta_s-\theta_r-\underline{/F(\omega_t+\omega_1)}-\underline{/G(\omega_1-\omega_t)}-\pi/2+(2k-1)\pi$$
$$\text{gain} = |F(\omega_t+\omega_r)||G(\omega_1-\omega_t)|\times\frac{V_aK_0K_d}{V_i2(\omega_t+\omega_r)}$$

For an upper-sideband receiver, only solutions (i) and (iii) need be considered as the gains in (ii) and (iv) are very small owing to the $G(\omega_1-\omega_t)$ term. For a long-loop receiver with $F(s)=(1+s\tau_2)/s\tau_1$ and $|\omega_s-\omega_r|\gg\omega_n$, the loop natural frequency, eqns. 7 and 8 become

$$\text{gain} = |G(\omega_1+\omega_t)|\frac{V_a2\zeta\omega_n}{V_i(\omega_s-\omega_r)}$$

and

$$\text{gain} = |G(\omega_1+\omega_t)|\frac{V_a2\zeta\omega_n}{V_i(\omega_s+\omega_r)}$$

respectively, since

$$\omega_n^2 = \frac{K_0K_d}{\tau_1}$$

and

$$\zeta = \frac{\tau_2\omega_n}{2} = \text{the loop damping factor}$$

7.2 *Derivation of first local oscillator sidebands*

A demodulated speech term, $v_b(t)=V_b\sin(\omega_bt+\theta_b)$, and the demodulated reference tone, $v_c(t)=V_c\sin(\omega_rt+\theta_c)$, at the SSB detector output of the long-loop receiver mix with the receiver reference, $v_r(t)=V_r\cos(\omega_rt+\theta_r)$, in the phase detector. With phase lock between the reference tones, the phase detector output consists of a DC term and three AC

terms, which are:

$$\frac{V_c V_r}{2} \sin(2\omega_r t + \theta_c + \theta_r) \quad \text{twice reference frequency term}$$

$$\frac{V_b V_r}{2} \sin(\omega_b t - \omega_r t + \theta_b - \theta_r) \quad \text{speech difference frequency term}$$

$$\frac{V_b V_r}{2} \sin(\omega_b t + \omega_r t + \theta_b + \theta_r) \quad \text{speech sum frequency term}$$

If the reference frequency and the spacing between the demodulated speech and pilot-tone frequencies are both much greater than the phase-locked loop bandwidth, the three terms pass through the loop filter with a gain of τ_2/τ_1. Assuming, for the present, that the modulation on the first local oscillator is narrowband, it can simply be shown [11] that the oscillator output single-sideband/carrier power ratios are given by:

$$10 \log_{10} \left(\frac{V_c V_r \tau_2 K_0}{8 \tau_1 \omega_r} \right)^2 \text{dB}$$

$$10 \log_{10} \left(\frac{V_b V_r \tau_2 K_0}{4 \tau_1 (\omega_b - \omega_r)} \right)^2 \text{dB}$$

$$10 \log_{10} \left(\frac{V_b V_r \tau_2 K_0}{4 \tau_1 (\omega_b + \omega_r)} \right)^2 \text{dB}$$

for each of the terms, respectively. Noting that $V_c V_r/2$ is the phase detector constant and that $(V_b/V_c)^2$ is the speech/reference-tone power ratio, the above expressions simplify to:

$$10 \log_{10} \left(\frac{\zeta \omega_n}{2 \omega_r} \right)^2 \text{dB}$$

$$10 \log_{10} \left(\frac{\text{speech-tone power}}{\text{reference-tone power}} \right) + 10 \log_{10} \left(\frac{\zeta \omega_n}{(\omega_b - \omega_r)} \right)^2 \text{dB}$$

$$10 \log_{10} \left(\frac{\text{speech-tone power}}{\text{reference-tone power}} \right) + 10 \log_{10} \left(\frac{\zeta \omega_n}{(\omega_b + \omega_r)} \right)^2 \text{dB}$$

The extent of local-oscillator modulation by speech terms must be limited in a pilot-tone system, and in the present Wolfson system a peak speech tone will modulate the oscillator with a modulation index up to 0.2. This would give rise to second- and third-order sidebands -46 dB and -75 dB relative to the carrier. Their effect on adjacent-channel performance is negligible compared with the sum and difference first-order sidebands and with the loop instability case.

The effect of noise at the SSB detector output may be approximated as follows. Assume that the SSB detector output consists of the demodulated reference tone, $v_c(t) = V_c \sin(\omega_r t + \theta_c)$, together with noise, RMS voltage V_n, bandlimited to B rad/s (see Fig. 11*a*). The phase detector output will then be as shown in Fig. 11*b*, the noise being mixed with the reference tone, $V_r \cos(\omega_r t + \theta_r)$, and folded over at 0 rad/s, resulting in a 3 dB drop in noise power density at $(B - \omega_r)$ rad/s. The RMS oscillator derivation [11] is then given by

$$\Delta\omega^2_{RMS} = \frac{K_0^2 \tau_2^2 V_n^2 V_r^2}{\tau_1^2 B 2} = \frac{4\zeta^2 \omega_n^2}{SB} \text{ rad/sec}$$

$$\text{for } \omega_n \ll \omega_m < (B - \omega_r)$$

and

$$\Delta\omega^2_{RMS} = \frac{2\zeta^2 \omega_n^2}{SB} \text{ rad/s}$$

$$\text{for } (B - \omega_r) < \omega_m < (B + \omega_r)$$

where ω_m = modulation frequency, and

$$S = \frac{V_c^2}{2 V_n^2} = \text{reference-tone signal/noise ratio}$$

At the oscillator output,

$$\frac{\text{(noise power density)}}{\text{(carrier power)}} = \frac{\Delta\omega^2_{RMS}}{2\omega_m^2} \text{ s/rad}$$

and is shown in Fig. 11*c*.